Investigating the role of TLDc proteins in neuroprotection and disease-associated comorbidities



Anna L. M. Parsons

Word count: 42,951

Submitted for the degree of Doctor of Philosophy (DPhil)
Trinity 2022

Supervisors: Professor Peter Oliver & Professor Francis Szele

Department of Physiology, Anatomy and Genetics, University of Oxford
Mammalian Genetics Unit, Medical Research Council, Harwell

Abstract

The TLDc family of proteins is characterized by a conserved Tre2/Bub2/Cdc16 (TBC), lysin motif (LysM), domain catalytic (TLDc) domain. While the domain has been shown to protect against oxidative stress (OS), the mechanism of its protection and the distinct molecular functions of the TLDc family members are yet to be fully ascertained. In this thesis, the function and dysfunction of Tbc1d24 and Oxr1, two clinically important members of the TLDc family, are investigated.

Mutations in TBC1D24 are associated with a broad spectrum of neurological disorders, including epilepsy and the gene is implicated in synaptic transmission and neuronal development. Using knock-in mouse models, this thesis has studied the functional and physiological consequences of disruption in Tbc1d24, determining that loss-of-function mutations within Tbc1d24 result in a significant knock down of protein expression, ultimately resulting in seizures. Furthermore, a key interaction between Tbc1d24 and the V-ATPase has been confirmed, supporting a role for Tbc1d24 in the endolysosomal pathway. Unexpectedly, data from the new mouse models implicated Tbc1d24 in anaemia, revealing a novel role for the gene in the haematological system.

Oxr1 has been demonstrated to effectively protect against OS-induced cell death in neuronal cells, while overexpression of Oxr1 *in vivo* is able to delay neurodegeneration and neuroinflammation in mouse models of ALS. These findings support the promise of Oxr1 as a safe therapeutic target against OS-related neurodegeneration. This thesis has investigated the pharmacological induction of Oxr1 as a viable protective strategy, through generation of a stable cell line based on the highly conserved Oxr1 promoter element. Compound screening using this line has produced some early leads for exogenous upregulation of Oxr1. Furthermore, the *in vivo* genetic over-expression system was used to determine whether Oxr1 could functionally compensate for a loss-of-function Tbc1d24 mutation, shedding light on the lack of functional redundancy between TLDc family members.

This thesis addresses both the deleterious consequences of disruption, and the protective potential of overexpression of the TLDc family, combining new mouse genetic models with a range of molecular and cellular techniques. These studies have furthered understanding of the TLDc family and elucidated its therapeutic potential in protecting against OS and neurodegeneration.

Acknowledgements

Throughout my DPhil I have been fortunate to receive support from a great many people to whom I am deeply grateful. First and foremost, I would like to thank my supervisor Dr Peter Oliver for his mentorship and scientific guidance, and whose advice and support has challenged me to grow as a scientist and has encouraged me throughout the writing of this thesis. My thanks also to Dr Silvia Corrochano, whose useful discussions and teaching helped me to become an independent researcher, and whose kindness and energy have been a great example. My sincere gratitude also to Dr Gareth Banks, my postdoc supervisor, who has given me great encouragement. I am thankful to all who have been members of the Oliver lab; Dr Daniel Rial, Dr Enrico Castroflorio, Dr Tania Soares, Eboni Bucknor and Dominic Simpson; and to all of the students at MRC Harwell. You have all supported and inspired me with your teamwork and valuable discussion.

I am deeply grateful for the scientific support I have received from many of the teams at MRC Harwell, including the GEMS team and especially Dr Debbie Williams, whose insight and teaching have been valuable at all stages of my research. I'd also like to thank Dr Chris Esapa and Protein Core, and Dr Lydia Teboul and the CRISPR team, who have lent expertise that has been vital for this research. I would sincerely like to thank Simon Gillard and Ward 6 at the Mary Lyon Centre, who have been brilliantly attentive in the care of my mice and without whom much of this research would not have been possible. I have been honoured to be able to research using mice as the gold standard for genetic modelling, and am forever grateful for their sacrifice.

I would like to thank my collaborators in this research, whose outside perspective and generous teaching have enabled me to broaden the scope of my research, and have been shining examples of scientific cooperation. Thank you to Dr Samira Lakhal-Littleton and Dr Goran Mohammad for their help with understanding and analysing plasma chemistry, and to Dr Katja Simon and her lab for their help with planning cytometric analysis. My thanks to Alexandra Preston for her enthusiastic collaboration and help with performing

flow cytometry. I am grateful also to my examiners, Dr Hal Drakesmith and Dr Frances Wiseman, whose insightful and engaging discussion of my research made the final stages of my PhD enjoyable and interesting.

I have been lucky to have access to incredible professional support, and would like to thank Clare Graham, to whom I am extremely grateful for her study skills tuition, which was always compassionate and encouraging. I would like to thank Sarah Noujaim for her tireless and enthusiastic help in navigating all things administrative. Thank you also to Claire Chesworth for her encouragement with pursuing the next stages of my career, and thank you to my current tutors and students at Hughes Hall for supporting me during my preparation for my viva while studying my first term of Medicine.

Thank you to my wonderful family, Ruth, Jeremy, Louis and Raphie Parsons, for your encouragement, unconditional love and constant supply of warmth and humour. Knowing that you are there for me no matter what has been an endless source of comfort. Thank you to my friend Helen Long for supporting me in all your weird and wonderful ways. To Natasha, Lou and Primothy, thank you for your friendship, which has stood the test of distance and a global pandemic. Thank you to Charlie for being a great friend, and for always being up for the pub. Thank you to Balliol Chapel Choir who have filled difficult times with music and light, and especially Leah and Kate for our evenings of excellent food and cackling. Finally, thank you George, my partner and love of my life, for all you have done to support me, and all you continue to do to make my life better in every way.

Abbreviations used repeatedly in this thesis

AED	**Anti-Epileptic Drug**
EEG	**Electroencephalogram**
GLT-1	**Glutamate transporter 1**
HEK	**Human Embryonic Kidney**
N2a	**Neuro-2a**
NCOA7	**Nuclear Receptor Coactivator 7**
NMJ	**Neuromuscular Junction**
OS	**Oxidative Stress**
OXR1	**Oxidation Resistance 1**
PME	**Progressive Myoclonic Epilepsy**
ROS	**Reactive Oxygen Species**
SV	**Synaptic Vesicle**
TBC1D24	**TBC1 domain family member 24**
TLDc	**Tre2/Bub2/Cdc16 (TBC), lysin motif (LysM), domain catalytic**
V-ATPase	**Vacuolar ATPase**

Table of Contents

ABSTRACT **2**

ACKNOWLEDGEMENTS **3**

ABBREVIATIONS USED REPEATEDLY IN THIS THESIS **5**

TABLE OF CONTENTS **6**

TABLE OF FIGURES **10**

CHAPTER 1: INTRODUCTION **12**

1.1 EPILEPSY 12
1.1.1 Definition, Incidence and Aetiology of Epilepsy *12*
1.1.2 Genetic Causes of Epilepsy *13*
1.1.3 Anti-Epileptic Drugs *16*
1.1.4 Mouse Models of Epilepsy *17*
1.1.5 Oxidative Stress and Epilepsy *19*
1.2 THE TLDC FAMILY 22
1.2.1 Background of the TLDc Family *22*
1.2.2 TBC1D24 in Disease *24*
1.2.3 OXR1 in Disease *26*
1.3 RESEARCH AIMS AND OBJECTIVES 28

CHAPTER 2: MATERIALS AND METHODS **30**

2.1 ETHICS STATEMENT 30
2.2 ANIMALS, HUSBANDRY AND HOUSING 30
2.2.1 Generation of CRISPR/Cas9 mouse lines *30*
2.2.2 Genotyping *31*
2.2.3 Behavioural Phenotyping *32*
2.3 HISTOPATHOLOGY 33
2.3.1 Tissue collection *33*
2.3.2 Immunohistochemistry *33*
2.3.3 Nissl staining *34*
2.3.4 DAB-enhanced Perls stain *34*
2.4 PROTEIN ANALYSIS 35
2.4.1 Protein extraction *35*
2.4.2 Western blotting *35*
2.4.3 Co-immunoprecipitation *36*
2.4.4 Table of antibodies *36*
2.5 RNA ANALYSIS 36
2.5.1 RNA extraction of large tissue *36*
2.5.2 RNA extraction of small tissue *37*
2.5.3 Synthesis of cDNA *37*
2.5.4 RT-qPCR *37*
2.5.5 Allele-specific RT-qPCR assay *37*
2.5.6 In situ hybridization *38*
2.5.7 Table of RT-qPCR primers *38*
2.6 TRANSCRIPTOMICS 39
2.7 HAEMATOLOGICAL ANALYSIS 39
2.7.1 Blood and sera collection *39*
2.7.2 Clinical chemistry *40*
2.7.3 Giemsa staining *40*
2.7.4 Serum analysis *40*

2.7.5 Heme assay ... *40*
2.7.6 Glycine assay ... *40*
2.8 Flow cytometry ... 41
2.8.1 Erythroid cells ... *41*
2.8.2 Hematopoietic progenitors ... *41*
2.9 Generation and maintenance of cell lines ... 42
2.9.1 Neuro2a cells ... *42*
2.9.2 Cloning ... *42*
2.9.3 Transfection ... *42*
2.9.4 Nano-Glo Dual Luciferase assay ... *43*
2.9.5 Coincidence reporter validation ... *43*
2.9.6 Generation of stable cell lines ... *43*
2.9.7 Compound Screen ... *44*
2.9.8 CRISPRa ... *44*
2.9.9 Statistical analysis ... *45*

CHAPTER 3: CHARACTERIZATION OF CRISPR MOUSE MODELS OF *TBC1D24* DYSFUNCTION ... 46

3.1 Introduction ... 46
3.1.1 Models of TBC1D24 dysfunction ... *46*
3.1.2 CRISPR Models of TBC1D24 dysfunction: R360L, P135L and INS2 ... *49*
3.2 Characterization of the Tbc1d24$^{R360L/R360L}$ mouse ... 51
3.2.1 Phenotype of Tbc1d24$^{R360L/R360L}$ ... *51*
3.2.2 Expression studies of Tbc1d24$^{R360L/R360L}$ ... *54*
3.2.3 Neuropathology of Tbc1d24$^{R360L/R360L}$ ... *57*
3.2.4 Functional studies of the V-ATPase in Tbc1d24$^{R360L/R360L}$ ... *60*
3.2.5 Summary of findings in the Tbc1d24$^{R360L/R360L}$ mutant ... *62*
3.3 Characterization of the *Tbc1d24$^{P135L/P135L}$* mutant ... 63
3.3.1 Phenotype of Tbc1d24$^{P135L/P135L}$ ... *63*
3.3.2 Expression studies in the Tbc1d24$^{P135L/P135L}$ mutant ... *64*
3.3.3 Summary of findings in the Tbc1d24$^{P135L/P135L}$ mutant ... *65*
3.4 Characterization of the *Tbc1d24$^{INS2/INS2}$* mutant ... 65
3.4.1 Expression studies of Tbc1d24$^{INS2/INS2}$ ... *66*
3.4.2 Neuropathology of Tbc1d24$^{INS2/INS2}$ ... *69*
3.4.3 Summary of findings in the Tbc1d24$^{INS2/INS2}$ mutant ... *71*
3.5 Discussion ... 72
3.5.1 The phenotypes of Tbc1d24 mutant mouse lines ... *72*
3.5.2 The interaction between the TLDc family and the V-ATPase ... *80*
3.5.3 Concluding Remarks ... *82*

CHAPTER 4: EXPLORING THE FUNCTIONAL EFFECTS OF DISRUPTION OF TBC1D24 ON THE HAEMATOLOGICAL SYSTEM ... 84

4.1 Introduction ... 84
4.1.1 Anaemia and Erythropoiesis ... *84*
4.1.2 Aetiological links between anaemia and oxidative stress ... *85*
4.1.3 Iron homeostasis, the endolysosomal pathway, and Tbc1d24 ... *86*
4.2 Haematological studies in the *Tbc1d24$^{INS2/INS2}$* mutant ... 87
4.2.1 Visible anaemia in the embryonic mutant ... *87*
4.2.2 Peripheral blood smears of Tbc1d24$^{INS2/INS2}$ exhibit haemolytic anaemia ... *88*
4.3 Expression studies in loss-of-function *Tbc1d24* mouse mutants ... 89
4.3.1 RNA-Sequencing in the Tbc1d24$^{INS2/INS2}$ mutant ... *89*
4.3.2 Microarray studies in the Tbc1d24$^{R360L/R360L}$ mutant ... *93*
4.3.3 RNA-Sequencing in the Tbc1d24$^{R360L/R360L}$ mutant ... *96*
4.3.4 A comparison of the transcriptomic studies of the two Tbc1d24 mutants ... *99*

4.3.5 Validation of transcriptomics confirms drive towards haemoglobin synthesis 100
4.3.6 In situ hybridization of haematology markers 102
4.3.7 Saline perfusion confirms vascular origin of expression changes in the Tbc1d24$^{R360L/R360L}$ mutant 103
4.4 HAEMATOLOGICAL STUDIES IN THE *TBC1D24$^{R360L/R360L}$* MUTANT 104
4.4.1 Peripheral blood smears appear normal 104
4.4.2 Clinical chemistry shows reduced haemoglobin and erythrocyte volume 105
4.5 INVESTIGATING IRON HOMEOSTASIS 110
4.5.1 Iron marker mRNA expression changes in the Tbc1d24$^{R360L/R360L}$ and Tbc1d24$^{INS2/INS2}$ liver 110
4.5.2 Serum analysis of Tbc1d24$^{R360L/R360L}$ reveals disrupted iron homeostasis 113
4.5.3 Concentration of circulating free heme is reduced in the Tbc1d24$^{R360L/R360L}$ mutant 115
4.5.4 Glycine assay shows increased glycine, may indicate Alas2 dysfunction 116
4.5.5 Iron staining of the Tbc1d24$^{R360L/R360L}$ mutant spleen indicates iron loading anaemia 117
4.6 ERYTHROPOIETIC CHANGES IN *TBC1D24$^{R360L/R360L}$* 118
4.6.1 Splenomegaly indicates stress erythropoiesis 118
4.6.2 Flow cytometry indicates stress erythropoiesis in the Tbc1d24$^{R360L/R360L}$ mutant 119
4.7 DISCUSSION 121
4.7.1 Expression and haematological studies confirm that loss-of-function in Tbc1d24 results in anaemia 121
4.7.2 Hypothesised mechanism of action 126
4.7.3 Concluding Remarks 127

CHAPTER 5: INVESTIGATING THE NEUROPROTECTIVE ROLE OF OXR1 *IN VITRO* AND *IN VIVO* 129

5.1 INTRODUCTION 129
5.1.1 The role of Oxr1 in neuroprotection, and therapeutic potential of endogenous neuroprotective mechanisms to rescue neurodegeneration 129
5.1.2 OXR1-C is functionally sufficient and confers neuroprotection 131
5.2 INVESTIGATION OF OXR1-C PROMOTER FOR USE IN COMPOUND SCREENING 133
5.2.1 Transient transfection reciprocal inhibition with NanoGlo 136
5.2.2 Transient transfection transcriptional assays with NanoGlo 137
5.3 GENERATION OF A STABLE CELL LINE 138
5.3.1 Antibiotic selection kill curve 138
5.3.2 Colony validation by PCR and Luciferase assay 140
5.3.3 Stable cell line reciprocal inhibition 141
5.4 COMPOUND SCREENING 142
5.4.1 Establishing a protocol for cell based compound screening 142
5.4.2 Compound Screen Results 143
5.4.3 Dose-response curves of lead compounds 145
5.4.4 Validation of lead compounds by polyclonal line assay 146
5.4.5 Validation of lead compounds by qPCR 147
5.5 CRISPR ACTIVATION TESTING IN NEURO2A CELLS 148
5.6 OVEREXPRESSION OF OXR1 TO MODIFY SEIZURE PHENOTYPE OF TBC1D24 MUTANT 150
5.6.1 Oxr1^{Prnp} x Tbc1d24^{R360L} protein expression 151
5.6.2 Preliminary video tracking analysis shows extended survival in Oxr1^{Prnp} x Tbc1d24^{R360L} compared with Tbc1d24^{R360L} 152
5.6.3 The gene c-Fos is influenced by neuronal overexpression of Oxr1 154
5.7 EFFECT OF OXR1 OVEREXPRESSION ON HAEMATOLOGICAL DISRUPTION IN LOSS-OF-FUNCTION TBC1D24 MUTANTS 155
5.7.1 Rescue of Alas2 coincides with enhanced survival in Oxr1^{Prnp} x Tbc1d24^{R360L} 156
5.7.2 Haematological markers in Oxr1^{Prnp} x Tbc1d24^{INS2} 157
5.7.3 Summary of the effects of overexpression of Oxr1 in vivo 159
5.8 DISCUSSION 160
5.8.1 Strategies for the transcriptional control of Oxr1 expression 160

5.8.2 Overexpression of Oxr1 produces mild amelioration of pathology caused by loss-of-function mutations in Tbc1d24 ..... *165*
5.8.3 Concluding Remarks *168*

CHAPTER 6: DISCUSSION & CONCLUSION **170**

6.1 GENERAL SUMMARY OF DATA 170
6.2 TBC1D24 PROTEIN STABILITY AND FUTURE TREATMENT FOR TBC1D24-RELATED PATHOLOGY 172
6.3 TBC1D24, THE V-ATPASE AND THE ENDOLYSOSOMAL PATHWAY 175
6.4 THE OVERLAPPING AETIOLOGIES OF ANAEMIA AND EPILEPSY 179
6.5 GLUTAMATE, EPILEPSY AND THE V-ATPASE 181
6.6 OXR1 AS A FUTURE THERAPEUTIC TARGET 185
6.7 CONCLUSION 186

CHAPTER 7: APPENDICES **188**

BIBLIOGRAPHY **196**

Table of Figures

FIGURE 1.1 SCHEMATIC SHOWING THE TLDC PROTEIN FAMILY.. 23
FIGURE 3.1 MUTATION SCHEMATIC FOR TBC1D24^{R360L}, TBC1D24^{P135L} AND TBC1D24^{INS2} MUTANT MOUSE MODELS.. 49
FIGURE 3.2 SEQUENCE ALIGNMENT BETWEEN HUMAN TBC1D24 AND MOUSE TBC1D24 PROTEIN. 50
FIGURE 3.3 OPEN FIELD BEHAVIOURAL TESTING SHOWS NO SIGNIFICANT CHANGES IN BEHAVIOUR OF THE TBC1D24$^{R360L/R360L}$ MOUSE MUTANT 54
FIGURE 3.4 THE TBC1D24$^{R360L/R360L}$ MUTANT SHOWS KNOCK DOWN IN PROTEIN LEVELS 55
FIGURE 3.5 TBC1D24$^{R360L/R360L}$ SHOWS NO DIFFERENCE IN EXPRESSION OF TBC1D24 MRNA COMPARED WITH TBC1D24$^{+/+}$. 56
FIGURE 3.6 EXPRESSION ANALYSIS BY RT-QPCR INDICATES SIMILAR EXPRESSION OF TBC1D24^{+} AND TBC1D24^{R360L} ALLELES ..... ERROR! BOOKMARK NOT DEFINED.
FIGURE 3.7 IN SITU HYBRIDISATION OF TBC1D24 SHOWS SIMILAR EXPRESSION BETWEEN TBC1D24$^{+/+}$ AND TBC1D24$^{R360L/R360L}$. 57
FIGURE 3.8 COMPARABLE GROSS MORPHOLOGY BETWEEN TBC1D24$^{+/+}$ AND TBC1D24$^{R360L/R360L}$ BRAIN SHOWN BY NISSL STAINING 58
FIGURE 3.9 UPREGULATION OF C-FOS IN THE PIRIFORM CORTEX OF THE TBC1D24$^{R360L/R360L}$ MUTANT 59
FIGURE 3.10 CONFIRMATION OF THE INTERACTION BETWEEN TBC1D24 AND V-ATPASE SUBUNITS, DEMONSTRATED BY CO-IMMUNOPRECIPITATION. 62
FIGURE 3.11 THE TBC1D24$^{P135L/P135L}$ MUTANT SHOWS KNOCK DOWN IN PROTEIN LEVELS. 64
FIGURE 3.12 EXPRESSION ANALYSIS BY RT-QPCR SHOWS SIMILAR EXPRESSION OF TBC1D24 MRNA IN TBC1D24$^{P135L/P135L}$ AND TBC1D24$^{+/+}$ 65
FIGURE 3.13 REDUCED ABUNDANCE OF TBC1D24 PROTEIN IN THE TBC1D24$^{INS2/INS2}$ MUTANT 67
FIGURE 3.14 EXPRESSION OF TBC1D24 MRNA IS DECREASED IN TBC1D24$^{INS2/INS2}$ COMPARED WITH TBC1D24$^{+/+}$ 67
FIGURE 3.15 DECREASED EXPRESSION OF TBC1D24 IN THE DEVELOPING TBC1D24$^{INS2/INS2}$ BRAIN 68
FIGURE 3.17 DISRUPTION IN PATTERNING OF THE DEVELOPING CORTEX IN THE TBC1D24$^{INS2/INS2}$ MUTANT. 71
FIGURE 4.1 ANAEMIA IS VISIBLE IN EMBRYONIC TBC1D24^{INS2} MUTANT. 88
FIGURE 4.2 PERIPHERAL BLOOD SMEARS OF INS2 MUTANT MICE SHOW HAEMOLYTIC ANAEMIA 89
FIGURE 4.3 RNA SEQUENCING SHOWS SIGNIFICANT UPREGULATION OF KEY HAEMATOLOGICAL GENES IN THE TBC1D24$^{INS2/INS2}$ CORTEX. 90
FIGURE 4.4 ENRICHMENT ANALYSIS INDICATES IRON HOMEOSTASIS, GLUCOSE METABOLISM AND EMBRYONIC DEVELOPMENT AS ENRICHED BIOLOGICAL PROCESSES IN THE TBC1D24$^{INS2/INS2}$ MUTANT. 91
FIGURE 4.5 FUNCTIONAL ENRICHMENT ANALYSIS OF THE TBC1D24$^{INS2/INS2}$ MUTANT INDICATES DIFFERENTIAL EXPRESSION OF GENES IN PATHWAYS RELATING TO ANAEMIA. 93
FIGURE 4.6 MICROARRAY OF TBC1D24$^{R360L/R360L}$ MUTANT SHOWS UPREGULATION OF KEY HAEMATOLOGY GENES ACROSS CORTEX, CEREBELLUM AND HIPPOCAMPUS 95
FIGURE 4.7 - GENES CHOSEN FOR PRIMER DESIGN BASED ON MICROARRAY OF TBC1D24$^{R360L/R360L}$ CORTEX, CEREBELLUM AND HIPPOCAMPUS 96
FIGURE 4.8 RNA SEQUENCING SHOWS SIGNIFICANT UPREGULATION OF KEY HAEMATOLOGICAL GENES IN THE TBC1D24$^{R360L/R360L}$ PREFRONTAL CORTEX. 98
FIGURE 4.9 PRINICPAL COMPONENT ANALYSIS (PCA) OF RNA-SEQUENCING OF TBC1D24$^{R360L/R360L}$ COMPARED TO WILD TYPE CONTROLS 98
FIGURE 4.10 COMPARISON OF DIFFERENTIALLY EXPRESSED GENES BETWEEN TWO TBC1D24 MUTANTS. 99
FIGURE 4.11 VALIDATION OF EXPRESSION CHANGES IN CRITICAL HAEMATOLOGICAL GENES AS A RESULT OF TBC1D24 MUTATION 101
FIGURE 4.12 IN SITU HYBRIDIZATION OF TBC1D24$^{R360L/R360L}$ SHOWS VISIBLE UPREGULATION OF HAEMOGLOBIN SUBUNITS 103
FIGURE 4.13 SALINE PERFUSION OF TBC1D24$^{R360L/R360L}$ REMOVES UPREGULATION OF HAEMATOLOGICAL GENES. 104

FIGURE 4.14 PERIPHERAL BLOOD SMEARS OF TBC1D24$^{R360L/R360L}$ MICE SHOW NO OBVIOUS DIFFERENCES COMPARED WITH TBC1D24$^{+/+}$ 105
FIGURE 4.15 THE TBC1D24$^{R360L/R360L}$ MUTANT SHOWS SMALLER ERYTHROCYTE VOLUME WITH HIGHER CELL COUNT, INDICATIVE OF MICROCYTIC ANAEMIA. 106
FIGURE 4.16 HAEMOGLOBIN CONCENTRATION IS DECREASED IN TBC1D24$^{R360L/R360L}$ 107
FIGURE 4.17 LARGE PLATELETS ARE OBSERVED IN THE TBC1D24$^{R360L/R360L}$ MUTANT. 108
FIGURE 4.18 THE BASOPHIL AND PEROXIDASE METHODS OF WHITE BLOOD CELL COUNTING GIVE CONFLICTING READINGS FOR THE TBC1D24$^{R360L/R360L}$ MUTANT 109
FIGURE 4.19 INCREASED EXPRESSION OF MARKERS OF IRON HOMEOSTASIS IN THE LIVER OF TBC1D24$^{INS2/INS2}$. 111
FIGURE 4.20 INCREASED EXPRESSION OF HAEMOGLOBIN SYNTHESIS MARKERS AND DECREASED EXPRESSION OF IRON HOMEOSTASIS MARKERS IN THE LIVER OF THE TBC1D24$^{R360L/R360L}$ MUTANT. 112
FIGURE 4.21 SERUM ANALYSIS OF THE TBC1D24$^{R360L/R360L}$ MUTANT SHOWS AN INCREASE IN IRON CONCENTRATION AND A DECREASE IN GLUCOSE CONCENTRATION 115
FIGURE 4.22 CONCENTRATION OF FREE HEME IS DECREASED IN THE TBC1D24$^{R360L/R360L}$ MUTANT. 116
FIGURE 4.23 GLYCINE CONCENTRATION IS INCREASED IN THE TBC1D24$^{R360L/R360L}$ 117
FIGURE 4.24 INCREASED IRON DEPOSITS IN THE TBC1D24$^{R360L/R360L}$ SPLEEN INDICATES IRON LOADING ANAEMIA 118
FIGURE 4.25 SPLENOMEGALY IS OBSERVED IN THE TBC1D24$^{R360L/R360L}$ MUTANT 119
FIGURE 4.26 FLOW CYTOMETRY INDICATES SPLENIC STRESS ERYTHROPOIESIS IN THE TBC1D24$^{R360L/R360L}$ MUTANT 121
FIGURE 4.27 FUNCTIONAL TBC1D24 PROTEIN IS REQUIRED FOR IN HEME SYNTHESIS 128
FIGURE 5.1 SEQUENCE ALIGNMENT OF HUMAN AND MOUSE PROMOTER REGIONS OF OXR1-C (WILLIAMSON, 2015). 134
FIGURE 5.2 TRANSFECTION WITH OXR1-C PROMOTER CONSTRUCT DRIVES LUMINESCENCE IN NANOGLO SYSTEM 135
FIGURE 5.3 VALIDATION OF THE COINCIDENCE REPORTER SYSTEM USING OXR1-C PROMOTERS OF 400 BP AND 1 KB LENGTH, USING TRANSIENT TRANSFECTION 136
FIGURE 5.4 IDENTIFICATION OF TRANSCRIPTION FACTORS THAT AFFECT LUMINESCENCE WITHIN THE TRANSIENTLY TRANSFECTED REPORTER SYSTEM. 138
FIGURE 5.5 DETERMINING THE CONCENTRATION OF HYGROMYCIN FOR USE IN ANTIBIOTIC SELECTION. 139
FIGURE 5.6 VALIDATION OF SUCCESSFUL MONOCLONES BY LUCIFERASE ASSAY 140
FIGURE 5.7 VALIDATION OF THE STABLY EXPRESSED COINCIDENCE REPORTER SYSTEM USING OXR1-C PROMOTERS OF 400 BP AND 1 KB LENGTH. 141
FIGURE 5.8 REPRESENTATIVE RESULTS OF THE COMPOUND SCREEN. 144
FIGURE 5.9 A POSITIVE HIT IDENTIFIED FROM THE INITIAL COMPOUND SCREEN. 144
FIGURE 5.10 DOSE-RESPONSE CURVES PRODUCED WITH VARYING CONCENTRATIONS OF PUTATIVE OXR1-C UPREGULATORS IN STABLE CELL LINES 145
FIGURE 5.11 DOSE-RESPONSE CURVES PRODUCED WITH VARYING CONCENTRATIONS OF PUTATIVE OXR1-C UPREGULATORS IN A POLYCLONAL STABLE CELL LINE. 146
FIGURE 5.12 INVESTIGATION OF EFFECT OF LEAD COMPOUNDS ON EXPRESSION OF OXR1-C 147
FIGURE 5.13 BRIGHT FIELD AND FLUORESCENT IMAGING OF CRISPRA-TRANSFECTED CELLS. 149
FIGURE 5.14 INCREASED EXPRESSION OF OXR1-C FOLLOWING TRANSFECTION WITH CRISPRA CONSTRUCTS 150
FIGURE 5.15 PROGENY OF THE OXR1^{PRNP} X TBC1D24^{R360L} CROSS SHOW EXPECTED PROTEIN LEVELS. 152
FIGURE 5.16 MRNA EXPRESSION OF C-FOS IN PROGENY OF THE OXR1^{PRNP} X TBC1D24^{R360L} CROSS 155
FIGURE 5.17 OVEREXPRESSION OF OXR1 RESCUES PATHOLOGICAL INDUCTION OF ALAS2 IN TBC1D24^{R360L} 157
FIGURE 5.18 OVEREXPRESSION OF OXR1 MAY REDUCE MARKER OF NEURODEVELOPMENTAL DYSFUNCTION IN TBC1D24^{INS2} 159
FIGURE 6.1 ELECTROPHYSIOLOGICAL RECORDINGS SHOW HYPEREXCITABILITY AND INCREASED SATURATION OF GLT-1 IN THE TBC1D24$^{R360L/R360L}$ MUTANT 182
FIGURE 6.2 – THE INTERACTION BETWEEN TBC1D24 AND THE V-ATPASE IS REQUIRED FOR GLUTAMATE HOMEOSTASIS BETWEEN NEURONS AND ASTROCYTES 184

Chapter 1: **Introduction**

1.1 Epilepsy

1.1.1 Definition, Incidence and Aetiology of Epilepsy

Epilepsy refers to a group of neurological diseases characterized by a chronic predisposition to epileptic seizures, with a wide variety of causes [1]. Seizures are caused by abnormal, excessive or synchronous neuronal activity, affecting the cerebral cortex [2]. An estimated 65 million people worldwide experience epilepsy, with an increased disease burden on low-income countries; mortality rate in epilepsy patients is 2-5 times higher than that of the general population in high-income countries, but up to 37 times higher in low income countries [3]. The disproportionate impact of epilepsy in low income populations is due to several factors, including increased risk of induced epilepsy, for example due to infection or head trauma, and lack of access to treatments such as antiepileptic drugs (AEDs) [4]. Epilepsy is associated with multiple psychiatric and somatic comorbidities, increasing the complexity of therapeutic need [5]. The heterogeneity of epilepsy is evident in that up to 40% of epilepsies have genetic origin [6], but no individual gene is the underlying cause in more than 1% of epilepsies [7]. The remaining 60% of epilepsy cases are divided by aetiology into unknown causes (30%) and acquired causes (30%); the latter refers to epilepsy induced by events such as traumatic brain injury (TBI) [8], brain tumour [9] or infection [10].

The diagnosis of epilepsy applies to patients that have experienced two spontaneous seizures over 24 hours apart, have experienced a single spontaneous seizure with a high probability (>60%) of recurrence within 10 years, or have been previously diagnosed with an epileptic syndrome [11]. Further specificity can be applied to the diagnosis within the definition of epilepsy, based on the localization and presentation of seizures. In focal epilepsies, seizures originate from a particular region of the cortex, and can spread to other brain areas, while generalized epilepsies involve seizures with bilateral origin, occurring with aberrant activity throughout the cortex [12]. The features of seizure presentation enable classification of epilepsies as either motor or non-motor, with further subtypes including

myoclonic, involving rapid asynchronous muscle spasms; and tonic-clonic, involving muscle stiffening with twitching movements [13]. Clinical presentation of seizures can depend on the brain area affected by seizure, especially in focal epilepsies. Localization of the epileptogenic zone can be aided by recognising specific symptoms early in the time course of the seizure; for example, visual auras are associated with seizures originating from Broadmann areas 17 and 18 within the visual cortex [14]. Determining the origin of seizures in focal epilepsies is crucial for surgical treatment options, which are considered after the failure of AEDs to treat symptoms [15]. However, generalized epilepsies are more likely to have genetic causes, requiring AEDs that address the underlying pathologies of disrupted neurotransmission for successful treatment [16].

1.1.2 Genetic Causes of Epilepsy

Seizure events are triggered by an imbalance between excitatory and inhibitory neurotransmission, due to increase in glutamatergic activity or a decrease in GABAergic activity, although there are many causal mechanisms for an imbalance in neurotransmission [17] [18]. Acute seizures can be caused by a temporary factors, for example due to magnesium deficiency [19] or viral infection [20]. However, in epilepsy, which is characterized by recurrent seizures, neuronal networks are predisposed to cause seizures. This is due to a wide variety of permanent factors, resulting in imbalance between excitatory and inhibitory neurotransmission.

Neurotransmission is the process by which neurotransmitters are released from the presynaptic terminal by exocytosis, to cross the synaptic cleft and bind to postsynaptic receptors. A diverse range of chemical signalling molecules function as neurotransmitters, from amino acids, such as glutamate or gamma aminobutyric acid (GABA), and monoamines such as serotonin, to gases such as nitric oxide [21]. Neurotransmitters are packaged into synaptic vesicles (SVs) through the action of the vacuolar ATPase (V-ATPase), which consumes ATP to pump protons into the SVs. The V-ATPase creates the electrochemical gradient necessary for vesicular neurotransmitter transporters, for example the vesicular monoamine transporter (VMAT) or the vesicular glutamate transporter

(VGLUT), to drive the inward transport of neurotransmitters into the SV [22]. Stimulation of a presynaptic neuron by an action potential (AP) causes an influx of Ca^{2+} through voltage-gated Ca^{2+} channels, which induces exocytosis of neurotransmitter containing-SVs [23]. Neurotransmitter binding causes either depolarisation (due to the influx of cations such as sodium, Na^{+}) or hyperpolarisation (due to the influx of anions such as chloride, Cl^{-}) depending on the neurotransmitter and its receptor.

Channelopathies caused by mutations in ion channels are commonly associated with epilepsy, as they cause destabilisation of neuronal membrane potential, leading to disruption in neural networks [24]. The most common gene associated with epilepsy is sodium voltage-gated channel alpha subunit 1 (*SCN1A*), encoding $Na_v1.1$, although mutations in *SCN1A* are responsible for a wide range of epilepsy syndromes [25]. Pathogenic mutations alter the channel properties of $Na_v1.1$, for example, by increasing the voltage required for channel gating, causing slowed inactivation, or blocking the sodium current altogether. Characterization of mutations has been performed by expression in *Xenopus oocytes* and in human embryonic kidney (HEK) cells [26]. Gain-of-function mutations in hyperpolarization-activated cyclic nucleotide-gated channel 2 (*HCN2*) were shown to cause epilepsy due to alterations of both the voltage required for activation and the speed of activation [27].

Following neurotransmission, SV membranes are retrieved and reformation of SVs takes place to replenish the SV pool for future synaptic transmission [28]. Endocytosis of SVs at the presynaptic terminal is mediated by Dynamin-1 (DNM1), a large mechanochemical GTPase. Mutations in *DNM1* have been shown to cause epileptic encephalopathy in humans, and *Dnm1*^{Ftfl}, a spontaneous seizure-inducing mouse mutation in *Dnm1,* was shown to cause defects in endocytosis, showing fewer vesicles but enlarged vesicle size [29]. In addition, uptake of neurotransmitters from the synaptic cleft is necessary to prevent excitotoxicity; the accumulation of glutamate in the synaptic cleft instigates over-activation of the glutamate receptors AMPA and NMDA, which can lead to cell death following

excessive Ca^{2+} influx and activation of calcium-binding proteins which cause breakdown of organelles [30]. Astrocytes, responsible for glutamate clearance, express glutamate transporter 1 (GLT-1) for the transport of glutamate from the synapse to enter the glutamate-glutamine cycle, through which glutamate is converted into glutamine to be transported from astrocytes to neurons [31]. Glutamine is then converted back into glutamate to be repackaged into SVs as a neurotransmitter.

Thus, astrocytes contribute to neurotransmission through recycling neurotransmitters and preventing excitotoxicity. The neuronal glutamate transporter excitatory amino acid carrier-1 (EAAC-1) was determined not to contribute to glutamate clearance, but rather to synthesis of GABA [32]. Following antisense knockdown of *Eaac1* in the rat hippocampus, a 50% reduction in GABA synthesis was measured, indicating that EAAC-1 is vital for the synthesis of GABA, for which glutamate is the precursor. Furthermore, the rats displayed seizures, with neuronal hyperexcitability measured in thalamocortical and hippocampal slices [33]. Elevated extracellular glutamate has been described in many types of epilepsy, both chronically when compared to non-epileptic patients [34], and acutely, around the time of seizure events [35]. Microdialysis studies have demonstrated an acute rise in extracellular glutamate immediately following TBI in both humans and rats, postulated to contribute to posttraumatic epileptogenesis [36].

While the specific aetiologies of epilepsies vary widely, including channelopathies, metabolic defects and autoimmune causes, all can disrupt neuronal signalling, evident in the manifestation of seizures. Metabolic defects can cause epilepsy through the accumulation of toxins, or disruption of energy supply to the brain, leading to neuronal injury and disturbance of neural networks [37]. For example, epilepsy-associated mutations are found in *SLC2A1*, which encodes the glucose transporter GLUT1, and is required for transport of glucose across the blood-brain barrier to reach neurons, which are highly metabolically active [38]. Defects in GLUT1 lead to low glucose and low lactate availability to neurons, which results in seizures, although GLUT1 deficiency can be treated effectively

by the ketogenic diet [39]. Autoimmune causes of epilepsy have been described, including autoantibodies against GABA receptors, which reduce the number of GABA receptors found at the synapse, leading to encephalitis with refractory seizures [40].

1.1.3 Anti-Epileptic Drugs

Anti-epileptic drugs (AEDs) are able to successfully treat epilepsy in 60-70% of adult patients [41]. Many AEDs exert effects on neurotransmission that are well understood, by increasing inhibition or reducing excitatory neurotransmission. For example, Benzodiazepines bind to GABA receptors at allosteric sites, leading to potentiation of GABAergic signalling and increasing inhibitory neurotransmission [42]. Many successful AEDs are known to exert multiple mechanisms of action [43]. For example, the first-line AED Valproate is known to block voltage-gated sodium channels, reducing repetitive neuronal firing in cell culture [44], and has also been reported to elevate levels of GABA, suggesting potentiation of inhibitory neurotransmission resulting in an anticonvulsant effect [45]. Similarly, Topiramate exerts a blockade of voltage-gated sodium channels, potentiates GABA activity, and inhibits NMDA receptors to reduce excitatory neurotransmission. Topiramate was also shown to protect mitochondria isolated from rat brain against calcium insult *in vitro*, suggesting inhibition of mitochondrial permeability [46]. However, up to 30% of adult epilepsy patients display drug-resistant epilepsy, in which seizures are not attenuated by AEDs [47]. Unfortunately, despite several hypotheses having been proposed, the mechanism for drug resistance in epilepsy is not yet understood [48]. This lack of understanding highlights the need for further research into drug resistant epilepsies, and for new therapeutic strategies to address them. In particular, understanding of the wide variety of genetic mechanisms of epilepsy may shed light on the mechanisms for drug resistance.

Overall, many of the underlying mechanisms of epileptogenesis are well understood. A variety of biological pathways can disrupt neurotransmission when altered, with many epilepsy-related genes converging on common mechanisms, such as membrane channel

properties and endocytosis. However, treatments for epilepsy remain limited, highlighting the need for pharmacological mechanisms to modulate key pathways. The study of rare genetic disease provides the opportunity to elucidate and target specific pathways that may be applicable across different epileptic syndromes.

1.1.4 Mouse Models of Epilepsy

Mouse models of epilepsy are categorized as either genetic or induced, where genetic models express mutations in genes associated with epilepsy, and induced models are exposed to a stimulus to induce epileptic seizures [49]. Both genetic and induced models must show face validity for comparison with human epilepsy, and thus must exhibit seizures that enable electrophysiological or behavioural quantification [50].

Behavioural measurement, for example through video tracking or human observation, enables the quantification of seizure events that is direct and relatively simple, in comparison to electrophysiological alternatives, not requiring surgical intervention or expensive equipment to perform. Features of seizures, such as pre-ictal hyperactivity, convulsions or myoclonic jerks, may assist recognition of seizures; identification of seizures is aided by the Racine scale, which was developed to quantify epilepsy severity [51]. However, seizures can be difficult to observe and record, especially if they occur infrequently, or during sleep [52]. Electrophysiological methods, such as electroencephalogram (EEG) recording, provide high resolution quantification of seizure dynamics [53]. EEG methods are highly sensitive, and are able to distinguish seizures based on electrical activity, rather than physical manifestations. However, EEG can be invasive, requiring surgical intervention to implant electrodes into the skull [54]. This method is therefore unsuitable for very young mice, or mouse models showing early postnatal lethality. Both behavioural and electrophysiological methods can be useful for the quantification of seizures in mouse models of epilepsy, with individual experimental requirements taken into account.

Induced mouse models of epilepsy involve the chemical, electrical or auditory induction of seizures in wild type mice. Induction of seizures can be acute or chronic, where the latter

provides a more realistic clinical model of epilepsy. For example, the kindling model uses multiple seizure-generating insults over time, such as electrical stimulation or pentylenetetrazole injection, to generate a model that displays spontaneous seizures [55]. The exitotoxic glutamate agonist kainate is used to generate mouse models which recapitulate many of the features of human mesial temporal lobe epilepsy (MTLE), including spontaneous seizures [56]. This particular model shows a level of pharmacoresistance, which is especially useful in testing of novel anti-epileptic drugs (AEDs) [57]. The reliable generation of epileptic seizures by these methods necessitates predictable seizures, which are easier to study than in most genetic models, where seizures may be infrequent or difficult to detect [49]. However, induced mouse models do not recapitulate the physiological causes of epilepsy in humans, therefore their suitability for use in studies of human epileptogenesis is limited [58].

Genetic mouse models of epilepsy express mutations associated with epilepsy in humans [59]. The mouse is a useful model organism for the genetic study of neurological disease, both due to the high level of homology between human and mouse genomes [60], and the general conservation of spatial patterning of gene expression between the brains of the two organisms [61]. A key advantage of genetic mouse models of epilepsy is that they are hypothesis driven. Thus, they allow specific study of the molecular mechanisms involved in epilepsy, enabling the production of therapies targeted to the precise aetiology of different epileptic syndromes. For example, certain missense mutations in *Scn8a*, encoding the neuronal sodium channel $Na_v1.6$, have been shown to cause epileptic encephalopathy in humans, and cause seizures when modelled in mice. The mutations were shown to be gain-of-function, leading to neuronal hyperexcitability and impaired inactivation of $Na_v1.6$. Treatment with a sodium channel modulator, GS967, was found to reduce seizure frequency by more than half in mice, and the drug is now in clinical trials for use as an AED in humans [62].

Genetic mouse models have helped to elucidate the wide range of molecular pathways that can lead to epilepsy when disrupted. The gene SV2A, encoding a synaptic vesicle protein, was shown to be mutated in epilepsy. Knockout of *Sv2a* in mice resulted in seizures and early lethality [63]. It was demonstrated in mouse primary neuronal culture that the epilepsy mutation R383Q in Sv2a prevents binding to Synaptotagmin-1, a protein necessary for neurotransmitter release following calcium influx, indicating that the mutation is loss-of-function and disrupts synaptic vesicle trafficking required for neurotransmitter release [64]. Disruption in glycogen metabolism has been linked to epilepsy, through mouse models of Lafora disease (LD), caused by mutations in the gene *EPM2A*, which encodes the phosphatase laforin, required for glycogen metabolism. A null mutant mouse model of *Epm2a* showed seizures and progressive ataxia, as observed in LD. Neuropathological analysis showed 'Lafora bodies', also reported in humans, which were found to contain end products of glycation, and neurodegeneration in hippocampal, cerebellar and cortical neurons, demonstrating that disruption of glycogen metabolism in LD causes neuronal death and seizures [65].

The recapitulation of genetic mechanisms by genetic mouse models is increasingly essential for development of effective AEDs, to be able to precisely target affected pathways in epilepsy [49].

1.1.5 Oxidative Stress and Epilepsy

The brain is a highly energetically active organ, especially due to the high ATP demand of synaptic transmission [66]. This high demand for energy corresponds with the need for the brain to have an abundant supply of oxygen; indeed, the human brain at rest uses over 20% of the oxygen available to the body [67]. The highly oxygenated environment of the brain facilitates aerobic metabolism, leading to the generation of reactive oxygen species (ROS) as a by-product. ROS exist in a balance in the brain to regulate such processes as redox signalling, bacterial phagocytosis, and even neurotransmission in the case of nitric oxide signalling [68]. However, disturbing this balance can lead to oxidative stress (OS) resulting in damage to DNA, proteins and lipids; if left unmanaged it can ultimately lead to

cell death [69]. Furthermore, glutamate signalling increases OS, demonstrated in neuronal cell lines which show increased ROS production, depletion of antioxidants and cell death in response to high concentrations of glutamate [70].

Signs of OS are present in epilepsy, demonstrated both in patients and animal models. In patients with severe motor and intellectual disabilities (SMID), a strong correlation was observed between epileptic seizure frequency and the degree of oxidation, as indicated by level of free radicals in the blood [71]. Markers of OS, including the antioxidant glutathione (GSH), were found to be elevated following seizures in a kainate model of epilepsy in rats, and protein and lipid oxidation were shown to be increased 24 hours after seizures [72]. OS is associated with neuronal apoptosis in epilepsy, and ROS have been shown to increase cell death following excitotoxic injury in cortical culture [73]. Lower antioxidant levels have been reported in blood plasma of patients with generalized epilepsy, indicating a relationship between seizure induction and OS [74].

Endogenous antioxidant systems, which are broadly classified as either enzymatic or non-enzymatic, usually maintain a healthy OS balance, by preventing production of ROS or by removing ROS when they occur. These endogenous mechanisms show potential as therapeutic targets to enhance neuroprotection, and ameliorate the deadly effects of OS in neurological disease [75].

Enzymatic antioxidant defence involves a neutralising chain of enzymes capable of reducing free radicals through electron scavenging, to prevent harmful build-up of ROS. The first of these enzymes, Superoxide Dismutase (SOD), contains either manganese, copper or zinc depending on cellular/extracellular location; these transition metals are capable of altering valence state to transfer electrons [76]. Following free radical formation, for example through mitochondrial respiration, SOD catalyses the superoxide anion, $O_2^{\cdot-}$, into hydrogen peroxide, (H_2O_2) which is then scavenged and converted into water and oxygen by either Catalase or Glutathione Peroxidase (GPx).

Non-enzymatic antioxidants are electron-scavenging molecules, which are usually soluble and are able to traverse the body through the circulatory system, for example, ascorbate (Vitamin C) and albumin. Vitamin C works both as a scavenger of ROS, and in conjunction with lipid-soluble tocopherols (Vitamin E) across liposomal membranes to reduce lipid hydroperoxyl radicals produced following ROS-scavenging by vitamin E [77]. Metal chelation also plays a key role in preventing the formation of ROS. While the property of redox-active metals such as iron ($Fe^{2+/3+}$) and copper ($Cu^{+/2+}$) to change their oxidation state enables their antioxidant capability, this same property enables unregulated circulating metal ions to cause dangerous chain reactions producing free radicals. Many circulating antioxidants, including albumin [78], have metal-chelating properties, and specific metal homeostasis molecules are also able to chelate metal ions, such as iron regulatory proteins (IRPs), which are able to target iron for storage by Ferritin or metabolism through the tricarboxylic acid (TCA) cycle [79].

OS induces a transcription factor cascade involving upregulation of antioxidant genes due to activation of the antioxidant response element (ARE) within their promoter regions [80]. ARE activation and expression is regulated by two genes of the Cap-N-Collar (CNC) gene family: Nrf1 and Nrf2. The genes differ in their expression patterns, as Nrf1 operates at a basal level to activate expression of genes involved in biosynthesis of GSH, whereas Nrf2 is inducible as part of the transcription factor cascade [81]. In a mouse double knockout study it was shown that knockout of both genes results in embryonic lethality and severe oxidative stress, indicating functional overlap between Nrf1 and Nrf2 [82]. Activation of ARE activity by Nrf2 causes induction of expression of hundreds of genes with antioxidant fuction, including GSH- and NADPH-dependent enzymes, metal chelating proteins including ferritin, and the heme-catabolizing enzyme heme oxygenase 1 [83]. Regulation of Nrf2 is controlled by Keap1, an adaptor protein bound to the cytoskeleton which promotes ubiquitylation of Nrf2 in the absence of OS, but is inhibited by OS, removing the degradation of Nrf2 and promoting activation of the ARE-mediated antioxidant cascade [84].

Antioxidant protection against epileptic syndromes is emerging as a relatively new field. The use of antioxidants therapeutically to enhance neuroprotection in epilepsy has had limited effect for a number of reasons; many therapies only target one source of OS, and some antioxidants are location-specific. For example, although GSH acts as a crucial antioxidant molecule in the cortex, neuroprotection against OS in the hippocampus is dependent on SOD, therefore enhancing GSH levels would have little to no effect on epilepsies originating from the hippocampus [72]. Antioxidant strategies have seen more success when used as add-on therapies, for instance, the supplementation of AEDs with Vitamin E has been shown to significantly reduce both seizure frequency and OS marker expression in epileptic patients [85]. As low plasma antioxidant levels are commonly reported in epileptic patients even when successfully treated with AEDs [74], additional antioxidant treatment could reduce seizure-induced OS and neuronal injury.

Overall, antioxidant strategies for treating neurological disorders such as epilepsy show great promise, especially in combination with existing anti-seizure drugs, or when a wide range of antioxidant molecules are deployed, such as in dietary interventions. In fact, protection against OS and resultant neuronal injury may be crucial for the long term success of current AEDs.

1.2 The TLDc Family

1.2.1 Background of the TLDc Family

The discovery of the TLDc family began with the identification of the gene oxidation resistance 1 (*OXR1*) in a functional genomics screen which aimed to identify factors that could be protective against oxidative DNA damage [86]. *Escherichia coli* were transformed with a human cDNA library, and exposed to peroxidase treatment to induce OS [87]. Transformation with *OXR1* caused a 5-fold reduction in oxidative mutagenesis, suggesting a protective function for the gene. In *Saccharomyces cerevisiae*, deletion of the *OXR1* homologue led to a reduction in cell survival when treated with H_2O_2, indicating increased sensitivity to OS in the absence of the gene [87]. OXR1 was found to contain a conserved domain named the Tre2/Bub2/Cdc16 (TBC), lysin motif (LysM), domain catalytic (TLDc)

domain, which was predicted to exert the protective function of the gene [88]. This prediction was supported by findings that a gene with 53% identity similarity to *OXR1* including expression of the TLDc domain, nuclear receptor coactivator 7 (*NCOA7*), was similarly able to supress oxidative mutagenesis when expressed in *E. coli* [89]. The TLDc domain itself is a conserved motif of approximately 200 amino acids, found at the C-terminus of all OXR1 isoforms [90]. While the TLDc domain of zebrafish OXR2 was crystallized in 2011, the solved structure had no similarity to any known proteins [91]; therefore no clues as to the molecular function could be predicted from these data. A further three proteins contain the TLDc domain in mammals: TBC domain family member 24 (TBC1D24), MTOR associated protein, eak-7 homolog (MEAK7, also referred to as KIAA1609 and TLDC1), and chromosome 20 open reading frame 118 (C20ORF118, also referred to as TLDC2) [92]. Together, these proteins comprise the TLDc family (**Figure 1.1**).

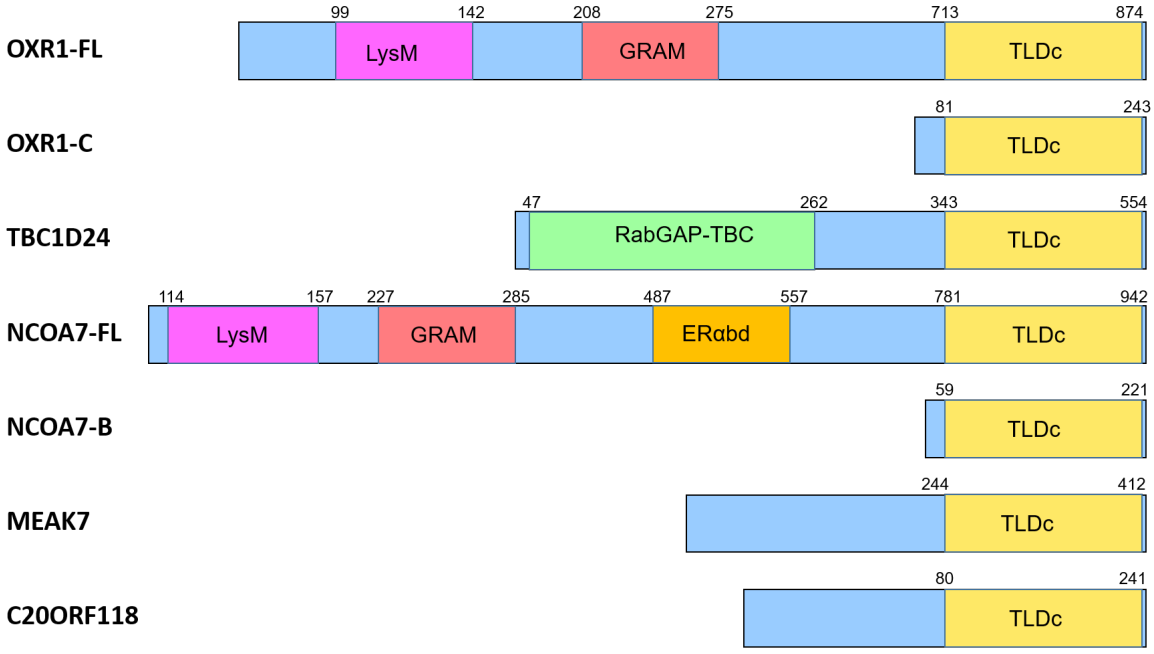


Figure 1.1 Schematic showing the TLDc protein family. *Domains marked as TLDc: Tre2/Bub2/Cdc16 (TBC), Lysin Motif (LysM), Domain Catalytic; LysM: lysin motif; GRAM: GRAM domain; ERαbd: estrogen receptor α binding domain; RabGAP: GTPase activating protein. Protein domain positions obtained from UniProt.org.*

TLDc family members show distinct tissue expression patterns when measure by *in situ* hybridization (ISH) in the mouse. *Tbc1d24*, *Oxr1* and *Ncoa7* are all highly expressed in the

central nervous system [92]. Expression of the TLDc family members has been demonstrated to protect against OS *in vitro*; cell death of a neuronal culture exposed to arsenite treatment was reduced following transfection with TLDc family constructs [92]. The largest isoform of *Ncoa7* and the shortest isoform of *Oxr1* were both found to be inducible under arsenite treatment, while other TLDc family members were not, suggesting a specific inducible role for the two genes under conditions of OS [92]. Accordingly, the different members are predicted to perform additional independent roles due to differing cellular localisation and structural differences. For instance, TBC1D24 also contains a Tre2/Bub2/Cdc16 (TBC) domain which is usually associated with roles in vesicular trafficking through interactions with Rab-GTPases [93]. Although enzymatic function was predicted initially based on sequence analysis of the TLDc domain, it appears not to possess any catalytic or scavenging activity to explain its protective function against OS [90].

1.2.2 TBC1D24 in Disease

Given the vital protective role played by the TLDc family, it follows that disruption of the function of TLDc proteins can produce severe consequences. In particular, *TBC1D24* is associated with a broad spectrum of neurological disorders, especially epilepsies, often accompanied by intellectual disability [94, 95, 96, 97, 98].*TBC1D24* is highly expressed in the brain, with a broad expression pattern spanning all layers of the cerebral cortex and the hippocampus [99]. More diverse phenotypes, including sensorineural hearing loss and DOORS (deafness, onchyodystrophy, osteodystrophy and intellectual disability) syndrome, the latter involving skeletal defects, are also associated with mutations in *TBC1D24* [100, 101]. Exome sequencing has shown that mutations in *TBC1D24* account for 0.5-1% of inherited epilepsies [101]. Mutations in *TBC1D24* are also associated with comparatively mild disease phenotypes, including recessive hearing loss, highlighting the wide spectrum of disease associated with *TBC1D24* mutation [102, 103].

TBC1D24 encodes a protein 553 amino acids in length, containing the TLDc domain and an additional TBC domain, found in Rab GTPase-activating proteins (RabGAPs) which

mediate membrane trafficking, although sequence analysis determined that TBC1D24 lacks the arginine finger necessary for RabGAP activity. However, TBC1D24 was shown to instead interact with ADP ribosylation factor 6 (ARF6), which is part of a family of GTPases that regulates exocytosis and endocytosis [99]. Initial indication for the involvement of *TBC1D24* in epilepsy came from genome mapping of a consanguineous family from which three patients experienced recessive, early onset myoclonic epilepsy. The causative gene was mapped to the p terminus of chromosome 16, 16p13.3 [104]. Later, a different consanguineous family was identified whose members displayed recessive focal epilepsy with intellectual disability, with the disease-causing mutation mapped to the same chromosomal region, 16p13.3. Target sequence enrichment was used to interrogate this region, which determined that the disease-causing mutation was in *TBC1D24* [105].

A study of mutations in *TBC1D24* associated with epilepsy included patients experiencing a diverse range of seizure types, including febrile convulsive, tonic and absence, with myoclonic or clonic seizures representing 60% of seizure types. No correlation was determined between location, or type, of mutations and disease phenotype of *TBC1D24*-associated syndromes [106]. However, correlation was reported between disease severity, including mortality, and predicted loss of function mutations, such as frameshift, nonsense or splice-site, as opposed to missense mutations, which were only associated with death when occurring in or before the TBC domain [106]. The majority of TBC1D24-related disorders display autosomal recessive inheritance [100]. Studies of the molecular function of TBC1D24, particularly using mouse models, are further detailed in Chapter Three.

The *Drosophila melanogaster* orthologue of TBC1D24, known as skywalker (sky), has provided useful insight into the structure and function of the protein. *Sky* was shown to be expressed at synapses and neuromuscular junctions (NMJs) in *Drosophila*. Fluorescent labelling of newly endocytosed SV membranes using a *sky* loss-of-function mutant showed SV trafficking defects, indicated by cisternal-like structures at the synaptic bouton.

Furthermore, the amplitude of excitatory currents was shown to be increased, suggesting a greater release of neurotransmitter at the *sky* mutant synapses [107]. Total loss of *sky* was determined to be lethal, but *Drosophila* homozygous for deletion of *sky* in the eyes alone survived. Electroretinogram (ERG) of the *sky* mutant eyes showed smaller transients, indicating desynchronous neuronal activity similar to that observed during seizures [108]. Solving of the crystal structure of the skywalker TBC domain revealed a cationic pocket, which was determined by sequence analysis to be conserved across TBC1D24 homologues [109]. The positive charge of the pocket enables direct binding to phosphoinositides present on liposome membranes, allowing TBC1D24 to associate with liposomes. Interestingly, DOORS-causing mutations map to residues within this binding pocket, and pathogenic mutations associated with epilepsy in humans prevented binding of sky with liposomes, and led to defective SV trafficking measured by fluorescent imaging [109]. Together, these data provide strong evidence for a role for sky, and in particular its TBC domain, in regulating SV trafficking and synaptic signalling. However, the molecular mechanism of this regulation is yet to be determined.

Further research is required to uncover the molecular mechanisms of TBC1D24 function in the mammalian CNS, and how disruption of these mechanisms might lead to epilepsy and other serious neurological disorders. Importantly, human pathogenic mutations are found in both the TBC and TLDc domains of TBC1D24. While useful insights into the function of the TBC domain have been provided from studies in *Drosophila*, the function of the highly conserved TLDc domain and its implications for protection against OS are yet to be fully ascertained.

1.2.3 OXR1 in Disease

Following the original discovery of *OXR1*, it was found that the gene is highly conserved throughout evolution, and appears to protect against OS throughout eukaryotes, from *Drosophila* [110], to mice [111], to humans [112]. This conservation has enabled effective study in genetic mouse models. The importance of *OXR1* to brain function was revealed in the homozygous *bella* mouse mutant. This mouse contained a spontaneous deletion

removing the entire coding region of the *Oxr1* gene, causing progressive ataxia and death between P24 and P26 [113]. From P19, progressive levels of apoptotic cell death are observed in the cerebellar granule cell layer, although no other brain regions appear to be affected at end-stage. In addition, markers of OS were found in the cerebellum of bella mice at P24. In humans, bi-allelic loss-of-function mutations in *OXR1* have been shown to cause severe developmental delay, intellectual disability, cerebellar atrophy and seizures [114]. Therefore, reduction in expression of OXR1 results in severe neurological and developmental phenotypes involving cerebellar cell death, which can be modelled in mice.

It is of note that overlapping disease phenotypes are observed as a result of loss-of-function in OXR1 and TBC1D24, including epileptic syndromes, often with developmental delay [115, 114, 94, 106, 100]. This may indicate overlapping functions due to the shared TLDc domain, and suggests the potential for compensatory mechanisms between TLDc family members.

Interestingly, mice homozygous for a construct that disrupts only the longest Oxr1 isoform (Oxr1-FL) do not show any neurodegeneration [116], revealing that presence of the remaining short isoform of the gene (Oxr1-C) is sufficient to prevent cell death. In humans, a heterozygous mutation disrupting expression of *OXR1-C* causes specific language impairment (SLI), indicating the developmental disruption caused by haploinsufficiency of this isoform alone [117].

Studies of the localization of *OXR1* in mice have shown that it is expressed in all major structures of the brain, but especially in the cortex, cerebellum and hippocampus [92]. Interestingly, *OXR1* expression is particularly enriched in neurons in the hippocampal CA3 subfield, which have been shown to be comparatively more resistant to OS than neurons of the cerebellar granule layer and of other hippocampal regions [118]. *OXR1* was found to be upregulated during the OS response in cells, and is accordingly induced in *Saccharomyces cerevisiae* by both heat and peroxide treatment [112]. *OXR1* is depleted in neurodegenerative diseases including Parkinson's disease (PD); microRNA targeting

OXR1, miR-137, was found to circulate in serum of PD patients [119]. Furthermore, depletion of *OXR1* by inhibitory RNA (RNAi) *in vitro* was found to increase levels of ROS, which led to cellular and mitochondrial damage and ultimately, cell death [120].

Due to the important role of *OXR1* in neuronal protection against OS it has been postulated that its overexpression could be restorative if applied to neurodegenerative diseases involving OS [86]. Overexpression of *OXR1* has been demonstrated to be neuroprotective both *in vitro* [121] and *in vivo* [122], in models of ALS-associated pathology (see Chapter Five for further description of neuroprotective strategies involving the overexpression of *OXR1*). These data suggest that there is promise of potential future treatments involving upregulation of *OXR1*, although the therapeutic potential of *OXR1* has not been thoroughly investigated.

1.3 Research Aims and Objectives

TLDc proteins are increasingly being implicated in a range of serious neurological disorders, yet there is still much to learn regarding their molecular function and why loss-of-function mutations cause certain specific clinical phenotypes and pathologies. In addition, several lines of study have demonstrated the protective activity of TLDc over-expression, but whether this could be harnessed therapeutically warrants further investigation. The aim of this thesis is to address these two questions, combining new mouse genetic models with a range of molecular and cellular techniques, in order to gain further understanding of the TLDc family, and elucidate the family's therapeutic potential in protecting against OS and neurodegeneration. The specific objectives of each chapter are listed below.

The first results chapter will determine the effects of epilepsy-associated TBC1D24 *in vivo*, in order to further current understanding of the aetiology of epilepsy in patients.

- Molecular characterisation and behavioural phenotyping of mouse knock-in mutants representing pathogenic TBC1D24 mutations.

The second results chapter will investigate the aetiology of the anaemic phenotype of TBC1D24 dysfunction, and to elucidate the role of Tbc1d24 in the haematological system.

- Transcriptomic analysis and haematological studies of mouse models of *TBC1D24* dysfunction.

The third results chapter will investigate neuroprotection by up-regulation of *OXR1*, both *in vitro* and *in vivo*.

- Develop and validate a dual luciferase reporter-based cell assay to screen for compounds that increase OXR1 expression *in vitro*. Validate lead compounds for further testing *in vitro*.
- Use an *in vivo* model of genetic overexpression of *OXR1* to investigate functional compensation between *OXR1* and *TBC1D24* in a mouse model of Tbc1d24 dysfunction.

Chapter 2: Materials and Methods

2.1 Ethics Statement

All experiments were conducted in adherence to UK Home Office regulations and guidelines.

2.2 Animals, husbandry and housing

Mouse lines were housed in the Mary Lyon Centre (MLC), at the MRC Harwell Institute. All lines were created or maintained on a C57BL/6J background. The day of birth was designated as P0. Mice received food and water *ad libitum*, and are housed in individually ventilated cages (IVCs) on a 12 hour on/off light cycle, 06:00 – 18:00.

2.2.1 Generation of CRISPR/Cas9 mouse lines

Three of the mouse models described in this thesis were generated using CRISPR/Cas9 technology by the MRC Harwell CRISPR group (Teboul, L.) [123]. Single guide RNA (sgRNA) sequences were designed around the regions within *Tbc1d24* containing the intended site to be altered. The web tool http://tefor.net/crispor/crispor.cgi [124] was used for design. Donor oligonucleotides (oligos) were designed with homology arms 60 nucleotides in length flanking the site of the intended mutation.

To generate each founder line, Cas9 and the sgRNA and donor oligo, suspended in microinjection buffer (10 mM Tris-HCl, 100 mM NaCl, 0.1mM EDTA, pH 7.5), were introduced into mouse embryos at the 1 cell stage by pronuclear microinjection. Embryos were implanted into pseudo-pregnant female hosts, which then littered the F1 progeny. Ear clips of F1 progeny were taken, and ddPCR copy counting experiments were performed to ensure that no additional insertions of the donor oligo had been made.

2.2.1.1 Tbc1d24^{R360L}

The R360L point mutation in *Tbc1d24* was introduced together with a silent mutation to prevent reprocessing of the engineered allele.

2.2.1.2 Tbc1d24^{P135L}

The P135L point mutation in *Tbc1d24* was introduced together with two silent mutations to prevent reprocessing of the engineered allele.

2.2.1.3 Tbc1d24^{INS2}

The null mouse model of Tbc1d24 expression was generated during the production of the *Tbc1d24^{P135L}* mouse line by the MRC Harwell CRISPR group (Teboul, L.). Sequencing of one of the founder (F0) lines revealed a 2 nucleotide insertion that was predicted to introduce a frameshift, leading to an early stop codon within exon 3, after position 135 in the translated protein product.

2.2.1.4 Tg(mPrnp-Oxr1)

Mice expressing a full-length isoform of Oxr1 (Oxr1-FL) driven by a prion promoter [125] were imported from DPAG, Oxford, and rederived from sperm at the MLC, Harwell. Hemizygous mice were intercrossed with both the *Tbc1d24^{R360L}* and *Tbc1d24^{INS2}* lines.

2.2.2 Genotyping

Genotyping was performed in house, by the author herself and with assistance from the MRC Harwell GEMS core group. For genotyping performed using a gel-based assay, this consisted of RedTaq ReadyMix PCR Reaction Mix (Sigma) (15 µl), primers (**Table 2.1**) (0.5 µl of 5 pmol stock), genomic DNA (1 µl) and water (13.5 µl). Following PCR, DNA purification was performed using the QIAquick PCR purification kit (Qiagen) followed by enzyme digest (Table 1) and gel electrophoresis of the digested product, Sanger sequencing or presence/absence of the PCR product. As below, the mutant sequence contained the additional restriction enzyme site versus the wild-type sequence.

Table 2.1 Genotyping Primers

Mouse line	**Primer sequence (5'-3')**	**Enzyme**
Tbc1d24^{R360L}	F: TGAGACGCACTTTCTAGGCTG R: AGGACGAGGCATGACTTACG	SacI
Tbc1d24^{P135L}	F: TCTCTGGGACCCACATAGGG R: CACAGTGTGGAAAAGCTGGC	Sequencing required
Tbc1d24^{INS2}	F: GGAAAGTGTACCAGCGCCT R: CATCGCTGCCAGTCAGAGTAG	BstXII
Tg(mPrnp-Oxr1)	F: GCCATTCCTGTAAAACGTTTG R: GCGTAATCTGGAACATCGTATG	N/A

2.2.3 Behavioural Phenotyping

2.2.3.1 Home cage video tracking

Mouse litters were housed in home cages placed into Home Cage Analyzer (HCA) units, which each contain a high-definition infrared video camera directed at the side of the IVC, enabling observation of behaviour and seizure pathology [126]. 12 hour on/off light cycling was maintained. Food and water was available *ad libitum*. Mice were recorded for 5 – 8 days. Videos were manually analysed using Simple Video Coder [127], with 2 hours of footage scored per day, selecting the time slot during which mice displayed the highest activity level (between 19:00 – 21:00).

2.2.3.2 Open Field

Four arenas (44 x 44cm) in an enclosed room were used for open field testing, with overhead video camera and adjustable lighting set at 150-200 lux. Mice were separated by sex, and individually placed into arenas with a minimum of two mice tested at a time. Ethovision video tracking software was used to record mouse movements over a period of 20 minutes. Arenas were divided into periphery, centre, and intermediate zones.

2.3 Histopathology

2.3.1 Tissue collection

Mice were euthanized by cervical dislocation at P16, and tissue (brain, liver or spleen) dissected.

For embryo collection at E15.5 and E18.5, pregnant female mice were euthanized by cervical dislocation, and embryos removed into chilled PBS. Decapitation of embryos was performed to confirm death, and embryo tissue (brain or liver) dissected.

For perfused tissue collection, mice were euthanized by anaesthetic overdose, followed by transcardial perfusion with either PBS alone or with PBS followed by 4% PFA in PBS. Perfusions were performed with assistance from the MRC Harwell Necropsy group.

2.3.2 Immunohistochemistry

Immunohistochemistry (IHC) was performed using embryonic brains fixed in 4% paraformaldehyde for 2 days, and embedded in wax then sectioned at 10 μm before mounting on bonding slides. Slides were dried for 1 hour at 37°C, followed by dewaxing by xylene and alcohol washes. Antigen retrieval was performed by boiling slides in 0.2% tri-sodium citrate buffer at pH 6. Blocking was performed using blocking solution (5% NGS in PBS with 0.1% triton X-100) placed on slides for 1 hour at room temperature. Antibodies (**Table 2.2**) were diluted in blocking solution and placed onto slides at 4°C overnight. Slides were washed in PBS with 0.05% triton X-100. Secondary antibodies were diluted in blocking solution and placed onto slides for 2 hours at room temperature, in the dark. Slides were washed in PBS with 0.05% triton X-100 before mounting using ProLong Gold Antifade mountant (Invitrogen).

Table 2.2 Antibodies used for Immunohistochemistry

Antibody	**Host species**	**Concentration**	**Product code**
Satb2	Mouse	1:200	Abcam ab51502
Ctip2	Rat	1:400	Abcam ab18465
Tbr1	Rabbit	1:400	Sigma AB10554
NeuN	Mouse	1:200	Sigma/Millipore MAB377
Anti-Rat IgG H&L Alexa Fluor 594	Goat	1:1000	Abcam ab150160
Anti-Mouse IgG H&L Alexa Fluor 594	Goat	1:1000	Invitrogen A-11032
Anti-Rabbit IgG H&L Alexa Fluor 594	Goat	1:1000	Invitrogen A-11012

2.3.3 Nissl staining

Brains were collected and mounted in OCT on dry ice for sagittal sectioning by cryostat and collection onto positively charged slides. Slides were subsequently fixed in 4% paraformaldehyde. Nissl staining was performed on slides following de-fat step by a 1:1 mix of chloroform and alcohol, and rehydration in decreasing concentrations of alcohol. Slides were immersed in Cresyl Violet solution for 5-10 minutes, followed by rinsing in water and dehydration by increasing concentrations of alcohol, and finally xylene, before mounting using DPX mountant (Sigma-Aldrich).

2.3.4 DAB-enhanced Perls stain

Spleens were collected and fixed in 4% paraformaldehyde for 2 days, and embedded in wax for sectioning at 14 µm and mounting on poly-L-lysine slides. Slides were dried at 37°C overnight, then dewaxed using xylene and rehydrated in decreasing concentrations of alcohol. The Prussian Blue staining kit (Abcam) was used according to manufacturer's instructions: briefly, slides were incubated in a 1:1 mix of potassium ferrocyanide and hydrochloric acid solutions for 15 minutes at room temperature, then washed and incubated in DAB solution (20 mg 3,3′-Diaminobenzidine, 4 µl 30% hydrogen peroxide in 40ml PBS)

for 15 minutes at room temperature. Slides were washed in PBS and dehydrated using increasing concentrations of alcohol, and finally xylene, before mounting using DPX mountant (Sigma-Aldrich).

2.4 Protein analysis

2.4.1 Protein extraction

Tissue was mechanically homogenized using bead homogenizer tubes, immersed in RIPA buffer (25mM Tris, 150mM NaCl, 0.1% SDS, 0.5% sodium deoxycholate, 1% Triton X-100) with cocktail protease (cOmplete Protease inhibitor cocktail, Roche) and phosphatase (PhosSTOP, Roche) inhibitors, 1 tablet per 10 ml, shaken at 5,500 rpm for 30 sec using the Fast Prep FP120 instrument. Homogenate was then centrifuged for 10 minutes at 14000 x g, 4 °C, and supernatant transferred to an Eppendorf tube on ice. Protein concentration was quantified using DC Assay (BioRad), using bovine serum albumin (BSA) standards (New England BioLabs) to produce a standard curve ranging between concentrations of 0.0625 – 1.4 mg/ml. Absorbance was measured at 750 nm using Epoch microplate spectrophotometer (BioTek).

2.4.2 Western blotting

Western blotting was performed on 4-12% NuPAGE Bis-Tris mini gels (ThermoFisher). Samples were loaded with NuPAGE LDS Sample Buffer 4x and NuPAGE Sample Reducing Agent (ThermoFisher) following denaturation at 90°C for 5 min. Electrophoresis was performed using MOPS SDS Running Buffer (ThermoFisher) at 200V for 45-60 minutes. Membrane transfer was performed using iBlot transfer system (ThermoFisher). Membranes were blocked in 10ml 4% skimmed milk (4g skimmed milk powder (Sigma-Aldrich), 100ml PBST) for 1-2 hrs before incubation with primary antibodies either overnight at 4°C or for 2 hrs at room temperature (**Table 2.3**). Membranes were washed three times in PBST, then incubated in the dark with secondary antibodies, at room temperature for 1-2 hrs (see Table X for all antibody host animals and dilutions). Membranes were washed again twice in PBST and once in PBS, before they were left in the dark at room temperature until dry and

scanned using an Odyssey CLx scanner (Licor). Image Studio software (Licor) was used to obtain raw data for western blot quantification.

2.4.3 Co-immunoprecipitation

Co-immunoprecipitation was performed by ProteinCore, MRC Harwell (Hopestone, S.) using the Pierce Crosslink IP kit (ThermoFisher) according to manufacturer instructions, using a protein:antibody ratio of 1 mg:4 µg.

2.4.4 Table of antibodies

Table 2.3 Antibodies used for Western blotting

Antibody	**Host species**	**Concentration**	**Product code**
Tbc1d24	Rabbit	1:500	NovusBio NBP1-82925
Oxr1	Rabbit	1:1000	Proteintech 13514-1-AP
Atp6v1b2	Rabbit	1:1000	Abcam ab73404
Atp6v1a	Rabbit	1:1000	Proteintech 17115-1-AP
Atp6v1c	Rabbit	1:1000	Proteintech 16054-1-AP
Atp6v0d	Mouse	1:1000	Abnova H00009114-M02
B-Actin	Mouse	1:10,000	CST 3700S
Anti-Rabbit IgG (H+L) 800CW	Goat	1:10,000	Licor 926-32211
Anti-Mouse IgG(H+L) 680RD	Goat	1:10,000	Licor 926-68070

2.5 RNA Analysis

2.5.1 RNA extraction of large tissue

Larger tissue (whole brain, liver) was mechanically homogenized using bead homogenizer tubes, immersed in QIAzol lysis reagent (Qiagen) shaken at 6,500 rpm for 30 sec using the Fast Prep FP120 instrument. Total RNA was purified using RNeasy lipid tissue mini kit spin

columns (Qiagen) and eluted into RNase-free water. Samples were treated with endonuclease DNase I (ThermoFisher) to digest single and double stranded DNA.

2.5.2 RNA extraction of small tissue

Smaller tissue (embryonic brain, subdissected brain structures) was processed using the Maxwell RSC extraction system (Promega). Tissue was mechanically homogenized using bead homogenizer tubes, immersed in homogenization solution (20 µl thioglycerol per 1 ml homogenization buffer), shaken at 6,500 rpm for 30 sec using the Fast Prep FP120 instrument. Total RNA was purified using the Maxwell cartridge system (Promega), which includes an endonuclease step to digest single and double stranded DNA.

2.5.3 Synthesis of cDNA

Concentration and purity of RNA was assessed by spectrophotometry (Nanodrop) and RNA integrity was assessed using a Bioanalyzer (Agilent). RevertAid H Minus Reverse Transcriptase (ThermoFisher) was used for cDNA synthesis with 1.5µg RNA.

2.5.4 RT-qPCR

RT-qPCR was performed in 96 well plates using ABI 7500 fast qPCR system (Applied BioSystems), with a total volume of 10µl per well (5µl fast SYBR green master mix (ThermoFisher), 0.2µl F&R primers at 18µM, 4.8µl diluted cDNA at 10 ng per well). See **Table 2.4** for primers. The following cycles were used: 1 cycle (20 sec at 95°C), 40 cycles (3 sec at 95°C, 30 sec at 60°C), followed by dissociation curve step. Individual gene cycle threshold (Ct) values obtained from qPCR were normalised to Ct values for S16 obtained on the same day, under the same conditions.

2.5.5 Allele-specific RT-qPCR assay

Allele-specific RT-qPCR was performed by GEMS (Williams, D.) using a previously described method [128]. Probes were specifically designed against mutant alleles *Tbc1d24*^{R360L} and *Tbc1d24*^{P135L}, and RT-qPCR was performed as above (2.5.4).

2.5.6 *In situ* hybridization

Brains were collected and mounted in OCT on dry ice for storage at -80°C prior to sectioning by cryostat at 15 µm and mounting onto slides. *In situ* hybridisation (ISH) was performed under RNAse free conditions, using baked glassware and DEPC-treated and autoclaved water. RNAse-Zap (Sigma Aldrich) was used to regularly clean surfaces. Slides were acetylized by being placed into 0.1M triethanolamine hydrochloride solution and acetic anhydride was added dropwise. Slides were incubated for 10 minutes, then washed. Slides were incubated in hybridization solution (50% formamide, 200 µg/ml E. coli tRNA, 1× Denhardt's solution, 0.25% SDS,10% dextran sulfate, 10 mM Tris at pH 7.6, 600 mM NaCl, 1 mM EDTA) for 1 hour at room temperature. Slides were then incubated in hybridization solution containing the DIG-labelled probe overnight at 65°C. Slides were then washed in a solution containing 30 mM NaCl and 3 mM sodium citrate. Slides were detected using DIG RNA labelling kit (Roche) according to manufacturer's instructions: briefly, slides were incubated in blocking solution for 1 hour at room temperature, then incubated in blocking solution containing anti-DIG antibody at 1:5000 overnight at 4°C. Slides were then washed and incubated in buffers supplied by kit, before slides were incubated in detection solution in the dark at room temperature, and checked until staining was complete (12-24 hours). Slides were then washed and mounted in Aquamount (Sigma-Aldrich).

2.5.7 Table of RT-qPCR primers

All primers were designed to span two or more exons ensuring specific amplification of cDNA.

Table 2.4 Primers used in RT-qPCR

Target	**Forward (5'-3')**	**Reverse (5'-3')**
Tbc1d24	GGAGATGAGAGACATTTGGTCC	GCTTGCCTCCGAATTTAGTC
Oxr1-C	CCATAAATACACTCTGGTAGTGTCG	TTTGGTCGGAAAGATTCAGG
Alas2	CACCAGCGCAATGTCAAACA	CGAGGCACAGTTGGGTAGTT

Hbb-bt	TGATGCTGAGAAGGCTGCTG	AAAGGTGCCCTTGAGGCTGT
Hba-a2	CAGGTCAAGGGTCACGGCAA	GGTGAAATCGGCAGGGTGGT
Cntn3	TTGGAATGCTTCGCCCTGGG	CCGCCCTCTCGCCACATTTT
C-fos	GAGAAACGGAGAATCCGAA	TGGGCTGCCAAAATAAACTC
Epb41	GACTCAAGCTCAGACCAGGCAA	ACTTCGGTCTGTGGACTCAGCA
Erdr1	CGTGGTCAAGATGTCTCTGCCATC	GGGCATTTCTGTACGCAGTCAGGC
Isg20	CAAGTACATCCGACCCGAGG	AGTCGTGCTTCAGGTCATGG
Tfr1	ATACGTTCCCCGTTGTTGAGG	GGCGGAAACTGAGTATGGTTGA
Ferritin	GCCCTGAAGAACTTTGCCAAAT	TGCAGGAAGATTCGTCCACCT
DMT1	GCTGAGCGAAGATACCAGCG	TGTGCAACGGCACATACTTG
Fpn1	TTCCGCACTTTTCGAGATGG	TACAGTCGAAGCCCAGGACTGT
S16	CCAAGCTTTCCTTTTCCGGT	CGAAGACTTGAACGGACTGCA

2.6 Transcriptomics

Brains were subdissected on ice into cortex, cerebellum and hippocampus then placed into Eppendorf tubes on dry ice for fast freezing. RNA extraction was performed as for larger tissue (2.5.1) and concentration and purity of RNA was assessed by spectrophotometry (Nanodrop) and RNA integrity was assessed by Bioanalyzer. RNA was shipped on dry ice to Cambridge Genomic Services (CGS) for transcriptomics analysis. Both microarray and RNA-Sequencing (RNA-Seq) services were provided by CGS.

2.7 Haematological analysis

2.7.1 Blood and sera collection

Mice were placed into a gas chamber and anaesthetized by inhalation of isofluorane. Once fully anaesthetized, a glass capillary tube was used to perforate the retro-orbital sinus and collect blood into EDTA coated or serum collection tubes (Starstedt). Following collection

of 50-150 µl blood, tubes were placed on a rotator and mice were euthanized by cervical dislocation. For serum preparation, blood was allowed to clot at room temperature for 30 minutes, then centrifuged at 1000 xg for 10 minutes at 4°C.

2.7.2 Clinical chemistry

Haematological analysis was performed using the Advia 2120 analyser (Siemens). Assays were performed by Clinical Chemistry services at MRC Harwell.

2.7.3 Giemsa staining

Giemsa staining was performed on blood smears according to manufacturer instructions (Sigma): briefly, slides were incubated in May-Grünwald stain for 5 minutes at room temperature, then washed in PBS, and incubated in Giemsa stain diluted 1:20 in distilled water for 15 minutes at room temperature. Slides were washed briefly in deionized water and air dried before mounting using Aquamount (Sigma-Alrich).

2.7.4 Serum analysis

Analysis of the following serum parameters was performed using the Pentra C400 clinical chemistry analyser (Horiba): Glucose HK, Glucose PAP, Lactic Acid, Lactate Dehydrogenase, Ferritin and Transferrin. Specific calibrators and controls were used as required for each parameter. Serum samples were diluted 1:5 in distilled water. Assays were performed at DPAG, Oxford, under supervision by Dr Goran Mohammad.

2.7.5 Heme assay

Serum heme concentration was measured using a colorimetric heme assay kit (ab272734, Abcam), using serum samples diluted 1:10 in distilled water. Assay was performed in clear 96 well plate, in triplicate, and absorbance measured using the Epoch microplate spectrophotometer at 400 nm.

2.7.6 Glycine assay

Serum glycine concentration was measured using a fluorometric glycine assay kit (ab211100, Abcam), using serum samples deproteinized using 10 kD spin columns

(Abcam) and diluted 1:20 using assay buffer. Assay was performed in flat bottomed black 96 well plate, in triplicate, and fluorescence readings measured using the VarioSkan automated plate reader (ThermoFisher) at Ex/Em = 535/587 nm.

2.8 Flow cytometry

2.8.1 Erythroid cells

Whole spleens were dissociated and passed through a 40-µm cell strainer prior to counting. A total of 1x106 cells / spleen were plated into a 96-well plate and washed with flow buffer (PBS + 2% FBS), then incubated for 15 minutes on ice with CD16/32 blocking antibody (dilution, 1:100) and LIVE/DEAD™ Fixable Near-IR Dead Cell Stain (dilution, 1:500; Invitrogen). Following washing with flow buffer, the cells were incubated with the following antibodies for 20 minutes on ice: Te119-PE (dilution, 1:200), CD44-APC (dilution, 1:200), CD71-FITC (dilution, 1:400). Lineage exclusion was performed using B220-APC-Cy7, Ly6C-APC-Cy7 and CD5 APC-Cy7 (dilution, 1:200). All antibodies were purchased from Biolegend. After washing off the antibody cocktail, cells were run through the flow cytometer in flow buffer.

2.8.2 Hematopoietic progenitors

Whole spleens were dissociated and passed through a 40-µm cell strainer prior to counting. Bone marrow was extracted from femurs using a centrifugation method [129]. A total of 2.5x106 cells / sample were plated into a 96-well plate and washed with flow buffer (PBS + 2% FBS), then incubated for 15 minutes on ice with CD16/32-PerCP-Cy5.5 (dilution, 1:200) and LIVE/DEAD Fixable Near-IR Dead Cell Stain (dilution, 1:500; Invitrogen). Following washing with flow buffer, the cells were incubated with the following antibodies for 20 minutes on ice: Te119-PE (dilution, 1:200), Sca-1-PE-Cy7 (dilution, 1:200), CD71-APC (dilution, 1:200), c-kit-BV421 (dilution, 1:100), CD41-BV605 (dilution, 1:150) and CD34-FITC (dilution, 1:400). Lineage exclusion was performed using B220-APC-Cy7, NK1.1-APC-Cy7 and Gr1-APC-Cy7 (dilution, 1:200). All antibodies were purchased from

Biolegend. After washing of the antibody cocktail, cells were run through the flow cytometer in flow buffer.

2.9 Generation and maintenance of cell lines

2.9.1 Neuro2a cells

Neuro2a (N2A) cells were maintained in Dulbecco's Modified Eagles Medium (DMEM-GlutaMAX) (Invitrogen) supplemented with 10% fetal bovine serum (FBS) (Invitrogen) and 1% Penicillin-Streptomycin solution (Invitrogen). Cells were passaged every 3-4 days and split in a 1:20 ratio.

2.9.2 Cloning

The conserved upstream human OXR1-C promoter sequence had previously been cloned into the vector pGL4.0[luc2] (Promega) by the Oliver lab, as well as the longer 1kb OXR1-C promoter sequence. The plasmids were cut using Kpn1 and Xho1 enzymes, while the coincidence reporter vector pNLCol1[luc2-P2A-NlucP/Hygro] (GenBank ID: KM359771) was also cut at the two enzyme sites Kpn1 and Xho1. The promoters were then ligated into the coincidence reporter vector to produce two separate constructs. Both promoter-constructs, and the empty vector, were used for transformation into bacteria, followed by colony picking, for miniprep in Lysogeny Broth (LB) with Ampicillin at 0.05mg/ml. Colonies were validated by enzyme digestion with Kpn1 and Xho1. The validated colonies were grown for maxiprep in LB with Ampicillin at 0.05mg/ml, sequence verified and stocks purified using the maxi plasmid DNA purification kit (QIAGEN).

2.9.3 Transfection

24 hours prior to transfection, cells were seeded in opaque-bottomed 96-well plates at a density of 1×10^4 cells per well, in OptiMEM (Invitrogen) supplemented with 5% FBS (Invitrogen) and 1% Penicillin-Streptomycin solution (Invitrogen). Cells were transfected with DNA constructs using Lipofectamine 3000 (ThermoFisher) according to manufacturer's instructions. Cells were transfected with 40ng DNA construct per well.

2.9.4 Nano-Glo Dual Luciferase assay

Transfected N2A cells were lysed and assayed for Firefly and Nano luciferase activity using the Nano-Glo Luciferase assay system (N1630, Promega), in an add-read-add-read method according to manufacturer's instructions. Cells were incubated in luciferase reagents for 10 minutes before luminescence readings were taken using the VarioSkan automated plate reader (ThermoFisher). Each well was read for 1 second. All experiments were performed in duplicate at minimum (see results for individual experiment n numbers).

2.9.5 Coincidence reporter validation

Cells were seeded in opaque-bottomed 96-well plates, following the same method as for transfection, 24 hours prior to administration of selective inhibitor compounds at the following titrations ranges: PTC124 10^{-12} - 10^{-15} M, Cilnidipine 10^{-9} - 10^{-4} M. Luminescence reading using the Nano-Glo system was performed 24 hours later. Methods used according to Schuck et al [130].

2.9.6 Generation of stable cell lines

Stable cell lines were generated according to the methodology described by Schuck et al [130], further described in Chapter Five. Briefly, promoter constructs were transfected into N2a cells, as above (2.9.3) and cells were passaged into growth media (DMEM-GlutaMAX (Invitrogen) supplemented with 10% FBS (Invitrogen) and 1% Penicillin-Streptomycin solution (Invitrogen)). GFP-transfected cells were used as a control. Growth media was replaced after 24 hours with growth media containing 800 µg/ml Hygromycin and cells were monitored until GFP-transfected cells were all dead, and construct-transfected cells were confluent for expansion. Cells were then split, taking polyclonal lines for expansion and using limited-dilution cloning to generate monoclones. Monoclones were allowed to grow until colony picking could be performed, then cells were picked under a microscope using a sterile pipette tip, and grown individually in wells of a 96 well plate. Validation was performed firstly using PCR to confirm expression of the construct, then by luciferase assay

to confirm sufficient luciferase expression. Monoclones were expanded for use in the compound screen.

2.9.7 Compound Screen

Screening of a small compound library was performed as described by Schuck et al [130] and in Chapter Five. Cells stably expressing the promoter construct were seeded in opaque bottomed 96 well plate. The PHARMAKON 1600 library (MicroSource Discovery Systems) was screened by application in triplicate at a concentration of 10 μM per well in OptiMEM media (Invitrogen) containing 0.1% DMSO. Luciferase assay was performed as described above (2.9.4) following incubation with test compounds 24 hours following cell seeding, for 48 hours. Luminescence was read using a VarioSkan automated plate reader (ThermoFisher).

2.9.8 CRISPRa

For cloning into the gene activation vector, three independent double-stranded fragments were synthesized commercially (GeneWiz) each containing an individual gRNA 20-mer sequence adjacent to a PAM (NGG) triplet upstream of mOxr1-C first exon (mouse GRCm38.p5, Chr15:41830658-41830957; TCTGCAGTCACATGGGATCT / GTGCAACCTAACTTGAGCTT / CAGCTTTACAGTCTCCACTC). The total critical region synthesized for sub-cloning was 177bp between the BamHI and the Bsp1407I sites of pCas-Guide-GFP-CRISPRa and the DNA fragments were initially supplied in a general-use pUC-Kan vector (GeneWiz). Plasmid DNA from each individual pUC clone was digested with BamHI and Bsp1407I (Fast Digest, Thermofisher) and run on a 2% agarose gel for purification of the 177bp fragment (Qiaquick gel purification kit, Qiagen). In parallel, pCas-Guide-GFP-CRISPRa DNA was digested with the same enzymes, followed by alkaline phosphatase treatment (FastAP, Thermofisher) and the larger plasmid band (10.5kb) gel purified. A 3:1 molar ratio of each individual insert to the plasmid (2.5ng to 50ng) was ligated overnight at 16^{o}C (T4 DNA ligase, NEB). As a negative control, one reaction contained no insert. 10% of the ligation mix was transformed into TOP10 competent cells (Invitrogen) by

heat shock and plated onto ampicillin plates. Bacterial colonies were picked for mini-prep DNA purification from 5ml overnight cultures (Qiagen) and the plasmids sequenced using a primer 80bp upstream of the BamHI site of pCas-Guide-GFP-CRISPRa (5' ACGATACAAGGCTGTTAGAGAG 3'). Endotoxin-free maxi-prep DNA was purified for sequence verified clones from 200ml overnight cultures (Qiagen) derived from the original mini-prep bacterial colony.

Cells were transfected with DNA constructs using Lipofectamine 3000 (ThermoFisher) according to manufacturer's instructions. Guide RNA was transfected 2 µg per well, with 0.6 µg enhancer. Transfections were performed in 6 well plate format, with a total liquid volume of 2 ml.

2.9.9 Statistical analysis

Analysis of results was performed using Excel 2016 and Prism version 7 (GraphPad Software Inc.). Data are presented as mean ± standard error of mean (SEM), with indicated values for 'n', as the number of independent samples within each group. Individual mice were considered 'biological replicates', and were controlled for age. Sample size is specified for individual results, and can be found in figures within each chapter. No biological replicates were excluded from analyses.

The two tailed Student's t test was performed to compare means between two groups, while one-way ANOVA was performed to compare means between three or more groups. Both tests were performed under the assumptions that data were continuous, independent and normally distributed, and there was similar variance between each group. For the two tailed Student's t test it was also assumed that means between groups could be significantly different in either direction compared with the control range of values. Difference between means was determined to be significant if $p < 0.05$.

Blinding could not be performed on behavioural analyses, as the phenotype of Tbc1d24 mutants was striking. There were no procedures performed requiring randomization.

Chapter 3: Characterization of CRISPR mouse models of *Tbc1d24* dysfunction

3.1 Introduction

3.1.1 Models of TBC1D24 dysfunction

Mutations in *TBC1D24* are associated with a pleiotropic spectrum of human diseases, including a variety of drug refractory epileptic disorders [99] also characterised by intellectual disability [105], neurodegeneration [131] and deafness, onychodystrophy, osteodystrophy, mental retardation and seizures (DOORS) syndrome [132]. Investigation into any possible interaction between disease phenotypes and the exonic locations and types of mutations has found no obvious correlation, although recessive loss-of-function mutations were generally found to produce more severe phenotypes [106]. Thus, it was predicted that the structure-function relationship of TBC1D24 would give further insight into genotype-phenotype correlation of deleterious mutations.

Through the systematic study of *TBC1D24* mutations, important roles of the gene have been uncovered in presynaptic function and neuronal development. Solving of the crystal structure of the *Drosophila* orthologue of *TBC1D24*, skywalker (*sky*), revealed a lipid-binding pocket, found to be conserved across *TBC1D24* homologs [109]. It was found that conserved disease-causing mutations in this pocket disrupted synaptic vesicle trafficking in *Drosophila*, and led to epilepsy-like defects such as seizures and loss of coordination. Modelling *TBC1D24* mutations associated with Rolandic epilepsy-exercise induced dystonia (RE-EID) in *sky* elucidated a link between the effect of mutations on protein stability within the TLDc crystal structure, and severity of disease mutation [133]. Disease-associated *TBC1D24* mutations conserved in *sky* showed defects in synaptic vesicle trafficking, which were exacerbated by exposure to oxidative stress (OS) through H_2O_2 treatment, but rescued by antioxidant treatment, suggesting a role for TBC1D24 in OS-dependent vesicle trafficking. As such, work in *Drosophila* has provided some valuable insights into TBC1D24. However, studies using *Drosophila* provide only limited insight into complex disease mechanisms, such as those involved in epilepsy, due to differences

between fly and mammalian physiology, including the lack of a complex nervous system [134]. Further details of *TBC1D24* modelling in the fly can be found in Introduction, Chapter One.

Work in mammalian *in vitro* systems has furthered understanding of TBC1D24 in neuronal development. Expression of *Tbc1d24* in mouse hippocampal neurons taken at E18.5 and cultured for 14 days *in vitro*, and in mouse whole brain at E15.5, correlates with terminal differentiation of neurons, and overexpression of Tbc1d24 protein increased the length of axons and number of neurites in primary culture of hippocampal neurons [105]. This suggests a role for TBC1D24 in brain development, and neuronal arborisation. Silencing of Tbc1d24 in rat cortical primary neurons led to defects in axonal specification and impaired endocytosis at the growth cone, suggesting that Tbc1d24 is required for membrane trafficking during neurodevelopment [135]. Studies in cultured mouse neurons (N2a) with total deletion of *Tbc1d24* showed that cells were less viable, more sensitive to OS, and showed reduction in neurite outgrowth compared to wild type cells [136]. Acute viral knockdown of *TBC1D24* in cultured mature hippocampal neurons caused significant reduction in the number of dendritic spines and excitatory synapses, indicating that TBC1D24 plays a role in maintaining synaptic function [137]. In the developing rat cortex, knockdown of *Tbc1d24* leads to defects in neuronal migration and maturation, which was found to result from disruption in interaction between Tbc1d24 and ADP ribosylation factor 6 (ARF6), which is a small GTPase protein required for membrane trafficking in the endolysosomal pathway [138]. Mutations within a different ARF6-interacting gene, IQ motif and Sec7 domain ArfGEF 2 (*IQSEC2*), are associated with drug-resistant epilepsy, autism and severe intellectual disability [139]. Studies of mutations in *IQSEC2* support a role of ARF6 in neurodevelopment, in that mutations modelled in mice lead to the aberrant activation of Arf6, causing disrupted neuronal signalling *in vitro* and formation of immature neuronal networks *in vivo* [140]. Overall, these data support a key role for TBC1D24 at the synapse, both in neurodevelopment and in regulating neuronal excitability.

A mouse model of Tbc1d24 haploinsufficiency, *Tbc1d24*^{tm1b}, harbours one copy of a disrupted allele of *Tbc1d24*, in exons 3-5 are removed due to expression of a ubiquitous cre-recombinase, leading to an early stop codon at position 380 in the Tbc1d24 protein sequence. This mouse expresses approximately half of wild-type *Tbc1d24* at both the RNA and protein levels, and shows defects in neuronal growth and increased sensitivity to OS in primary cortical neurons; although no overt defects in neuronal migration were observed through quantification of cortical layer markers [136]. Investigation of synaptic physiology *in vitro* showed a reduction of excitatory neurotransmission in hippocampal neurons. It was also found that haploinsufficient neurons had larger and denser endosomal-like compartments, consistent with results found when the orthologue *Sky* was mutated in drosophila [109], which suggests a role for TBC1D24 in synaptic vesicle recycling and the maintenance of excitatory nerve terminals. No seizures were observed in *Tbc1d24*^{tm1b} mice, nor were there any signs of neurodevelopmental delay despite the synaptic defects observed in the mutant, consistent with findings in human carriers of loss-of-function mutations in *TBC1D24*, who did not experience seizures [136]. However, the disease mechanism of mutations in *TBC1D24* was yet to be uncovered.

In summary, at the start of this project, the data was consistent with a role for TBC1D24 in synaptic vesicle trafficking and neuronal development. However, due to the lack of correlation between genotype and clinical phenotype, there was still a limited understanding regarding role of TBC1D24 in neurological disease. Furthermore, no mammalian models of TBC1D24 dysfunction had been generated which showed seizures, thus the understanding of the *in vivo* effects of mutations in *TBC1D24* was limited. Studies in *Drosophila*, despite providing interesting structural and electrophysiological data, could not be extrapolated into understanding of the function of TBC1D24 in a complex nervous system.

Therefore, the aim of this project was to generate new *in vivo* knock-in mouse models to study the functional and physiological consequences of TBC1D24 disruption.

While the importance of *TBC1D24* mutations in epilepsy had already been demonstrated, the insight into the potential role of TBC1D24 in disease mechanisms of epilepsy would depend on the phenotypes observed.

3.1.2 CRISPR Models of TBC1D24 dysfunction: R360L, P135L and INS2

Mouse models are invaluable tools for investigating the molecular mechanisms involved in pathogenic mutations. To investigate the functional consequences of disrupted Tbc1d24 *in vivo*, mouse lines harbouring human disease mutations were generated using CRISPR-mediated methods. Three mouse lines in total were generated, each to provide different insight into TBC1D24 function: *Tbc1d24*^{R360L}, *Tbc1d24*^{P135L} and *Tbc1d24*^{INS2} (**Figure 3.1**).

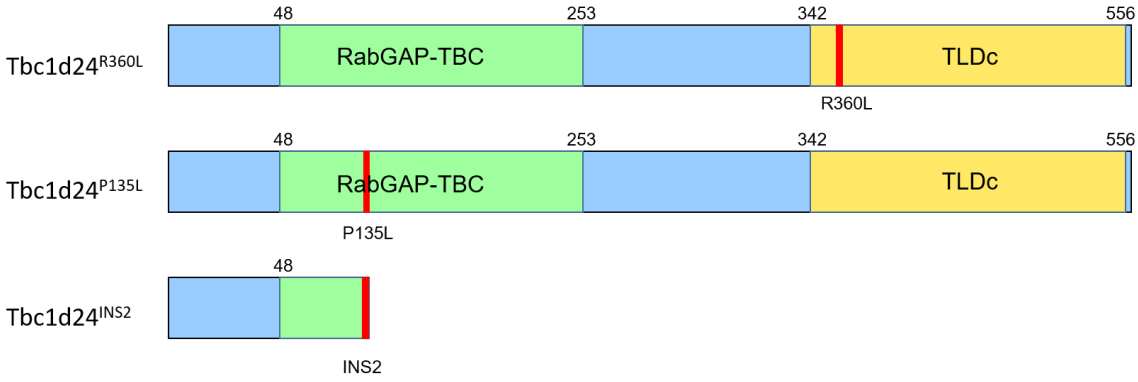


Figure 3.1 Mutation schematic for* Tbc1d24^{R360L}, Tbc1d24^{P135L} *and* Tbc1d24^{INS2} *mutant mouse models. *Mutants generated for the study of Tbc1d24 dysfunction. The* Tbc1d24^{R360L} *mutant line contains an Arginine to Leucine missense mutation at position 360, which is in the TLDc domain of Tbc1d24 protein. The* Tbc1d24^{P135L} *mutant line contains a Proline to Leucine missense mutation at position 135, which is the in the RabGAP-TBC domain of Tbc1d24. The* Tbc1d24^{INS2} *mutant line contains an early stop codon at position 135 of Tbc1d24, causing early truncation of the protein.*

The first mutant to be generated was the *Tbc1d24*^{R360L} mouse line, containing the knock-in mutation R360L, which is an arginine to leucine missense mutation within the TLDc domain of Tbc1d24 (**Figure 3.1**). The R360 residue in the *Drosophila* orthologue of Tbc1d24 forms part of a salt bridge, with residue R425; mutation in either residue was predicted to cause a mild effect on protein stability [133]. The arginine amino acid residue at position 360 is conserved across human and mouse, with 95% sequence conservation between the two species of the 10 residues either side of R360 (**Figure 3.2**) [141]. This mutation is directly associated with epilepsy in humans, causing a recessive form of PME

with neurodegeneration, enabling particular focus on the pathogenic consequences of disruption in the TLDc domain, with its links to OS [142], and cerebellar degeneration [143]. Of note, it had been shown in primary mouse cortical cells that transfection with a *TBC1D24* construct containing the R360L mutation led to significantly reduced neurite outgrowth [106]. This finding suggested promise that an *in vivo* mouse model of this mutation would display a neurological phenotype, enabling study of the potential molecular mechanisms involved in human disease.

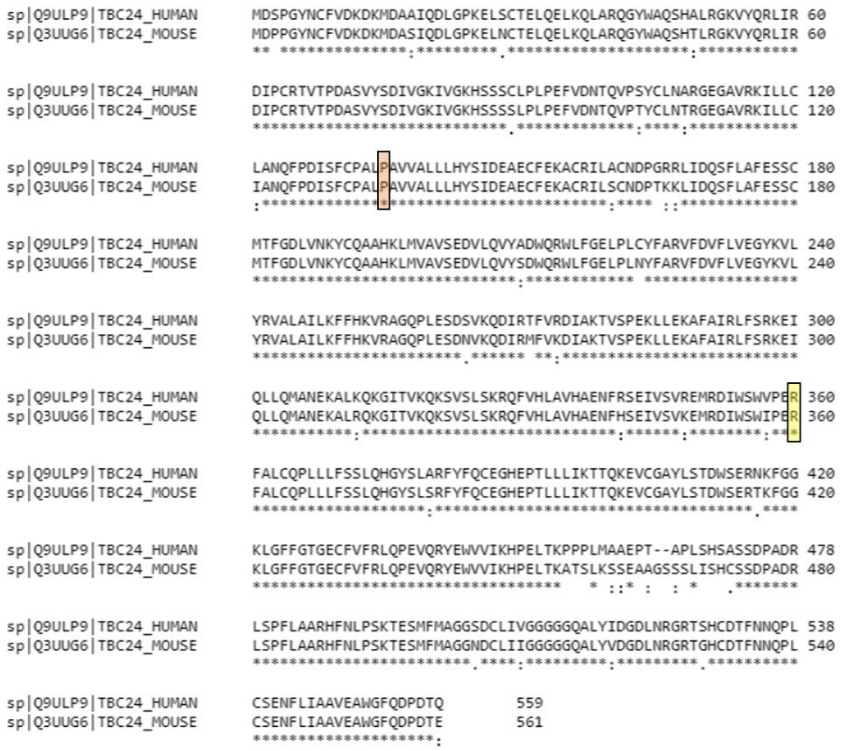


Figure 3.2 Sequence alignment between human TBC1D24 and mouse Tbc1d24 protein. *TBC1D24 is predicted to be 94.2% conserved across human and mouse, including at key mutation sites P135 (orange) and R360 (yellow). Ten residues either side of mutation sites show sequence conservation of 100% (P135) and 95% (R360). Alignment performed using UniProt.org.*

Given that the association between genotype and phenotype in *TBC1D24* mutations is poorly understood, it is useful to investigate mutations representing disruption in both of the major domains in TBC1D24. The *Tbc1d24*^{P135L} mutant mouse line containing a knock-in mutation P135L, a proline to leucine missense mutation within the RabGAP-TBC domain of TBC1D24 (**Figure 3.1**). The proline amino acid residue at position 135 is conserved across human and mouse, with 100% sequence conservation between the two species of the 10 residues either side of P135 (**Figure 3.2**) [141]. At the time of mutant mouse line

selection, this mutation had been shown to cause tonic-clonic and myoclonic epilepsy, with an autosomal dominant pattern of inheritance [144]. Thus we were interested to determine whether this apparent gain-of-function mechanism could recapitulated in vivo in the mouse. Furthermore, a patient carrying compound heterozygous mutations P135L in tandem with an arginine to cysteine mutation (R360C) is associated with epilepsy, intellectual disability, Parkinsonism and psychosis, producing a more severe neurological syndrome than the P135L mutation alone [144]. Therefore, we were interested in investigating the R360L/P135L compound heterozygous if that was possible.

During the production of the *Tbc1d24*^{P135L} mouse line, one of the founder (F0) lines was found when sequenced to contain a 2 nucleotide insertion, introducing an early stop codon after position 135 in Tbc1d24, producing an null model of Tbc1d24 (named here *Tbc1d24*^{INS2}). This mutant is predicted to be a complete null or loss-of-function model with no full-length protein expression. It was not known whether homozygous mutants would be viable at this stage; although preliminary studies on the Tbc1d24^{tm1b} allele had suggested that it would be homozygous lethal postnatally. In humans, a truncation mutation in *TBC1D24* with a predicted protein product 42% shorter than wild-type TBC1D24 is associated with severe, lethal epileptic encephalopathy [131].

The aim for this chapter is to phenotypically and pathologically characterize the three Tbc1d24 mouse mutants, in order provide insight into the aetiology of epilepsy in human patients through the study of Tbc1d24 dysfunction, and thus help to elucidate the molecular functions of TBC1D24.

3.2 Characterization of the Tbc1d24$^{R360L/R360L}$ mouse

3.2.1 Phenotype of Tbc1d24$^{R360L/R360L}$

3.2.1.1 Description of phenotype through video tracking analysis

A human patient with the homozygous R360L mutation in TBC1D24 was found to experience progressive myoclonic epilepsy (PME), characterized by myoclonus, tonic-clonic seizures and progressive neurological damage including cerebellar degeneration [142]. Following generation of founder F0/F1 CRISPR positive carrier R360L lines,

intercrossing was performed to generate wild type, heterozygous and homozygous offspring. In the first litters produced by intercross, some offspring were found dead at P16 and P17, which were subsequently genotyped and identified as homozygous for the R360L mutation. Home cage video tracking was then performed to look for behavioural signs to explain the early death, through which a hyperactive episode was observed in a mouse at P17. The mouse later died, during the dark phase of the video recording, and genotyping revealed it to be homozygous for the R360L mutation. In accordance with Home Office guidance, the humane end-point for the mutant was then determined to be P16. The ratio of homozygous mice across litters was determined to follow Mendelian inheritance, at approximately 1 in 4, suggesting that no overt prenatal lethality is caused by the mutation. Furthermore, both male and female mice were observed to experience seizures.

The *Tbc1d24*$^{R360L/R360L}$ mutant mouse exhibits seizures from P15 onwards, which become fatal from P17. As observed through video-tracking analysis, the seizure phenotype of *Tbc1d24*$^{R360L/R360L}$ consists of three stereotypic phases: a period of intense hyperactivity, followed by seizure (known as the ictal phase), then a period in which the mouse enters a postictal state. In the earlier disease stage, between P15 – P16, mice are observed to recover from shorter (30 second) myoclonic seizures, however, from P17 onwards, mice do not recover following postictal state (Home Office licence restrictions prevented a longitudinal survival study). It was noted that movement of the cage or handling could instigate ‘jumpy’ behaviour prior to a hyperactive episode from P15 in some cases. This phenotype has been observed both in light phase and in dark phase using video-tracking cages. Mice heterozygous for the R360L mutation show no seizures or apparent deleterious effects of the mutation, and exhibit survival comparable to wild type littermates (not shown). Given the pronounced and stereotypic character of the seizure presentation in the *Tbc1d24*$^{R360L/R360L}$ mutant, especially considering the hyperactive period preceding the ictal phase, seizure confirmation by a secondary method (such as EEG or IHC of seizure markers) was not deemed necessary (Home cage analysis (HCA) was performed on

offspring from the Oxr1^{Prnp} x Tbc1d24^{R360L} cross, and survival and seizure incidence data reported in **Chapter Five**).

3.2.1.2 Open Field shows no changes in *Tbc1d24$^{R360L/R360L}$* behaviour

Behavioural analysis of the *Tbc1d24$^{R360L/R360L}$* mutant was performed using the open field (OF) test, to potentially quantify hyperactive behaviour observed through home cage video tracking. The OF test, during which mice are individually placed in an open arena, can be used to measure a range of behaviours, and assess motor function in mice. Due to the instinctive aversion of mice to open spaces, anxiety-like behaviour can be assessed according to the number of times a mouse enters the centre of the arena (frequency to centre), the time taken for the mouse to first enter the centre (latency to arena), and the percentage of time the mouse spends in the centre overall (percentage time in centre) [19]. As shown by Figure 3, there was no significant difference in any of these parameters across *Tbc1d24$^{+/+}$*, *Tbc1d24$^{+/R360L}$* and *Tbc1d24$^{R360L/R360L}$* mice, although the *Tbc1d24$^{R360L/R360L}$* mutant appeared to show decreased latency to centre, with a mean decrease of 42.1% compared with Tbc1d24+/+ ($p = 0.193$) and 20.1% compared with *Tbc1d24$^{+/R360L}$* ($p = 0.809$). *Tbc1d24$^{+/R360L}$* showed an intermediary latency to centre between the other two genotypes.

Parameters measuring total distance moved and overall velocity also give insight into locomotor activity [145]. There was no significant difference between *Tbc1d24$^{+/+}$*, *Tbc1d24$^{+/R360L}$* and *Tbc1d24$^{R360L/R360L}$* mice for either total distance moved ($p = 0.529$) or velocity ($p = 0.635$). However, for both total distance moved and velocity, there were increases in *Tbc1d24$^{R360L/R360L}$* compared with *Tbc1d24$^{+/+}$*, with an intermediary result in *Tbc1d24$^{+/R360L}$*. This suggests a potential dose-dependent effect of the mutation, although the results were not statistically significant. Overall, open field behavioural analysis suggest no detrimental effect of the R360L mutation on either anxiety-like behaviour or locomotor activity. Decreased latency to centre may indicate a lower level of anxiety in the *Tbc1d24$^{R360L/R360L}$* mutant, although the effect is not statistically significant [146]. One *Tbc1d24$^{R360L/R360L}$* mouse was observed to experience a hyperactive episode, followed by

seizure, during OF testing (**Figure 3.3**, demarcated by▲). This mouse was not identified as an outlier within any of the parameters tested, although latency to centre was measured as 572.96 seconds, which is 2.9 fold higher than the mean latency to centre for *Tbc1d24*$^{R360L/R360L}$. As stated above, an increase in this parameter may indicate increased anxiety, which may relate to the subsequent seizure experienced by the mouse.

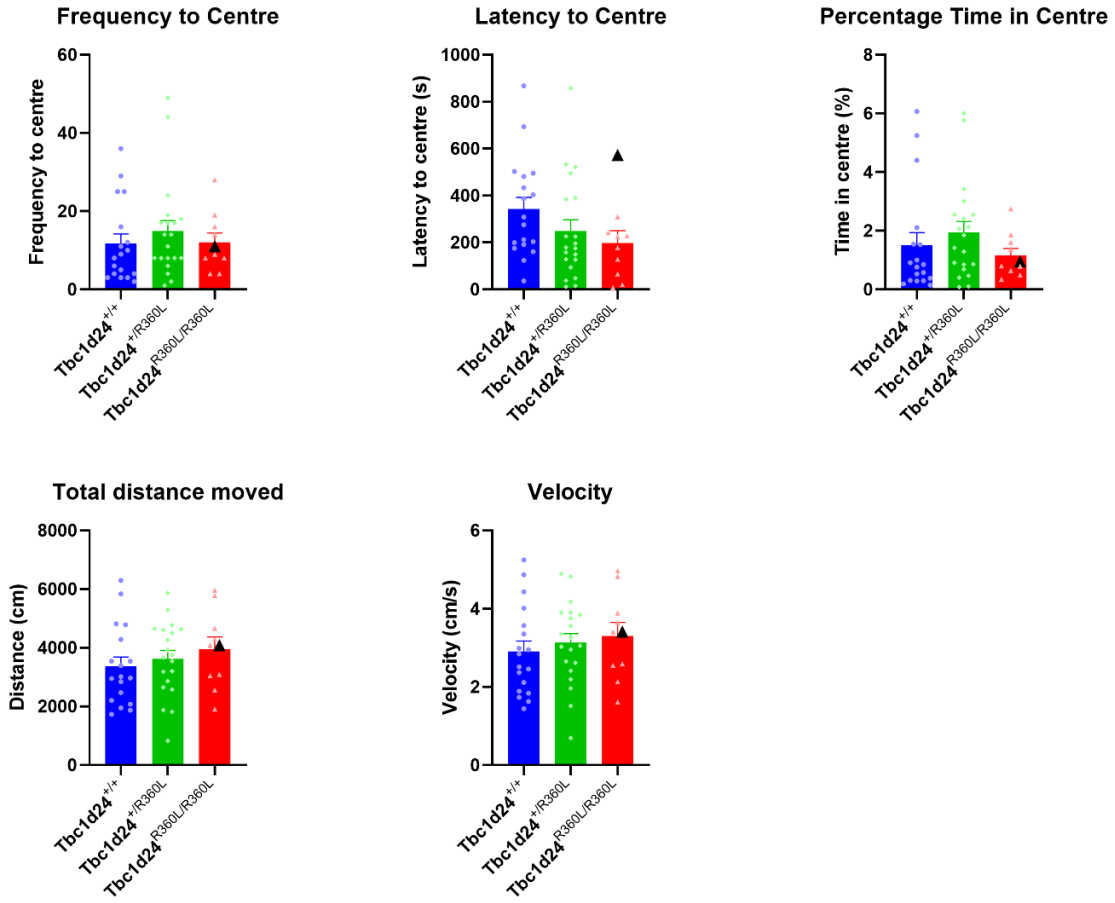


Figure 3.3 Open Field behavioural testing shows no significant changes in behaviour of the* Tbc1d24$^{R360L/R360L}$ *mouse mutant. Tbc1d24$^{+/+}$, Tbc1d24$^{+/R360L}$ *and* Tbc1d24$^{R360L/R360L}$ *mice were individually placed into the Open Field arena test, and their movement was tracked over twenty minutes using EthoVision tracking software. Analysis was performed to calculate frequency to centre, latency to centre, percentage time spent in centre, total distance moved, and velocity. The data point for one mouse which experienced a hyperactive seizure episode is demarcated by a symbol: ▲. One way ANOVA with Tukey's multiple comparisons test was performed. However, no significant changes were observed. (Testing performed on male and female mice at P16, Tbc1d24 $^{+/+}$ N = 18, Tbc1d24$^{+/R360L}$ N = 20, Tbc1d24$^{R360L/R360L}$ N = 10).*

3.2.2 Expression studies of *Tbc1d24*$^{R360L/R360L}$

3.2.2.1 The *Tbc1d24*$^{R360L/R360L}$ mutant shows decreased Tbc1d24 expression

To investigate the effect of the R360L mutation on the expression of Tbc1d24 protein, Western blotting was performed using protein extracted from whole brains of *Tbc1d24*$^{+/+}$,

Tbc1d24$^{R360L/R360L}$ mice at P16. Surprisingly, as shown by **Figure 3.4**, the *Tbc1d24*$^{R360L/R360L}$ mutant showed a dramatic decrease in expression of Tbc1d24, with a mean decrease of 90.8% compared to *Tbc1d24*$^{+/+}$ ($p < 0.0001$). Decreased protein expression may indicate either a reduction in transcription of mRNA, or post-translational degradation of the protein itself.

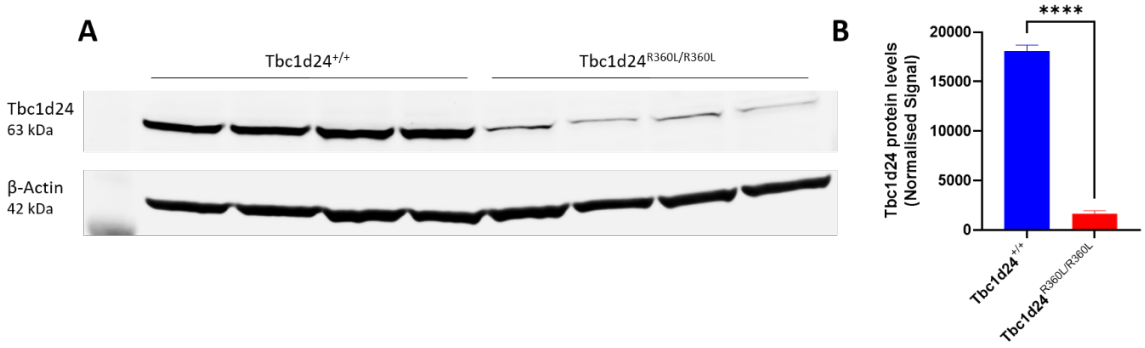


Figure 3.4 The* Tbc1d24$^{R360L/R360L}$ *mutant shows knock down in protein levels. *Western blotting was performed using protein extracted from whole brains of* Tbc1d24$^{+/+}$ *and* Tbc1d24$^{R360L/R360L}$ *mice at P16. (**A**) Representative western blot showing bands at 63kDa for Tbc1d24 and at 42kDa for β-Actin. (**B**) Quantification of Tbc1d24 protein levels normalized to β-Actin. Student's t test was performed. Graph shows mean ± SEM (n = 4).*

3.2.2.2 Expression and stability of the mutant *Tbc1d24*^{R360L} allele

To investigate whether decreased expression of *Tbc1d24* is observed at the mRNA level, RT-qPCR was performed using mRNA extracted from whole brains of *Tbc1d24*$^{+/+}$, *Tbc1d24*$^{+/R360L}$ and *Tbc1d24*$^{R360L/R360L}$ mice at P16. As shown by **Figure 3.5**, there was no difference in expression between the three genotypes, *Tbc1d24*$^{R360L/R360L}$, *Tbc1d24*$^{+/R360L}$ and *Tbc1d24*$^{+/+}$ ($p = 0.1206$).

Of note, RNA sequencing (RNA-Seq) was later performed using mRNA extracted from the prefrontal cortex of *Tbc1d24*$^{R360L/R360L}$, using *Tbc1d24*$^{+/+}$ littermate controls (see Chapter Four). Concordantly with RT-qPCR findings, no difference in expression of *Tbc1d24* was observed (FDR = 0.9756).

To further investigate the expression of *Tbc1d24* mRNA in the *Tbc1d24*$^{R360L/R360L}$ mutant, a separate RT-qPCR assay was developed to specifically amplify either the wild type or R360L mutant transcript of *Tbc1d24*. The results confirmed the specificity of the

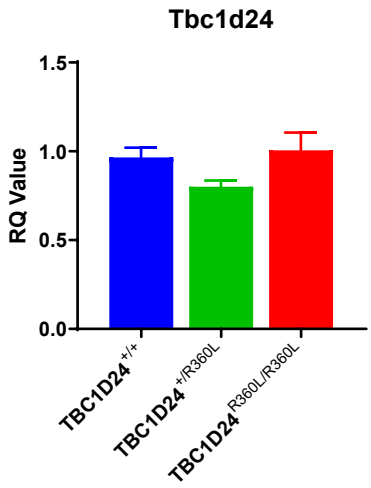


***Figure 3.5* Tbc1d24$^{R360L/R360L}$ *shows no difference in expression of* Tbc1d24 *mRNA compared with* Tbc1d24$^{+/+}$.** *RT-qPCR was performed using mRNA extracted from male and female* Tbc1d24$^{+/+}$ *(blue),* Tbc1d24$^{+/R360L}$ *(green) and* Tbc1d24$^{R360L/R360L}$ *(red) whole brains at P16. Expression of the gene* Tbc1d24 *was measured. One way ANOVA with Tukey's multiple comparisons test was performed using ΔCT values. Values show mean ± SEM (n = 4 - 5).*

mutant and wild type probes, indicating that expression of the *Tbc1d24*$^{+}$ allele in the *Tbc1d24*$^{+/R360L}$ mice was approximately half that in the *Tbc1d24*$^{+/+}$ mice, and expression of the *Tbc1d24*^{R360L} allele in the *Tbc1d24*$^{+/R360L}$ mice was approximately half that in the *Tbc1d24*$^{R360L/R360L}$ mice (**Figure 3.6**), indicating that both wild type and R360L mutant alleles are expressed at similar levels. This suggests that the R360L mutation leads to post-translational alterations in expression.

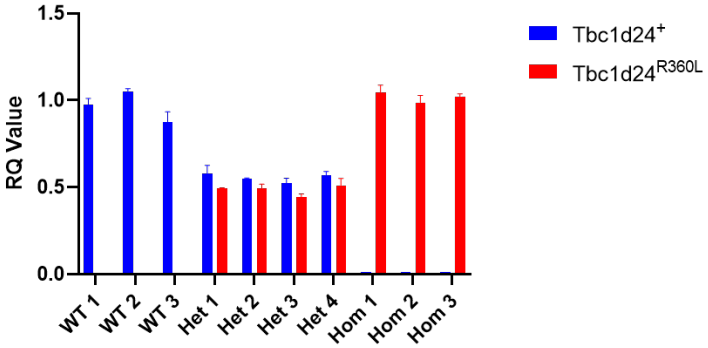


Figure 3.6 Expression analysis by RT-qPCR indicates similar expression of* Tbc1d24^{+} *and* Tbc1d24^{R360L} *alleles. *Allele specific RT-qPCR was performed using specific probes for* Tbc1d24^{+} *(wild type allele, blue) and* Tbc1d24^{R360L} *(mutant allele, red). mRNA was extracted from whole brains of male and female mice at P16. RQ values were plotted for individual mice, with* Tbc1d24$^{+/+}$ *(WT),* Tbc1d24$^{+/R360L}$ *(Het) and* Tbc1d24$^{R360L/R360L}$ *(Hom) showing specificity of the probes. RQ values of the probes were calculated independently. Student's t test was performed using ΔCT values. Values show mean ± SEM (n = 3 - 4). Allele-specific RT-qPCR experiment (excluding analysis) was performed by D. Williams, MRC Harwell.*

3.2.2.3 *In situ* hybridisation of Tbc1d24 in the *Tbc1d24*$^{R360L/R360L}$ mutant

Previous studies of *Tbc1d24* have shown by *in situ* hybridisation (ISH) that wild type *Tbc1d24* mRNA is expressed throughout the adult mouse brain, including the cerebral cortex and cerebellum, with particularly strong expression in the hippocampus [147]. In order to observe any potential differences in *Tbc1d24* spatiotemporal expression caused by the R360L mutation, ISH was performed using sagittal sections of *Tbc1d24*$^{+/+}$ and *Tbc1d24*$^{R360L/R360L}$ brains at P16. As shown in **Figure 3.7**, expression of *Tbc1d24* mRNA is comparable between *Tbc1d24*$^{+/+}$ and *Tbc1d24*$^{R360L/R360L}$. *Tbc1d24* is visibly expressed in the cortex and hippocampus of the *Tbc1d24*$^{R360L/R360L}$ mutant, with no discernible differences in expression compared with Tbc1d24$^{+/+}$. This is consistent with findings by RT-qPCR and RNA-Seq, that *Tbc1d24* mRNA does not undergo significant nonsense mediated decay in the Tbc1d24$^{R360L/R360L}$ mutant and that the significant protein level reduction is a post-transcriptional event.

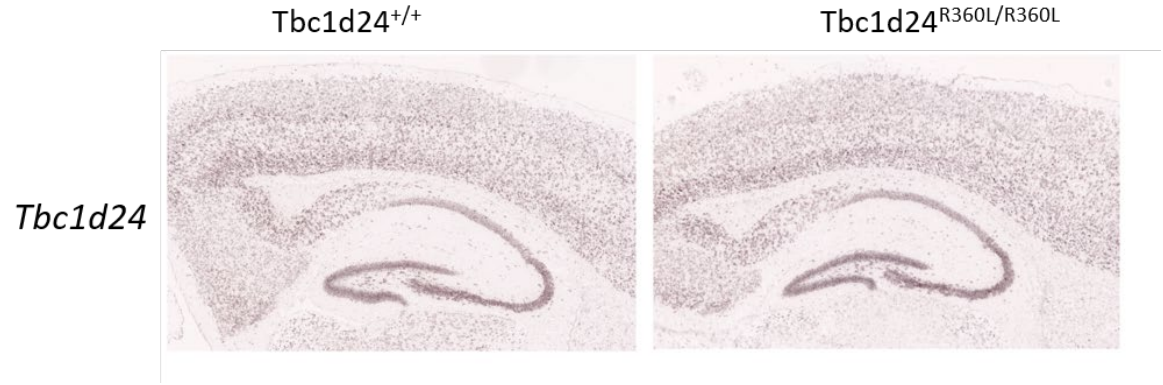


Figure 3.7* In situ *hybridisation of* Tbc1d24 *shows similar expression between* Tbc1d24$^{+/+}$ *and* Tbc1d24$^{R360L/R360L}$*. *Representative images showing* Tbc1d24 *expression in cortex and hippocampus of* Tbc1d24$^{+/+}$ *and* Tbc1d24$^{R360L/R360L}$ *mice. ISH was performed using sagittal sections of brains of male mice at P16.*

3.2.3 Neuropathology of *Tbc1d24*$^{R360L/R360L}$

3.2.3.1 Gross brain morphology

Many forms of epilepsy are associated with alterations in brain morphology, such as a decrease of hippocampal volume in mesial temporal lobe epilepsy (MTLE) [148], and increased brain volume and increased cortical width demonstrated across several models of heritable epilepsy in rats [149]. Interestingly, patients with homozygous loss-of-function variants of the TLDc family-member *OXR1* display neurological disease including seizures,

and show marked cerebellar atrophy resulting in shrinkage of the cerebellum [150]. In order to visualise gross morphology of the *Tbc1d24*$^{R360L/R360L}$ brain, sagittal sections of *Tbc1d24*$^{+/+}$ and *Tbc1d24*$^{R360L/R360L}$ brains were Nissl stained. As shown in **Figure 3.8**, the *Tbc1d24*$^{R360L/R360L}$ brain at P16 is comparable to the *Tbc1d24*$^{+/+}$ brain, with no difference in appearance of the cerebellum, hippocampus, cortex or midbrain. No striking neuropathological alterations are observed either on a gross morphology level, or in cortical layers at higher magnifications. More detailed neuropathology is being carried out by the Oliver laboratory.

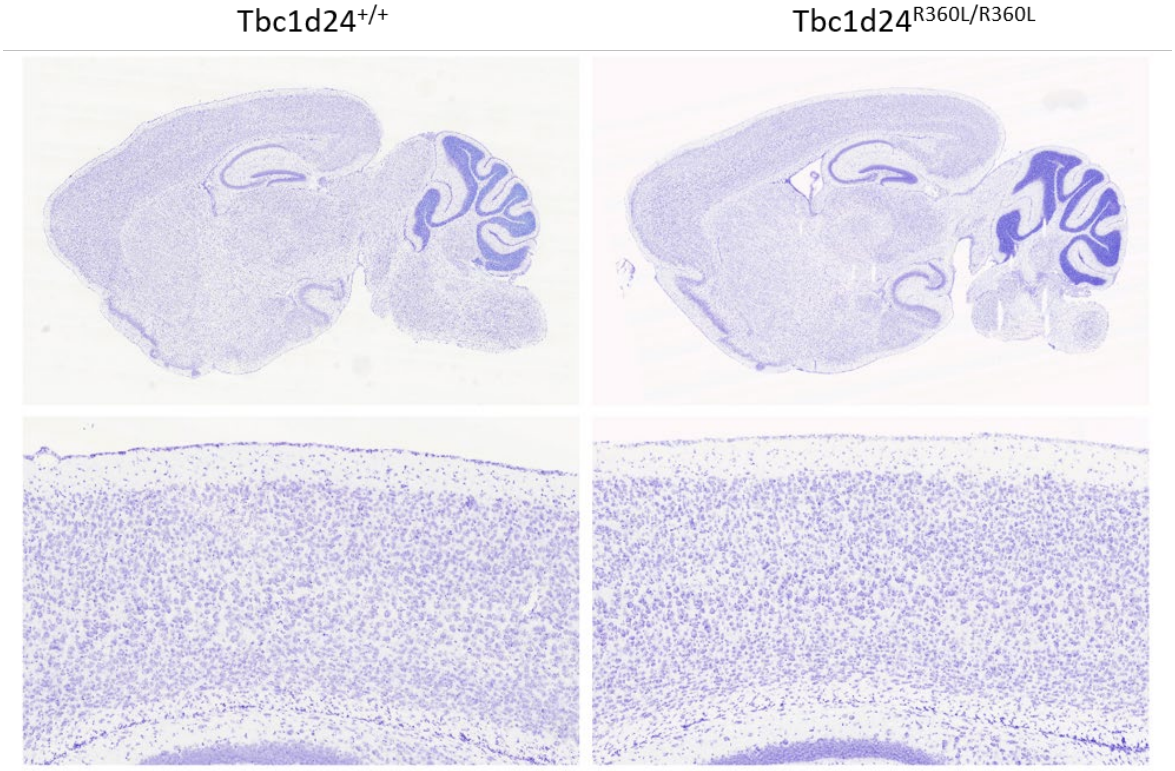


Figure 3.8 Comparable gross morphology between* Tbc1d24$^{+/+}$ *and* Tbc1d24$^{R360L/R360L}$ *brain shown by Nissl staining. *Representative images of Nissl-stained brains of male mice at P16. Top: sagittal sections of whole brains, showing comparable structural morphology between* Tbc1d24$^{+/+}$ *(left) and* Tbc1d24$^{R360L/R360L}$ *(right) brains. Bottom: Cortical layers at greater magnification.*

3.2.3.2 C-Fos as a marker of neuronal activity

The immediate early gene (IEG) c-fos is a transcription factor that regulates neuronal excitability, and is used as an indicator of neuronal activation and seizure-related neuronal excitation [151] [152]. Expression of *c-Fos* at the mRNA level can therefore be utilised as a proxy for seizure-like activity. Therefore, in order to determine whether the

seizure phenotype of the *Tbc1d24*$^{R360L/R360L}$ mutant could be observed at a molecular level, ISH was performed using a riboprobes against *c-fos* on coronal sections of *Tbc1d24*$^{+/+}$ and *Tbc1d24*$^{R360L/R360L}$ brains. As shown in **Figure 3.9**, expression of *c-Fos* is markedly upregulated in the *Tbc1d24*$^{R360L/R360L}$ brain, in the piriform cortex (PC), which is thought to be crucial in seizure initiation in epilepsy, and the area of the cortex most susceptible to epileptogenic stimulation [153, 154]. Upregulation of *c-fos* in this region provides a clear indication that there is epileptiform activity in the *Tbc1d24*$^{R360L/R360L}$ mutant. Upregulation of *c-fos* is also visible in the anterior cingulate area (ACA). Studies have described the proliferation of electrical activation from the PC to the ACA in patients with focal epilepsies, interpreted as electrical discharge spreading from the PC between seizure events [155].

In summary, the *Tbc1d24*^{R360L} line is characterized by a large and significant reduction in abundance of Tbc1d24 protein expression. No gross pathological changes were observed in the brain of the mutant, although molecular indications of seizures were observed through the upregulation of *c-fos* in brain areas pertinent to seizure pathology, including the piriform cortex.

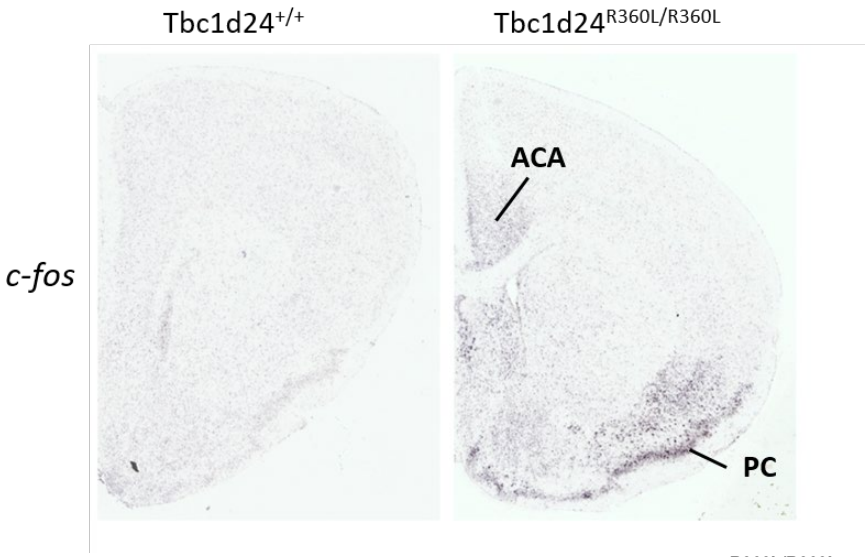


Figure 3.9 Upregulation of* c-fos *in the piriform cortex of the* Tbc1d24$^{R360L/R360L}$ *mutant. *Representative images showing ISH performed using a riboprobes against the IEG* c-fos *on coronal sections of* Tbc1d24$^{+/+}$ *(left) and* Tbc1d24$^{R360L/R360L}$ *(right) brains of male mice at P16. Labels show areas of staining in the piriform cortex (PC) and anterior cingulate area (ACA).*

3.2.4 Functional studies of the V-ATPase in *Tbc1d24*$^{R360L/R360L}$

The V-ATPase is a large protein complex involved in vesicle acidification, using hydrolysis of ATP to generate energy to act as a proton pump, and consists of transmembrane (V0) and cytosolic (V1) subunits [156]. The initial indication that the function of Tbc1d24 may be tied to the action of the V-ATPase arose from a mass spectrometry screen in 2014, which identified subunits of the V-ATPase as common binding partners with all members of the TLDc family (Finelli, M. – Oliver lab, unpublished). Mutations in V-ATPase subunits, such as ATP6V1A, have been reported to cause epilepsy, associated with decreased stability of the V-ATPase complex and disrupted lysosomal acidification [157]. Transfection of hippocampal neurons with ATP6V1A mutant constructs resulted in a reduction of excitatory synapses, highlighting the importance of V-ATPase function in neuronal development. Furthermore, fibroblasts of patients with epilepsy-related *de novo* missense mutations in *ATP6V1A* show lysosomal acidification defects and decreased expression of lysosomal-associated membrane protein-1 (LAMP1), indicating lysosomal impairment [158]. Additionally, compound heterozygous variants in the V-ATPase subunit ATP6V0A1 show progressive myoclonic epilepsy (PME) and ataxia [159]. Stable expression of these mutants in Neuro2a cell lines resulted in decreased lysosomal acidification compared to a cell line expressing wild type ATP6V0A1. A mouse line homozygous for a knock-in human mutation, R741Q, in ATP6V01A showed embryonic lethality, providing further evidence for the essential role of the V-ATPase [160]. Missense mutations in *ATP6V0C* affecting proton transport and complex assembly are associated with febrile seizures and epilepsy [161].

Mutations in *ATP6V1B2* have been described in dominant deafness-onychodystrophy (DDOD) syndrome [162], which is highly similar to DOORS syndrome, associated with certain mutations in *TBC1D24* [132]. Both syndromes include sensorineural deafness and onychodystrophy. In addition, a truncating variant of *ATP6V1B2* has recently been identified in patients with DOORS syndrome [163]. Furthermore, the V-ATPase subunit *ATP6V0C* and *TBC1D24* are deleted from one copy of chromosome 16 in a 16p13.3

microdeletion syndrome recently reported to cause epilepsy, intellectual disability and skeletal abnormalities [164] [165]. This overlap between rare disease phenotypes of mutations in V-ATPase subunits and TBC1D24 indicates shared functional significance between the two proteins.

Co-immunoprecipitation was performed to confirm the interaction between V-ATPase subunits and Tbc1d24, using protein extracted from *Tbc1d24*$^{+/+}$ and *Tbc1d24*$^{R360L/R360L}$ whole brain at P16. The antibody for Tbc1d24 was produced in-house for use in co-immunoprecipitation. As shown by **Figure 3.10**, a clear interaction is observed between wild type Tbc1d24 protein and the V-ATPase cytoplasmic subunits Atp6v1b2, Atp6v1a and Atp6v1c, as shown by specific bands at 57 kDa, 68 kDa and 44 kDa, respectively, in the *Tbc1d24*$^{+/+}$ immunoprecipitate (IP) lanes. Interestingly, no band was observed at 38 kDa in the IP lane when blotted with an antibody against Atp6v0d, indicating that Tbc1d24 does not interact with this subunit, which forms part of the membrane-bound V0 domain of the V-ATPase.

No bands were visible for Atp6v1b2, Atp6v1a or Atp6v1c in the *Tbc1d24*$^{R360L/R360L}$ IP lane (Atp6v0d was not tested in this mutant) (**Figure 3.10**). The severe reduction in expression of Tbc1d24 protein in the *Tbc1d24*$^{R360L/R360L}$ mutant is evident, in that no band is visible at 63 kDa in the IP lane when blotted with an antibody for Tbc1d24. Therefore, the apparent lack of interaction between Tbc1d24 and V-ATPase subunits in the *Tbc1d24*$^{R360L/R360L}$ mutant is not surprising, given the low level of expression of Tbc1d24 protein. It is unclear, therefore, whether the R360L mutation itself disrupts interaction with the V-ATPase.

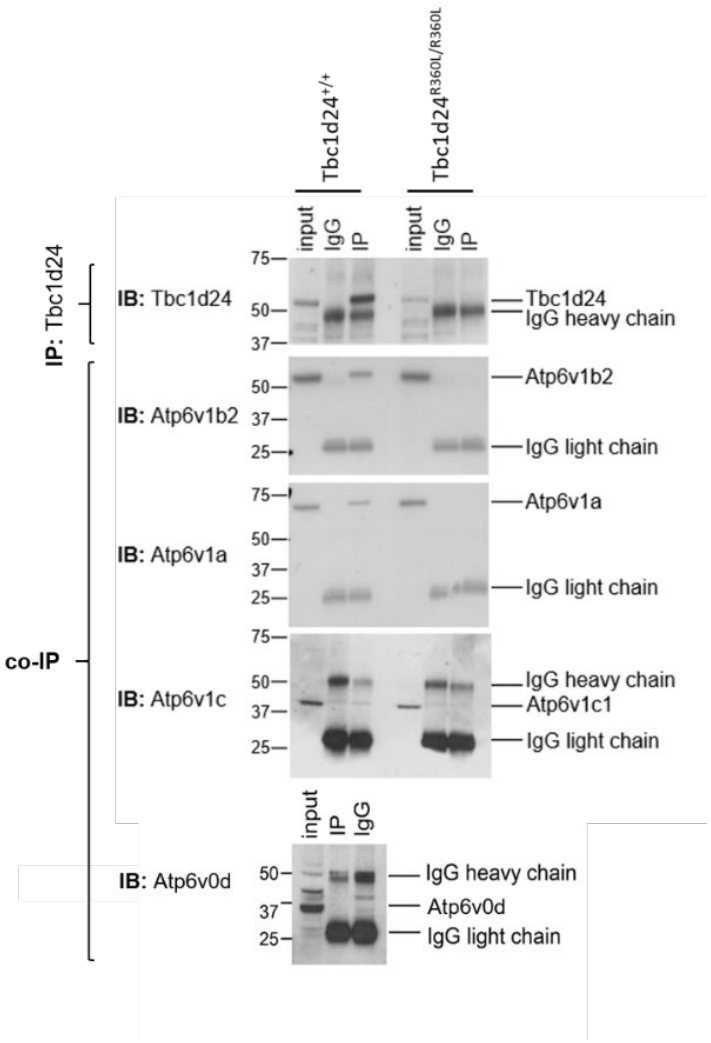


Figure 3.10 Confirmation of the interaction between Tbc1d24 and v-ATPase subunits, demonstrated by co-immunoprecipitation. *Co-immunoprecipitation was performed using protein extracted from Tbc1d24$^{+/+}$ and Tbc1d24$^{R360L/R360L}$ whole brains of male mice at P16. Western blotting was performed using input, IgG control, and immunoprecipitate (IP) protein, blotted using antibodies for Atp6v1b2, Atp6v1a, Atp6v1c and Atp6v0d. Co-immunoprecipitation and western blotting were performed by Protein Core, MRC Harwell.*

3.2.5 Summary of findings in the *Tbc1d24$^{R360L/R360L}$* mutant

The R360L mutation in Tbc1d24 leads to a form of childhood-onset epilepsy in humans, which is mirrored by seizures in the *Tbc1d24$^{R360L/R360L}$* mouse. Furthermore, the mutation shows the same recessive pattern of inheritance in mice as reported in humans, with *Tbc1d24$^{+/R360L}$* mice showing no visible seizures, and comparable survival with wild type, *Tbc1d24$^{+/+}$,* mice. Although the open field test indicated normal locomotor function, the early death of *Tbc1d24$^{R360L/R360L}$* mice at P17 limits more complex cognitive behavioural analysis.

Expression studies of the *Tbc1d24*$^{R360L/R360L}$ mutant reveal a 90.9% decrease in protein expression, but no significant decrease in mRNA expression, which suggests that post-translational degradation of the mutant protein may occur. Co-immunoprecipitation confirms the interaction between Tbc1d24 and V1 subunits of the V-ATPase, supporting a functional role for Tbc1d24 in vesicle acidification. Further evidence is needed to understand the importance of this interaction, and its potential links with the aetiology of epilepsy in the *Tbc1d24*$^{R360L/R360L}$ mutant.

3.3 Characterization of the *Tbc1d24*$^{P135L/P135L}$ mutant

3.3.1 Phenotype of *Tbc1d24*$^{P135L/P135L}$

In humans, the *Tbc1d24*$^{P135L/P135L}$ mutation shows an autosomal dominant pattern of inheritance associated with tonic-clonic and myoclonic epilepsy [144]. Therefore, it was interesting to ascertain whether a phenotype would be observed in the heterozygous carrier mice. Indeed, the founder F0/F1 CRISPR positive P135L carrier lines used to establish the colony had no breeding issues or early, unexpected fatalities. Subsequently, a small cohort of heterozygous mice, *Tbc1d24*$^{+/P135L}$, were aged to 12 months, and no adverse effects were observed. The intercrosses were also established, and in very similar circumstances to the R360L mutant, pups were found dead at P17, which were genotyped to be homozygous. The homozygous *Tbc1d24*$^{P135L/P135L}$ mutants also showed the same seizure profile as *Tbc1d24*$^{R360L/R360L}$ mutants in live mice at P16, displaying a hyperactive phase preceding seizures, followed by post-ictal recovery or death. P16 was determined to be the humane end point for mice homozygous for the P135L mutation. Seizures were observed in both male and female *Tbc1d24*$^{P135L/P135L}$ mutants.

In summary, these data are contrary to the original P135L mutation described that is autosomal dominant, with the patient heterozygous for the mutation experiencing epileptic seizures [144]. Unfortunately, due to time constraints, no further behavioural or pathological analysis was performed on the *Tbc1d24*$^{P135L/P135L}$ mutant.

3.3.2 Expression studies in the *Tbc1d24*$^{P135L/P135L}$ mutant

3.3.2.1 *Tbc1d24*$^{P135L/P135L}$ mutant shows decreased Tbc1d24 protein expression

To investigate the effect of the P135L mutation on Tbc1d24 protein levels, Western blotting was performed using protein extracted from whole brains of *Tbc1d24*$^{+/+}$, *Tbc1d24*$^{+/P135L}$ and *Tbc1d24*$^{P135L/P135L}$ mice. As shown in **Figure 3.11**, Tbc1d24 protein expression in the *Tbc1d24*$^{P135L/P135L}$ mutant was 94.2% decreased compared to Tbc1d24$^{+/+}$ ($p < 0.0001$), and 89.4% decreased compared to *Tbc1d24*$^{+/P135L}$ ($p = 0.0002$). *Tbc1d24*$^{+/P135L}$ showed intermediary protein expression between *Tbc12d4*$^{+/+}$ and *Tbc1d24*$^{P135L/P135L}$, with a 45.5% reduction in expression compared with *Tbc1d24*$^{+/+}$ ($p = 0.0002$). The P135L mutation appears to cause near-total knockdown in expression of Tbc1d24 protein, similar to the level seen in *Tbc1d24*$^{R360L/R360L}$ mice.

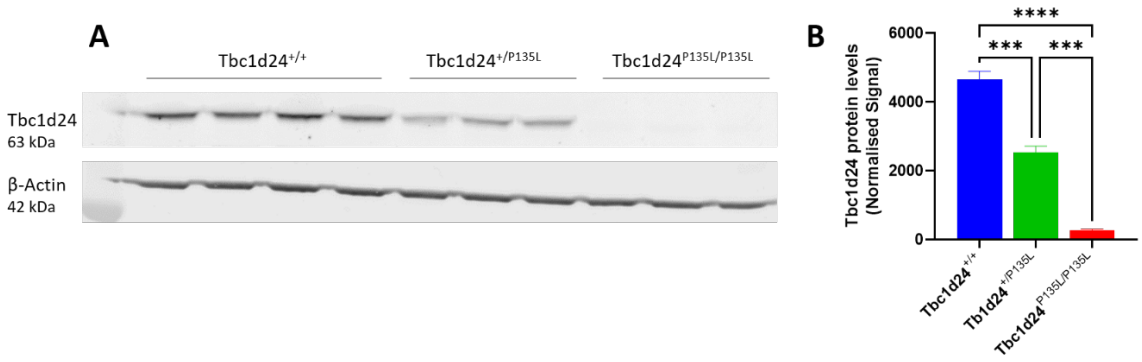


Figure 3.11 The* Tbc1d24$^{P135L/P135L}$ *mutant shows knock down in protein levels. *Western blotting was performed using protein extracted from whole brains of* Tbc1d24$^{+/+}$, Tbc1d24$^{+/P135L}$ *and* Tbc1d24$^{P135L/P135L}$ *male and female mice at P16. (**A**) Representative western blot showing bands at 63kDa for Tbc1d24 and at 42kDa for β-Actin. (**B**) Quantification of Tbc1d24 protein levels normalized to β-Actin. One way ANOVA with Tukey's multiple comparisons test was performed. Graph shows mean ± SEM (n = 3 – 4).*

3.3.2.2 Expression and stability of the mutant *Tbc1d24*^{P135L} allele

To investigate expression of *Tbc1d24* in the *Tbc1d24*$^{P135L/P135L}$ mutant at the mRNA level, RT-qPCR was performed using mRNA extracted from frontal cortex of *Tbc1d24*$^{+/+}$ and *Tbc1d24*$^{P135L/P135L}$ mice at P16. As shown in **Figure 3.12A**, no difference was observed in the expression of *Tbc1d24* mRNA between *Tbc1d24*$^{+/+}$ and *Tbc1d24*$^{P135L/P135L}$. Allele-specific RT-qPCR, using probes designed to specifically amplify either the wild type or

P135L mutant transcript of *Tbc1d24*, indicating that both wild type and P135L mutant alleles are expressed at similar levels (**Figure 3.12B**).

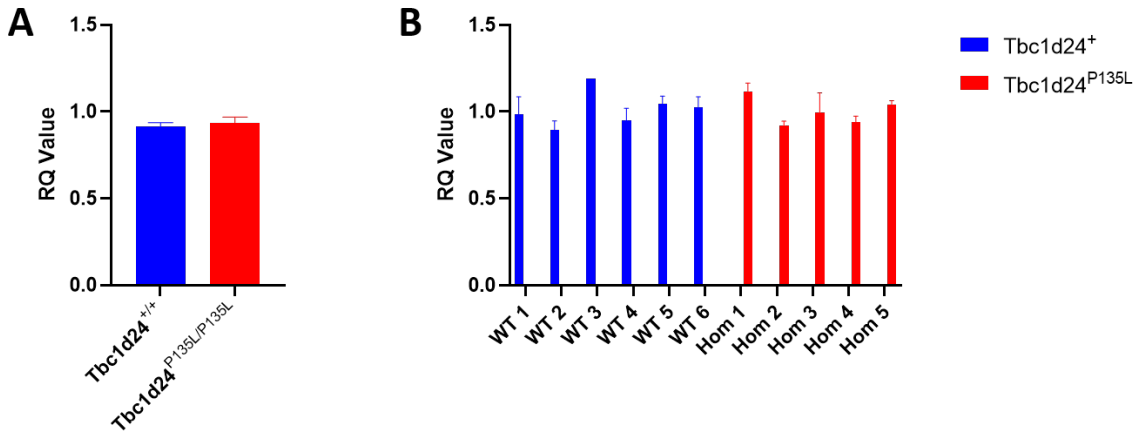


Figure 3.12 Expression analysis by RT-qPCR shows similar expression of Tbc1d24 mRNA in* Tbc1d24$^{P135L/P135L}$ *and* Tbc1d24$^{+/+}$.** ***A *- RT-qPCR to measure expression of* Tbc1d24 *was performed using mRNA extracted from* Tbc1d24$^{+/+}$ *(blue), and* Tbc1d24$^{P135L/P135L}$ *(red) whole brains of male and female mice at P16 (n = 5-6).* ***B*** *- Allele specific RT-qPCR was performed using specific probes for* Tbc1d24^{+} *(wild type allele, blue) and* Tbc1d24^{P135L} *(mutant allele, red). mRNA was extracted from frontal cortex at P16. RQ values were plotted for individual mice, with* Tbc1d24$^{+/+}$ *(WT) and* Tbc1d24$^{R360L/R360L}$ *(Hom) showing specificity of the probes (n = 5 - 6). Allele-specific RT-qPCR (excepting analysis) was performed by D. Williams, MRC Harwell. Values show mean ± SEM.*

3.3.3 Summary of findings in the *Tbc1d24$^{P135L/P135L}$* mutant

The P135L mutation in Tbc1d24 leads to epilepsy in humans, and recurrent seizures are observed in the *Tbc1d24$^{P135L/P135L}$* mutant, although the mouse shows a different pattern of inheritance from that reported in humans. The mutation shows autosomal dominant inheritance in patients, but appears to show recessive, loss-of-function inheritance in the mouse mutant, with *Tbc1d24$^{+/P135L}$* mice showing no seizures but a significant decrease in Tbc1d24 protein expression, with no significant decrease in *Tbc1d24* mRNA expression, similarly to the *Tbc1d24$^{R360L/R360L}$* mutant. This model suggests that protein expression level may be driving the seizures in the two loss-of-function mouse models.

3.4 Characterization of the *Tbc1d24$^{INS2/INS2}$* mutant

The *Tbc1d24$^{INS2/INS2}$* mutant contains an insertional null allele that leads to an early stop codon in *Tbc1d24*. Given the predicted disruption caused by this mutation on the protein product, it was not known whether homozygous embryos would be produced. In the initial intercrossing of mice heterozygous for the mutation, litters were produced containing mice

that were found dead at P0, which were subsequently genotyped to be homozygous for the INS2 mutation, *Tbc1d24*$^{INS2/INS2}$. No homozygous mice survived to weaning age (approximately P21), which is when genotyping is routinely performed. Embryo harvesting was performed at E15, and several embryos were found to be homozygous. Later, a live birth was observed of mice subsequently genotyped to be *Tbc1d24*$^{INS2/INS2}$ mutants; these pups were responsive to touch. Therefore, the INS2 mutation was determined to cause early postnatal death, at approximately P0. The *Tbc1d24*$^{INS2/INS2}$ embryo exhibits pallor suggestive of anaemia from E14.5, which is explored in depth in Chapter Four. Heterozygous *Tbc1d24*$^{+/INS2}$ mice show survival comparable to wild type *Tbc1d24*$^{+/+}$ littermates, and do not exhibit pallor.

3.4.1 Expression studies of *Tbc1d24*$^{INS2/INS2}$

3.4.1.1 The *Tbc1d24*$^{INS2/INS2}$ mutant shows significant reduction in abundance of Tbc1d24 protein expression

To investigate the effect of the INS2 mutation on Tbc1d24 protein levels, Western blotting was performed using protein extracted from whole brains of *Tbc1d24*$^{+/+}$, *Tbc1d24*$^{+/INS2}$ and *Tbc1d24*$^{INS2/INS2}$ mice at E18.5. As shown in **Figure 3.13**, Tbc1d24 protein expression in the *Tbc1d24*$^{INS2/INS2}$ mutant was 93.5% decreased compared to *Tbc1d24*$^{+/+}$ ($p < 0.0001$), and 82.8% decreased compared to *Tbc1d24*$^{+/INS2}$ ($p = 0.0116$). Given the severity of the mutation, which prevents expression of a full-length Tbc1d24 protein produce, it is likely that the knockdown in protein expression is closer to 100% in the *Tbc1d24*$^{INS2/INS2}$ mutant, and that the small level of signal measured is due to background. *Tbc1d24*$^{+/INS2}$ showed intermediary protein expression between Tbc1d24+/+ and *Tbc1d24*$^{INS2/INS2}$, with a 61.8% reduction in expression compared with Tbc1d24+/+ ($p = 0.0004$). The INS2 mutation thus causes dramatic reduction in abundance of Tbc1d24 protein, therefore, loss of Tbc1d24 expression is incompatible with life.

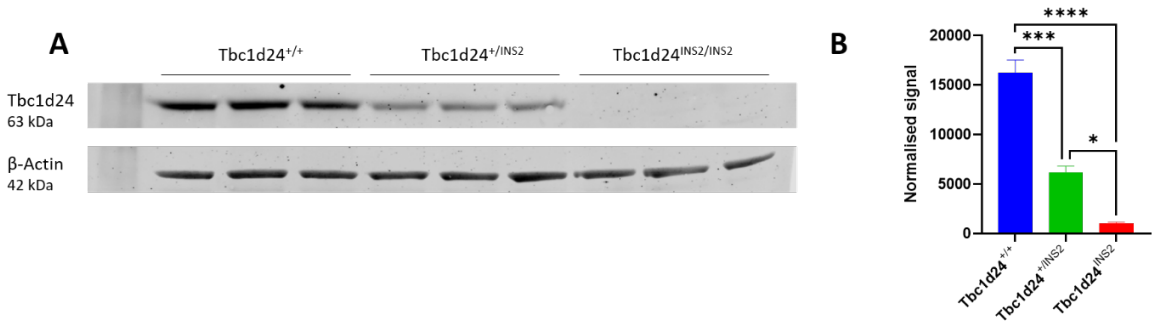


Figure 3.13 Reduced abundance of Tbc1d24 protein in the* Tbc1d24$^{INS2/INS2}$ *mutant. *Western blotting was performed using protein extracted from whole brains of* Tbc1d24$^{+/+}$, Tbc1d24$^{+/INS2}$ *and* Tbc1d24$^{INS2/INS2}$ *male and female mice at E18.5. (**A**) Representative western blot showing bands at 63kDa for Tbc1d24 and at 42kDa for β-Actin. (**B**) Quantification of Tbc1d24 protein levels normalized to β-Actin. One way ANOVA with Tukey's multiple comparisons test was performed. Graph shows mean ± SEM (n = 3).*

3.4.1.2 Partial knockdown of *Tbc1d24* mRNA expression in *Tbc1d24*$^{INS2/INS2}$

To investigate expression of *Tbc1d24* mRNA in the *Tbc1d24*$^{INS2/INS2}$ mutant, RT-qPCR was performed using mRNA extracted from whole brains of *Tbc1d24*$^{+/+}$, *Tbc1d24*$^{+/INS2}$ and *Tbc1d24*$^{INS2/INS2}$ at E15.5. As shown in **Figure 3.14**, RT-qPCR showed decreased expression of *Tbc1d24* mRNA in *Tbc1d24*$^{INS2/INS2}$, with a mean decrease of 55.9% compared with *Tbc1d24*$^{+/+}$ ($p < 0.0001$), and mean decrease of 33.6% compared with *Tbc1d24*$^{+/INS2}$ ($p = 0.0004$). *Tbc1d24*$^{+/INS2}$ showed an intermediary expression of

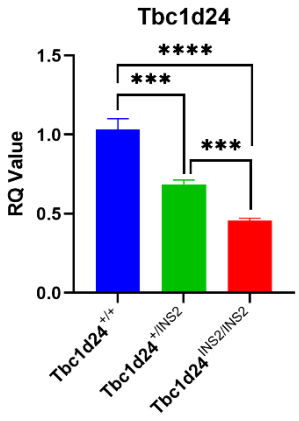


***Figure 3.14 Expression of* Tbc1d24 *mRNA is decreased in* Tbc1d24$^{INS2/INS2}$ *compared with* Tbc1d24$^{+/+}$.** *RT-qPCR was performed using mRNA extracted from cortex of male and female* Tbc1d24$^{+/+}$ *(blue),* Tbc1d24$^{+/INS2}$ *(green) and* Tbc1d24$^{INS2/INS2}$ *(red) mice at E18.5. Expression of the gene* Tbc1d24 *was measured. One way ANOVA with Tukey's multiple comparisons test was performed using ΔCT values. Values show mean ± SEM (n = 4).*

Tbc1d24 mRNA between *Tbc1d24*$^{+/+}$ and *Tbc1d24*$^{INS2/INS2}$, with a mean decrease of 33.6% compared with *Tbc1d24*$^{+/+}$ ($p < 0.0001$).

Of note, RNA-Seq was also performed using mRNA extracted from *Tbc1d24*$^{INS2/INS2}$ and *Tbc1d24*$^{+/+}$ brain cortices at E18.5 (see Chapter Four). Expression of *Tbc1d24* was shown to be decreased in *Tbc1d24*$^{INS2/INS2}$, with a fold change of 0.58 (FDR = 6.7 x 10^{-84}), which is consistent with the results of RT-qPCR.

3.4.1.3 *In situ* hybridization of *Tbc1d24* in the *Tbc1d24*$^{INS2/INS2}$ mutant

Expression of *Tbc1d24* has been demonstrated in the developing mouse brain, where expression increases over time, and in cultured E18.5 mouse hippocampal neurons, which also show increasing *Tbc1d24* expression after culturing *in vitro* [105]. In order to visualise *Tbc1d24* expression in the *Tbc1d24*$^{INS2/INS2}$ mutant as demonstrated by RT-qPCR of whole brain and RNA-Seq of prefrontal cortex, ISH was performed using sagittal sections of mouse embryonic brains. As shown in **Figure 3.15**, *Tbc1d24* is widely expressed in the *Tbc1d24*$^{+/+}$ brain at E18.5, particularly in the outer layers of the cerebral cortex. At E16.5,

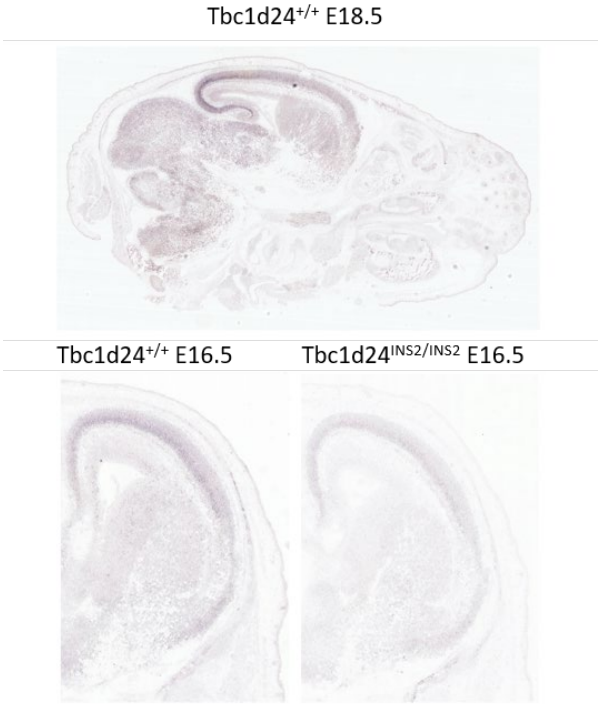


Figure 3.15 Decreased expression of* Tbc1d24 *in the developing* Tbc1d24$^{INS2/INS2}$ *brain. *Representative images showing* Tbc1d24 *expression in the developing mouse brain.* ***Top****: expression of* Tbc1d24 *in sagittal section of male Tbc1d24*$^{+/+}$ *embryonic head at E18.5.* ***Bottom****: expression of* Tbc1d24 *in coronal sections of* Tbc1d24$^{+/+}$ *(left) and* Tbc1d24$^{INS2/INS2}$ *(right) brains at E16.5.*

expression of *Tbc1d24* is visible in the cortex of *Tbc1d24*$^{+/+}$ embryo. However, a visible reduction in *Tbc1d24* expression is observed in the *Tbc1d24*$^{INS2/INS2}$ cortex compared to *Tbc1d24*$^{+/+}$, which is consistent with the qPCR and RNA-seq expression data.

3.4.2 Neuropathology of *Tbc1d24*$^{INS2/INS2}$

Increasing levels of *Tbc1d24* expression at E18.5 is correlated with terminal neuronal differentiation [105], which is crucial for the maturation of electrophysiological properties and the formation of functional neural networks [166]. Expression of *TBC1D24* constructs with pathological mutations leads to neurite outgrowth defects in mouse cortical culture *in vitro*, compared with transfection with wild type *TBC1D24*, suggesting that TBC1D24 is required for neuronal maturation [106]. Therefore, loss of *Tbc1d24* expression in the *Tbc1d24*$^{INS2/INS2}$ mutant may disrupt this key process.

3.4.2.1 Gross anatomy of the *Tbc1d24*$^{INS2/INS2}$ mutant brain

In order to visualise gross anatomy of the brain in the *Tbc1d24*$^{INS2/INS2}$ mutant, Nissl staining was performed using sagittal sections of embryonic heads at E18.5, with *Tbc1d24*$^{+/+}$ littermate controls. As shown in **Figure 3.16**, *Tbc1d24*$^{+/+}$ and *Tbc1d24*$^{INS2/INS2}$ brains show no striking differences in morphology of the developing cortex, cerebellum, hippocampus or midbrain.

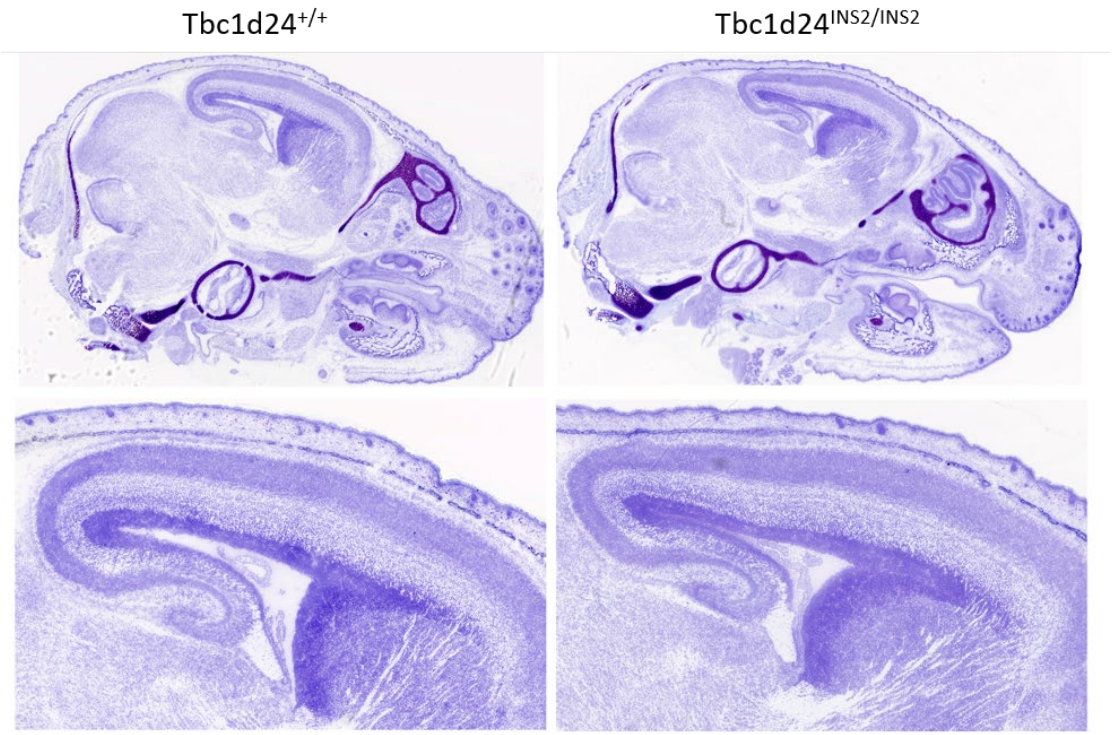


Figure 3.16 Comparable gross morphology between* Tbc1d24$^{+/+}$ *and* Tbc1d24$^{INS2/INS2}$ *brain shown by Nissl staining. *Representative images of Nissl-stained embryonic heads at E18.5. Top: sagittal sections of heads, showing comparable structural morphology between male* Tbc1d24$^{+/+}$ *(left) and* Tbc1d24$^{INS2/INS2}$ *(right) brains at E18.5. Bottom: Dorsal and medial pallium at greater magnification. The dorsal and medial pallium develop into the cerebral cortex and hippocampus, respectively.*

3.4.2.2 Cortical layer disruption in *Tbc1d24$^{INS2/INS2}$* mutant

In addition to its effects on neurite outgrowth [106] and presynaptic function [136], Tbc1d24 has been shown to play an important role in cranial neural crest (CNC) cell migration, through its interaction with ephrinB2, mediated by Dishevelled (Dsh) [167]. Disruption of this interaction leads to defective CNC migration. Knockdown of Tbc1d24 in rat cerebral cortical neurons *in vivo* was demonstrated to impair axonal projections, including callosal projections connecting the two cerebral hemispheres [135]. In order to examine cortical layer patterning in the *Tbc1d24$^{INS2/INS2}$* mutant, immunohistochemistry (IHC) was performed on coronal sections of *Tbc1d24$^{+/+}$* and *Tbc1d24$^{INS2/INS2}$* brains at E18.5, using antibodies against cortical layer markers Satb2 (Layers 2 - 4), Ctip2 (Layer 5) and Tbr1 (Layer 6). Measurements were taken of the cortical layer widths, and the distance from the outer edge of each layer to the edge of the developing cortex. As shown in **Figure 3.17**, no difference between the *Tbc1d24$^{+/+}$* and *Tbc1d24$^{INS2/INS2}$* brains was observed in the

widths of any of the cortical layers. Interestingly, a decrease in the distance from layer to cortex edge was observed for both Ctip2 ($p = 0.0002$) and Tbr1 ($p = 0.0071$), suggesting a potential disruption in cortical layer patterning caused by the INS2 mutation in Tbc1d24.

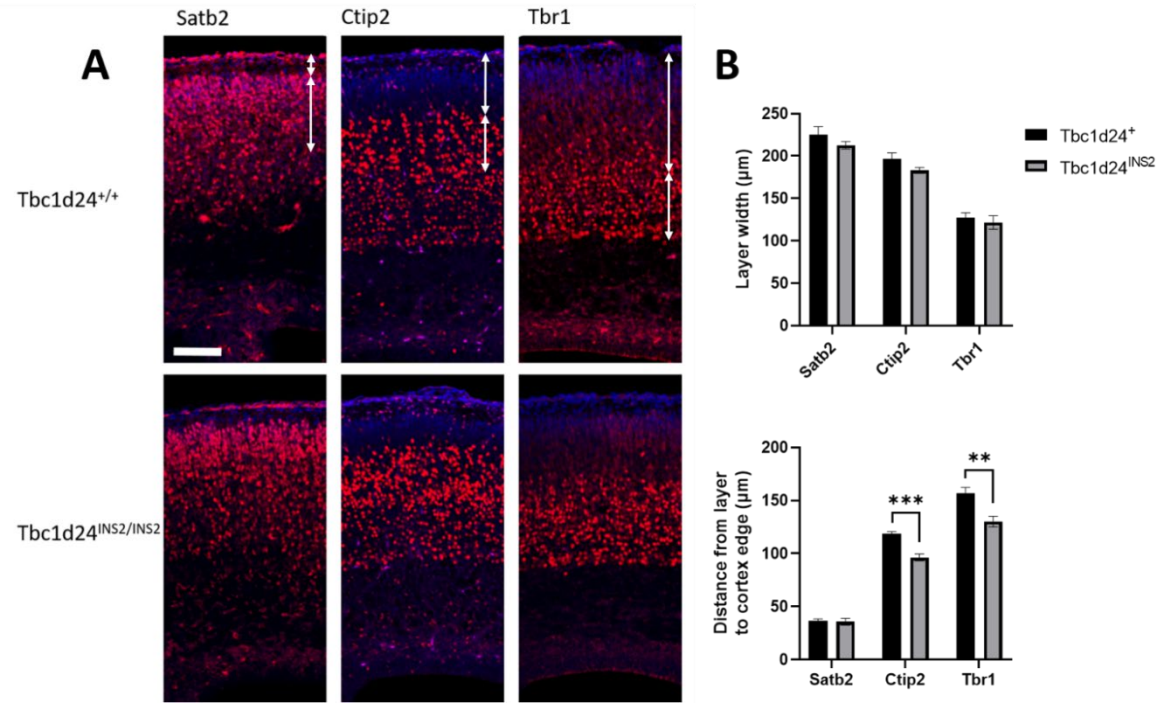


Figure 3.17 Disruption in patterning of the developing cortex in the* Tbc1d24$^{INS2/INS2}$ *mutant. *IHC staining of layer markers Satb2 (L2-4), Ctip2 (L5) and Tbr1 (L6) was performed using coronal sections of male and female* Tbc1d24$^{+/+}$ *and* Tbc1d24$^{INS2/INS2}$ *brains at E18.5.* ***A*** *– Representative images of developing cortex of* Tbc1d24$^{+/+}$ *(top) and* Tbc1d24$^{INS2/INS2}$ *(bottom), at 20x magnification. From left to right, Satb2, Ctip2 and Tbr1 markers in red showing stained neurons. All markers counterstained with Hoescht 33342 in blue. Scale bar of 100 µm. Arrows marked on* Tbc1d24$^{+/+}$ *showing measurements taken.* ***B*** *– Measurements were made of layer width (top, corresponding to top arrows in* ***A****) and distance from layer to cortex edge (bottom, corresponding to bottom arrows in* ***B****). Student's t-tests performed between biological groups (N = 3, measurements in triplicate).*

3.4.3 Summary of findings in the *Tbc1d24$^{INS2/INS2}$* mutant

The INS2 mutation in Tbc1d24, which causes an early stop codon in *Tbc1d24*, is postnatally lethal in *Tbc1d24$^{INS2/INS2}$* mutant mice. Expression studies of the mutant reveal that expression of Tbc1d24 protein is decreased by 88.0% compared with *Tbc1d24$^{+/+}$* mice, and *Tbc1d24* mRNA is decreased by 55.9%. In addition, ISH shows general knockdown in *Tbc1d24* expression, including in the cortex. The heterozygous *Tbc1d24$^{+/INS2}$* mice do survive to birth, although they show 33.6% decrease in *Tbc1d24* mRNA expression compared with *Tbc1d24$^{+/+}$* littermates.

Neuropathological studies of the *Tbc1d24*$^{INS2/INS2}$ mutant show disruption in the organisation of developing cortical layers, with layer 5 and layer 6 markers closer to the outer edge of the developing cortex, suggesting defects in neuronal migration. Overall, the *Tbc1d24*$^{INS2/INS2}$ mutant supports a crucial role for Tbc1d24 in neurological function and development.

3.5 Discussion

3.5.1 The phenotypes of Tbc1d24 mutant mouse lines

In this chapter, three mouse models of *Tbc1d24* mutations have been characterized, which has provided insight into the function of Tbc1d24 and the pathogenic consequences of its dysfunction. Two human pathological mutations in *TBC1D24* have been modelled, and both the *Tbc1d24*^{R360L} and *Tbc1d24*^{P135L} mouse lines successfully display recurrent seizures, similar to the epileptic phenotype observed in human patients. These models show promise for use in future preclinical testing of AEDs, as they exhibit recurrent, spontaneous seizures within predictable timeframes. The *Tbc1d24*^{INS2} mouse model has provided a useful null model of Tbc1d24, and its embryonic lethal phenotype has highlighted the critical importance of functional Tbc1d24 expression, while still providing a tool that can be used for the generation of primary cell cultures.

Despite the original report that the epilepsy-associated P135L mutation shows an autosomal dominant pattern of inheritance in patients – hence the initial choice of the mutant - [144], an autosomal recessive pattern of inheritance of the same clinical mutation has been described more recently. Sequencing of a patient presenting with epilepsy and deafness revealed the P135L mutation was inherited as a compound heterozygous mutation with another *TBC1D24* mutation, R227W. No clinical features were identified in the carrier P135L parent, arguing against dominant inheritance for the mutation; this is also consistent with the loss-of-function recessive inheritance observed in the *Tbc1d24*^{P135L} mouse. It is unclear why the mutation was originally reported as showing dominant inheritance [144], although one explanation is differing genetic backgrounds of the two clinical populations.

Some mouse models of epilepsy exhibit variable severity based on genetic background, for example, the Scn2a^{Q54} transgenic mouse, which enabled the identification of the epilepsy modifier gene *Cacna1g* through RNA-Seq analysis [168]. While all of the Tbc1d24 mutants characterized in this chapter are maintained of a C57BL/6J background, the *Tbc1d24^{R360L}* mouse line was intercrossed onto a DBA/2J background in order to investigate the effect of genetic background on phenotypic severity. The offspring of this intercross showed the same pattern of survival shown by the *Tbc1d24^{R360L}* mouse line of C57BL/6J background, with early death from P18 exhibited in homozygous *Tbc1d24$^{R360L/R360L}$* mice (data not shown). The same genetic background, C57BL/6J, was also used to model the Tm1b, F251L and S324Tfs*3 mutations, enabling comparison between the mutations [136] [137] [169].

During this project, several mouse models of mutations in *TBC1D24* were generated, providing some invaluable insight into the function of TBC1D24, and the wide-ranging consequences of its dysfunction. Comparison between all known mouse models of Tbc1d24 mutations is shown in **Table 3.1**. The addition of *Tbc1d24^{R360L}*, *Tbc1d24^{P135L}* and *Tbc1d24^{INS2}* mouse lines builds on a growing body of research into the function and dysfunction of TBC1D24. The *TBC1D24* mutation F251L, associated with epilepsy in humans, causes spontaneous seizures and early death in mice, which was shown to be associated with destabilization of Tbc1d24 protein and reduced synaptic density [137]. Similarly, the human *TBC1D24* mutation S324Tfs*3, which leads to a premature stop codon in a splice variant of *TBC1D24*, is associated with early infantile epileptic encephalopathy, and, when modelled in mice, causes spontaneous seizures from P15, and early death [169]. Somewhat surprisingly, mouse models of TBC1D24 mutations associated with deafness in humans did not show any hearing loss, but some of these homozygous mutations led to seizures and early death [170]. It was determined in the same study (contrary to earlier published work) that *TBC1D24* is expressed in the hair cells of the inner ear in humans, but

surprisingly not in mice [170]. This highlights that recapitulating all the pleotropic aspects of TBC1D24 dysfunction using the mouse may not be possible.

Mouse models of Tbc1d24 dysfunction show striking similarity in the seizure phenotypes displayed, with near identical timing across all models; mice display seizures from approximately P15, and show early mortality at around P20 [94, 137, 170, 169]. The timing of the seizure phenotype of the S324Tfs*3 mouse mutant was originally ascribed to the alternate splicing of the mutant exon, as the appearance of the exon carrying the mutation was found to correlate with the onset of seizures [169]. However, this does not explain the seizure time course of other mutations, at different exonic locations within *Tbc1d24*. Rather, the timing of seizures may relate to key neurodevelopmental milestones, such as the dramatic increase in brain volume that takes place in mice between P7 and P20 [171]. This is supported by increasing expression of *Tbc1d24* in mouse hippocampal neurons during culturing *in vitro* for 14 days, correlating with the terminal differentiation of neurons [105].

Also consistent across mouse models of Tbc1d24 dysfunction is the significant reduction in abundance of protein expression, which is seen in the $Tbc1d24^{R360L}$, $Tbc1d24^{P135L}$ and $Tbc1d24^{INS2}$ mutants, in addition to the $Tbc1d24^{F251L}$ model [105] (protein expression was not measured in the $Tbc1d24^{S324Tfs*3}$ mouse, nor in any of the deafness-associated mutants) [169, 170] (**Table 3.1**). Mutations across both the TBC and TLDc domains of Tbc1d24 can therefore cause reduction in abundance of protein expression, coincident with similar phenotypes, indicating that these mutations are loss-of-function. This is in line with findings from a small number of patient fibroblasts that have been tested, where a significant decrease in expression of TBC1D24 protein was observed, with no significant decrease in *TBC1D24* mRNA expression [172]. That point mutations within *Tbc1d24* lead to dramatic decrease in Tbc1d24 protein levels likely indicates that the mutations cause functional disruption of the protein. The recent solving of the TLDc crystal structure of human NCOA7-B revealed that the arginine residue disrupted by the R360L

mutation is involved in a salt-bridge interaction with another highly conserved residue, Glu139 [173]. Mutations at either residue were predicted to break this interaction, causing destabilization of a crucial long loop within the tertiary structure of the TLDc domain. It is probable that loss-of-function mutations of Tbc1d24 cause similar destabilization of its protein structure, resulting in severe phenotypic consequences as seen in the Tbc1d24 mouse mutants.

Misfolded proteins are degraded in the cell through several mechanisms, including the ubiquitin-proteasome system (UPS) and the autophagy-lysosome system [174]. In UPS, ubiquitin is activated by an enzyme cascade involving three enzymes – E1, E2 and E3 – and then binds to a protein targeted for degradation. The protein is then able to be recognised by the 26S proteasome, a multimeric protease enzyme with a proteolytic core, which then catalyses the degradation of the protein [175]. In the autophagy-lysosome system, proteins targeted for degradation are encapsulated within a vesicle, which fuses with lysosome in which both the denaturing acidic environment and the presence of hydrolase enzymes causes degradation of the protein cargo [176]. Both UPS and autophagy have been shown to mediate degradation of misfolded tau protein, involved in the pathogenesis of Alzheimer's disease [177]. However, disruption in the interaction between Tbc1d24 and the V-ATPase may lead to dysfunctional lysosomal acidification (further discussed in this chapter and later in thesis), therefore it may be predicted that the reduction in abundance of Tbc1d24 protein in the mutant mice is primarily due to degradation by the UPS.

Studies of the behavioural effects of mutations in Tbc1d24 have been limited by phenotypic severity. However, acute knockdown of Tbc1d24 by hippocampal injection with Tbc1d24-shRNA has been shown to cause behavioural changes. Mice with Tbc1d24 knockdown showed increased travel distance in OF testing, indicating hyperactivity, with increased anxiety-like behaviour indicated by preference for the peripheral zones of the arena [137]. These mice also showed reduced fear learning behaviours in the fear

conditioning test. Interestingly, mice heterozygous for the F251L mutation, which displayed normal survival (unlike homozygous mice), showed the same reduction in fear learning, suggesting that impaired expression of Tbc1d24 causes impaired synaptic function, although no increase in hyperactivity was observed [137]. The effect of Tbc1d24 protein expression on hyperactivity may therefore be dose-dependent. Importantly, despite the appearance of ataxia in patients harbouring *TBC1D24* mutations [106], in addition to patients with loss-of-function mutations in the TLDc gene *OXR1* [178] and the *Oxr1* knockout mouse, *bella* [143], this has not been studied in loss-of-function Tbc1d24 mouse mutants. Ataxia can be studied in mice using phenotyping tests such as gait analysis and the Locotronic motor coordination test, although many phenotyping tests are designed for use on adult mice [179]. Therefore, a conditional loss-of-function mouse mutant may be needed to study the effect of knockdown of Tbc1d24 expression on ataxia (see **Chapter 6**). In addition, more detailed studies of neuropathology of the cerebellum in the mouse models is warranted, given the multiple examples of cerebellar atrophy across TBC1D24-associated disorders [131, 132, 106, 180]. Importantly, the Oxr1 null model exhibits significant apoptosis in the granule cell (GC) layer of the cerebellum from P18 onwards, with signs of neuroinflammation [143]. However, there is no indication of activation of either apoptotic or neuroinflammatory pathways shown by microarray of the *Tbc12d4*^{R360L} mutant (**Chapter Four**). One possible explanation for this is that the end point of the *Tbc12d4*^{R360L} mutant at P16 may be too early to detect such markers.

Electrophysiological studies using the *Tbc1d24*^{R360L} mouse line have recently shed light on additional features of the brain that may underlie the seizure activity (D. Rial, T. Soares, Oliver group, unpublished). Single cell and local field potential recordings in L5 cortical neurons in the *Tbc1d24*$^{R360L/R360L}$ mutant at P16 show an elevated baseline spike frequency, confirming neuronal hyperexcitability. Interestingly, this is not detected in the hippocampus or striatum. One further experiment was to investigate the potential role of glutamate as a key excitatory neurotransmitter, and whether transport via the glutamate

transporter 1 (GLT-1) was playing a role. GLT-1 is responsible for clearing the excitatory neurotransmitter glutamate from the synaptic cleft, and maintaining a low level of extracellular glutamate prevents excitotoxicity [30]. Pharmacological blocking of Glt-1 using DL-threo-beta-benzyloxyaspartate (DL-TBOA) showed a lower saturation threshold in *Tbc1d24*$^{R360L/R360L}$ neurons compared with wild type control, indicating decreased functionality, formation or expression of Glt-1 in the mutant mouse, which was confirmed by Western blot. Thus, the epileptic phenotype and hyperexcitability of the *Tbc1d24*$^{R360L/R360L}$ mutant may in part be related to decreased astrocytic glutamate clearance.

Earlier models of human pathological Tbc1d24 mutations demonstrated alterations in neuronal morphology and neurite outgrowth. Knockdown of *Tbc1d24* expression in N2a culture led to reduced neurite outgrowth [136]. However, the effects of altered neuronal morphology on anatomical organisation of the brain have not been previously quantified in a mouse model of Tbc1d24 dysfunction. The *Tbc1d24*$^{INS2/INS2}$ mutant shows a reduction in distance between the edge of the developing cortex and layers 5 and 6, indicating disruption in cortical layer patterning as a result of knockdown in *Tbc1d24* expression. Cortical lamination defects are observed in mice lacking the protein p35, which is needed to activate a neuronal specific kinase, cdk5. The p35-deficient mice also show seizures and early lethality, although the cortical defects are more severe than those observed in the *Tbc1d24*$^{INS2/INS2}$ mutant, with general disorganization throughout the cortex and enlarged ventricles [181]. Network alterations have been shown to cause seizures in patients of temporal lobe epilepsy (TLE), due to disruption in functional connections within the cortical network leading to increased seizure susceptibility [182]. Tbc1d24 has been shown to form a complex with the cell-surface signalling ligand EphrinB2, mediated by the scaffold protein Dishevelled (Dsh), with this complex regulating contact inhibition of locomotion (CIL) during neural crest migration [167]. Morpholino oligonucleotide (MO) silencing of Tbc1d24 causes defects in CNC migration in tailbud stage *Xenopus* embryos, due to the disruption of CIL

and subsequent invasion of neural crest tissue into other neural crest tissue. The cortical patterning defects observed in the *Tbc1d24*$^{INS2/INS2}$ mutant, which shows reduction in expression of *Tbc1d24* mRNA and protein, may result from disruption of the interaction between Tbc1d24 and ephrinB2.

Table 3.1 Mouse models of human pathological mutations in Tbc1d24 to date.

Tbc1d24 Mutation	Human disease and inheritance	Mouse phenotype	Tbc1d24 expression	Associated findings	Ref
Tm1b (Heterozygous expression of tm1b allele, early stop codon at 380)	N/A	None	50% expression of protein. 50% expression of mRNA.	Reduced neurite growth in hippocampal, cortical neurons. Increased sensitivity to OS. Reduced mEPSP frequency at excitatory synapses. Reduced endocytosis and SV recycling in primary neurons. Increased endosomal volume.	[136]
F251L (Within TBC domain)	Epilepsy Intellectual disability. Autosomal recessive	Spontaneous seizure Early death (P21) Adult het memory defect	>50% decrease in protein expression. No change in mRNA.	Increased neuronal excitability. Dendritic spine defects. Reduced synapse density.	[105] [137]
Acute viral knockdown of *Tbc1d24* in hippocampus	N/A	Memory defect. Anxiety-like behaviour.	>50% decrease in protein expression. No change in mRNA.	Dendritic spine defects.	[137]
S324Tfs*3 (frameshift with early stop codon)	Early infantile epileptic encephalopathy (EIEE). Autosomal recessive	Spontaneous (tonic clonic) seizure from P15 Early death (P21)	Not measured.	Tbc1d24 localization at TGN and hippocampal synapses (sites of endocytosis). No expression of *Tbc1d24* in mouse hair cells, contrary to findings in humans.	[169]
Asp70Tyr (Within TBC domain)	Deafness DFNB86	No deafness	Not measured		[170]
Ser178Leu (Within TBC domain)	Deafness DFNA65	No deafness	Not measured	Ser178 residue critical for stabilization of the TBC domain fold.	[170]
Ser324Thrfs*3/ His336GInfs*12 (No predicted domain)	N/A (Predicted DOORS or EIEE16 with deafness)	No deafness Spontaneous seizure Early death (P20)	Not measured		[170]
R360L (Within TLDc domain)	Progressive myoclonic epilepsy (PME), Neurodegeneration. Autosomal recessive	Spontaneous seizure from P15 Early death (P17)	90.8% decrease in protein expression. No change in mRNA	Disrupted interaction with v-ATPase subunits. Hyperexcitability of neurons. Reduced neurite outgrowth in hippocampal cultures.	[132] [106]
P135L (Within TBC domain)	Epilepsy. Likely autosomal recessive	Spontaneous seizure from P15 Early death (P17)	94.2% decrease in protein expression No change in mRNA		[144] [183]
INS2 (Nonsense early stop codon within TBC domain)	N/A	Postnatal lethal	93.5% (to 100%) decrease in protein expression. 55.9% decrease in mRNA expression	Cortical layer marker disruption	

3.5.2 The interaction between the TLDc family and the V-ATPase

Functional synaptic transmission relies on the packaging of neurotransmitters into vesicles, followed by their release at the appropriate place and time. Providing the electrochemical gradient for concentration of neurotransmitters into vesicles, the v-ATPase plays a vital role in neurotransmission [184]. Endocytosis and SV recycling require lysosomal acidification by the v-ATPase, and disrupted acidification is associated with neurological diseases such as AD, ALS and Parkinson's disease (PD) [185]. As shown in the Tbc1d24^{tm1b} mouse model, disruption of *Tbc1d24* expression results in impaired endocytosis and recycling of synaptic vesicles [147]. In the *Tbc1d24*^{S324Tfs*3} model, immunogold electron microscopy was used to investigate Tbc1d24 localization, which revealed that the protein associates with clathrin-coated vesicles of the trans-Golgi network and at synapses of hippocampal neurons, providing evidence for the role of TBC1D24 in vesicle trafficking and synaptic transmission. Furthermore, proteomic analysis of v-ATPase interactions has now revealed that members of the TLDc family, including TBC1D24, OXR1 and NCOA7, in addition to the TLDc domain itself, interact with the v-ATPase, suggesting a new role for the TLDc family as v-ATPase regulatory proteins [186]. Interestingly, certain deleterious TLDc mutations associated with neurological disease in humans, such as G376A in TBC1D24, were found to correspond to regions of the TLDc domain required for binding with the v-ATPase, indicating the severe pathological consequences of disruption of this interaction. Alternatively, this mutation may result in reduced protein abundance, as seen in the *Tbc1d24*^{R360L} and *Tbc1d24*^{P135L} mutants, resulting in loss-of-function due to post-translational events, rather than as a result of the site of the G376A mutation itself. Described in this chapter is the reduction of Tbc1d24 protein expression caused by the R360L mutation, such that no interaction is observed between Tbc1d24 and V1 subunits, as shown by co-immunoprecipitation. Given the importance of v-ATPase function in both synaptic transmission and SV recycling, the impairments in both processes observed in mouse models of human *TBC1D24* mutations suggests the functional importance of the interaction between Tbc1d24 and the v-ATPase.

Differences in phenotypic severity between the *Tbc1d24*$^{R360L/R360L}$ and *Tbc1d24*$^{INS2/INS2}$ mutants may be explained by the strength of disruption in the interaction between Tbc1d24 and the v-ATPase. While the R360L mutation causes loss of Tbc1d24 protein expression, the INS2 mutation is upstream of the TLDc domain, at position 135, thus any protein product of the *Tbc1d24*^{INS2} allele would be made up of only the first 135 amino acids of Tbc1d24. RNA expression of *Tbc1d24* is detected in the *Tbc1d24*$^{INS2/INS2}$ mutant, therefore a short Tbc1d24 protein product is possible, although unlikely due to post-transcriptional modification. Confirmation of this could be obtained using a C-terminal antibody. Moreover, the loss of the TLDc domain is likely to prevent any interaction with the V-ATPase. It is possible that some interaction with the V-ATPase is maintained in the *Tbc1d24*$^{R360L/R360L}$ mutant, for example, at other amino acid residues or at different subunits.

A mouse model of *Ncoa7* deletion was used to demonstrate the interaction between Ncoa7 and the V1 complex of the v-ATPase, and regulates the assembly of the V1/V0 complex. In primary cortical neurons, subcellular fractionation experiments showed that deletion of *Ncoa7* led to a significant reduction in V1 subunits in the membrane, despite no alteration in protein levels of V1 subunits overall, indicating that the V-ATPase complex assembly is disrupted by deletion of *Ncoa7* [187]. Deletion of *Ncoa7* was found to cause defects in lysosomal homeostasis in neurons, and led to a reduction in inhibitory contacts. The study found no changes in expression of either Tbc1d24 or Oxr1, suggesting a lack of compensatory mechanism amongst the TLDc family, which is consistent with the findings in this chapter. NCOA7 was shown by protein-lipid overlay assay to interact with membrane-associated phosphoinositides (PIPs) [187]. Similarly, solving of the crystal structure of the TBC1D24 orthologue *Sky* revealed a pocket within the TBC domain which enables bindings with PIPs [109]. PIPs have been shown to interact with the V-ATPase, and regulate activity through assembly of the complex [188, 189]. The interactions of TBC1D24 and NCOA7 with both the V-ATPase and membrane-bound PIPs provides evidence for the role of the TLDc family in anchoring the V-ATPase at vesicle membranes. The expectation that all

TLDc proteins share common functional interactions with the V-ATPase has been challenged by very recent cryo-EM studies that will be discussed further in Chapter 6.

It is now evident that disruption in function of the V-ATPase is involved in a wide range of neurological disorders, including epilepsy. The clinical overlap between V-ATPase mutations and TLDc family mutations supports a shared functional significance. Furthermore, there is a growing body of evidence for the role of the TLDc family in regulating v-ATPase function, supported by the association between mutations in proteins of this family, particularly *TBC1D24*, and epilepsy. However, further research is required to understand the link between lysosomal acidification defects and epileptic seizures. The potential mechanism may include the disruption of glutamate uptake, given the decrease in Glt-1 expression in the *Tbc1d24*$^{R360L/R360L}$, and the importance of glutamate-induced excitotoxicity in the aetiology of epileptic syndromes [190]. The vesicular glutamate transporters (VGLUT) transports glutamate into vesicles for neurotransmission, using the electrochemical gradient produced by proton transport of the V-ATPase [191]. Inhibition of the v-ATPase may prevent the concentration of glutamate into vesicles for release in neurotransmission. This could instead lead to increased intracellular glutamate, with deleterious consequences. Interestingly, the v-ATPase is inhibited by increased OS, as shown by H_2O_2 treatment of purified bovine synaptic vesicles, which also caused the inhibition of glutamate uptake [192]. Further research into the TLDc family and its interaction with the V-ATPase should, therefore, include study of neurotransmitters such as glutamate.

3.5.3 Concluding Remarks

In this chapter, three mouse models of Tbc1d24 dysfunction been characterized: *Tbc1d24*^{R360L}, *Tbc1d24*^{P135L} and *Tbc1d24*^{INS2}.

Surprisingly, the same phenotype is observed in both the *Tbc1d24*^{R360L} and *Tbc1d24*^{P135L} mutant models. However, both models display a very similar level of knockdown of Tbc1d24 protein expression, likely due to post-transcriptional events. It is likely that knock-down of Tbc1d24 protein drives the onset of seizures in these models, with

seizures prevented in mice heterozygous for either mutation due to sufficient protein expression.

Recurrent seizure phenotypes in the two viable models of epilepsy-related mutations in *TBC1D24* have provided useful *in vivo* tools that are now undergoing detailed electrophysiological analysis and could be used in future for testing of AEDs. Confirmation of the interaction between Tbc1d24 and V-ATPase subunits from tissue suggests an important mechanistic for further study.

Chapter 4: Exploring the functional effects of disruption of Tbc1d24 on the haematological system

4.1 Introduction

4.1.1 Anaemia and Erythropoiesis

Anaemia is a haematological disease characterised by decreased capacity of red blood cells (RBCs) to transport oxygen to body tissues, which affects approximately one third of the global population [193]. There is a wide range of anaemia subtypes, all with subtly different causes and pathology. For example, iron deficiency anaemia - representing half of all anaemia cases worldwide [194] - occurs when there is insufficient iron available to associate with haemoglobin [195]. Iron deficiency anaemia can be categorized as either absolute iron deficiency, when total body iron stores are depleted (for example due to diet), or functional iron deficiency, when iron is present in body stores but unable to reach sites of erythropoiesis such as the bone marrow [194]. Aplastic anaemia is caused by failure of stem cells in the bone marrow to produce blood cells of all types, which can be an inherited disease or acquired as a result of immune deficiency [196]. Haemolytic anaemias are caused by aberrant destruction of RBCs, which can occur due to enzyme deficiency [197], autoimmune attack [198], and unstable haemoglobin, as is the case in sickle cell anaemia [199]. Due to the wide variety of causes within anaemia, understanding of specific aetiology is required for effective treatments to be developed and for haematological dysfunction to be addressed.

The clinical diagnosis of anaemia is based on the concentration of the oxygen-carrying molecule haemoglobin [200]. Haemoglobin is made up of four globin subunits, each of which carries a molecule of heme. Heme contains iron, which is able to bind to oxygen (O_2) due to its variable transition state. Each heme molecule carries one oxygen molecule, and haemoglobin therefore transports up to four molecules of O_2 [201]. Haemoglobin is synthesised during erythropoiesis, when the combination of erythropoietin release from the kidneys, in tandem with the bioavailability of iron, stimulates the synthesis

of heme by an eight step enzymatic cascade in the mitochondria and cytosol, and for which δ-aminolevulinic acid synthase 2 (ALAS2) is the first and rate-limiting enzyme [202]. Disruption of Alas2 expression in mouse embryonic stem cells prevents the induction of the seven other heme synthetic pathway enzymes, in addition to globin proteins, indicating that Alas2 is vital for the formation of functional haemoglobin, and viable erythrocytes [203]. The accumulation of heme induces the transcription and translation of globin genes, which then associate with heme to form haemoglobin [204]. Both excess heme and excess globin are toxic. Diamond Blackfan anaemia (DBA) is caused by insufficient globin production leading to excess heme accumulation and the accumulation of reactive oxygen species (ROS), which causes cell death and the failure of erythropoiesis [205]. While in β-thalassemia, impaired production of β-globin results in the accumulation of α- globin, leading to the formation of globin aggregates which cause apoptosis [206]. Therefore, the careful regulation of both heme and globin synthesis is essential both for the production of haemoglobin and the prevention of accumulation of toxic species.

4.1.2 Aetiological links between anaemia and oxidative stress

The pathology of anaemia is inextricably linked with oxidative stress (OS). Iron deficiency anaemia, the most common form of anaemia, is associated with an increase in OS following the degradation of heme and the generation of reactive oxygen species (ROS) [207], in addition to a decrease in antioxidant defence by the enzyme glutathione peroxidase (GPx) [208]. Fanconi anaemia, the most common form of aplastic anaemia, involves the failure of bone marrow to produce all types of blood cells, caused by hypersensitivity to the oxidant species generated as part of normal metabolism [209]. ROS also play key roles in expansion of hematopoietic stem cells (HSCs), so that more HSCs proliferate in oxygenated environments, and production of platelets, as elevated levels of ROS lead to megakaryocyte (MK) fragmentation, which generates platelets [210].

Iron, which is essential for the oxygen-carrying function of haemoglobin, is highly susceptible to the generation of OS due to its variable oxidation state, existing as either ferrous (Fe^{2+}) or ferric (Fe^{3+}) iron. The transport and storage of iron are therefore tightly

controlled in order to prevent circulation of free iron, which could enter a state of redox cycling, leading to the unbridled generation of ROS. Iron is stored by ferritin, which is made up of H-ferritin and L-ferritin subunits; H-ferritin in particular is responsible for regulating cytosolic iron [211]. Ferritin has an antioxidant function, as it sequesters iron to prevent redox cycling. The gene FTH, encoding H-ferritin, is activated by the antioxidant response element (ARE) under conditions of OS [212].

4.1.3 Iron homeostasis, the endolysosomal pathway, and Tbc1d24

Iron homeostasis involves the careful regulation of iron uptake, storage and excretion, such that sufficient iron is available for the daily synthesis of billions of erythrocytes, while circulating iron is tightly modulated, and bound during transport to prevent toxicity caused by redox cycling due to the variable transition state of iron [213] [214]. Iron uptake occurs in the duodenum, where divalent metal transporter 1 (DMT1) transports iron across enterocyte plasma membranes [215]. The iron transporter ferroportin (*SLC40A1,* also known as *FPN1*) is responsible for all iron extrusion, including at the enterocyte basolateral membrane, and is regulated by the hormone hepcidin in a delicate balance of the ferroportin/hepcidin axis [216]. Once it enters the circulation, iron is transported in the circulation by the iron carrier transferrin, which binds ferrous iron (Fe^{2+}). Iron can then be utilised in erythropoiesis, metabolism and other key cellular processes, or stored inertly in the liver and spleen by the iron storage protein ferritin. To enter erythroblasts for erythropoiesis, iron-bound transferrin binds to Transferrin Receptor-1 (TfR1, also known as CD71), which is followed by endocytosis. Fe^{2+} is freed from the transferrin/receptor complex in the endosome due to the acidic environment generated by the V-ATPase proton pump. Iron can then be transported by DMT1, which uses the pH gradient of the endosome to cotransport Fe^{2+} and H^{+} into the cytosol or mitochondria, allowing iron to then be utilized in haemoglobin synthesis, metabolic processes, or storage by ferritin [217] [218].

The endocytosis and subsequent intracellular release of iron is essential for the synthesis of haemoglobin, and dependent upon acidification of the endosome by the V-

ATPase [219]. Inhibition of the V-ATPase leads to functional iron deficiency, activation of hypoxia-inducible factor-1α (HIF-1α), and decreased mitochondrial respiration [220]. Therefore, molecular mechanisms that modulate V-ATPase functionality in the haematopoiesis system are likely to have a profound influence on blood cell development. Importatly, the V-ATPase interacts with the TLDc protein family, including Tbc1d24 [221]. As discussed in Chapter Three, dysfunction of Tbc1d24 leads to severe neurological phenotypes, which is believed to be in-part due to the disruption of the interaction between Tbc1d24 and the V-ATPase. Interestingly, mutations in either TBC1D24 or subunits of the V-ATPase can cause a subset of rare syndromes with highly specific clinical presentations including DOORS (deafness, onchyodystrophy, intellectual disability and seizures) syndrome [222] and epilepsy [223] [224].

The emerging role of Tbc1d24 in the endolysosomal pathway posits a novel link with iron homeostasis and anaemia. The aims of this chapter are to understand the aetiology of the anaemic phenotype of Tbc1d24 dysfunction, and to elucidate the role of Tbc1d24 in the haematological system.

4.2 Haematological studies in the *Tbc1d24*$^{INS2/INS2}$ mutant

As introduced in Chapter Three, the *Tbc1d24*$^{INS2/INS2}$ mutant contains an insertional null allele that leads to an early stop codon in *Tbc1d24*, causing decreased RNA expression and a total knockdown in expression of Tbc1d24 protein. This mutation is postnatally lethal, with some homozygous mice observed to reach P0.

4.2.1 Visible anaemia in the embryonic mutant

In the *Tbc1d24*$^{INS2/INS2}$ mouse model, it was observed that mutant embryos of both sexes were visibly paler than *Tbc1d24*$^{+/+}$ littermates from E14.5, with barely visible developing vascular networks (Figure 1). The phenotype is consistent between litters, although there is some variation observed by eye. From multiple embryos dissections, heterozygous embryos do not show any overt alteration in body pigmentation (data not shown). Interestingly, E14.5 is critical for mouse haematopoiesis, as it moves from

occurring predominantly in the yolk sac and placenta to the embryonic liver [225]. The anaemic appearance of this mutant persists to E18.5 (**Figure 4.1**).

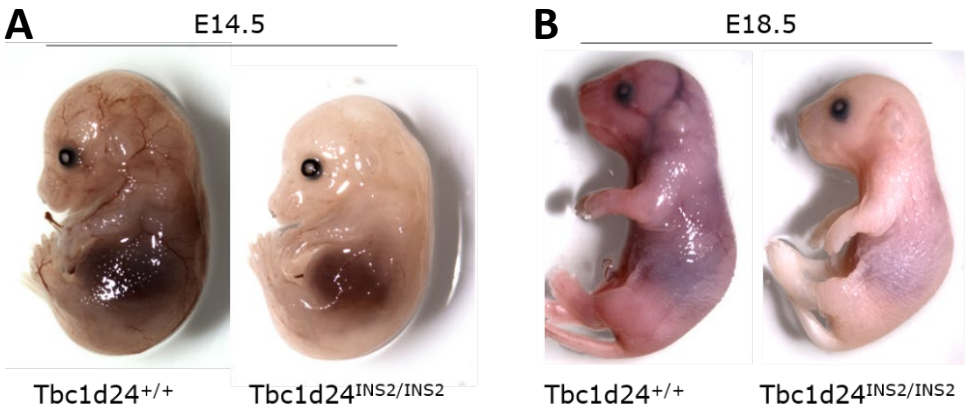


Figure 4.1 Anaemia is visible in embryonic* Tbc1d24^{INS2} *mutant *– Representative* Tbc1d24$^{INS2/INS2}$ *embryo compared with wild type littermate at Embryonic Day 14.5 (**A**) and 18.5 (**B**) (unknown sex). The* Tbc1d24$^{INS2/INS2}$ *mutant (**A**,**B** – right) is visibly paler than* Tbc1d24$^{+/+}$*(**A**,**B** – left), without the visible vascular networks that are seen clearly in* Tbc1d24$^{+/+}$*.*

4.2.2 Peripheral blood smears of *Tbc1d24$^{INS2/INS2}$* exhibit haemolytic anaemia

The pallid appearance of the *Tbc1d24$^{INS2/INS2}$* mice suggest strong haematological phenotype and severe anaemia. Peripheral blood smears enable the visualisation of blood cell morphology and are used in the diagnosis of haematological diseases [226]. Peripheral blood smears were taken from *Tbc1d24$^{INS2/INS2}$* mice and wild type littermates at E18.5 and subjected to Giemsa staining, a method that marks cellular components according to pH, staining nucleic acids blue and basic organelles, such as cytoplasmic granules, red [227]. Compared to *Tbc1d24$^{+/+}$* mice, the blood smears from *Tbc1d24$^{INS2/INS2}$* embryos exhibit anisocytosis (varying sizes within RBC population) and poikilocytosis (varying shapes of RBCs), with many ghost erythrocytes indicating haemolytic anaemia (**Figure 4.2**). Increased central pallor within RBCs, known as hypochromia, signifies a disproportionate reduction in haemoglobin content of the cells [228]. The phenotype of polychromasia, described as varying colour of stained RBCs, is to be expected in a blood smear from mice at E18.5, due to high levels of erythropoietic activity and circulating erythroblasts [229]. Polychromasia is seen in blood smears from both *Tbc1d24$^{INS2/INS2}$* and *Tbc1d24$^{+/+}$*. Overall, the blood smears of the *Tbc1d24$^{INS2/INS2}$* mutant confirm severe haematological disruption,

affecting the haemoglobin content and cellular integrity of erythrocytes, which likely contributes to the lethal phenotype of this mutant, as the oxygen-carrying capacity of the erythrocytes is likely decreased.

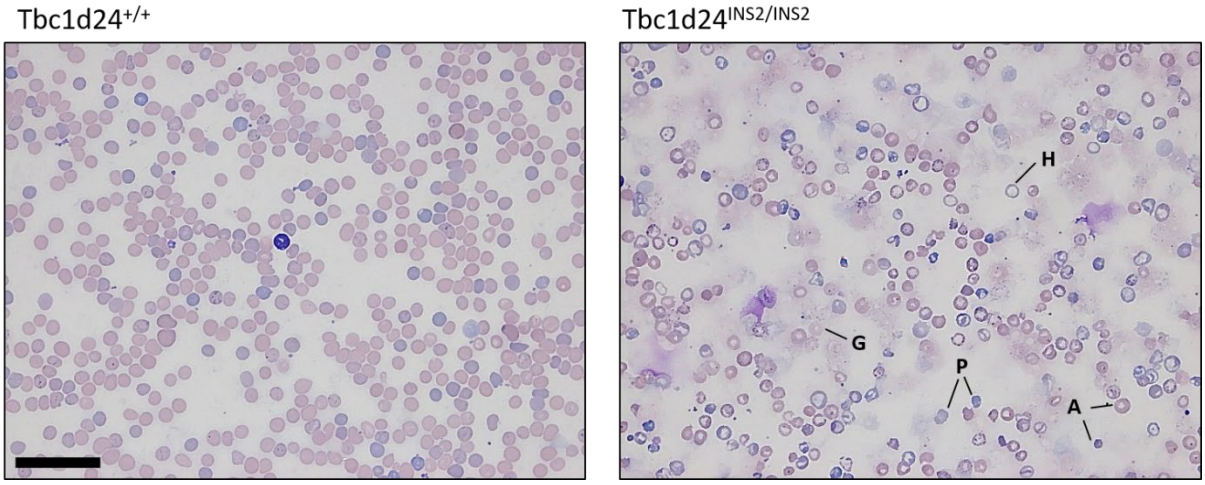


Figure 4.2 Peripheral blood smears of INS2 mutant mice show haemolytic anaemia. *Representative bright field images of Giemsa-stained blood smears from* Tbc1d24$^{+/+}$ *(left) and* Tbc1d24$^{INS2/INS2}$ *(right) mice at E18.5.* Tbc1d24$^{INS2/INS2}$ *blood smears exhibit haemolytic anaemia, with hypochromia (**H**), anisocytosis (**A**), poikilocytosis (**P**), and many visible ghost erythrocytes (**G**). Images taken at 40x magnification. Scale bar shows 50 µm. Smears were analysed from both male and female mice at E18.5. Representative images from female mice.*

4.3 Expression studies in loss-of-function *Tbc1d24* mouse mutants

4.3.1 RNA-Sequencing in the *Tbc1d24$^{INS2/INS2}$* mutant

Having ascertained that the INS2 mutation in Tbc1d24 leads to haematological disruption, transcriptomics (RNA-Seq) was performed in order to identify genetic alterations that might contribute to the anaemic phenotype of the mutant as well as other molecular pathways that might be informative regarding neurodevelopment. Due to the role played by Tbc1d24 in neurological development, and electrophysiological findings of hyperexcitability in the cortex of *Tbc1d24$^{R360L/R360L}$* mutant mice (discussed in Chapter Three), RNA was extracted from the sub-dissected cortices of sex-matched, male *Tbc1d24$^{+/+}$* and *Tbc1d24$^{INS2/INS2}$* mice at E18.5 (n = 5). Cambridge Genomic Services (CGS) performed RNA-Seq experiments using the extracted RNA. Of 12,092 genes detected in the tissue samples, 37 genes were identified as differentially expressed between genotypes with false discovery rate-adjusted P (FDR) value below 0.05, and 26 of these had FDR values below 0.01 (**Table 7.1**). **Figure 4.3** shows a volcano plot of the RNA-Seq results, annotated with

the top ten genes by FDR value. From most significant to least, these are: *Tbc1d24*, *Alas2*, Terminal nucleotidyltransferase 5C *(Tent5c)*, Monocarboxylate transporter 4 *(Slc16a3, also known as Mct4)*, Haemoglobin beta adult t chain *(Hbb-bt)*, Haemoglobin beta adult s chain *(Hbb-bs)*, Ferroportin *(Slc40a1)*, Heme oxygenase 1 *(Hmox1)*, Enolase 1 *(Eno1)* and Lactate dehydrogenase A *(Ldha)*. The top gene by FDR value is *Tbc1d24* (FDR = 6.7 x 10^{-84}), with a fold change of 0.58. This indicates a significant downregulation in *Tbc1d24* expression in the *Tbc1d24*$^{INS2/INS2}$ mutant, which is consistent with qPCR expression data in discussed in Chapter Three.

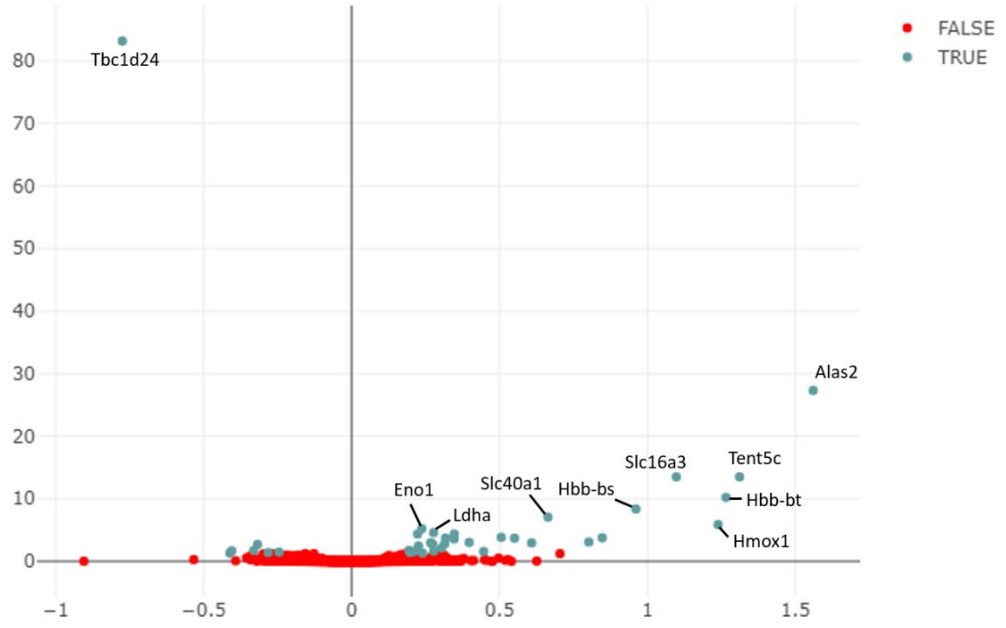


Figure 4.3 RNA Sequencing shows significant upregulation of key haematological genes in the* Tbc1d24$^{INS2/INS2}$ *cortex. *Volcano plot produced using plotly showing gene expression changes, with logFC on the x-axis plotted against significance level (-log(adjusted p value)) on the y-axis. RNA was extracted from* Tbc1d24$^{INS2/INS2}$ *cortex, and analysed against* Tbc1d24$^{+/+}$ *littermate controls. Male mice were used. The top ten genes by FDR value are labelled, and all genes with FDR ≤ .5 highlighted as 'TRUE' (blue) as opposed to 'FALSE' (red).*

Strikingly, the genes encoding all four haemoglobin subunits – *Hba-a1* (FDR = 0.000174), *Hba-a2* (FDR = 0.000829), *Hbb-bs* (FDR = 4.38 x 10^{-9}) and *Hbb-bt* (FDR = 6.15 x 10^{-11}) – and the haemoglobin synthesis gene *Alas2* (FDR = 4.83 x 10^{-28}), are all significantly upregulated in the *Tbc1d24*$^{INS2/INS2}$ cortex, indicating transcriptional de-regulation of haemoglobin synthesis caused by the INS2 mutation. Haemoglobin is made up of α-type and β-type globin subunits, which, in mice, are encoded by *Hba-a1*, *Hba-a2*,

Hbb-bt and *Hbb-bs*. The globin subunits associate with heme, which is produced through the heme biosynthetic pathway for which the first, rate-limiting enzyme is Alas2 [230]. The upregulation in expression of all four haemoglobin subunits and Alas2 indicates a potential molecular shift in gene expression to drive haemoglobin synthesis in the *Tbc1d24*$^{INS2/INS2}$ mutant.

Enrichment analysis was performed firstly using the web-based application GOrilla, which identifies enriched gene ontology terms from ranked lists of genes, (in this case, the

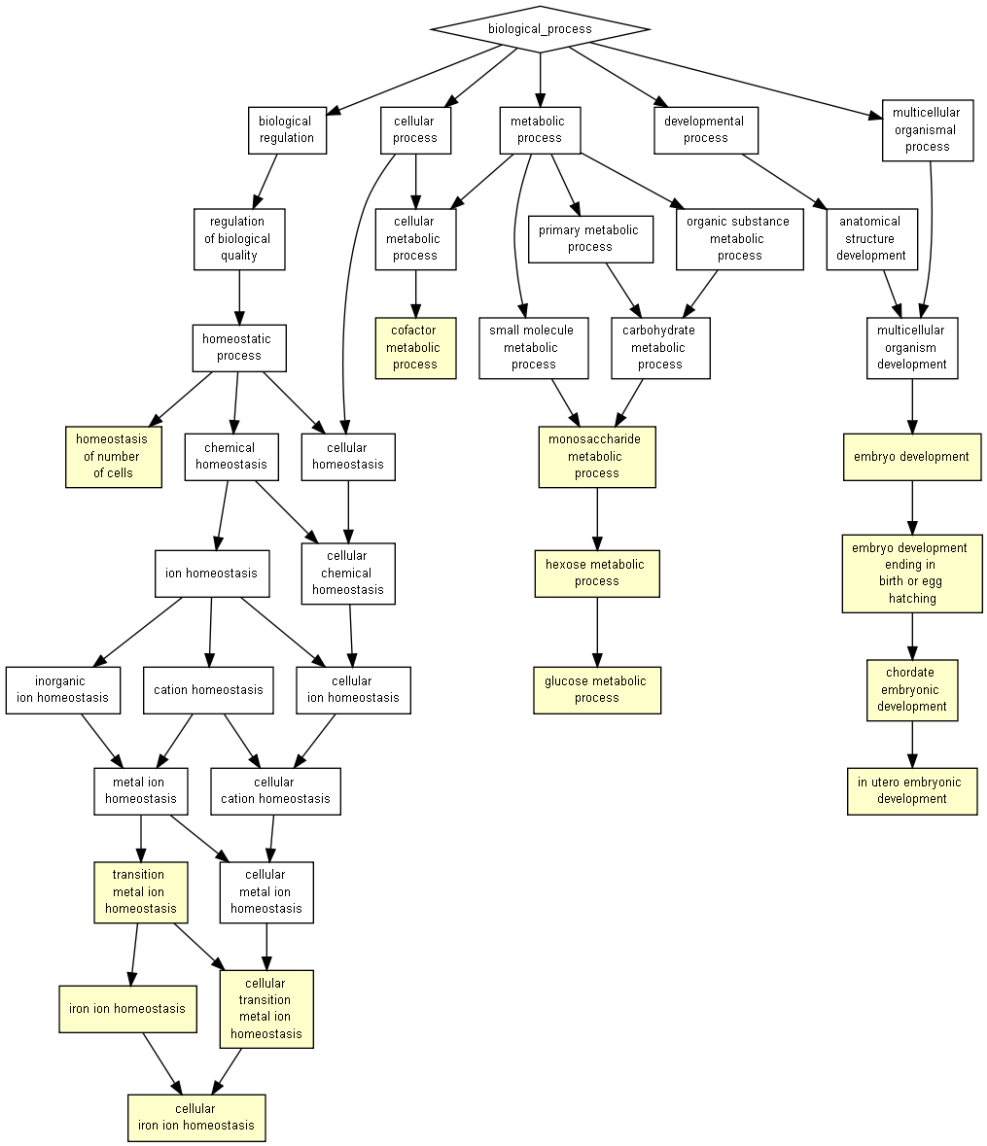


Figure 4.4 Enrichment analysis indicates iron homeostasis, glucose metabolism and embryonic development as enriched biological processes in the* Tbc1d24$^{INS2/INS2}$ *mutant. *The web-based tool GOrilla was used to analyse the top 37 hits (FDR < 0.05) from RNA-Seq data from the* Tbc1d24$^{INS2/INS2}$ *mutant, shown here as a hierarchy of enriched gene terms, colour coded according to significance level of the observed enrichment (WHITE: P > 10^{-3}, YELLOW: 10^{-3} ≤ P < 10^{-5}).*

37 genes identified by RNA-Seq of *Tbc1d24*^{INS2} with FDR < 0.05), to produce maps of the functional hierarchies of altered genes [231] [232]. Using GOrilla to analyse the *Tbc1d24*$^{INS2/INS2}$ RNA-Seq data identified a number of key processes predicted to be significantly altered by the INS2 mutation, especially cellular iron ion homeostasis, glucose metabolic processes and *in utero* embryonic development ($10^{-3} \leq P < 10^{-5}$) (**Figure 4.4**).

Secondly, functional enrichment analysis was performed using the g:Profiler web server to map gene enrichment alterations to databases of known functional information [233]. Using the web-based analysis tool g:GOSt, the top 37 hits from RNA-Seq data from the *Tbc1d24*$^{INS2/INS2}$ mutant were mapped against the Gene Ontology Databases of molecular function, biological processes, and cellular component; the Kyoto Encyclopedia of Genes & Genomes (KEGG) database; Reactome; and the Human Phenotype Ontology database (**Figure 4.5**). Enrichment analysis against the Gene Ontology molecular function database demonstrated gene term enrichment in a range of functions highly relevant to anaemia, including haemoglobin binding, oxygen binding, and oxygen carrier activity, indicating a possible effect of the INS2 mutation on haemoglobin function (**Figure 4.5A**). Analysis against the Gene Ontology cellular component database similarly highlighted the haptoglobin-haemoglobin complex and the haemoglobin complex as enriched terms, in addition to the cytosol (**Figure 4.5C**). Interestingly, analysis against the biological process database highlighted pyruvate metabolism as the most significantly enriched process ($-\log_{10}(P_{adj}) = 6.65$), together with other significantly enriched biological processes including oxygen transport and erythrocyte homeostasis (**Figure 4.5B**). Enrichment analysis against the Reactome database highlighted both pyruvate metabolism and glycolysis as differentially expressed pathways, in addition to multiple erythrocytic processes involving O_2/CO_2 exchange (**Figure 4.5D**). Differentially regulated KEGG database pathways identified by g:GOst include the Hypoxia Inducible Factor (HIF)-1 signalling pathway, Glycolysis/Gluconeogenesis, and Ferroptosis pathways (**Figure 4.5E**). HIF-1 is an oxygen-sensitive transcription factor which regulates the cellular response to hypoxia, inducing

transcription of genes related to angiogenesis, anaerobic metabolism and erythropoiesis [234]. Finally, enrichment analysis against human disease phenotypes from the Human Phenotype Ontology database highlighted enrichment in pathways related to three types of anaemia: hypochromic microcytic anaemia, nonspherocytic haemolytic anaemia and Heinz body anaemia (**Figure 4.5F**).

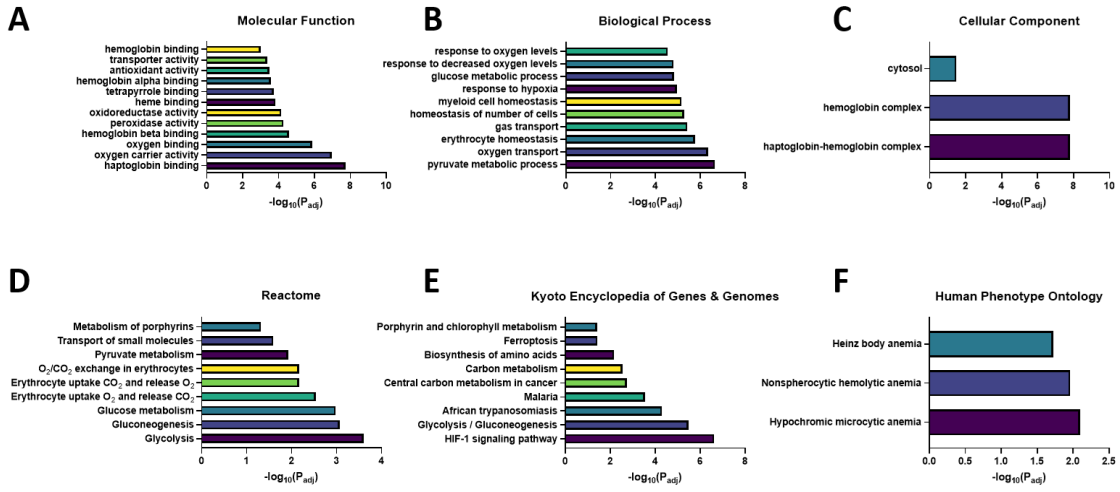


Figure 4.5 Functional enrichment analysis of the* Tbc1d24$^{INS2/INS2}$ *mutant indicates differential expression of genes in pathways relating to anaemia. *The web-based tool g:Profiler was used to analyse RNA-Seq data from the* Tbc1d24$^{INS2/INS2}$ *mutant, using the programme g:GOst to compare differentially expressed genes in the* Tbc1d24$^{INS2/INS2}$ *mutant against databases of gene ontology. The databases are as follows: GO Molecular Function (A), GO Biological Process (B), GO Cellular Component (C), Reactome (D), Kyoto Encyclopaedia of Genes & Genomes (E), and Human Phenotype Ontology (F).*

Enrichment analysis using both GOrilla and g:Profiler indicates differentially expressed genes within pathways in common, including iron homeostasis, hypoxia and glycolysis. Furthermore, these pathways relate to anaemia, providing transcriptomic evidence for haematological disruption as a result of mutation in *Tbc1d24*.

4.3.2 Microarray studies in the *Tbc1d24*$^{R360L/R360L}$ mutant

The *Tbc1d24*$^{R360L/R360L}$ mutant (introduced in **Chapter Three**) models a recessive epilepsy syndrome; mice homozygous for the mutation experience seizures from P16, which become fatal from P18. Prior to the RNA-seq experiment above and generation of the *Tbc1d24*$^{INS2/INS2}$ line, transcriptomic analysis using microarrays was performed in order to potentially find clues relating to the seizure phenotype. However, consistent with the

anaemic phenotype of the *Tbc1d24*$^{INS2/INS2}$ mutant, differential expression was almost exclusively observed in genes relating to the haemoglobin synthesis, supporting a role for Tbc1d24 in the haematological system.

Microarray analysis uses a set of nucleic acid hybridization probes to measure genome-wide expression in a given biological sample [235]. Due to the interesting neurological phenotype of the *Tbc1d24*$^{R360L/R360L}$ mutant, RNA was extracted from brain subdissected into cortex, cerebellum and hippocampus, from *Tbc1d24*$^{R360L/R360L}$ mice at P16, with sex-matched *Tbc1d24*$^{+/+}$ littermate controls. Cambridge Genomic Services (CGS) performed microarray experiments using the Affymetrix assay, and performed quality controls and bioinformatics analysis. Note that these experiments were carried out before the RNA-seq analysis above.

Figure 4.6 shows volcano plots obtained from RNA-Seq of the sub-dissected cortex (**Figure 4.6A**), cerebellum (**Figure 4.6B**) and hippocampus (**Figure 4.6C**). Across the three brain regions, only a small selection of genes were shown to be differentially expressed in the *Tbc1d24*$^{R360L/R360L}$ mutant. The same six genes were identified as significantly upregulated in the cortex and cerebellum (adjusted p-value < 0.05): *Hba-a1*, *Hba-a2*, *Hbb-bs*, *Hbb-bt*, *Alas2* and Interferon Stimulated Exonuclease Gene 20 (*Isg20*). In the hippocampus, only *Hbb-bs* and *Hbb-bt* were significantly upregulated (adjusted p-value < 0.05). As explained previously, *Hba-a1*, *Hba-a2*, *Hbb-bs*, *Hbb-bt* are the four genes for the haemoglobin subunits expressed in mouse, and *Alas2* is the first enzyme in the heme biosynthetic pathway. However, *Isg20* is an interferon-stimulated RNA exonuclease that functions as an antiviral factor by blocking translation of non-self genetic material [236]. *Isg20* is upregulated in the cortex (adjusted p-value = 0.0147), cerebellum (adjusted p-value = 0.0269) and hippocampus (adjusted p-value = 0.0691) of *Tbc1d24*$^{R360L/R360L}$.

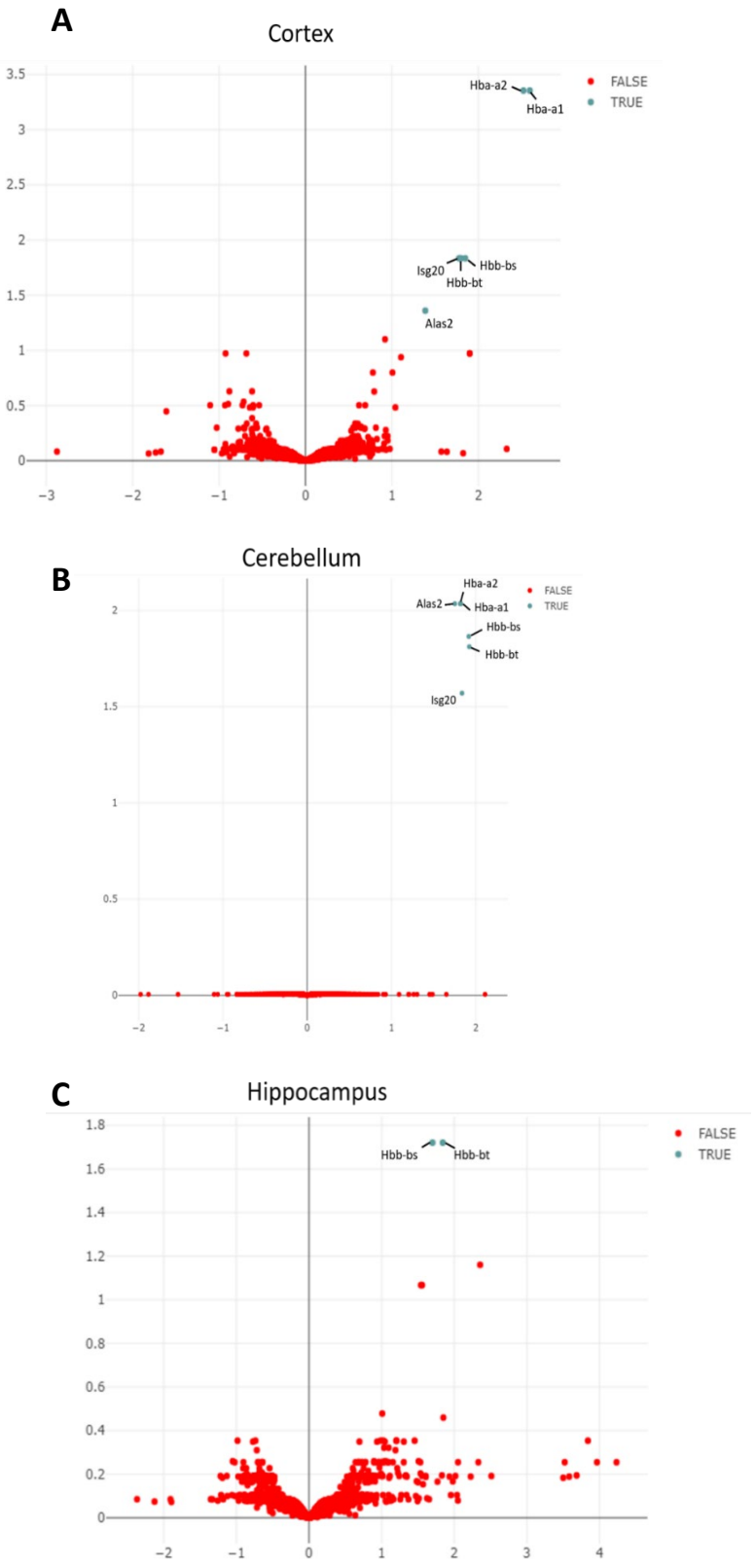


Figure 4.6 Microarray of* Tbc1d24$^{R360L/R360L}$ *mutant shows upregulation of key haematology genes across cortex, cerebellum and hippocampus. *Volcano plots produced using plotly showing gene expression changes, with logFC on the x-axis plotted against significance level (-log(adjusted p value)) on the y-axis. RNA extracted from* Tbc1d24$^{R360L/R360L}$ *cortex (**A**), cerebellum (**B**) and hippocampus (**C**), and analysed against* Tbc1d24$^{+/+}$ *littermate controls. Male mice were used. Significant genes according to adjusted p-value are labelled, all genes with adjusted p-value < 0.05 highlighted as 'TRUE' (blue) as opposed to 'FALSE' (red).*

Based on these results, primers were designed for validation by RT-qPCR (See 3.4). Additionally, a further three genes were chosen for primer design based on raw p-values, especially when consistent between brain regions, and biologically relevant to the epileptic and anaemic phenotypes of the *Tbc1d24*$^{R360L/R360L}$ mutant. These genes are: Contactin 3 (*Cntn3)*, Erythrocyte Membrane Protein Band 4.1 (*Epb41)* and Erythroid Differentiation Regulator 1 (*Erdr1)* (**Figure 4.7**). *Cntn3* was shown to be downregulated in the cerebellum of the *Tbc1d24*$^{R360L/R360L}$ mutant. Cntn3 is involved in cell adhesion and specifically plays a role in neural interactions during brain development [237]. *Epb41*, upregulated in both the cortex and hippocampus of the *Tbc1d24*$^{R360L/R360L}$ mutant, encodes Epb41, a key protein complex in the erythrocyte cytoskeletal network. Mutations in this protein lead to defects in erythrocyte morphology [238]. Finally, *Erdr1*, upregulated in both the cerebellum and hippocampus of the *Tbc1d24*$^{R360L/R360L}$ mutant, encodes Erdr1, which controls the differentiation of hematopoietic progenitors, especially as a response to cellular stress [239]. These three genes – *Cntn3*, *Epb41* and *Erdr1* – were therefore chosen for further validation, due to their potential biological relevance.

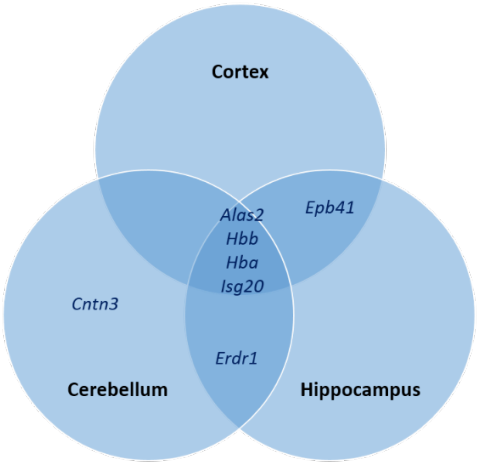


Figure 4.7 - Genes chosen for primer design based on microarray of* Tbc1d24$^{R360L/R360L}$ *cortex, cerebellum and hippocampus. *Venn diagram showing in which brain region(s) genes were found to be significantly differentially expressed ($p < 0.05$). Genes were chosen for primer design based on significance across brain regions, and biological relevance.*

4.3.3 RNA-Sequencing in the *Tbc1d24*$^{R360L/R360L}$ mutant

Further transcriptomic analysis was performed on the *Tbc1d24*$^{R360L/R360L}$ mutant, following electrophysiological studies which identified cortical layer 5 (L5) as a key region

of hyperexcitability in the mutant; random bursts of excitation consistent with epileptiform activity and a lower excitation threshold are detected from ex-vivo electrophysiology at P16 (Rial, D. – Oliver lab, unpublished). A 3mm-wide region of the frontal cortex was subdissected from *Tbc1d24*$^{R360L/R360L}$ mice and wild type littermate controls at P16, and sent to CGS for RNA-Seq analysis. A comparatively larger selection of genes were determined to be differentially expressed compared to RNA-Seq of*Tbc1d24*$^{INS2/INS2}$ tissue, likely due to the precise region of subdissection of the *Tbc1d24*$^{R360L/R360L}$ cortex that is known to be a focal point of hyperexcitability and likely contributes to the increase in selection of significant hits. Of 11,797 genes detected, a total of 302 genes were differentially expressed, with FDR values under 0.05, and 150 of these had FDR values below 0.01 (shown in **Table 7.2**); the haemoglobin genes *Alas2*, *Hba-a1*, *Hba-a2*, *Hbb-bs* and *Hbb-bt* were in the top fifteen of these hits when sorted by FDR value (highest to lowest significance) (**Figure 4.8**). Therefore, transcriptomic studies of the *Tbc1d24*$^{R360L/R360L}$ mutant, both through microarray of cortex, cerebellum and hippocampus, and RNA-Seq of subdissected prefrontal cortex, show significant upregulation of crucial haematology genes including all four haemoglobin subunits and the primary enzyme in heme synthesis.

Of note, RNA-Seq also revealed the upregulation of critical immediate early genes, including *c-fos* (also known as *Fos*), in *Tbc1d24*$^{R360L/R360L}$ (**Table 2**). As discussed in Chapter Three, immediate early genes are markers of neuronal activity, and *c-fos* can be used as a proxy to indicate seizure activity [151] [152]. *Fos* showed a 2.8-fold increase in expression in the *Tbc1d24*$^{R360L/R360L}$ mutant (FDR = 3.48 x 10^{-5}). As shown by **Figure 4.9**, principle component analysis (PCA) shows variability, with some mutant (R360L) data-points clustering separately from wild type (WT) data points, while some cluster together with the wild type dataset. This likely reflects the seizure prone status of individual animals. Furthermore, variability is evident within the wild type data set, suggesting that seizure status is not the only source of variation in the mutant set. Rather, the time course of gene expression changes may be responsible for differences between individual mice, which

PCA is sensitive to. However, differential expression within haemoglobin-related genes, such as *Alas2* and the haemoglobin subunits, shows less variability. These data, related to variability within the mutant group, will be discussed in more detail in Chapter Six, Discussion.

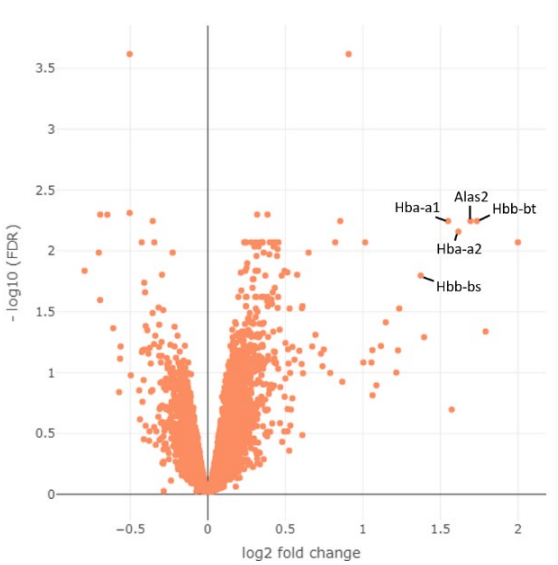


Figure 4.8 RNA Sequencing shows significant upregulation of key haematological genes in the* Tbc1d24$^{R360L/R360L}$ *prefrontal cortex. *Volcano plot produced using VolcaNoseR showing gene expression changes, with logFC on the x-axis plotted against significance level (-log10(FDR)) on the y-axis. RNA extracted from* Tbc1d24$^{R360L/R360L}$ *prefrontal cortex, and analysed against* Tbc1d24$^{+/+}$ *littermate controls. Key haematological genes are labelled, which represent 5 of the 150 differentially expressed genes with FDR value < 0.01. In total, 302 genes were significantly differentially expressed (FDR value < 0.05).*

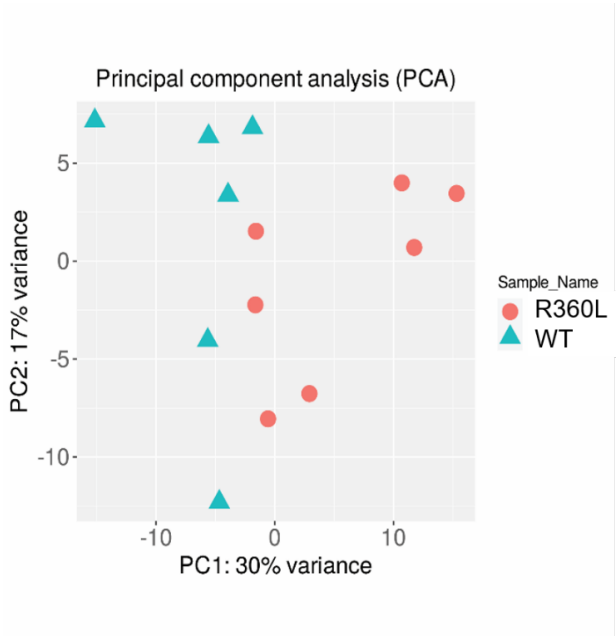
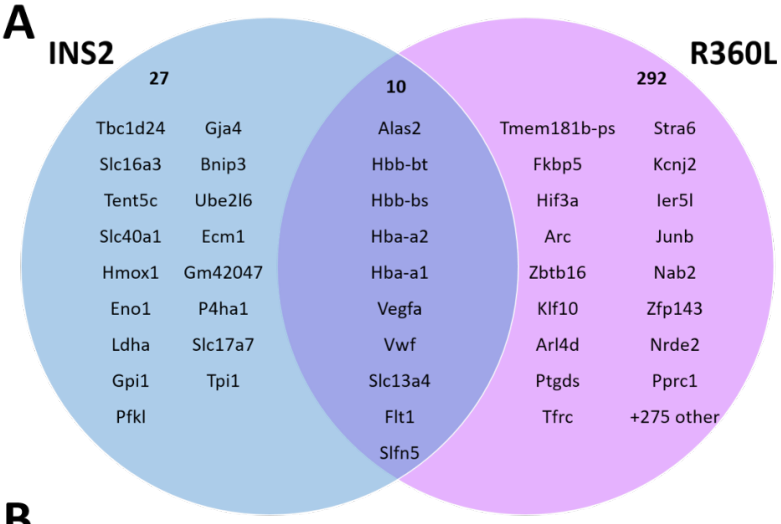


Figure 4.9 Prinicpal component analysis (PCA) of RNA-Sequencing of* Tbc1d24$^{R360L/R360L}$ *compared to wild type controls. *PCA reveals variability within the* Tbc1d24$^{R360L/R360L}$ *biological group.*

4.3.4 A comparison of the transcriptomic studies of the two Tbc1d24 mutants

The two mutant models, *Tbc1d24*$^{INS2/INS2}$ and *Tbc1d24*$^{R360L/R360L}$, both model disruption in the levels of Tbc1d24 protein expression. As indicated by the transcriptomic studies in this chapter, both models also experience haematological disruption, with key haematological genes differentially expressed in each. Ten differentially expressed genes in total overlap between the two Tbc1d24 mutants based on the same statistical threshold of FDR value < 0.05 (**Figure 4.10**), of which four encode haemoglobin subunits and one encodes *Alas2*, the primary heme synthesis enzyme; these five genes were all upregulated in both mutants. A further two upregulated genes, *Vegfa* and *Flt1*, encode vascular endothelial growth factor (Vegfa) and its receptor (Vegfr1), which are involved in angiogenesis and blood vessel morphogenesis [240] [241]. Von Willebrand factor (vWF) is a large glycoprotein that regulates platelet adhesion during vascular injury, and is

A



B

	Tbc1d24$^{INS2/INS2}$	Tbc1d24$^{R360L/R360L}$
Number of genes tested	12,092	11,797
FDR < 0.01	26	150
FDR < 0.05	37	302

Figure 4.10 Comparison of differentially expressed genes between two Tbc1d24 mutants. *RNA Sequencing was performed on two Tbc1d24 mutants, using RNA extracted from* Tbc1d24$^{INS2/INS2}$ *cortex at E18.5, and from Tbc124*$^{R360L/R360L}$ *frontal cortex at P16. Both experiments were performed using age- and sex-matched wild type controls. RNA Sequencing was performed by Cambridge Genomics Services.* ***A*** *– Venn diagram showing the overlap between differentially expressed genes in* Tbc1d24$^{INS2/INS2}$ *(INS2) and* Tbc124$^{R360L/R360L}$ *(R360L). 10 genes in total were found to be differentially expressed in both mutants.* ***B*** *– Table showing the number of genes tested in each mutant, and number of which genes were differentially expressed according to false discover rate-adjusted p-value (FDR).*

upregulated in both Tbc1d24 mutants. Slc13a4 is a transmembrane cotransporter of sodium and sulphate, believed to play a key role in postnatal brain development [242], which is downregulated in both mutants. Finally, Slfn5 is involved in cell differentiation, although its role is largely unknown and appears to be dependent on cell type [243]; the gene is upregulated in the *Tbc1d24*$^{R360L/R360L}$ mutant but downregulated in the *Tbc1d24*$^{INS2/INS2}$ mutant. Overall, the two Tbc1d24 mutants' expression profiles show significant upregulation of fundamental haemoglobin synthesis genes.

4.3.5 Validation of transcriptomics confirms drive towards haemoglobin synthesis

Transcriptomic analysis of the two *Tbc1d24* mutants identified significant upregulation in expression of critical haematological genes. Furthermore, microarray of the *Tbc1d24*$^{R360L/R360L}$ mutant showed differential expression of genes according to brain region, such as *Cntn3*, *Epb41* and *Erdr1*. To validate these findings of the transcriptomics data, RT-qPCR was performed using an independent set of RNA, extracted from the *Tbc1d24*$^{R360L/R360L}$ mutant cortex, cerebellum and hippocampus at P16, with *Tbc1d24*$^{+/+}$ controls (**Figure 4.11**). Genes were selected for primer design as described previously, with one each of the alpha and beta haemoglobin subunits selected for validation (*Hba-a2* and *Hbb-bt*).

Concordantly with the transcriptomic studies, expression of *Alas2* was dramatically upregulated, showing a 72 fold increase in *Alas2* expression in the cortex ($p = 0.0008$) and 5x increase in the cerebellum ($p = 0.049$), although the increase in expression in the hippocampus did not reach significance ($p = 0.174$) (**Figure 4.11**). Similarly, *Hbb-bt* was also dramatically upregulated, showing a 24x increase in expression in the cortex ($p = 0.00007$) and a 5 fold increase in the cerebellum ($p = 0.034$). Again, expression in the hippocampus was not significantly increased ($p = 0.206$).

Surprisingly, RT-qPCR showed no significant difference in the expression of *Hba-a2*, as shown in Figure 10, although there is an apparent increase in expression in the *Tbc1d24*$^{R360L/R360L}$ cerebellum ($p = 0.12$), despite this gene having been consistently shown

to be upregulated in Tbc1d24 mutants, through microarray and RNA-Seq. This result is unexpected, and may result from individual variation between biological groups.

The gene *Cntn3*, involved with neuronal migration, was found by microarray to be downregulated in the *Tbc1d24*$^{R360L/R360L}$ cerebellum. In agreement, RT-qPCR showed a 16 fold decrease in *Cntn3* expression in the cortex ($p = 0.000088$), in addition to a 20% decrease in expression in the cerebellum ($p = 0.002$) (**Figure 4.11**).

As **Figure 4.11** shows, RT-qPCR showed no difference across any of the brain regions tested in the expression of the genes *Epb41*, involved in erythrocyte morphology, and *Erdr1*, involved with erythrocyte differentiation and the induction of haemoglobin synthesis, in *Tbc1d24*$^{R360L/R360L}$ compared with wild type mice. This result is not surprising, given that microarray data did not show that either *Epb41* or *Erdr1* were differentially expressed across brain regions. Finally, RT-qPCR showed significant upregulation in *Isg20*, the exonuclease enzyme with antiviral properties, across cortex, cerebellum and hippocampus of the *Tbc1d24*$^{R360L/R360L}$ mutant compared with wild type. The cortex showed

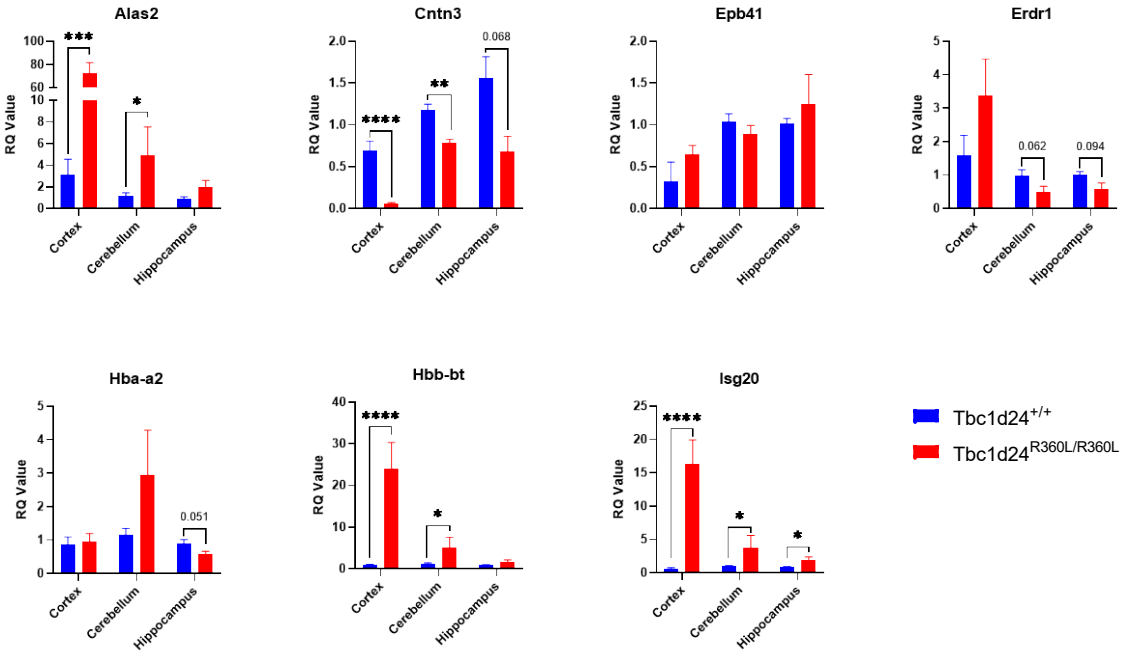


Figure 4.11 Validation of expression changes in critical haematological genes as a result of Tbc1d24 mutation. *RT-qPCR was performed using mRNA extracted from subdissected cortex, cerebellum and hippocampus of male and female* Tbc1d24$^{R360L/R360L}$ *mutants (red) at P16, with* Tbc1d24$^{+/+}$ *controls (blue). Expression of haematology genes* Alas2, Hba-a2 *and* Hbb-bt*, erythrocyte development genes* Epb41 *and* Erdr1*, antiviral gene* Isg20 *and neuronal migration gene* Cntn3*, were measured by RT-qPCR. T tests were performed using ΔCT values. Graphs show mean ± SEM, n = 4 for each genotype.*

a 16x increase in *Isg20* expression (p = 0.00006), the cerebellum, a 4x increase (p = 0.033) and the hippocampus, a 2x increase (p = 0.016).

4.3.6 *In situ* hybridization of haematology markers

In order to determine whether the bulk tissue expression changes from RNA-Seq were as a result of regional or cell-specific differential expression, *in situ* hybridization (ISH) was performed. Probes against *Alas2*, *Hba* and *Hbb were* tested on parasagittal sections of whole brains from *Tbc1d24*$^{R360L/R360L}$ and *Tbc1d24*$^{+/+}$ mice at P16. The upregulation in expression of both *Hba* and *Hbb* in the *Tbc1d24*$^{R360L/R360L}$ mutant was clear, with a 38% increase in expression of *Hba* in whole brain (p = 0.023) and a 63% increase in expression of *Hbb* (p = 0.0014), where expression is indicated by integrated density (**Figure 4.12**). In the *Tbc1d24*$^{R360L/R360L}$ mutant, expression of *Hba* is significantly increased in cerebellum (p = 0.0039) and hippocampus (p = 0.0066). Upregulation of *Hba* in the cortex does not reach significance (p = 0.178), however, there is no apparent regional specificity in expression of *Hba* in the mutant. Similarly, expression of *Hbb* is significantly increased in the cortex (p = 0.0003), cerebellum (p = 0.002) and hippocampus (p = 0.001) of the *Tbc1d24*$^{R360L/R360L}$ mutant. The increase in expression of both *Hba* and *Hbb* is not specific to any brain region, indicating that both genes are upregulated generally throughout the brain; these data are likely to indicate a vascular origin for the upregulation of haematological genes, rather than a neuronal origin.

Although ISH was also performed using an RNA probe against *Alas2*, it appears that this was unsuccessful, as there is no clear difference in expression across whole brains of *Tbc1d24*$^{R360L/R360L}$ compared with *Tbc1d24*$^{+/+}$ mice.

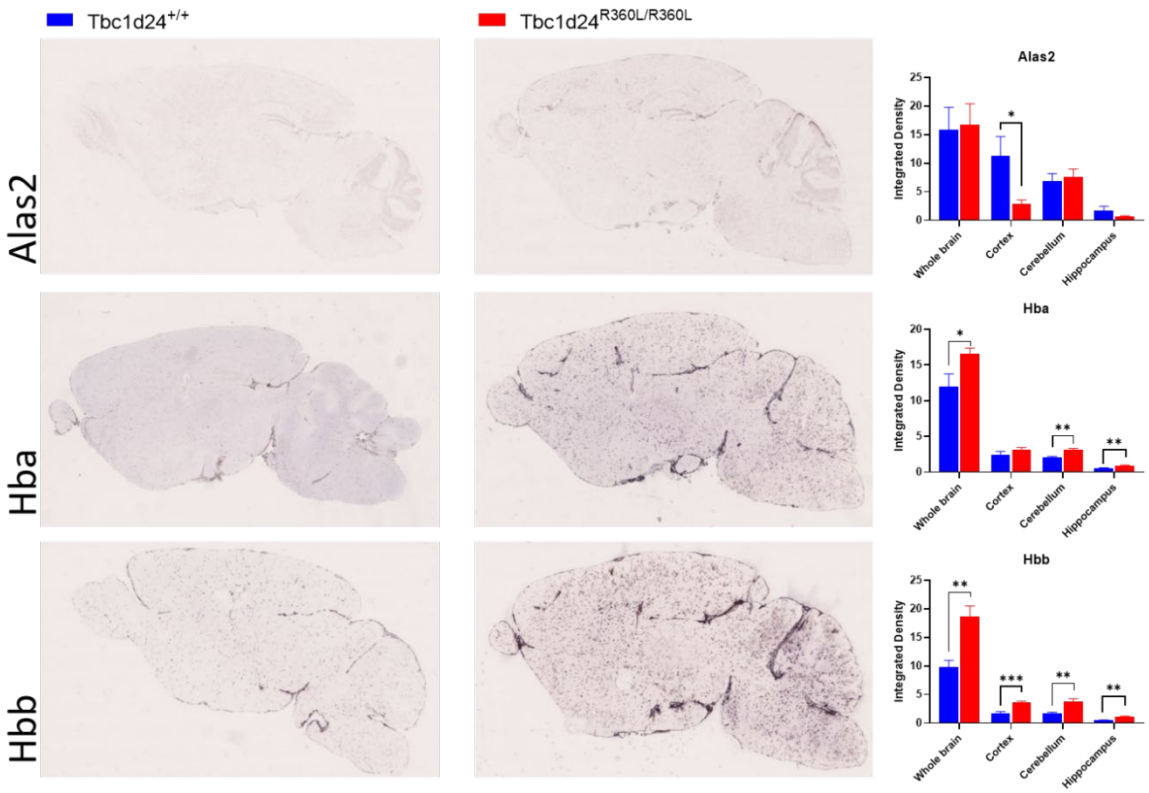


Figure 4.12* In situ *hybridization of* Tbc1d24$^{R360L/R360L}$ *shows visible upregulation of Haemoglobin subunits. *Sagittal sections of male and female* Tbc1d24$^{+/+}$ *(blue) and* Tbc1d24$^{R360L/R360L}$ *(red) brains at P16 were incubated with riboprobes against* Alas2*,* Hba *and* Hbb *(n = 4). Analysis was performed using ImageJ to measure raw integrated density, and T tests performed between genotypes, with graphs showing mean ± SEM.*

4.3.7 Saline perfusion confirms vascular origin of expression changes in the *Tbc1d24$^{R360L/R360L}$* mutant

Haemoglobin synthesis predominantly occurs in erythroblasts, prior to removal of organelles and development into mature erythrocytes that are capable of transporting oxygen around the body. However, all cells containing mitochondria are capable of synthesising haemoglobin, including neurons, where production of haemoglobin has been linked to cellular stress and neurotoxicity [244]. This is in contrast with neuroglobin, a heme-binding globin specific to neurons, which has been shown to provide neuroprotection during hypoxia and ischaemia [245]. The brain is highly vascular, with a complex network of blood vessels that supply all regions of the brain with sufficient oxygen and nutrients to meet its high energetic demands. Therefore, it was necessary to determine the origin of increased expression of haemoglobin synthesis genes. Mice at P16 were perfused with saline to

remove blood from the brain's vascular network, then cerebellum and brain were subdissected and RNA extraction was performed, followed by RT-qPCR. As shown in **Figure 4.13**, *Alas2*, *Hba* and *Hbb* showed no significant difference in expression between *Tbc1d24*$^{+/+}$ and *Tbc1d24*$^{R360L/R360L}$ mice when blood was removed from brain tissue by saline perfusion. Therefore, changes in expression of these haemoglobin synthesis genes were determined to originate from the blood, suggesting a vascular origin for upregulation in the *Tbc1d24*$^{R360L/R360L}$ mutant (**Figure 4.12**).

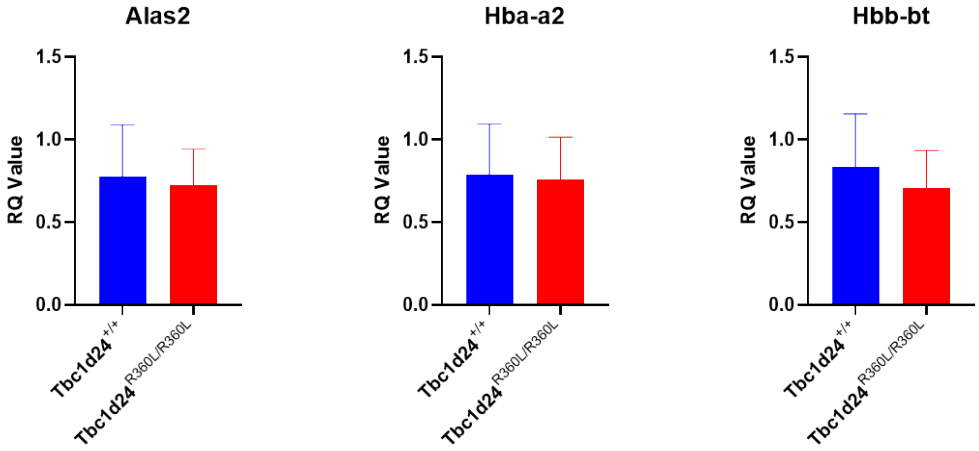


Figure 4.13 Saline perfusion of* Tbc1d24$^{R360L/R360L}$ *removes upregulation of haematological genes. *RT-qPCR was performed using mRNA extracted from cerebellum of* Tbc1d24$^{R360L/R360L}$ *(red) and* Tbc1d24$^{+/+}$ *(blue) male and female mice at P16. Expression of haematology genes* Alas2, Hba-a2 *and* Hbb-bt *was measured by RT-qPCR. T tests were performed using ΔCT values. Graphs show mean ± SEM, n = 4 for each genotype.*

4.4 Haematological studies in the *Tbc1d24*$^{R360L/R360L}$ mutant

4.4.1 Peripheral blood smears appear normal

As previously, for the *Tbc1d24*$^{INS2/INS2}$ mutants, visualisation of blood cell morphology was important to gain insight into type and severity of anaemia present in the *Tbc1d24*$^{R360L/R360L}$ mutant. Peripheral blood smears were taken from *Tbc1d24*$^{R360L/R360L}$ mice and wild type controls and Giemsa stained. However, in contrast with the *Tbc1d24*$^{INS2/INS2}$ mutant, no obvious changes in blood cell morphology were observed (**Figure 4.14**). Erythrocytes appear normal in size and shape, with no increase in central pallor compared with wild type blood smears. Blood smears were taken at P16, at which

time point circulating erythroblasts exist widely in circulation in wild type mice [229], and accordingly, a mixture of red-stained and blue-stained cells are observed in peripheral blood smears taken from both genotypes. This finding suggests that the anaemic phenotype of the *Tbc1d24*$^{R360L/R360L}$ mutant is less severe than that of the *Tbc1d24*$^{INS2/INS2}$ mutant, which may reflect the degree of disruption in Tbc1d24 expression in each mutant.

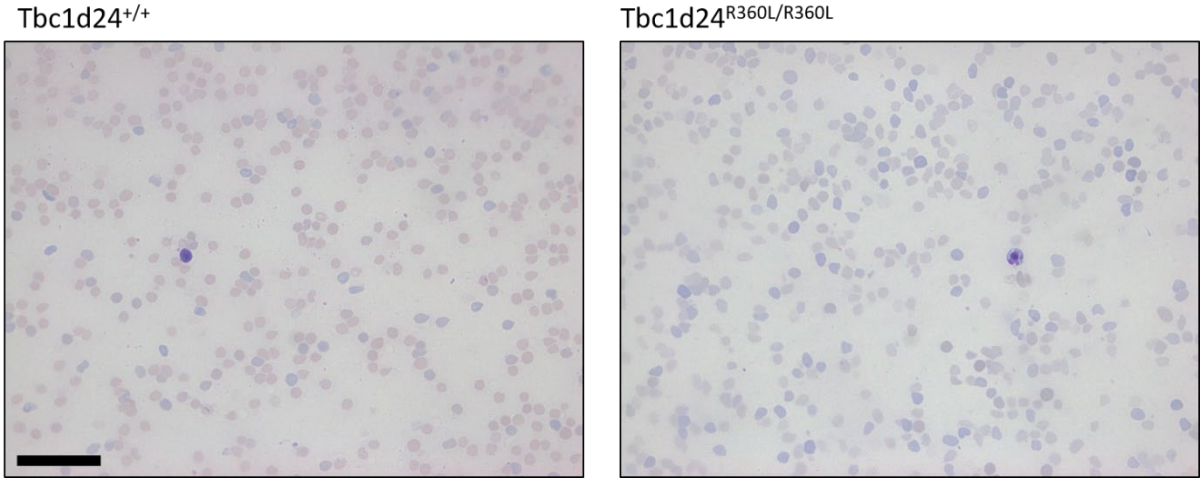


***Figure 4.14 Peripheral blood smears of* Tbc1d24$^{R360L/R360L}$ *mice show no obvious differences compared with* Tbc1d24$^{+/+}$.** *Representative bright field images of Giemsa-stained blood smears from* Tbc1d24$^{+/+}$ *(left) and* Tbc1d24$^{R360L/R360L}$ *(right) mice at P16. There are no obvious differences between genotypes. Images taken at 40x magnification. Smears were analysed from both male and female mice at E18.5. Representative images from female mice. Scale bar shows 50 µm.*

4.4.2 Clinical chemistry shows reduced haemoglobin and erythrocyte volume

To further investigate the haematological phenotype of the *Tbc1d24*$^{R360L/R360L}$ mutant, blood was collected by retro-orbital bleed at P16, and haematological testing was performed using the Advia 2120 analyser. The analyser uses flow cytometry, staining and colorimetric tests to provide a full panel of haematological measurements, including RBC count and size data, haemoglobin parameters, WBC counts, and platelet count and size data [246].

As shown in **Figure 4.15**, RBC count showed a 24.3% increase in number of RBCs in the *Tbc1d24*$^{R360L/R360L}$ mutant compared with wild type ($p = 0.0052$), however, the mean corpuscular volume (MCV) was 11.4% lower in the *Tbc1d24*$^{R360L/R360L}$ mutant ($p = 0.0005$). RBC distribution width was 9.92% higher in the *Tbc1d24*$^{R360L/R360L}$ mutant compared with *Tbc1d24*$^{+/+}$ mice ($p < 0.0001$), indicating higher variation in volume and size of erythrocytes

in the mutant. Hematocrit, which measures the relative volume of RBCs compared with full blood volume, showed no significant difference between the two genotypes (p = 0.1341), although mean haematocrit was 5.0% higher in *Tbc1d24*$^{R360L/R360L}$ compared with *Tbc1d24*$^{+/+}$ mice. Overall, analysis of RBC parameters indicate an increase in number of RBCs in *Tbc1d24*$^{R360L/R360L}$, in addition to a decrease in RBC size. Smaller erythrocytes are an indication of microcytic anaemia.

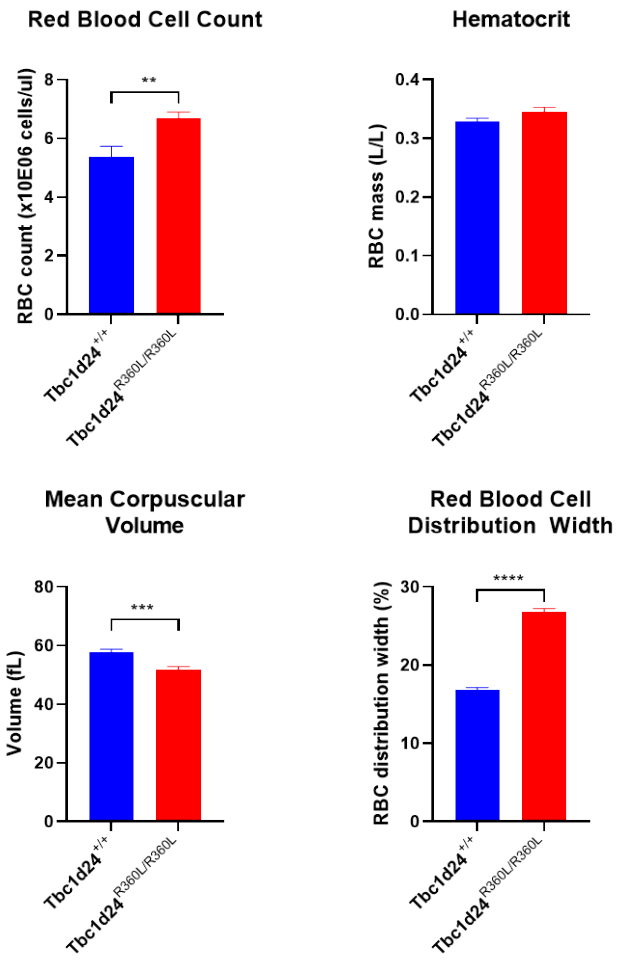


Figure 4.15 The* Tbc1d24$^{R360L/R360L}$ *mutant shows smaller erythrocyte volume with higher cell count, indicative of microcytic anaemia. *Haematological testing of red blood cell (RBC) parameters was performed using the Advia 2120 analyzer to measure RBC count (top left), haematocrit (top right), mean corpuscular volume (bottom left) and RBC distribution width (bottom right). The* Tbc1d24$^{R360L/R360L}$ *mutant showed increased number of RBCs compared with* Tbc1d24$^{+/+}$*, with smaller RBC volume and a higher distribution width. Hematocrit was not significantly different between the genotypes. Blood collected from both male and female mice. Graphs show mean ± SEM, (n = 7-10). T tests were performed.*

Strikingly, all parameters measured relating to haemoglobin content within the blood show significant decreases in the *Tbc1d24*$^{R360L/R360L}$ mutant compared with *Tbc1d24*$^{+/+}$ (**Figure 4.16**). Mean haemoglobin concentration, by colorimetric measurement, is 6.9 g/dL

in *Tbc1d24*$^{R360L/R360L}$, which is significantly lower compared with 8.8 g/dL in *Tbc1d24*$^{+/+}$ ($p = 0.0218$). The cellular haemoglobin concentration mean (CHCM), measured by light scatter, is 18.8 g/dL in *Tbc1d24*$^{R360L/R360L}$ and 24.2 g/dL in *Tbc1d24*$^{+/+}$ ($p < 0.0001$). Mean corpuscular haemoglobin (MCH) by mass is also significantly lower in the mutant ($p = 0.0004$), with 10.1 pg in *Tbc1d24*$^{R360L/R360L}$ compared with 15.4 pg in *Tbc1d24*$^{+/+}$. Finally, mean corpuscular haemoglobin concentration (MCHC), which is determined from the values for haemoglobin concentration and hematocrit, is predictably significantly lower in the mutant ($p = 0.0039$), with 19.5 g/dL in *Tbc1d24*$^{R360L/R360L}$ compared with 26.8 g/dL in *Tbc1d24*$^{+/+}$. Decreased haemoglobin in the *Tbc1d24*$^{R360L/R360L}$ mutant indicates an anaemic phenotype, consistent with expression data.

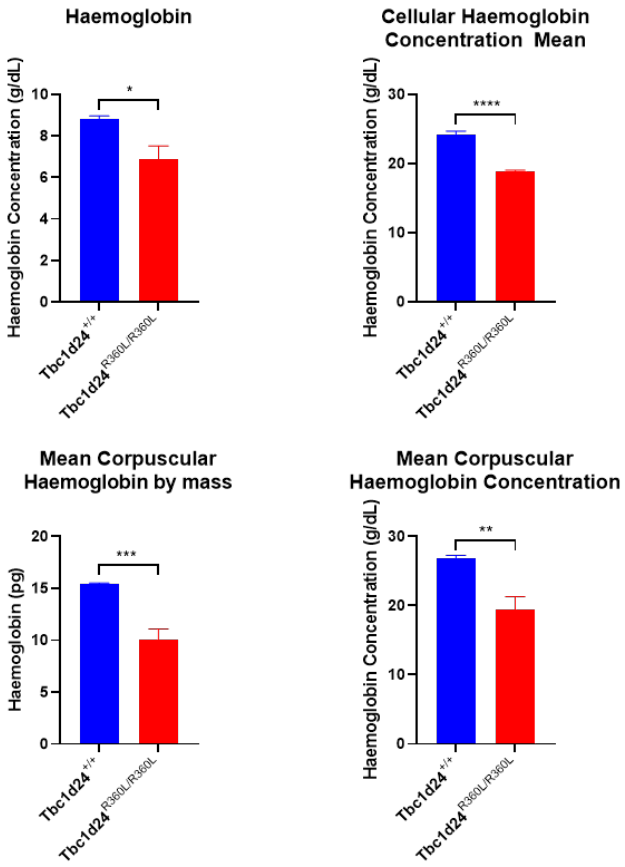


Figure 4.16 Haemoglobin concentration is decreased in Tbc1d24$^{R360L/R360L}$. *Haematological testing of haemoglobin concentration was performed using the Advia 2120 analyser to measure haemoglobin (top left), cellular haemoglobin concentration mean (CHCM) (top right), mean corpuscular haemoglobin (MCH) (bottom left) and mean corpuscular haemoglobin concentration (MCHC) (bottom right). The Tbc1d24$^{R360L/R360L}$ mutant showed decreased levels of haemoglobin compared with Tbc1d24$^{+/+}$ consistently across all measurements. Blood collected from both male and female mice. Graphs show mean ± SEM, (n = 7-10). T tests were performed.*

Platelet parameters are measured by high and low angle light scatter, which give accurate measurements of platelet count and properties including size (**Figure 4.17**). Interestingly, although platelet count is not significantly different between the two genotypes ($p = 0.309$), the *Tbc1d24*$^{R360L/R360L}$ mutant shows a higher mean platelet volume (MPV) of 10.7 fL, compared with 7.7 fL in *Tbc1d24*$^{+/+}$ ($p < 0.0001$). Platelet distribution width (PDW) is also higher in *Tbc1d24*$^{R360L/R360L}$, with 81.9% distribution width compared with 47.0% in *Tbc1d24*$^{+/+}$ ($p < 0.0001$). This finding is consistent with an increase in large platelets, which is seen in *Tbc1d24*$^{R360L/R360L}$ with a large platelet count of 48.2 x 10^{-3} cells/µl, compared with 4.4 x 10^{-3} cells/µl in *Tbc1d24*$^{+/+}$ ($p < 0.0001$). Large platelets are classified as having a diameter greater than 4 µm [247]. Microcytic anaemias characterised by small or

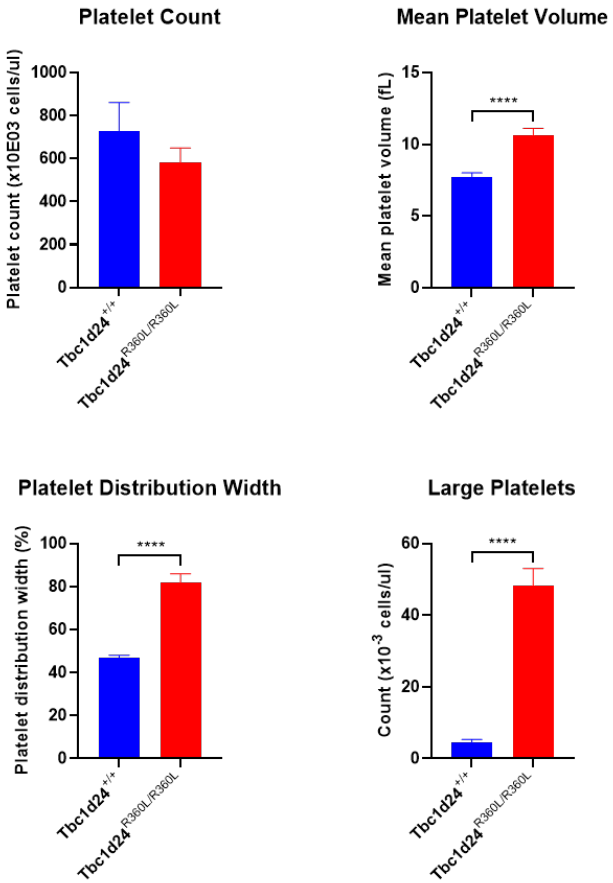


Figure 4.17 Large platelets are observed in the* Tbc1d24$^{R360L/R360L}$ *mutant. *Haematological testing of platelet parameters was performed using the Advia 2120 analyser to measure platelet count (top left), mean platelet volume top right), platelet distribution width (bottom left) and large platelet count (bottom right). The* Tbc1d24$^{R360L/R360L}$ *mutant increased mean platelet volume, platelet distribution width, and large platelet count compared with* Tbc1d24$^{+/+}$. *Blood collected from both male and female mice. Graphs show mean ± SEM, (n = 7-10). T tests were performed.*

fragmented erythrocytes can give rise to false readings of large platelets or platelet clumps [248].

White blood cells (WBCs) are measured using two different methods: the peroxidase method and the basophil method. The peroxidase method stains white cells with peroxidase, and the cells are counted based on staining and size. However, this method is known to give artificially high readings in samples containing platelet clumps, or abnormally large platelets, which are mistakenly counted as WBCs. The basophil method, which counts nuclei following removal of WBC cytoplasm, is more accurate [249]. As shown in **Figure 4.18**, there is no significant difference in WBC count between *Tbc1d24*$^{R360L/R360L}$ and *Tbc1d24*$^{+/+}$ when measured using the basophil method. However, WBC count using the peroxidase method showed a significant increase in the number of WBCs in the *Tbc1d24*$^{R360L/R360L}$ mutant ($p < 0.0001$), with a mean of 23.75 x 10^3 cells/µl in *Tbc1d24*$^{R360L/R360L}$ compared with only 3.43 x 10^3 cells/µl in *Tbc1d24*$^{+/+}$. This reading is likely to be falsely inflated by platelet clumping, consistent with the high large platelet count in the mutant (**Figure 4.17**), and the basophil method therefore gives the more accurate reading.

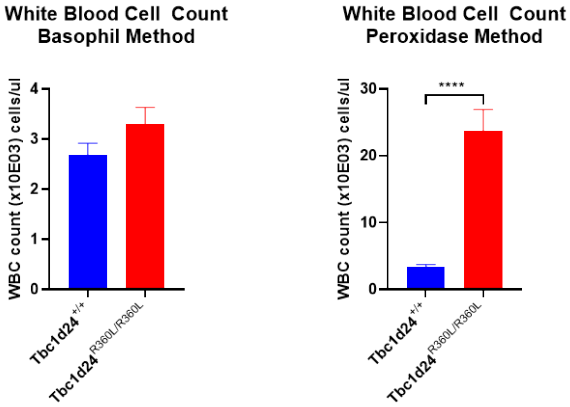


Figure 4.18 The basophil and peroxidase methods of white blood cell counting give conflicting readings for the* Tbc1d24$^{R360L/R360L}$ *mutant. *WBC counts performed using the Advia 2120 analyzer, using the basophil method (left), and the peroxidase method (right). The peroxidase method is known to give falsely high readings for WBC count in samples where platelet clumping is present. Blood collected from both male and female mice. Graphs show mean ± SEM (n = 8), T tests were performed.*

4.5 Investigating iron homeostasis

4.5.1 Iron marker mRNA expression changes in the *Tbc1d24*$^{R360L/R360L}$ and *Tbc1d24*$^{INS2/INS2}$ liver

Iron plays a vital role in the transportation of oxygen around the body by haemoglobin, and is involved in the aetiology of many types of anaemia, such as β-thalassemia [250] and iron deficiency anaemia [194]. Iron is required for the maintenance of erythropoiesis, which takes place throughout life, although there are dynamic changes in the location of erythropoiesis between embryonic, postnatal and later stages of development. In mice, primitive erythropoiesis takes place in the liver during embryonic development, and then shifts to the spleen and bone marrow from E17.5 [229]. The liver retains erythropoietic function until P9, and then continues to contribute to iron homeostasis [213].

Transcriptomics analysis of the *Tbc1d24*$^{INS2/INS2}$ showed differentially expressed genes in pathways involving iron homeostasis, and the upregulation of *Slc40a1*, encoding ferroportin, supporting a potential a link between Tbc1d24 and iron transport (**Table 7.1**). Furthermore, the transferrin receptor *Tfrc* was shown by RNA-Seq to be downregulated in the *Tbc1d24*$^{R360L/R360L}$ mutant by 0.74 fold (FDR = 7.02 x 10^{-8}) (**Table 7.2**). The decrease in haemoglobin shown by haematological analysis in the *Tbc1d24*$^{R360L/R360L}$ mutant also indicates dysfunction in haemoglobin biosynthesis, where iron plays a crucial role.

To therefore measure key markers of iron homeostasis, expression analysis was performed using RNA extracted from livers of *Tbc1d24*$^{R360L/R360L}$ and *Tbc1d24*$^{INS2/INS2}$ mutants, with wild type controls. Primers were designed to measure expression of transferrin (*Tfr1)*, ferritin heavy chain (*Ferritin H*), DMT1 (*Dmt1*) and ferroportin (*Fpn1*), in addition to haemoglobin synthesis enzyme *Alas2* and haemoglobin subunits *Hba-a2* and *Hbb-bt*. Due to the shift in location of erythropoiesis during early development, it was expected that expression data may show differences in iron homeostasis in the liver of the *Tbc1d24*$^{INS2/INS2}$ mutant at E18.5, compared with the *Tbc1d24*$^{R360L/R360L}$ mutant at P16.

As shown in **Figure 4.19**, there is no significant difference in expression of *Alas2* in the *Tbc1d24*$^{INS2/INS2}$ mutant compared with *Tbc1d24*$^{+/+}$ (p = 0.7919). *Alas2* expression is known to increase during erythropoiesis, however, expression of *Alas2* has been shown by transcriptomic data to be low in the fetal liver [251]. Additionally, at E17.5, erythropoiesis moves from the liver to the spleen and bone marrow. Surprisingly, expression of *Hba-a2* is decreased by 47.4% in *Tbc1d24*$^{INS2/INS2}$ compared with *Tbc1d24*$^{+/+}$ (p = 0.0348), although there is no difference in expression of *Hbb-bt* between the two genotypes (p = 0.4142). Expression of both *Hba-a2* and *Hbb-bt* is known to be very low in the liver at E18, in fact, expression of both genes is higher in the brain at this timepoint [252]. This may explain the difference between expression analysis by RT-qPCR of liver mRNA, and findings from transcriptomics analysis of expression in the *Tbc1d24*$^{INS2/INS2}$ cortex.

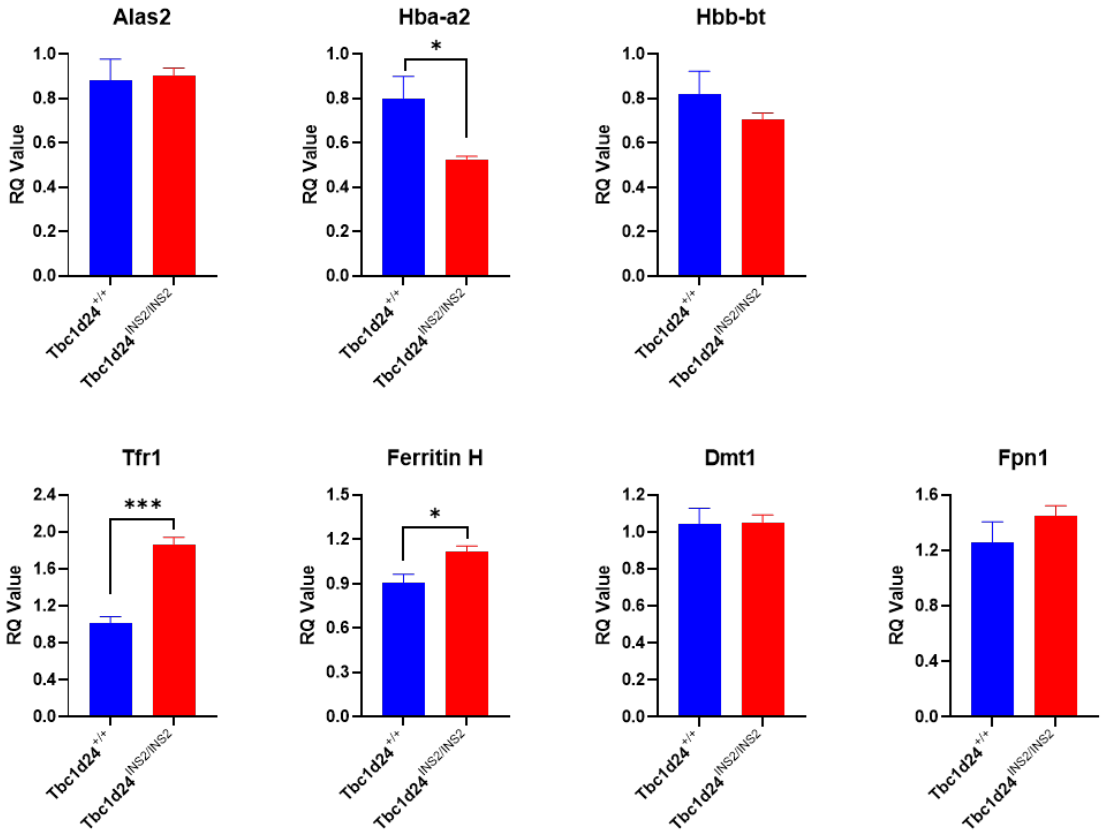


***Figure 4.19 Increased expression of markers of iron homeostasis in the liver of* Tbc1d24$^{INS2/INS2}$.** *RT-qPCR was performed using mRNA extracted from livers of* Tbc1d24$^{INS2/INS2}$ *mutants (red) and* Tbc1d24$^{+/+}$ *controls (blue) at E18.5. Expression of haematology genes* Alas2, Hba-a2 *and* Hbb-bt, *and iron homeostasis markers* Tfr1, Ferritin H, Dmt1 *and* Fpn1, *was measured by RT-qPCR. T tests were performed using ΔCT values. Blood collected from both male and female mice. Graphs show mean ± SEM, n = 4 for each genotype.*

Mean expression of *Tfr1* is upregulated by 85.5% in the *Tbc1d24*$^{INS2/INS2}$ mutant (p = 0.0006). An increase in expression of *Tfr1* may indicate an increase in circulating iron, requiring transferrin for transport. *Ferritin H* mean expression is also upregulated in *Tbc1d24*$^{INS2/INS2}$ by 11.4% compared with *Tbc1d24*$^{+/+}$ (p = 0.0343), which may indicate an increase in iron for storage. There is no significant difference in expression of either *Dmt1* (p = 0.8545), which relates to iron uptake, or *Fpn1* (p = 0.2614), relating to iron extrusion, between *Tbc1d24*$^{INS2/INS2}$ and *Tbc1d24*$^{+/+}$.

Expression of haemoglobin synthesis and iron homeostasis genes in the *Tbc1d24*$^{R360L/R360L}$ mutant was measured at the later timepoint of P16 (**Figure 4.20**). Predictably, based on transcriptomic data and expression analysis in the brain, the haemoglobin biosynthesis enzyme *Alas2* was significantly upregulated in the

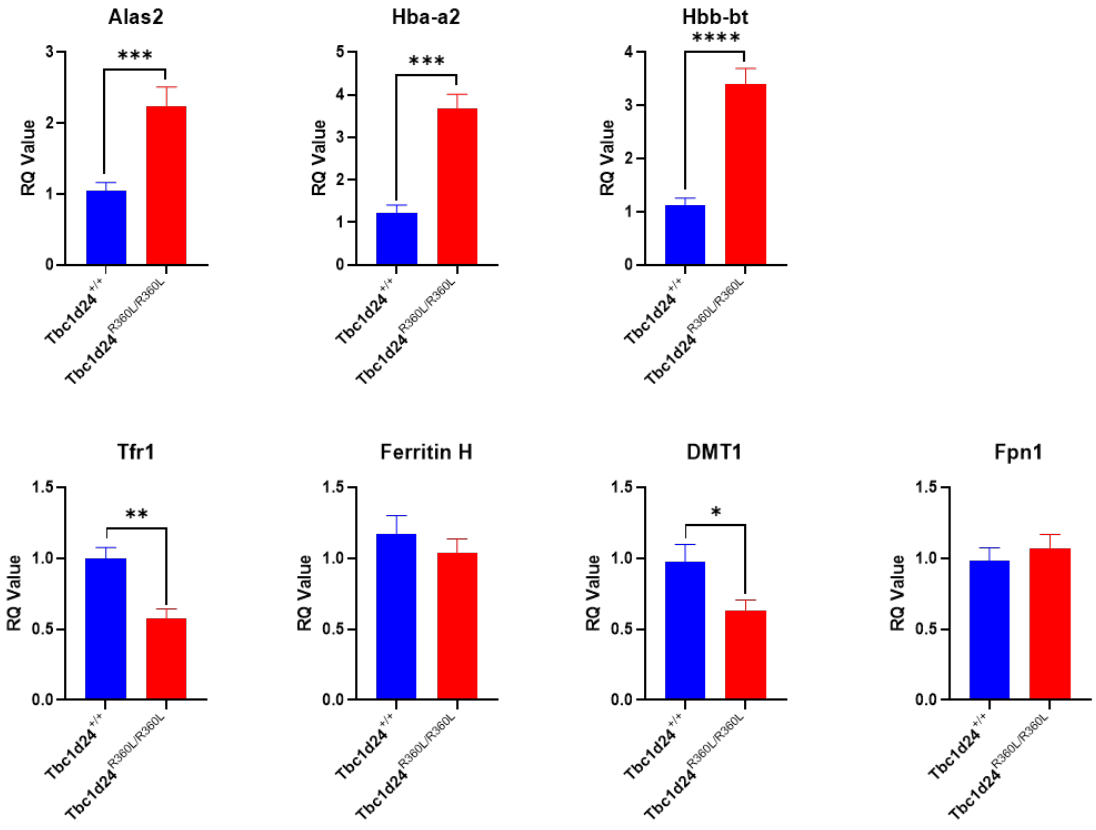


Figure 4.20 Increased expression of haemoglobin synthesis markers and decreased expression of iron homeostasis markers in the liver of the* Tbc1d24$^{R360L/R360L}$ *mutant. *RT-qPCR was performed using mRNA extracted from livers of* Tbc1d24$^{R360L/R360L}$ *mutants (red) and* Tbc1d24$^{+/+}$ *controls (blue) at P16. Expression of haematology genes* Alas2, Hba-a2 *and* Hbb-bt, *and iron homeostasis markers* Tfr1, Ferritin H, Dmt1 *and* Fpn1, *was measured by RT-qPCR. T tests were performed using ΔCT values. Blood collected from both male and female mice. Graphs show mean ± SEM, n = 5 for each genotype.*

Tbc1d24$^{R360L/R360L}$ mutant, with a 2.24 fold increase in expression (p = 0.0009). The haemoglobin subunits were also upregulated, with a 3.69 fold increase in expression of *Hba-a2* (p = 0.0001) and a 3.40 fold increase in expression of *Hbb-bt* (p = 0.00008).

Mean expression of *Tfr1* is downregulated by 42.6% in the *Tbc1d24*$^{R360L/R360L}$ mutant (p = 0.0038), conversely to the *Tbc1d24*$^{INS2/INS2}$ mutant. Mean *DMT1* expression is also downregulated in *Tbc1d24*$^{R360L/R360L}$ by 36.6% compared with *Tbc1d24*$^{+/+}$ (p = 0.0384), which may lead to a reduction in uptake of iron from the duodenum, or reduced release of iron into the cytoplasm following endocytosis. There is no significant difference in expression of either *Ferritin H* (p = 0.4117), or *Fpn1* (p = 0.5448) between *Tbc1d24*$^{INS2/INS2}$ and *Tbc1d24*$^{+/+}$.

4.5.2 Serum analysis of *Tbc1d24*$^{R360L/R360L}$ reveals disrupted iron homeostasis

To determine serum levels of ferritin, transferrin, and iron, in addition to metabolic indicators glucose, lactic acid and lactic dehydrogenase (LDH), spectrophotometric analysis was performed using a Pentra C400 analyser (**Figure 4.21**). Mice heterozygous for the R360L mutation, *Tbc1d24*$^{+/R360L}$, were included in this analysis to determine whether the mutation induces dose-respondent effects on serum parameters.

The three measurements relating to iron homeostasis each give useful and distinct information. Ferritin predominantly exists in the liver and spleen where it stores up to 4500 Fe^{3+} ions per molecule of ferritin, with a small amount of ferritin circulates in serum, where it can be used to indicate level of iron storage [253]. An increase in ferritin concentration is observed in *Tbc1d24*$^{R360L/R360L}$ serum, with an increase in mean concentration of 27.8% compared with *Tbc1d24*$^{+/+}$ (p = 0.0307) and 60.6% compared with *Tbc1d24*$^{+/R360L}$ (p = 0.0002). This suggests that iron storage is higher in the *Tbc1d24*$^{R360L/R360L}$ mutant, and may indicate iron loading anaemia. However, no increase in ferritin expression is observed in *Tbc1d24*$^{R360L/R360L}$ liver by RT-qPCR, which may indicate that increased expression occurs at an earlier time-point than P16, to produce an increase in serum ferritin. Transferrin is responsible for transport of iron in the circulation, where each molecule of transferrin carries

up to two Fe^{3+} ions, and facilitates the cellular uptake of iron through binding to transferrin receptors [254]. Serum concentration of transferrin was not significantly different between *Tbc1d24*$^{+/+}$, *Tbc1d24*$^{+/R360L}$ and *Tbc1d24*$^{R360L/R360L}$ ($p = 0.9250$), indicating that transport of iron by transferrin is as normal in the *Tbc1d24*$^{R360L/R360L}$ mutant. Iron, as quantified by the Pentra analyser, includes measurement of iron in both ferric and ferrous states, except for iron bound to heme. Strikingly, a dramatic increase in serum iron concentration was observed in the *Tbc1d24*$^{R360L/R360L}$ mutant, which showed a mean increase of 101.0% compared with *Tbc1d24*$^{+/+}$ ($p < 0.0001$) and 120.0% compared with *Tbc1d24*$^{+/R360L}$ serum concentration ($p < 0.0001$). Increased iron is a likely indicator of iron overload, which is clinically termed hemochromatosis. Hemochromatosis is usually associated with increase in both ferritin and transferrin [255]. However, high ferritin and normal transferrin levels are observed in ferroportin disease, which is caused by mutation in *Slc40a1* that leads to impaired iron export [256].

Glucose concentration was analysed by both the glucose oxidase (PAP) and hexokinase (HK) methods. Both methods found glucose concentration to be reduced in *Tbc1d24*$^{R360L/R360L}$ serum compared with *Tbc1d24*$^{+/+}$, with glucose concentration for *Tbc1d24*$^{+/R360L}$ at an intermediary level between the two. Mean serum concentration of glucose (PAP) in Tbc1d24$^{+/+}$ is 17.0% higher than in *Tbc1d24*$^{+/R360L}$ ($p = 0.0393$), and 31.6% higher than in *Tbc1d24*$^{R360L/R360L}$ ($p = 0.0006$). Similarly, mean serum concentration of glucose (HK) in *Tbc1d24*$^{+/+}$ is 17.0% higher than in *Tbc1d24*$^{+/R360L}$ ($p = 0.0647$), and 34.8% higher than in *Tbc1d24*$^{R360L/R360L}$ serum ($p = 0.0023$). Lactic acid concentration shows a trend towards increase in the *Tbc1d24*$^{R360L/R360L}$ serum, showing a mean increase of 16.6% ($p = 0.1755$) compared with *Tbc1d24*$^{+/+}$ and 31.7% ($p = 0.0106$) compared with *Tbc1d24*$^{+/R360L}$ serum. However, there was no significant difference between means of LDH concentration in serum of any of the three genotypes ($p = 0.2105$). A decrease in glucose and increase in lactic acid are consistent with increased glycolysis, which occurs under conditions of reduced oxygen [257]. There is no significant difference in lactic acid

concentration, or LDH concentration, between *Tbc1d24*$^{+/+}$ and *Tbc1d24*$^{R360L/R360L}$, which suggests there is no significant increase in lactate fermentation, which occurs under extreme hypoxia.

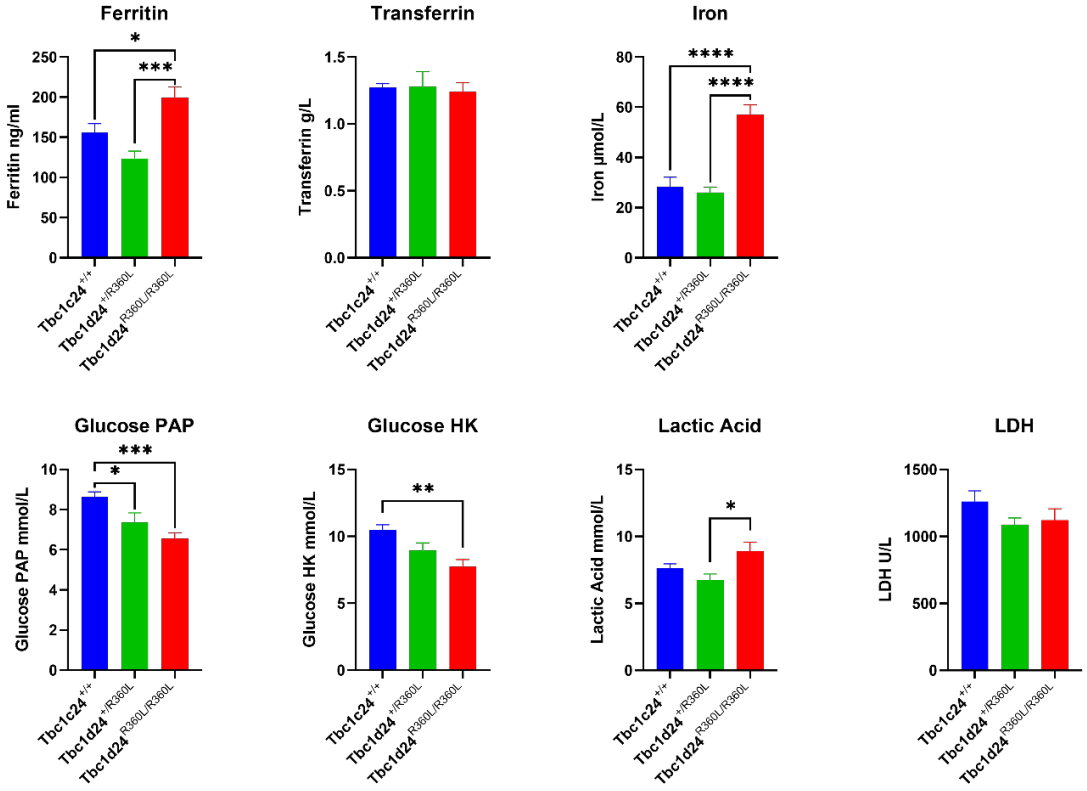


Figure 4.21 Serum analysis of the* Tbc1d24$^{R360L/R360L}$ *mutant shows an increase in iron concentration and a decrease in glucose concentration. *Spectrophotometric analysis was performed on serum from* Tbc1d24$^{+/+}$ *(blue),* Tbc1d24$^{+/R360L}$ *(green) and* Tbc1d24$^{R360L/R360L}$ *(red) mice using the Pentra C400 analyser. Measurements were taken of Ferritin, Transferrin, Iron, Glucose (PAP – glucose oxidase method), Glucose HK (hexokinase method), Lactic Acid and Lactate Dehydrogenase (LDH). Serum collected from both male and female mice. Graphs show mean ± SEM, N = 12-14 (except for Glucose HK, where N = 9-13). One way ANOVA was performed with Tukey's multiple comparisons test.*

4.5.3 Concentration of circulating free heme is reduced in the *Tbc1d24*$^{R360L/R360L}$ mutant

Heme is released from erythrocytes following haemolysis, and free heme is toxic due to its inclusion of iron, which has variable transition states and is therefore capable of generating ROS [258]. Furthermore, increased levels of circulating heme induces platelet activation [259]. To determine the presence or absence of haemolysis, and thereby help to ascertain the aetiology of anaemia in the *Tbc1d24*$^{R360L/R360L}$ mutant, the circulating concentration of free heme was measured in blood serum by colorimetric assay (**Figure**

4.22). The concentration of heme in Tbc1d24$^{R360L/R360L}$ was found to be decreased by 33.9% compared with *Tbc1d24*$^{+/+}$ (p = 0.0241). In addition, the concentration was decreased by 33.0% in *Tbc1d24*$^{+/R360L}$ compared with *Tbc1d24*$^{+/+}$ (p = 0.0355). This data is consistent with observations from peripheral blood smears of the *Tbc1d24*$^{R360L/R360L}$ mutant, which showed no apparent haemolysis. Together, these data are sufficient to exclude haemolytic anaemia [260].

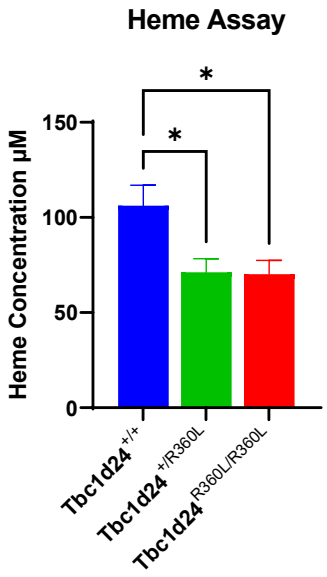


Figure 4.22 Concentration of free heme is decreased in the* Tbc1d24$^{R360L/R360L}$ *mutant. *Colorimetric assay was performed using serum samples taken from* Tbc1d24$^{+/+}$ *(blue),* Tbc1d24$^{+/R360L}$ *(green) and* Tbc1d24$^{R360L/R360L}$ *(red), in order to determine concentration of circulating free heme. One way ANOVA was performed, with Tukey's multiple comparisons test. Serum collected from both male and female mice. Graph shows mean ±SEM (N = 8-12).*

4.5.4 Glycine assay shows increased glycine, may indicate Alas2 dysfunction

Glycine is required for the synthesis of heme, through the reaction catalysed by Alas2 in the first step of the heme synthesis pathway [202]. Given that expression of *Alas2* is increased in both Tbc1d24 mutants, a reduction in glycine concentration may be expected due to increased consumption by the Alas2 enzyme. A fluorometric assay was used to measure the concentration of glycine in blood serum of *Tbc1d24*$^{+/+}$, *Tbc1d24*$^{+/R360L}$ and *Tbc1d24*$^{R360L/R360L}$ (**Figure 4.23**). The concentration was found to be increased by 70.1% in the *Tbc1d24*$^{R360L/R360L}$ mutant compared with *Tbc1d24*$^{+/+}$ (p = 0.0013). Concentration of glycine in *Tbc1d24*$^{+/R360L}$ appears to be at an intermediate level between

Tbc1d24$^{+/+}$ and *Tbc1d24*$^{R360L/R360L}$, with a 32.7% increase in glycine concentration compared with *Tbc1d24*$^{+/+}$ (p = 0.0528), and 28.2% lower concentration than *Tbc1d24*$^{R360L/R360L}$ (p = 0.0545). Contrary to prediction, the increased concentration of glycine in the *Tbc1d24*$^{R360L/R360L}$ mutant does not suggest increased Alas2 activity. An increase in glycine concentration may in fact suggest a decrease in Alas2 activity, especially together with the finding that heme concentration is decreased in the *Tbc1d24*$^{R360L/R360L}$ mutant. However, glycine is biologically active in several other pathways, including synthesis of the ATP-regenerating metabolite creatine [261], inhibitory neurotransmission [262] and synthesis of the antioxidant glutathione [263]. Elevated glycine in the

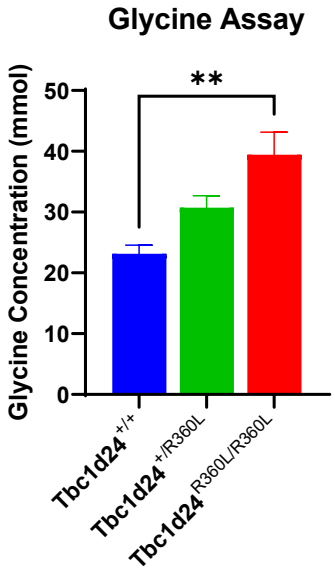


***Figure 4.23 Glycine concentration is increased in the* Tbc1d24$^{R360L/R360L}$.** *Flurorometric assay was performed using serum samples taken from* Tbc1d24$^{+/+}$ *(blue),* Tbc1d24$^{+/R360L}$ *(green) and* Tbc1d24$^{R360L/R360L}$ *(red), in order to determine concentration of circulating free heme. One way ANOVA was performed, with Tukey's multiple comparisons test. Serum collected from both male and female mice. Graph shows mean ±SEM (N = 3-5).*

Tbc1d24$^{R360L/R360L}$ mutant may therefore indicate an alteration in metabolism, neurotransmission or antioxidant defence.

4.5.5 Iron staining of the *Tbc1d24*$^{R360L/R360L}$ mutant spleen indicates iron loading anaemia

Dysfunctional iron homeostasis and increased levels of serum iron and ferritin in the *Tbc1d24*$^{R360L/R360L}$ mutant are indicative of iron loading anaemia. Though it can have

different acquired or genetic causes, overall, iron loading anaemia is characterized by dysfunctional erythropoiesis and excessive uptake of iron, leading to the harmful accumulation of stored iron [264].

DAB-enhanced Perls staining is used to visualise iron outside of heme, and preferentially stains ferric iron (Fe^{3+}), in which state iron is stored within ferritin, over ferrous iron (Fe^{2+}); iron is stained brown, enabling visualisation of iron deposits [265]. As shown in **Figure 4.24**, DAB-enhanced Perls staining detected a significant increase in iron deposits in the *Tbc1d24*$^{R360L/R360L}$ spleen, which was found to be higher by a mean of 85.0% compared to *Tbc1d24*$^{+/+}$ ($p = 0.0181$). This strongly supports an iron loading anaemia phenotype in the *Tbc1d24*$^{R360L/R360L}$ mutant.

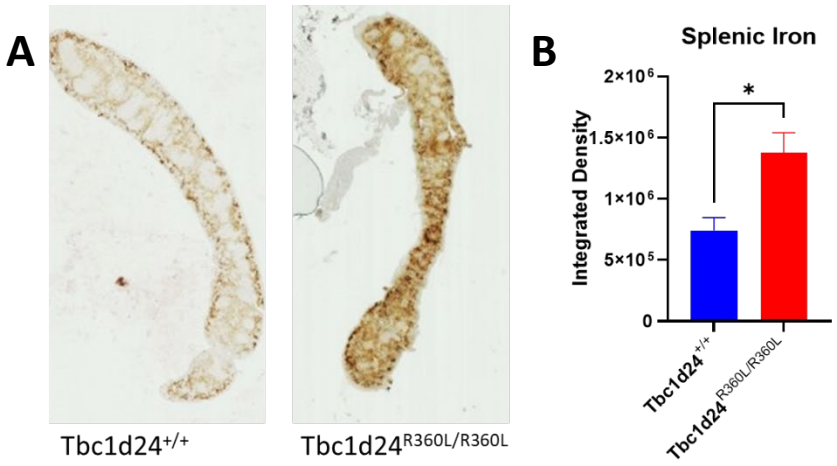


Figure 4.24 Increased iron deposits in the* Tbc1d24$^{R360L/R360L}$ *spleen indicates iron loading anaemia. *DAB-enhanced Perls staining was used to visualise iron deposits in spleens of* Tbc1d24$^{+/+}$ *and* Tbc1d24$^{R360L/R360L}$ *mice at P16. (**A**) Representative images of DAB-enhanced Perls-stained spleens in* Tbc1d24$^{+/+}$ *(left) and* Tbc1d24$^{R360L/R360L}$ *(right). Spleens were fixed in paraformaldehyde and embedded in paraffin wax before sectioning and staining. (**B**) Integrated density was calculated using ImageJ. Spleens collected from both male and female mice. Graph shows mean ± SEM, N = 4.*

4.6 Erythropoietic changes in *Tbc1d24*$^{R360L/R360L}$

4.6.1 Splenomegaly indicates stress erythropoiesis

Stress erythropoiesis can occur in response to hypoxia, and takes place mainly in the murine spleen. This can lead to enlargement of the spleen, or splenomegaly, caused by increased proliferation of erythroid progenitors [266]. Of note, stress erythropoiesis in humans predominantly occurs in the bone marrow, although splenic enlargement in mice

is often used as an indicator of anaemia [267]. As discussed previously, haematological analysis indicates an increase in the number of RBCs in the blood of the *Tbc1d24*$^{R360L/R360L}$ mutant (**Figure 4.16**). As shown in **Figure 4.25**, *Tbc1d24*$^{R360L/R360L}$ mice show enlarged spleens compared with *Tbc1d24*$^{+/+}$. Spleen weight normalised against body weight was increased by a mean of 94.9% in *Tbc1d24*$^{R360L/R360L}$ mice compared with *Tbc1d24*$^{+/+}$ mice ($p < 0.0001$) and by a mean of 73.6% compared with *Tbc1d24*$^{+/R360L}$ mice ($p < 0.0001$). The dramatic increase in spleen weight strongly indicates the presence of stress erythropoiesis in the *Tbc1d24*$^{R360L/R360L}$ mutant.

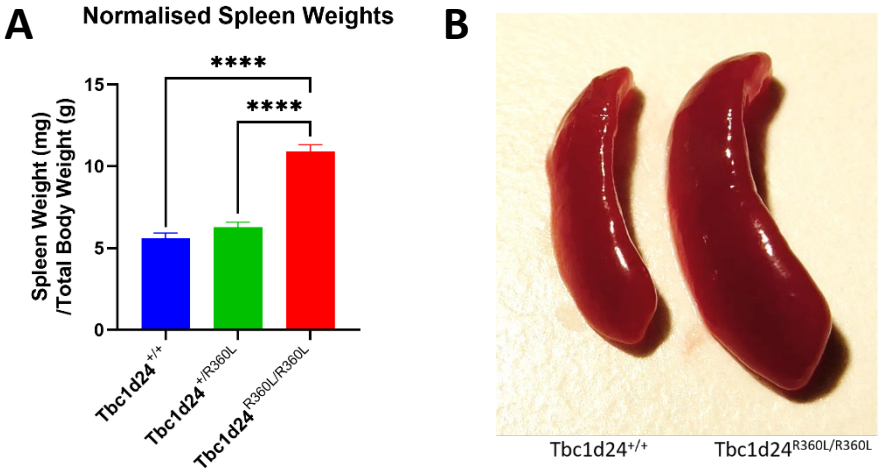


***Figure 4.25 Splenomegaly is observed in the* Tbc1d24$^{R360L/R360L}$ *mutant. (A)** Spleens dissected from male and female* Tbc1d24$^{+/+}$ *(blue),* Tbc1d24$^{+/R360L}$ *(green) and* Tbc1d24$^{R360L/R360L}$ *(red) mice were weighed and normalised to individual mouse body weight. Graph shows mean ± SEM (N = 4-7). One way ANOVA was performed with Tukey's multiple comparisons test. **(B)** Representative image of spleens dissected from both male and female* Tbc1d24$^{+/+}$ *(left) and* Tbc1d24$^{R360L/R360L}$ *(right) mice.*

4.6.2 Flow cytometry indicates stress erythropoiesis in the *Tbc1d24*$^{R360L/R360L}$ mutant

At P16, which is the end-point for the *Tbc1d24*$^{R360L/R360L}$ mutant mouse, erythropoiesis primarily occurs in the spleen, with no erythropoietic activity in the liver, and the beginnings of erythropoiesis in the bone marrow [229]. To investigate the effect of the haematological changes in the *Tbc1d24*$^{R360L/R360L}$ mutant, flow cytometry was performed in collaboration with the Wetherall Institute of Molecular Medicine (WIMM). A flow system employing CD44 and forward scatter was used to define stages of erythroblast maturity in the spleen, corresponding to basophilic (stage II), polychromatic (stage III) and

orthochromatic (stage IV) erythroblasts, and enucleated cells (stage V) [268]. Splenic stress erythropoiesis in the *Tbc1d24*$^{R360L/R360L}$ mutant was indicated by a 2.8 fold increase in number of early erythroblasts at stage III compared with *Tbc1d24*$^{+/+}$ littermates ($p = 0.0100$), and a 3.5 fold increase at stage II, although this did not reach significance ($p = 0.0918$) (**Figure 4.26A**). Furthermore, a 1.4 fold increase in reticulocytes was observed in the *Tbc1d24*$^{R360L/R360L}$ mutant compared with *Tbc1d24*$^{+/+}$ ($p = 0.0220$) (**Figure 4.26B**), which is consistent with stress erythropoiesis. Considering each erythroid progenitor stage as a proportion of all erythroid cells (Ter119+), no significant block of erythroid development is evident (data not shown). These data suggest that the increase in RBC number in peripheral blood of the *Tbc1d24*$^{R360L/R360L}$ mutant is not driven by an erythroid developmental defect. Rather, it is likely that low haemoglobin content, resulting in poor oxygen delivery, induces stress erythropoiesis. This is consistent with splenomegaly, described above (**4.6.1**).

As shown by clinical chemistry data (**4.5.2**), peripheral blood of the *Tbc1d24*$^{R360L/R360L}$ mutant shows large platelet size. This phenotype can be associated with developmental defects earlier in haematopoiesis, for example, the production of megakaryocyte-erythroid progenitor cells (MEPs) [269]. To investigate this possibility, specific surface markers for hematopoietic stem cells (HSCs), common myeloid progenitors (CMPs), granulocyte-monocyte progenitors (GMPs) and MEPs, were used to identify hematopoietic progenitor populations by flow cytometry in both spleen and bone marrow (**Figure 4.26C & D**). No difference was observed in absolute progenitor numbers between the *Tbc1d24*$^{R360L/R360L}$ mutant and *Tbc1d24*$^{+/+}$, in either spleen or bone marrow.

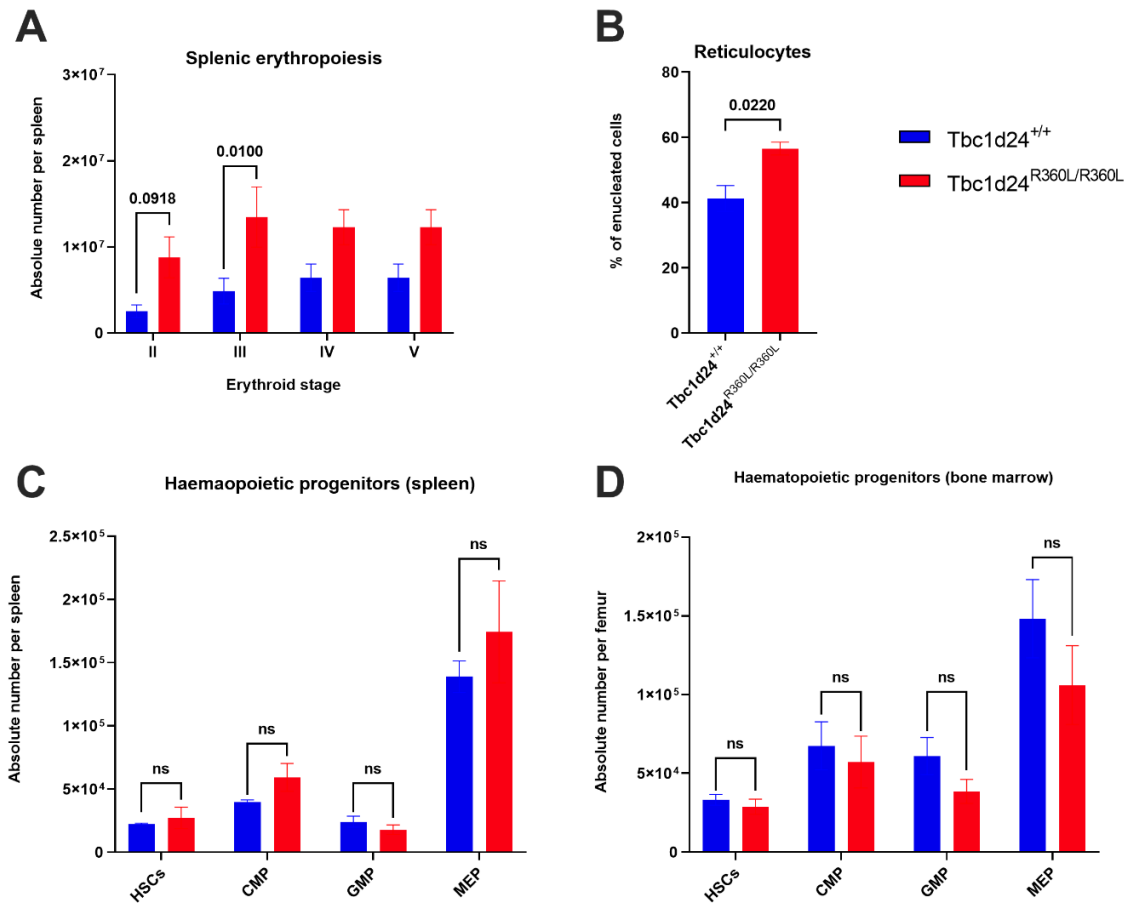


Figure 4.26 Flow cytometry indicates splenic stress erythropoiesis in the* Tbc1d24$^{R360L/R360L}$ *mutant. *Flow cytometry was performed to investigate erythropoiesis in the* Tbc1d24$^{R360L/R360L}$ *mutant (red) compared to* Tbc1d24$^{+/+}$ *littermate controls (blue).* ***A*** *– Increases in erythroblast stages II and III are observed in the mutant.* ***B*** *– Increased reticulocytes are observed in the mutant.* ***A*** *and* ***B*** *indicate splenic stress erythropoiesis (spleens dissected at P15).* ***C*** *and* ***D*** *– No differences are observed in surface specific markers between* Tbc1d24$^{R360L/R360L}$ *and* Tbc1d24$^{+/+}$ *in either spleen (****C****) or bone marrow (****D****).* ***C*** *and* ***D*** *indicate there is no effect of the R360L mutation on progenitor numbers (spleens and bone marrow dissected at P16).* ***A****,* ***C*** *&* ***D*** *2 way ANOVA with Šídák's multiple comparisons test was performed.* ***B*** *– Student's t test was performed. Flow cytometry and analysis performed in collaboration with Alexandra Preston, WIMM. Both male and female mice were used. Graphs show mean ± SEM, (N = 3-7).*

4.7 Discussion

4.7.1 Expression and haematological studies confirm that loss-of-function in Tbc1d24 results in anaemia

This chapter presents strong evidence, by way of transcriptomic studies, expression analyses, haematological measurements and cellular assays, for the novel role of Tbc1d24 in the haematological system. Loss of Tbc1d24 results in severe anaemia, as demonstrated by the *Tbc1d24$^{INS2/INS2}$* mutant, which exhibits haemolytic anaemia, and the *Tbc1d24$^{R360L/R360L}$* mutant, which exhibits iron loading anaemia with stress erythropoiesis.

The many lines of evidence described in this chapter are consistent in their indications of haematological dysfunction in the Tbc1d24 mutants, and also describe metabolic alterations corresponding to anaemia and hypoxia. Importantly, TBC1D24 has been found in the proteome of human erythroblasts, by mass spectrometry-based proteomics [270].

Transcriptomic studies consisting of RNA-Seq of both the *Tbc1d24*$^{INS2/INS2}$ and *Tbc1d24*$^{R360L/R360L}$ mutants, and microarray of the *Tbc1d24*$^{R360L/R360L}$ mutant, highlight the upregulation in expression of Alas2 and each of the Hba and Hbb globin subunits. This indicates increased drive towards haemoglobin synthesis, however, low haemoglobin content is measured in the blood of *Tbc1d24*$^{R360L/R360L}$ and indicated in peripheral blood smears of *Tbc1d24*$^{INS2/INS2}$. The *Tbc1d24*$^{INS2/INS2}$ mutant experiences a more severe anaemic phenotype than the *Tbc1d24*$^{R360L/R360L}$ mutant, evidenced by the visible pallor of *Tbc1d24*$^{INS2/INS2}$ mutant embryos, and clear haemolysis visible in blood smears.

RNA-Seq of *Tbc1d24*$^{INS2/INS2}$ revealed significant upregulation of 12 genes with FDR < 0.01 (**Table 1**) with links to anaemia, including *Tent5c*, *Slc40a1*, *Hmox1*, *Slc16a3*, *Ldha* and *Eno1*. The protein Tent5c is a nucleotidyl transferase enzyme involved in stabilization of mRNA [271]. Interestingly, Tent5c has been suggested to control erythrocyte proliferation, and *Tent5c* knockout mice experience anaemia [272]. *Slc40a1* encodes ferroportin, an iron transporter which is essential for iron homeostasis, and thus, haemoglobin synthesis; reduced ferroportin expression leads to iron accumulation and anaemia [273]. The upregulation of *Slc40a1* in the *Tbc1d24*$^{INS2/INS2}$ mutant may indicate disruption in iron homeostasis, and a compensatory mechanism to increase iron uptake. Conversely, *Hmox1* encodes Heme oxygenase 1 which catabolizes free heme into carbon monoxide, ferrous iron (Fe^{2+}) and biliverdin, and is upregulated under hypoxic conditions in a response mediated by hypoxia-inducible factor 1α (HIF-1α) [274]. *Hmox1* is also inducible under cellular stress, including OS [275]. Heme itself is pro-oxidant, and dysregulation in the levels of heme leads to OS and cytotoxicity. Given that haemolysis is visible in

Tbc1d24$^{INS2/INS2}$ blood smears, the upregulation of *Hmox1* in the *Tbc1d24*$^{INS2/INS2}$ mutant may indicate a cytoprotective response to an excess of heme.

The genes *Slc16a3*, *Ldha* and *Eno1* all relate to lactate metabolism and glycolysis. The enzyme lactate dehydrogenase A, encoded by *Ldha*, converts the end product of glycolysis, pyruvate, into lactate when oxygen is depleted. *Slc16a3* encodes Monocarboxylate Transporter 4 (MCT4), which preferentially transports lactate across the plasma membrane following glycolysis [276]. While MCT4 is most strongly expressed in glycolytic tissues such as white muscle, it is systemically upregulated under hypoxic conditions by HIF-1α [277], which also transcriptionally regulates both *Ldha* and *Eno1* [278] [279]. *Eno1* encodes the enzyme Enolase 1, which catalyses the final step of glycolysis, and has been shown to be upregulated in Fanconi anaemia [280]. In aerobic conditions, pyruvate, which is the end product of glycolysis, is metabolised to lactate and bicarbonate; pyruvate metabolism has been shown to be enriched in a mouse model of iron-deficiency anaemia, and is indicative of hypoxia [281]. In both Tbc1d24 mutants, expression analyses indicates the metabolic transition from oxidative phosphorylation to glycolysis. Remodelling to favour glycolytic metabolism has been reported in models of iron deficiency anaemia, due to the reduction in oxygen available for oxidative phosphorylation [281]. The upregulation of *Ldha*, *Eno1* and *Slc16a3* in the *Tbc1d24*$^{INS2/INS2}$ mutant, and the upregulation of HIF-1α-target genes *Vegfa* and *Flt1* supports a response to hypoxia. Interestingly, increased lactate concentrations have been reported during epileptic seizures in humans and mice, indicating increased glycolysis [282]. Thus, upregulation of *Slc16a3*, *Ldha* and *Eno1* indicate a metabolic switch favouring glycolysis in the *Tbc1d24*$^{INS2/INS2}$ mutant, consistent with anaemia and hypoxia in the mutant. In the *Tbc1d24*$^{R360L/R360L}$ mutant, a glycolytic phenotype is supported by the increase in lactic acid concentration and decrease in glucose concentration in serum. This provides evidence for the effect of disruption of *Tbc1d24* expression on metabolism.

Genes that were significantly differentially expressed in the *Tbc1d24*$^{R360L/R360L}$ mutant, but not in the *Tbc1d24*$^{INS2/INS2}$ mutant, include *Isg20*, *Cntn3*, *Epb41* and *Erdr1.* The antiviral exonuclease-encoding gene *Isg20* is upregulated in *Tbc1d24*$^{R360L/R360L}$ brain, as shown by microarray. Interestingly, *Isg20* and *Alas2* were both shown to be downregulated in mice homozygously expressing a null allele of erythroid Kruppel-like factor (EKLF), and both genes are upregulated in a cell line expressing tamoxifen-inducible EKLF, suggesting that both *Isg20* and *Alas2* are transcriptionally activated by EKLF, which is a key regulator of gene expression during both primitive and definitive erythropoiesis [283]. Given that both *Alas2* and *Isg20* are upregulated in the *Tbc1d24*$^{R360L/R360L}$ mutant, this could indicate upregulation by EKLF due to erythropoietic drive, which is supported by the stress erythropoiesis phenotype observed by flow data and splenomegaly. However, *Isg20* was not indicated by RNA-Seq as differentially expressed in the *Tbc1d24*$^{R360L/R360L}$ mutant. *Cntn3* encodes Contactin-3, which is a cell adhesion glycoprotein required for axon guidance during neuronal migration [284]. Interestingly, *Cntn3* has been found to be downregulated in patients with tuberous sclerosis complex (TSC) comorbid with drug refractory epilepsy [285]. Downregulation of *Cntn3* is likely relevant to the epileptic phenotype of the *Tbc1d24*$^{R360L/R360L}$, given the importance of tightly regulated neuronal migration in forming functional neuronal networks, although both the epileptic and anaemic phenotypes of the mutant are likely to be related. The potential overlapping aetiologies of anaemia and epilepsy in Tbc1d24 mutants, and their possible implications for treatment of both diseases, will be further discussed in Chapter Six, Discussion.

The protein Epb41 is a key constituent of the erythrocyte cell membrane, required for the formation of the cytoskeletal network and regulation of RBC morphology [286]. Although peripheral blood smears of *Tbc1d24*$^{R360L/R360L}$ did not show any striking morphological changes in RBCs, hypoxia is known to cause structural changes to erythrocytes [287], thus an increase in Epb41 may indicate a compensatory mechanism to resist these changes. Erdr1, which promotes cell survival under stress, has been shown to

induce haemoglobin synthesis in erythroid leukaemia cell lines from both human and mouse [239]. Upregulation of *Erdr1* is consistent with drive towards haemoglobin synthesis, and may also indicate a cellular stress response, due to low oxygen conditions.

In addition to haemoglobin subunits and *Alas2*, several genes were found to be differentially expressed in both Tbc1d24 mutants, including *Vwf*, *Vegfa*, *Flt1*, *Slc13a4* and *Slfn5*. *Vwf*, encoding von Willebrand factor (Vwf), is shown by RNA-Seq to be upregulated in both *Tbc1d24*$^{R360L/R360L}$ and *Tbc1d24*$^{INS2/INS2}$. Interestingly, large platelets are observed in platelet-type von Willebrand disease, which is caused by increased interaction between vWF and Glycoprotein Ib Platelet Subunit Alpha (GPIbα), due to gain-of-function mutation of the latter protein, and the subsequent increase in platelet activation [288]; large platelets are observed in *Tbc1d24*$^{R360L/R360L}$ blood. In addition, Vwf has been shown to be upregulated in patients with haemolytic anaemia [289]. Interestingly, both *Vwf* and *Vegfa* are upregulated in a neonatal rat model of iron-deficiency anaemia, which was postulated to indicate increased vascular complexity under hypoxic conditions [290]. Vascular endothelial growth factor A (Vegfa) interacts with the endothelial receptor Flk1 during angiogenesis, to enhance endothelial cell proliferation leading to the formation of blood vessels [291]. Expression of both *Vegfa* and *Flt1* is induced under hypoxia by HIF-1α [292] [293].

Slc13a4, downregulated in both Tbc1d24 mutants, is the most abundant sulphate transporter in the placenta, required in the maternal placenta for nutrient exchange and foetal development [294]. Downregulation of *Slc13a4* expression has been observed in the kidney of the *Vhl* mouse model of renal anaemia, under conditions of hypoxia, corresponding with metabolic changes in gene expression representing a shift from oxidative phosphorylation to glycolysis [295]. Slc13a4 consumes ATP; therefore, its downregulation may be in compensation for reduced oxygen availability and metabolic stress. Finally, the gene *Slfn5* is upregulated in the *Tbc1d24*$^{R360L/R360L}$ mutant but downregulated in the *Tbc1d24*$^{INS2/INS2}$ mutant. Slfn5 belongs to a family of interferon-

stimulated genes, although its role is not well understood, and varies depending on cell type [296].

4.7.2 Hypothesised mechanism of action

The controlled regulation of iron homeostasis is required for haemoglobin synthesis and erythropoiesis. Iron must be absorbed in the duodenum, passed to the circulation and transported to organs for utilization and storage, while preventing dangerous redox cycling due to the variable transition state of iron. Disruption in iron homeostasis has wide-ranging deleterious consequences. Iron regulatory proteins (IRPs) regulate expression of iron metabolism proteins including transferrin, ferritin and Alas2, and disruption in expression of IRPs results in microcytic anaemia and neurodegeneration [297]. Depletion in available iron, either by low levels of stored iron or disrupted iron mobilization from storage, results in iron-limited erythropoiesis, producing RBCs with low haemoglobin [298].

The data in this chapter point towards the *Tbc1d24*$^{R360L/R360L}$ mutant displaying iron loading anaemia due to disrupted iron homeostasis and a transcriptional drive towards haemoglobin synthesis. However, haematological measurements show a reduction in circulating haemoglobin and heme. *Tbc1d24*$^{R360L/R360L}$ serum shows dramatically increased concentrations of iron and ferritin, with normal levels of transferrin, indicating an increase in iron storage, which is confirmed by visualization of iron stores in the spleen. Flow cytometry shows increased stress erythropoiesis, and RBCs are shown to be smaller. Taken together, these results signify that, while iron uptake and storage are functional in the *Tbc1d24*$^{R360L/R360L}$ mutant, iron is unable to mobilize from stores to associate with haemoglobin. In order to characterise the underlying mechanism of iron loading anaemia, measurement of levels of hepcidin, the hormonal regulator of iron extrusion through ferroportin [216], and erythropoietin, which stimulates erythropoiesis in response to hypoxia [202], should be performed, in addition to analysis of inflammatory status markers such as IL-6 to preclude inflammatory hepcidin expression [299].

From the data in Chapter 3, combined with human genetic studies, suggests a strong functional link between Tbc1d24 and the V-ATPase. Circulating iron is transported by transferrin, which is taken up by cells when it binds to Tfr1 and endocytosis takes place. For iron to be released into the endosome within the cell, the endosomal pH must be sufficiently acidic for iron to dissociate from transferrin. Extrusion of iron from the endosome occurs through DMT1, which also relies on acidic pH to cotransport iron with H^+ into the cell [215]. Alternatively, DMT1 is also able to transport uncoupled iron in the absence of a H^+ gradient [217]. Endosomal acidification is essential for iron homeostasis, and the synthesis of haemoglobin. Acidification of the endosome occurs through the V-ATPase [300] and it has been shown that inhibition of the V-ATPase by bafilomycin *in vitro* results in decreased cellular heme and haemoglobin, indicating that the V-ATPase is essential for haemoglobin synthesis [301]. Furthermore, bafilomycin treatment of reticulocytes, containing endosomes labelled with the radioactive isotope ^{59}Fe bound to transferrin, blocked the synthesis of heme, providing evidence both for the essential role of the V-ATPase in heme synthesis, and for the necessary source of heme iron as being transferrin-derived, rather than from a chelatable pool [302]. Finally, the V-ATPase assembly factor CCDC115 has been identified as a determinant of transferrin-bound iron uptake by endocytosis, and disruption of CCDC115 by gene-specific CRISPR-Cas9 ribonucleoproteins, to produce a *CCDC114*$^{-/-}$ erythroid cell line, led to impaired heme trafficking [303].This indicates that factors influencing endosomal acidification can be essential for heme synthesis. Given the importance of the V-ATPase for vesicle acidification, and the proven interaction between Tbc1d24 and the cytosolic V1 subunits of the V-ATPase, this interaction may be critical for effective acidification and the downstream synthesis of heme.

4.7.3 Concluding Remarks

This chapter has investigated and quantified the unexpected anaemic phenotype of two mouse models of Tbc1d24 dysfunction, *Tbc1d24*$^{INS2/INS2}$ and *Tbc1d24*$^{R360L/R360L}$, and presented a novel role for Tbc1d24 in the haematological system. Furthermore, based on

the mechanistic hypothesis proposed in Chapter Three, one explanation is that the interaction between Tbc1d24 and V-ATPase is necessary for endolysosomal trafficking, and that disturbance of this interaction leads to disruption in iron homeostasis, resulting in anaemia (**Figure 27**).

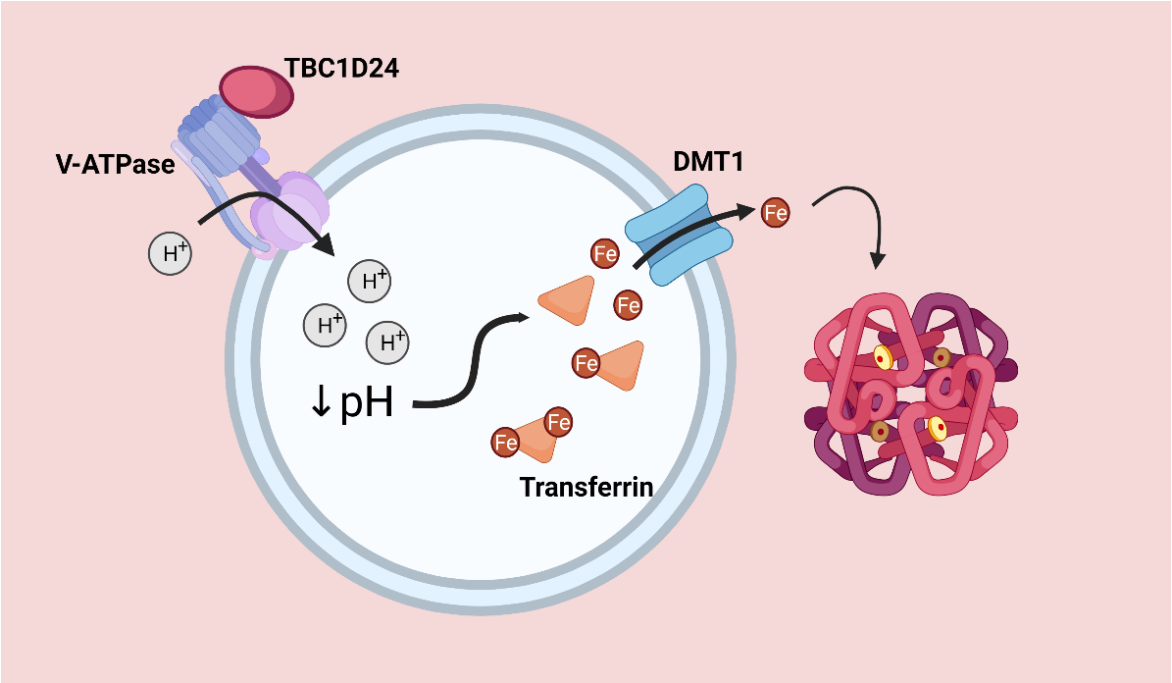


Figure 4.27 Functional Tbc1d24 protein is required for in Heme synthesis. *The proposed mechanism for the iron-loading anaemia observed in the Tbc1d24$^{R360L/R360L}$ mutant; disruption of the interaction between Tbc1d24 and the V-ATPase caused by the R360L mutation leads to dysfunctional acidification of the endosome, which prevents the release of transferrin-bound iron into the endosome, thus disrupting the synthesis of heme and impeding erythropoiesis. Created with Biorender.com.*

Chapter 5: Investigating the neuroprotective role of OXR1 *in vitro* and *in vivo*

5.1 Introduction

5.1.1 The role of Oxr1 in neuroprotection, and therapeutic potential of endogenous neuroprotective mechanisms to rescue neurodegeneration

The involvement of OXR1 in protecting against oxidative stress (OS) has been well established in recent years using loss-of-function model systems, including the *bella* mouse knockout model [304], *in vitro* knockdown of human OXR1 [305] and in an ischaemic model in which inhibition of Oxr1 expression is associated with oxidative injury [306]. The molecular function of OXR1 is still being elucidated, however; suggested mechanisms include the oligomerization of the antioxidant chaperone protein peroxiredoxin 2 (Prdx2), through which Prdx2 favours the formation of high molecular weight complexes with enhanced chaperone activity in response to OS [307], while another is the regulatory role of OXR1 in the cell cycle and apoptosis through its interaction with the p53 signalling pathway [308].

Interestingly, while the loss-of-function of OXR1 is detrimental to cellular function in many contexts and may instigate pathways related to OS, overexpression of the protein has proved to be a valuable method for protection against cell death both *in vitro* and *in vivo*. For example, overexpression of OXR1 has also been found to play a protective role when applied to neurodegenerative disease models involving a component of OS. *In vitro*, stable expression of human OXR1 (hOXR1) in the 661W photoreceptor cell line was shown to reduce levels of ROS and caspase cleavage when exposed to hydrogen peroxide (H_2O_2), while *in vivo,* subretinal injection of adeno-associated virus (AAV)-packaged hOXR1 into a mouse model of early-onset retinal degeneration improved photoreceptor function and delayed retinal degeneration [309]. Increasing Oxr1 levels in cells expressing mutant Fused in Sarcoma (FUS) and TAR DNA-binding protein 43 (TDP-43) has been shown to ameliorate ALS-associated cellular pathology, including cytoplasmic aggregation and mitochondrial morphology defects [310]. At the whole organism level, an ALS mouse model,

(*hSOD1*^{G93A}), was crossed with a neuron-specific Oxr1 overexpressor transgenic mouse line to investigate the potential for rescue of ALS-associated pathologies *in vivo* [125]. Interestingly, *hSOD*^{G93A} offspring from the cross expressing the Oxr1 transgene showed significantly extended survival and improved neuromuscular function and motor coordination. Furthermore, *in vivo* overexpression of Oxr1 in a further ALS mouse model, expressing the M337V mutant form of TDP-43, was found to reduce aberrant mislocalization of the mutant protein and improve muscle denervation and neuromuscular junction degeneration, significantly improving motor function in the mice expressing the Oxr1 transgene [311]. Importantly, transcriptomic studies within the *hSOD*^{G93A} mouse line have demonstrated that over-expression of the Oxr1 protein was not detrimental to spinal cord pathology; indeed, the only differentially expressed gene was from the Oxr1 transgene itself. Furthermore, presence of the transgene delayed early transcriptome changes related to ALS pathogenesis such as neuroinflammatory pathways in *hSOD*^{G93A} mice [125], suggesting the promise of future treatments to take advantage of Oxr1 neuroprotection [312].

Antioxidant therapies have been widely explored for the treatment of neurodegenerative diseases, such as Coenzyme Q10, which increases the levels of antioxidant enzymes [313], Sulforaphane, which activates the OS-defensive NRF2/ARE signal pathway [314], and the free radical scavenger Naringenin [315], all of which showed some ameliorative effect when applied to models of epilepsy. However, antioxidant therapies have had limited beneficial effect, which has been attributed to many factors, including difficulties in supplying the antioxidant to the site of damage for the right duration and also at a physiological beneficial level [316]. Importantly, these compounds only target one type of ROS and not the source of the OS itself [317]. Therefore, it may be more effective to target the body's endogenous cellular mechanisms to protect against OS. Endogenous antioxidant systems usually maintain a healthy oxidative balance, by preventing production of ROS or by removing ROS when they occur [318]. These

endogenous mechanisms show potential as therapeutic targets to enhance neuroprotection and ameliorate the detrimental effects of OS in neurological disease. For this purpose, Oxr1 shows real promise from multiple lines of evidence *in vitro* [309] [310] [319], and *in vivo* [309] [125] [311], combined with the apparent tolerability of artificially increased expression levels [122].

5.1.2 OXR1-C is functionally sufficient and confers neuroprotection

As introduced above (**1.2.3**), mammalian OXR1 is expressed as multiple isoforms, with a set of full-length (FL) isoforms containing all the functional domains, alongside a shorter isoform (C) with a unique promoter and first exon followed almost exclusively by the TLDc domain (**Figure 1.1**). In an initial attempt to compare the functionality of these isoforms, co-immunoprecipitation experiments revealed that Oxr1-C interacts with more binding partners when exposed to OS as opposed to in non-OS conditions, while Oxr1-FL interacts with the same binding partners regardless of conditions, thus supporting different functional roles for the two protein isoforms [310]. Crucially, there are several lines of evidence that the short isoform alone can functionally compensate for loss of the longer isoforms *in vivo*. Work in the fly has demonstrated that loss of the *OXR1* homolog *mtd*, which leads to pupal lethality or eclosion defects in *Drosophila*, can be rescued by expression of either human *OXR1-C* or truncated *NCOA7*, both of which contain only a functional TLDc domain [320]. Furthermore, in the mouse, the *bella* mutant - which lacks all of the OXR1 isoforms - exhibits severe cerebellar neurodegeneration [304], while a gene-trap insertional mutant mouse line with disrupted expression of all the FL isoforms (*Oxr1*$^{Gt(RRR195)Byg}$) do not show any pathological signs [304] [116], suggesting that presence of the remaining short isoform of the gene is sufficient to prevent cell death.

One of the currently available mouse models for overexpression of Oxr1, *Tg(mPrnp-Oxr1)*, expresses a full-length isoform (Oxr1-FL) driven by a prion promoter [125], in line with the majority of the overexpression studies that have used these isoforms [125] [311]. Importantly, others have also investigated the protective potential of the OXR1-C isoform,

for example, expression of OXR1-C has been demonstrated to supress spontaneous oxidative mutation in a bacterial mutagenesis assay [321]. The clinical significance of this isoform has also been suggested by the discovery of a heterozygous nonsense mutation near the start codon of *OXR1-C* that is associated with specific language impairment (SLI); this apparent haploinsufficiency of OXR1-C indicates that loss of only one copy of the short isoform leads to detectable neurodevelopmental disorder [322].

While both OXR1-FL and OXR1-C are protective against oxidative stress, there are key differences in the expression regulation of each protein. Isoforms of *Oxr1* expressed in the mouse brain show different subcellular localizations, with *Oxr1-FL* localised in the cytosol while *Oxr1-C* is associated with the outer mitochondrial membrane [323]. Additionally, different levels of antioxidant protection are observed depending on subcellular localization, with *Oxr1-C* conferring greater protection against OS-induced apoptosis when expressed in the cytosol than in its endogenous localization [323]. The two isoforms were demonstrated *in vivo* to be induced at different time points during the OS response, with Oxr1-FL induced 30 minutes after H_2O_2 treatment and Oxr1-C induced 120 minutes after treatment, suggesting that they are not co-regulated [310]. *In silico* analysis has confirmed that the isoforms are expressed under different promoters (Williamson, unpublished). Furthermore, *Oxr1-FL* itself is expressed under two different promoter regions, and transcriptional activity switches between the two across development and adulthood, in contrast to the single promoter of *Oxr1-C*, which regulates transcription of the protein throughout (Svistunova, unpublished). Crucially, while comparison of the genomic sequences between human and mouse *OXR1* isoforms showed no conservation of the FL promoter region across species, a short sequence of approximately 400bp immediately upstream of the translation start site of *OXR1-C* was found to be highly conserved between human and mouse, suggesting that this region plays a key role in the regulation of OXR1-C expression (Figure 1 below). Due to this high level of promoter conservation, and compelling evidence that expression of Oxr1-C alone is functionally sufficient, Oxr1-C

therefore appears a promising target for translational research into protection against OS as a therapeutic strategy in neurological disease.

The aim of this Chapter was to investigate two independent modes of OXR1 up-regulation as protective factors: first, to apply a small-molecule approach to modulate the OXR1-C endogenous promoter, and second, to utilise the *in vivo* genetic over-expression system to determine whether OXR1 could functionally compensate for a loss-of-function Tbc1d24 mutation *in vivo*.

5.2 Investigation of OXR1-C promoter for use in compound screening

Recent advancements in high-throughput screening have increased the efficiency and accuracy of therapeutic compound identification, in particular through the development of coincidence reporters [324]. These systems use two separate reporter enzymes to detect biological changes in parallel, enabling reliable readouts of biologically active compounds. The Nano-Glo Dual-Luciferase Reporter Assay System (henceforth referred to as NanoGlo), designed by Promega, enables expression of Firefly luciferase and Nano luciferase under a chosen promoter, and is therefore suitable for assay of transcriptional regulation of the OXR1-C promoter and use in a compound screen. Firefly luciferase, a bioluminescent enzyme found in the firefly family *Lampyridae* [325], is structurally different to Nano luciferase, which was engineered from the deep sea shrimp *Oplophorus gracilirostris* [326], and is quenched using the 'Stop & Glo' format to enable independent measurements of the two enzymes, irrespective of overlap between the two signal emission wavelengths.

The NanoGlo coincident reporter assay applies measurement of two luminescent signals at different time points in an add-read-add-read experimental assay. Used with the Promega vector pNLCol1[*luc2*-P2A-*NlucP*/Hygro], the system allows coincident measurement of the activity of a chosen promoter, when transfected into cells. The vector contains two luciferase genes, Firefly luciferase (FireflyLuc) and Nano luciferase (NanoLuc), separated by a P2A peptide sequence which allows the two luciferase proteins

to be expressed separately as functional enzymes. In addition, the vector contains antibiotic resistance genes, allowing antibiotic selection, and a cloning region, allowing insertion of the chosen promoter.

Analysis *in silico* of the promoters of the OXR1 isoforms revealed a region of the OXR1-C promoter which shows a high level of conservation between humans and mice (**Figure 5.1**). The sequence is approximately 400 bp in length, and immediately upstream of the start site of translation, indicating that the sequence is important in regulating expression of Oxr1 protein. This highly conserved region is promising in its suitability for translational research, as any transcriptional regulation of Oxr1 at this promoter region observed in murine studies, can be applied to human pharmacological screens.

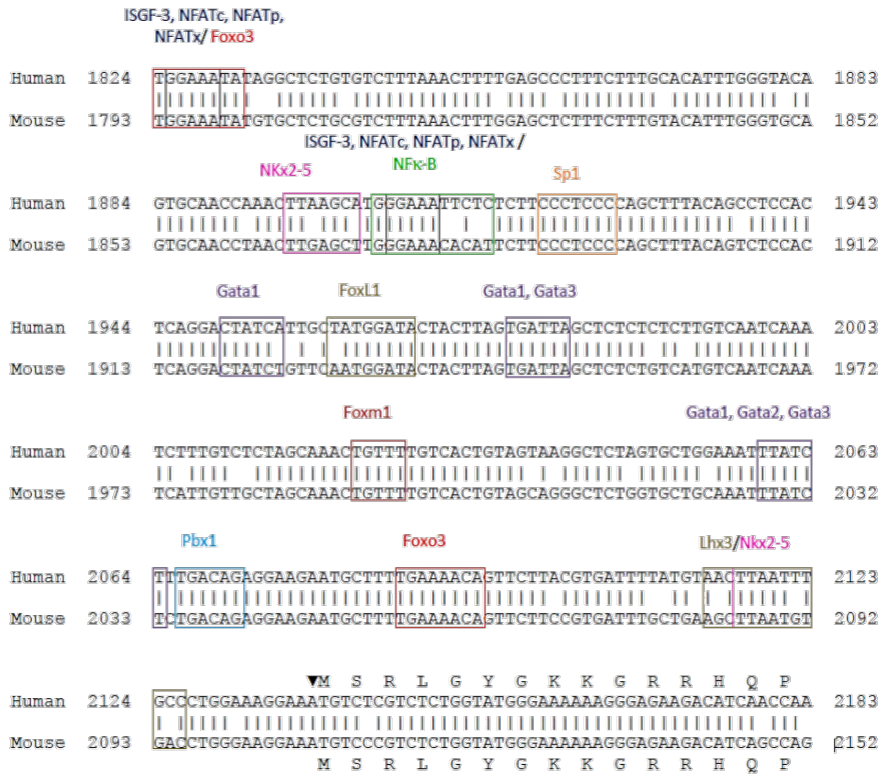


Figure 5.1 Sequence alignment of human and mouse promoter regions of Oxr1-C (Williamson, 2015). *Sequences show high level of conservation between human (top: NM_001198534) and mouse (bottom: NM_001130164) promoter regions of Oxr1-C. * = start site of transcription of 5' untranslated region. ▾= start site of translation, with corresponding amino acids shown from translated exon. Boxes show putative transcription factor binding sites for the following transcription factors: Foxl1, Foxm1, Foxo3, Gata1/2/3, Isgf-3, Lhx3, Nf-κB, NFATc/p/x, Nκx2.5, Pbx1, and Sp1.*

The 400bp region of the OXR1-C promoter was inserted ahead of the luciferase genes within the vector by cloning to produce a construct which, when transfected into cells or when stably expressed, enables formation of a biocircuit which expresses the two luciferases under the control of the OXR1-C promoter. Therefore, any compound which interacts with the promoter to alter luciferase expression in transfected cells could be assumed to exert the same alteration on endogenous OXR1 expression. Following transfection of the construct into Neuro2a (N2a) cells, the resulting biocircuit was tested by luciferase assay, and produced a strong signal from both luciferases, with a 19-fold increase in luminescence from FireflyLuc and 4-fold increase from NanoLuc, compared to transfection with the Promega vector without promoter (**Figure 5.2**). This demonstrates that the conserved promoter region of OXR1-C is functional, and capable of driving luminescence from the luciferase reporters.

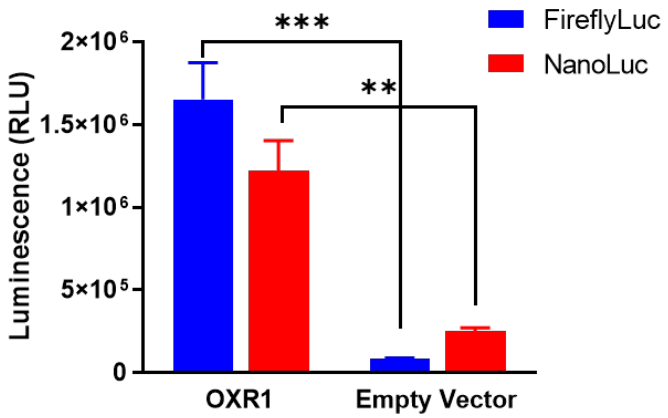


Figure 5.2 Transfection with OXR1-C promoter construct drives luminescence in NanoGlo system. *N2a cells were transfected with luciferase reporter constructs with (OXR1) and without (Empty Vector) the OXR1-C promoter to drive expression of two luciferases, FireflyLuc (blue) and NanoLuc (red). Graphs show mean ± SEM (n = 7).*

While the 400 bp OXR1-C promoter was chosen for the assay due to the high degree of sequence conservation, a construct was also made using a larger putative promoter region including an additional 600bp of upstream genomic sequence (1kb in total). This would likely increase the chance of obtaining positive screening hits while adding a confirmatory second stable cell line, although it is noteworthy that the sequence identity between mouse and human for the additional 600bp is very low.

5.2.1 Transient transfection reciprocal inhibition with NanoGlo

The coincident reporter system relies on the use of two genes with reporter activity that are expressed, and therefore modified, independently of each other, while being measured in parallel. To validate the coincident activity of the reporters, stabilizing inhibitors are used to obtain specific responses from each reporter. In the NanoGlo system, Firefly and Nano luciferases are inhibited by the drugs PTC124 and Cilnidipine, respectively, in a stabilizing manner, producing an increase in luminescent signal at low to medium concentrations of the drug, followed by a decrease in signal at high concentrations. Pharmacologically, this response is explained by initial binding and activation by the drug at lower concentrations, followed by stabilisation and inhibition of the luminescent signal as concentrations increase [327]. When the inhibitor is applied to the system, stable inhibition is observed in the specific channel of the luciferase it inhibits, while activity in the alternate

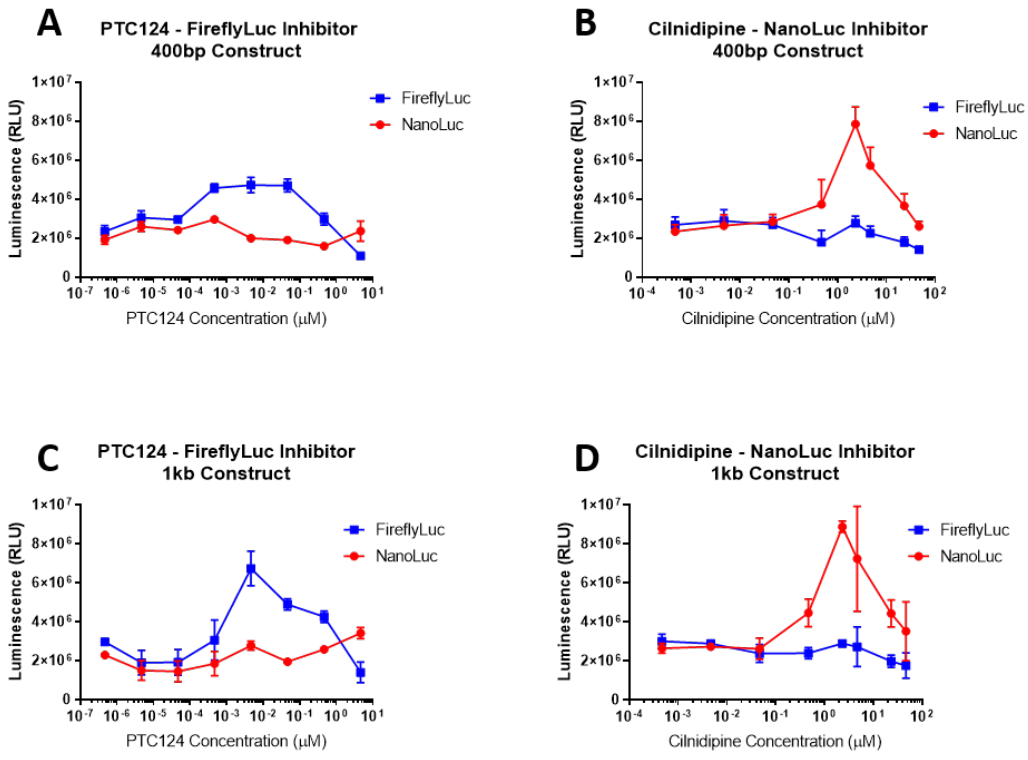


Figure 5.3 Validation of the coincidence reporter system using OXR1-C promoters of 400 bp and 1 kb length, using transient transfection. *The selective inhibitors PTC124 and Cilnidipine were applied exogenously to the cell-based transiently transfected reporter system at a range of concentrations, to observe specific responses from FireflyLuc (blue, inhibited by PTC124) and NanoLuc (red, inhibited by Cilnidipine). Two promoter constructs were tested, of lengths 400 bp (A & B) and 1 kb (C & D). Selective inhibition was found to produce reporter-specific responses measured as luminescent readings. Graphs show mean ± SEM, n = 4.*

channel remains constant. This is in contrast to the activity of a biologically active compound, which would alter activity in the channels of both luciferases [324].

Selective stabilizing inhibition was therefore applied to the NanoGlo system following transient transfection with each promoter construct in N2a cells, and specific responses were obtained from each luciferase: each channel was modulated by varying concentration of its own selective inhibitor (either PTC124 or Cilnidipine), producing a bell-shaped curve, while the alternate produced a stable signal (**Figure 5.3**). This therefore validated the coincident activity of the dual reporter system.

5.2.2 Transient transfection transcriptional assays with NanoGlo

Several putative transcription factor (TF) binding sites have been identified within the conserved 400bp OXR1-C promoter region (**Figure 5.4**). In order to further validate the coincidence reporter system, and to probe its sensitivity and ability to be modified by exogenous compound application, three TFs were selected for assay by transient transfection: Sp1, Pbx1 and Nκx2.5. The transcription factors were cloned from mouse cDNA to produce constructs driven by the cytomegalovirus (CMV) promoter. All three TFs were found to significantly enhance luminescence in the FireflyLuc channel, compared with luminescence when transfected with the biocircuit alone, including an increase in luminescence of over 15-fold when transfected with Nκx2.5. (**Figure 5.4A**). However, NanoLuc luminescence was significantly enhanced in response to only one of the three TFs tested, Pbx1, and showed a potential increase when transfected with Sp1, while transfection with Nκx2.5 did not significantly alter luminescent signal at all (**Figure 5.4B**). The two luminescence readings taken together suggest that Nκx2.5 induced a false-positive response from FireflyLuc. This highlights – and validates – an important feature of the coincidence reporter, desirable in any drug-discovery system: namely, the inbuilt capacity for detection of false-positive results.

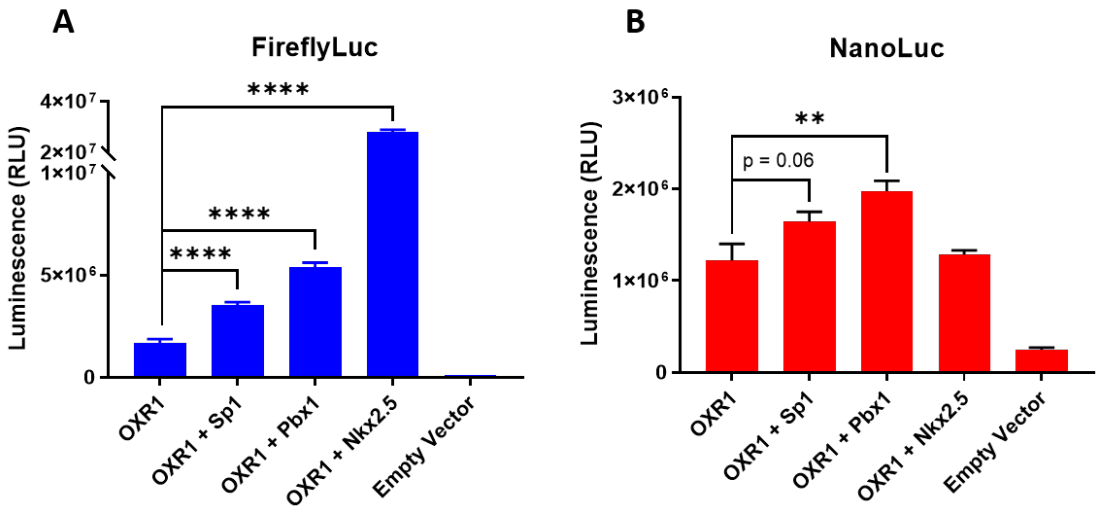


Figure 5.4 Identification of transcription factors that affect luminescence within the transiently transfected reporter system. *Luminescence readings shown in response to transient transfection with a reporter driven by the conserved 400 bp OXR1-C promoter, along with transcription factors Sp1, Pbx1 or Nkx2.5. Firefly luciferase (**A**, blue) and Nano luciferase (**B**, red) luminescence readings are both significantly increased when cells are transfected with the reporter and Pbx1, indicating a true interaction with the promoter, whereas Nkx2.5 increases luminescence only in Firefly luciferase, indicating a false positive interaction. Graphs show mean ± SEM, n = 7.*

5.3 Generation of a stable cell line

Having validated the suitability of the OXR1-C luciferase coincidence reporter system for use in compound screening, the system could then be transitioned into a stably-expressing cell line, to enhance consistency across and facilitate higher throughput screening [328]. Stable cell lines exhibit consistent expression of the integrated construct, yet with typically lower expression levels than transient transfection experiments. Both promoter constructs were transfected to produce stable cell lines, and it was decided that the initial compound screen would be performed using the line expressing the full-length promoter construct, while the line containing the 400 bp promoter construct would be used to validate results and to determine potential suitability for future *in vivo* testing in both mice and humans.

5.3.1 Antibiotic selection kill curve

Selection of stably transfected cells is enabled by the hygromycin resistance gene, which is built into the original coincidence reporter construct. Before these cell lines could be generated, the concentration of hygromycin in cell media first needed to be determined,

such that it would reliably kill most cells incubated without causing total cell death, ensuring that cells expressing the hygromycin-resistant construct were still viable. Based on this principle, a hygromycin kill curve experiment was performed (**Figure 5.5**). As expected, increasing concentration of the antibiotic led to decreasing cell survival with immediate effect. Between 10 and 14 days post seeding, a decline was observed in cell survival for all concentrations except 200 µg/ml, representing cell death due to starvation and/or overcrowding past 10 days [329]. At day 10 post seeding, at a concentration of 800 µg/ml, cell survival was 74% lower than at 100 µg/ml, which showed the maximum cell survival. At concentrations of 1000 µg/ml and 1200 µg/ml, cell survival was 14.9% and 14.3% respectively, indicating stabilization of the effect of antibiotic concentration. Therefore, it was determined that cell-selection media would contain 800 µg/ml hygromycin.

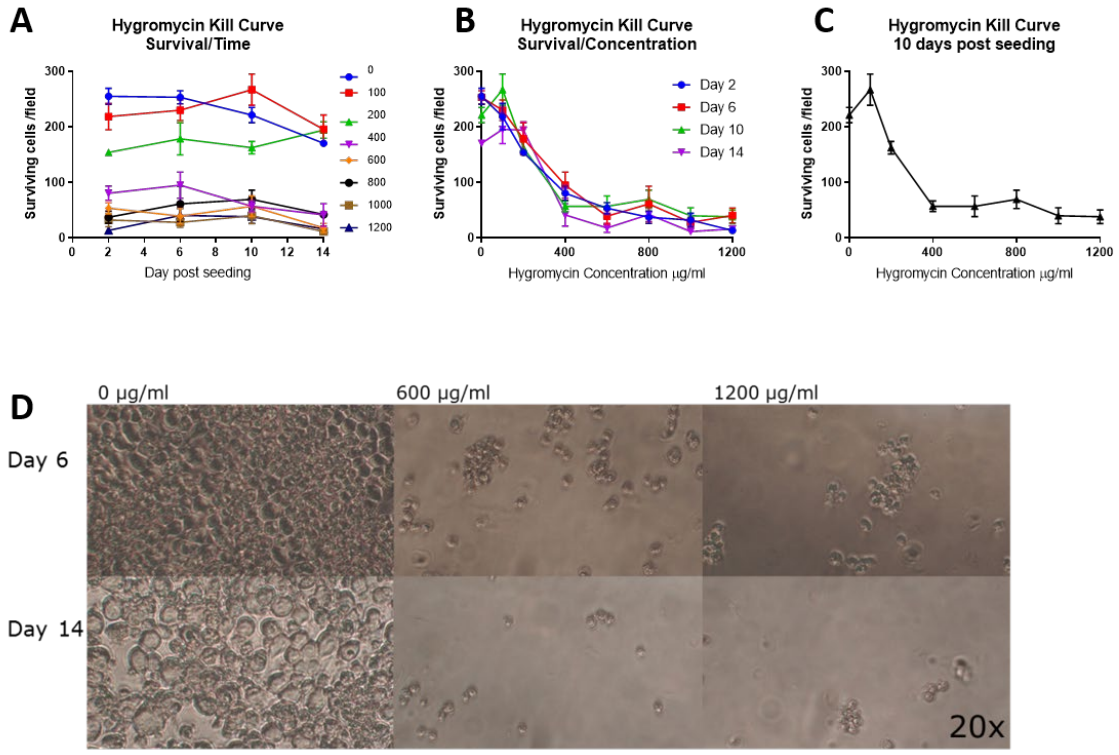


Figure 5.5 Determining the concentration of hygromycin for use in antibiotic selection. *N2a cells were grown in media containing the antibiotic hygromycin at concentrations ranging between 0 – 1200 µg/ml and survival was monitored by cell counting using bright field images.* ***A*** *– Cell survival plotted over time up to 14 days post seeding, with key showing concentrations of hygromycin (µg/ml).* ***B*** *– Cell survival plotted depending on hygromycin concentration, with key showing days post seeding.* ***C*** *– Cell survival plotted depending on hygromycin concentration at 10 days post seeding.* ***D*** *– Bright field images taken at 20x magnification at 0, 600 and 1200 µg/ml hygromycin, on days 6 and 14 post seeding. Graphs show mean ± SEM, n = 4.*

5.3.2 Colony validation by PCR and Luciferase assay

Following transfection with either of the OXR1-C promoter constructs, cells were passaged into growth media, which was replaced after 24 hours with media containing Hygromycin. Cells were then monitored until those transfected with the promoter constructs were confluent while those transfected with the empty control construct were dead, confirming that the surviving adhered cells contained the correct constructs. These polyclonal lines were split and expanded, so that vials could be frozen for future confirmation experiments, while colony picking was performed to generate monoclones.

To determine which monoclones were successfully expressing the promoter constructs, colony PCR was performed initially, with the successful monoclones being taken forward for further validation. Finally, the clones were tested by luciferase assay, and one monoclone containing each promoter was selected for expansion and use in the compound screen; monoclone D11 was selected from the line stably expressing the 1 kb promoter construct, and monoclone B6 from the 400 bp promoter construct (**Figure 5.6**).

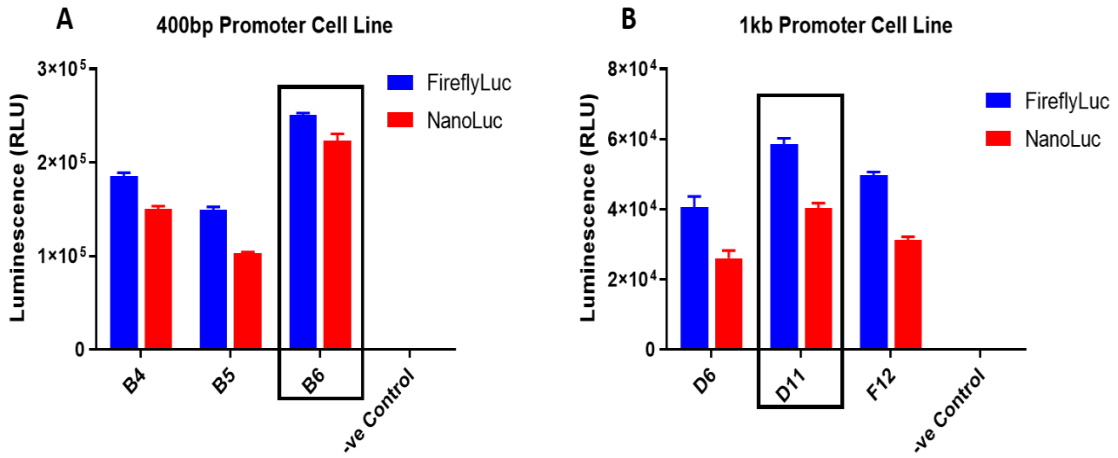


Figure 5.6 Validation of successful monoclones by luciferase assay. *Post validation by PCR, monoclones were tested by luciferase assay to ensure robust signal responses in both FireflyLuc (blue) and NanoLuc channels (red).* ***A*** *– Stable monoclones expressing the 400 bp Oxr1-C promoter luciferase construct - B4, B5 and B6 - were assayed and monoclone B6 was chosen.* ***B*** *– Stable monoclones expressing the 1kb Oxr1-C promoter luciferase construct - D6, D11 and F12 - were assayed and monoclone D11 was chosen. Graphs show mean ± SEM, n = 4.*

5.3.3 Stable cell line reciprocal inhibition

The final step in validating the stable cell lines for use in a compound screen was to assess the coincident activity of the stably expressed reporter genes. As previously tested using transient transfection, the stabilizing inhibitors PTC124 and Cilnidipine were applied to the cell lines, which were then assayed for luciferase activity. In each cell line, specific responses were obtained from each luciferase in a predictable manner showing an increase in luminescence at low to medium concentrations of each inhibitor, followed by a decrease in luminescence at high concentrations, while the luminescent signal of the uninhibited luciferase remained stable at all concentrations (**Figure 5.7**).

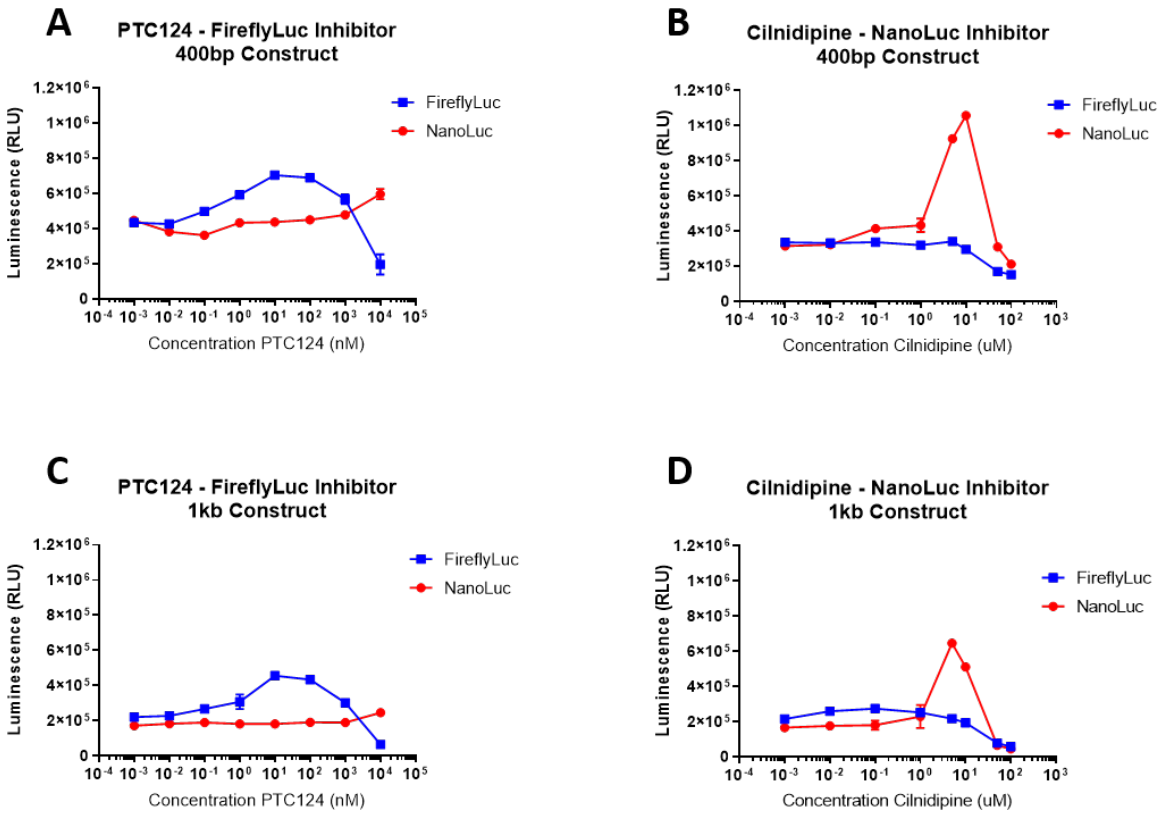


Figure 5.7 Validation of the stably expressed coincidence reporter system using OXR1-C promoters of 400 bp and 1 kb length. *The selective inhibitors PTC124 and Cilnidipine were applied exogenously to the stable cell line reporter system at a range of concentrations, to observe specific responses from FireflyLuc (blue, inhibited by PTC124) and NanoLuc (red, inhibited by Cilnidipine). Two stable cell lines were tested, expressing promoter constructs of lengths 400 bp (A & B) and 1 kb (C & D). Selective inhibition was found to produce reporter-specific responses measured as luminescent readings. Graphs show mean ± SEM, n = 3.*

5.4 Compound screening

The aim of the compound screen was to identify compounds that would upregulate expression of Oxr1-C through interaction with a conserved region of the OXR1-C promoter. The PHARMAKON 1600 compound library (MicroSource Discovery Systems) was selected due to its wide variety of small compounds, all of which had been approved for use by the FDA and had demonstrated biological activity when clinically evaluated. The compound library is contained within twenty 96 well plates, with 80 compounds per plate at a concentration of 10 mM.

5.4.1 Establishing a protocol for cell based compound screening

Having ascertained the suitability of both dual luciferase assay and stable cell line for compound screening, certain optimisation steps were required to establish a protocol for regular, repeatable compound screening in 96-well plate format. Cell density optimisation was performed (data not shown), which determined that cells would be seeded at 2.0 x 10^5 cells/well, ensuring a high level of confluence and robust luciferase signals when assayed 72 hours later. Cells were treated with compounds 24 hours following seeding, while actively dividing, at a concentration of 10 μM per well (following manufacturer recommendation), then incubated with the compounds for 48 hours to ensure sufficient time for effects on luciferase expression to be observed when assayed.

Within the 96-well plate format, a standardised plate layout was chosen including inbuilt controls (**Table 3.1**). The stabilizing inhibitors PTC124 and Cilnidipine were used as positive controls for FireflyLuc and NanoLuc respectively, with DMSO-containing media (0.1%) and media-only as controls [330]. Using this plate layout, up to 60 compounds were tested per batch of cells seeded.

	1	2	3	4	5	6	7	8	9	10	11	12
A	Compound 1	Compound 2	Compound 3	Compound 4	Compound 5	Compound 6	Compound 7	Compound 8	Compound 9	Compound 10	PTC124 1nM	Cilnidipine 1µM
B												
C												
D												
E	Compound 11	Compound 12	Compound 13	Compound 14	Compound 15	Compound 16	Compound 17	Compound 18	Compound 19	Compound 20	DMSO 0.1%	Media
F												
G												
H												

Table 5.1 Plate layout for compound screening. *Twenty compounds were tested per plate, with two positive controls (PTC124 1 nM & Cilnidipine 1 µM) and two negative controls (DMSO 0.1% and Media), with all conditions seeded at n = 4.*

5.4.2 Compound Screen Results

Over the course of the compound screen, 800 compounds were tested from the 1600 available in the PHARMAKON library, and testing was performed blinded to the identification of the compounds. Of the compounds tested, approximately 200 were found to significantly alter OXR1-C promoter activity, however the majority of these affected the reporter negatively.

Figure 5.8 shows representative results of the compound screen, with all eighty compounds from plate MS10 of the PHARMAKON library measured against controls built into the assay. As shown in the figure, many compounds were identified which increased reporter activity of only one of the two luciferases, and were therefore determined to be false positives. Overall, 56 targets were found to increase OXR1-C promoter activity; the criterion for selecting 'positive hits' was that the compound significantly increased luminescence in both FireflyLuc and NanoLuc channels, compared with negative controls. (**Figure 5.9**).

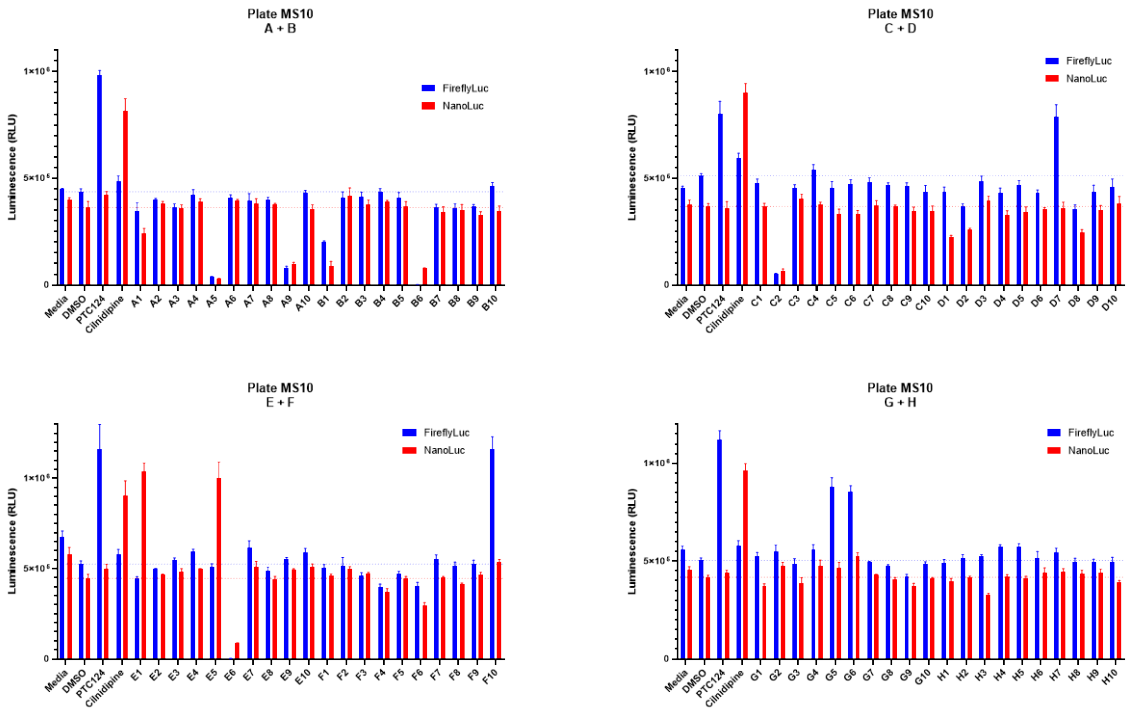


Figure 5.8 Representative results of the compound screen. *Each test plate assays 20 compounds, which translates to 20 compounds per graph, with positive and negative controls. FireflyLuc (blue) and NanoLuc (red) responses were measured 48hrs after incubation with test compounds. Graph shows mean ± SEM, n = 4.*

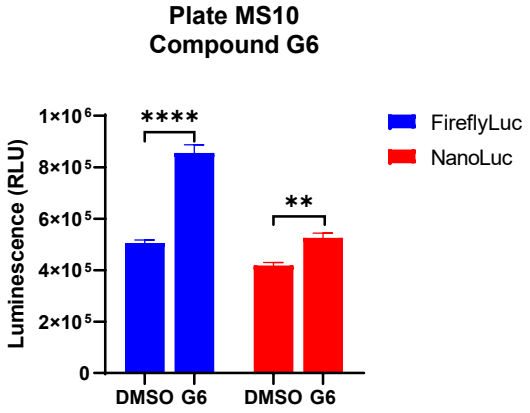


Figure 5.9 A positive hit identified from the initial compound screen. *Compound G6 from library plate MS10 produced a significant increase in luminescence from both FireflyLuc (blue) and NanoLuc (red) when compared with DMSO control. Graph shows mean ± SEM, n = 4.*

Secondary to the initial screen, these hit compounds were then tested using the cell line stably expressing the 400 bp promoter. This stage ruled out a large number of compounds which were shown not to drive reporter expression from this shorter conserved region. A total of eight compounds instigated increased activity of both reporters, in both cell lines, which were taken forward for further testing.

5.4.3 Dose-response curves of lead compounds

In dose-response testing, compounds are titrated at different concentrations to observe the relationship between concentration and magnitude of response, and enable determination of the active concentration. Dose-response curves were obtained through luciferase assay of both stable cell lines, using concentrations an order of magnitude either side of the test concentration used in the compound screen (10 μM). Several compounds tested were determined to be false positives at this stage, as they produced dose-dependent responses in only one of the two luciferase reporters, while the alternate reporter activity remained stable (data not shown). Three compounds of the eight tested exhibited the same dose-response relationship in both luciferases, and in both cell lines, and these were taken forward for validation as positive hits (**Figure 5.10**). Interestingly, all three of these compounds showed decreasing reporter activity at high concentrations, which suggests a degree of cellular toxicity.

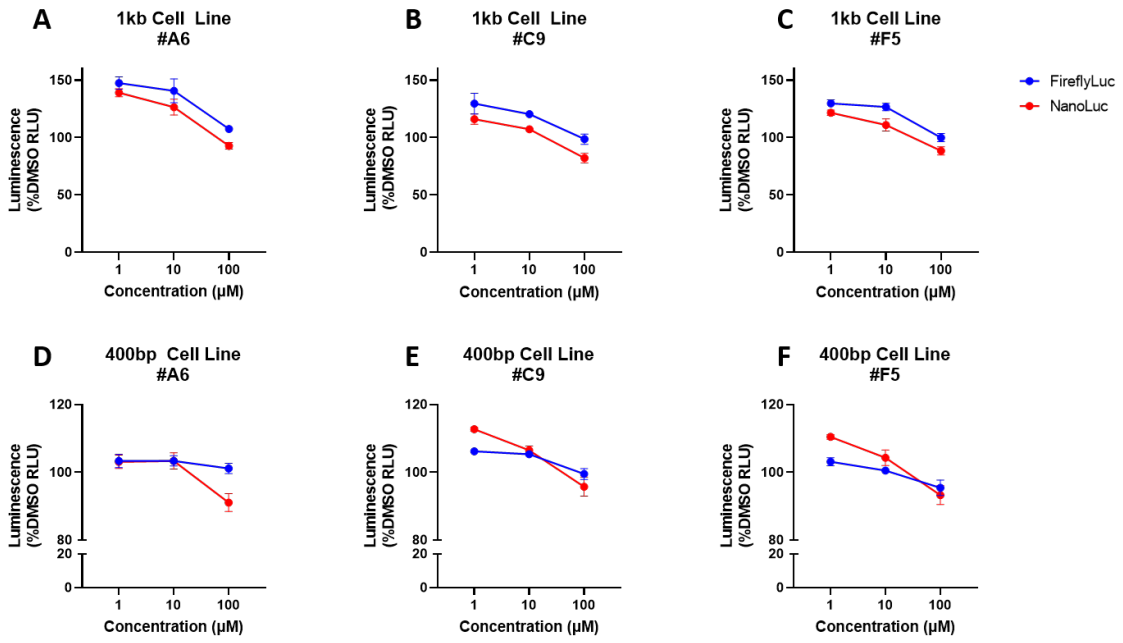


Figure 5.10 Dose-response curves produced with varying concentrations of putative Oxr1-C upregulators in stable cell lines. *Compounds identified in the compound screen were tested at 1, 10 and 100 μM concentrations in cell lines expressing either the 1 kb Oxr1-C promoter reporter construct (**A** – A6, **B** – C9, **C** – F5) or the 400 bp Oxr1-C promoter reporter construct (**D** – A6, **E** – C9, **F** – F5). Graphs show mean ± SEM, n = 4.*

5.4.4 Validation of lead compounds by polyclonal line assay

During generation of the stable cell lines, polyclonal lines were also produced and saved, for use in validating lead compounds. Polyclonal lines contain cells that stably express the construct of choice, however, the cells have not been selected or isolated and therefore there is a large amount of variation expected in the level of expression from each cell; in fact it is likely that the majority of cells do not express the construct at all. At the point of transfection, cells incorporate the chosen construct into their individual genomes at random locations. Following selection and isolation, monoclonal lines are produced in which all clonal cells express the construct from the same genomic location. Polyclonal lines can be used to validate results found in monoclonal cell lines, because if the same result is observed in both, then it is a true effect of the transfected construct, as opposed to an effect specific to one clone [328].

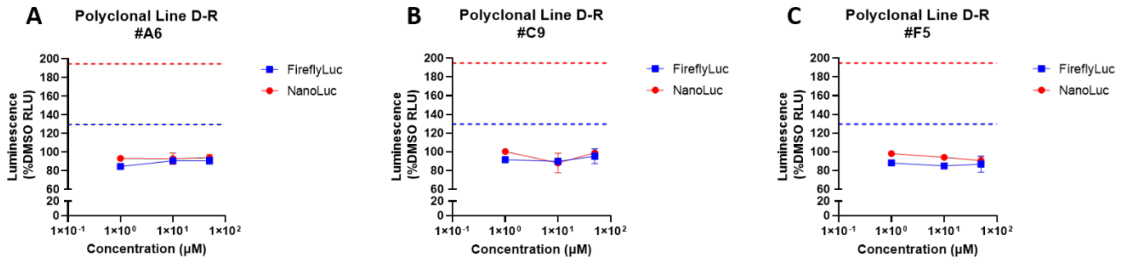


Figure 5.11 Dose-response curves produced with varying concentrations of putative Oxr1-C upregulators in a polyclonal stable cell line. *Compounds identified in the compound screen were tested at 1, 10 and 100 μM concentrations in a polyclonal cell line variably expressing the 400 bp OXR1-C promoter reporter construct.* ***A*** *– A6,* ***B*** *– C9,* ***C*** *– F5. Graphs show mean ± SEM, n = 4. Dashed lines show mean luminescence responses produced by PTC124 (blue) and Cilnidipine (red).*

The three lead compounds were therefore tested by luciferase assay in the polyclonal line expressing the 400 bp promoter construct. To observe dose-response relationships, compounds were tested at three concentrations: 1 μM, 10 μM and 50 μM (the latter concentration was chosen to prevent potential cellular toxicity effects observed in the previous dose-response experiment). As expected, a smaller effect was observed in response to incubation with the compounds compared with the effect observed in the monoclonal lines (**Figure 5.11**). However, a strong effect was still produced by incubation

with the positive control compounds, PTC124 and Cilnidipine (mean luminescence responses shown as dashed horizontal lines), confirming the activity of the two reporter genes. As the polyclonal line was therefore confirmed to be functional, the responses produced by the compounds can be described as weak, and there is doubt as to their genuine effect on expression driven by the OXR1-C promoter.

5.4.5 Validation of lead compounds by qPCR

Having ascertained that the three lead compounds did not produce a strong reporter response in the polyclonal cell line, it was still important to investigate whether any effect could be observed at the endogenous expression level of the Oxr1-C isoform itself. Following incubation of both cell lines with each compound, cells were harvested for RNA extraction, and RT-qPCR was performed. Interestingly, all three compounds significantly increased expression of OXR1-C in the cell line expressing the full-length promoter construct (**Figure 5.12B**). However, the compounds did not increase expression in the cell line expressing the shorter, conserved promoter construct **(Figure 5.12A)**, suggesting they may be acting via a promoter region upstream of the 400bp conserved region. In summary, although the compounds identified by the luciferase screen are able to upregulate expression of OXR1-C, this is likely through interaction with a region of the OXR1-C

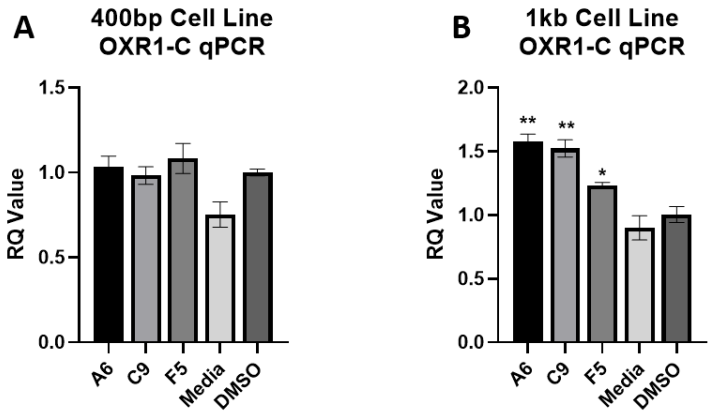


Figure 5.12 Investigation of effect of lead compounds on expression of OXR1-C. *Cell lines expressing either the 400 bp Oxr1-C promoter reporter construct (**A**) or the 1 kb Oxr1-C promoter reporter construct (**B**) were incubated with putative OXR1-C upregulators, and RT-qPCR was performed following mRNA extraction, to investigate expression of OXR1-C. Graphs show mean ± SEM, n = 3.*

promoter that is not conserved between human and mouse, and therefore would not be suitable for use in human therapeutics.

5.5 CRISPR activation testing in Neuro2a cells

At the inception of the project detailed in this chapter (building on a previous DPhil thesis), reporter-based assays were widely used in quantitative high throughput screening, with coincidence reporters, which were first developed in 2012 [331], viewed as the optimal system for such screens to identify therapeutic compounds with genuine biological activity capable of up- or down-regulation of a target gene [324]. However, during the intervening period, rapid progress has been made in a different technology, CRISPR activation (CRISPRa), also concerned with the specific upregulation of target genes. Proof of concept of CRISPRa technology was first published in 2013 [332], and in 2019, CRISPRa was approved for use in a clinical trial for treatment of a heritable form of retinal dystrophy (ClinicalTrials.gov Identifier: NCT03872479) [333]. CRISPRa uses CRISPR-Cas9 technology to activate gene transcription, utilising a catalytically inactive 'dead' Cas9 (dCas9) fused to a strong transcriptional activator and guided by one or more short guide RNAs (sgRNAs) to increase expression of endogenous genes [332]. The system can produce efficient and robust gene activation, especially when multiple sgRNAs are used, with high target specificity [334].

To investigate the use of CRISPRa to overexpress Oxr1-C, and for comparison with exogenous compound application, gene activation vectors were generated using one each of three independent guide RNAs designed in first exon of *Oxr1-C* and upstream sequence (see **Chapter Two**). The vector system expresses VP64 in tandem; this acts as the transcriptional activator through recruitment of transcriptional machinery to the target sequence [335].The vectors, named A, B and C, were each transfected into N2a cells, and transfection efficiency could be visualised through use of a GFP sequence contained within the vector. A CRISPRa Scramble vector (with no GFP) was transfected as a negative control. **Figure 5.13** shows N2as imaged both in bright-field and fluorescence illumination;

based on GFP signal, indicates a transfection efficiency of between 1.8% (Construct A) - 10.6% (Construct B).

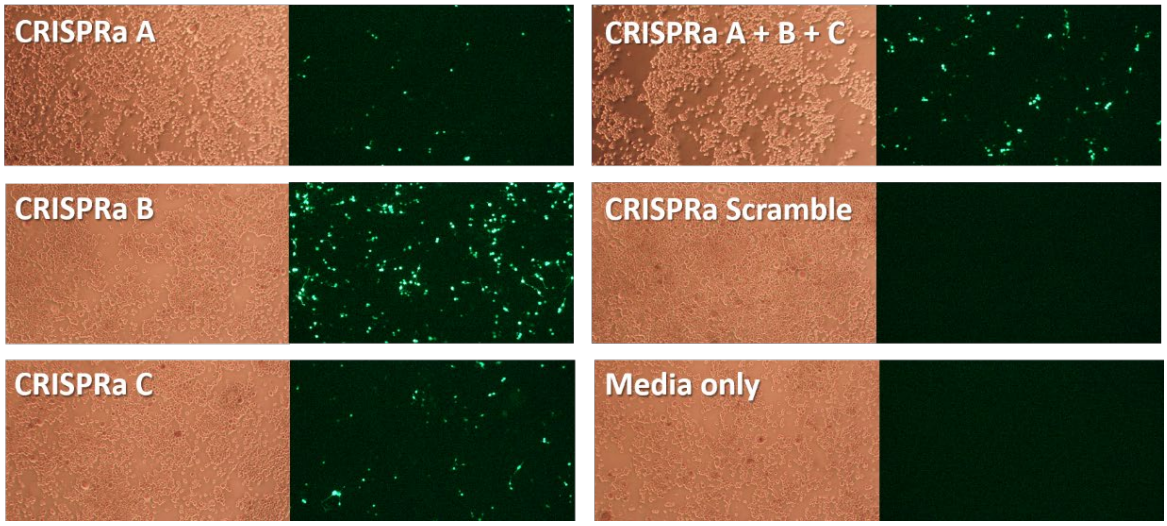


Figure 5.13 Bright field and fluorescent imaging of CRISPRa-transfected cells. *N2a cells were transfected with CRISPRa constructs A, B, C, (containing the* Oxr1-C *promoter) or Scramble (negative control), and incubated for 48 hrs before imaging at 20x magnification. Bright field images are shown on the left, and fluorescent images on the right. Inclusion of a GFP-coding sequence in CRISPRa constructs enables visualisation of transfected cells. Transfection efficiencies, calculated as number of fluorescent cells divided by total cells in bright field view, are as follows: construct A - 1.8%, construct B – 10.6%, construct C – 3.2%, constructs A, B & C – 5.0%.*

Following transfection, cells were harvested for RNA extraction and RT-qPCR was performed for endogenous Oxr1-C expression. Cells transfected with only one of the three vectors alone did not show any increase in expression when compared with the scramble vector, whereas interestingly, transfection with all three CRISPRa vectors in tandem (A, B & C) showed a significant increase in expression of *Oxr1-C* (**Figure 5.14**) compared to the control. It is noteworthy that the transfection efficiency was low and may be masking more promising results. For example, cells co-transfected with CRISPRa constructs A, B and C showed a transfection efficiency of 5.0%, but produced a 1.5 fold increase in expression of *Oxr1-C* by RT-qPCR. At a higher transfection efficiency, a greater increase in *Oxr1-C* would be expected. In summary, upregulation of OXR1 by CRISPRa was successful *in vitro*, showing promise for future potential use as a therapeutic strategy.

Given the low transfection efficiency of this experiment, which utilized the Lipofectamine 3000 vector system, the experiment should be repeated using different

experimental conditions, such as by varying RNA concentrations or using electroporation, in order to obtain more reliable and informative data.

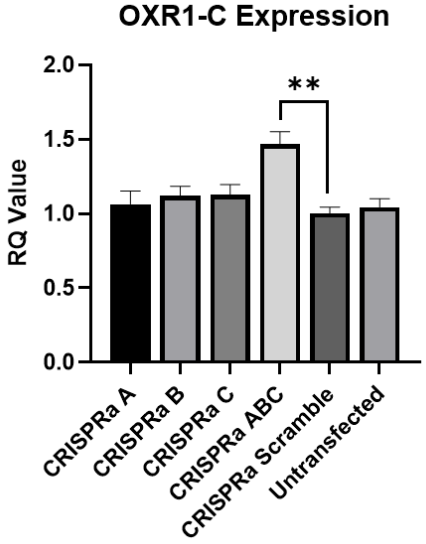


Figure 5.14 Increased expression of* Oxr1-C *following transfection with CRISPRa constructs. *N2a cells were transfected with CRISPRa constructs A, B, C, (containing the* Oxr1-C *promoter) or Scramble (negative control), and incubated for 48 hrs before RNA extraction was performed, followed by RT-qPCR. Although transfection with constructs A, B and C individually produced no significant increase in* Oxr1-C *expression, co-transfection with all three constructs (A, B & C) produced 1.4 fold upregulation when compared to transfection with a CRISPRa Scramble construct (p = 0.0021). Graphs show mean ± SEM (n = 4), one way ANOVA performed on CT values using Tukey's multiple comparisons test.*

5.6 Overexpression of Oxr1 to modify seizure phenotype of Tbc1d24 mutant

Overexpression of Oxr1 has been shown to ameliorate aberrant pathologies of OS-related neurodegeneration *in vivo*, including using the mouse model *Tg(mPrnp-Oxr1)* (henceforth referred to as *Oxr1*$^{Prnp/+}$), which overexpresses an Oxr1-FL isoform up to five-fold, at the protein level, driven by the mouse prion promoter so that it is expressed in neurons alone [125]. As shown previously by RNAseq (Chapter Three), there is no evidence for OS caused by the R360L mutation in Tbc1d24, however, similar epilepsy-related mutations in Tbc1d24 show increased OS sensitivity when modelled in *Drosophila*, which can be rescued by antioxidant treatment [336]. The emergent role of oxidative stress in epilepsy gives promise to potential rescue of seizure phenotypes by Oxr1 overexpression [337] [338] [339]. As OXR1 and TBC1D24 are both part of the synaptic proteome [340] and share functional domains, there is also a possibility of compensation between TLDc family

members and resultant rescue of disease phenotypes of the Tbc1d24 mouse mutants (described in Chapters Three & Four). Human mutations in *OXR1* and *TBC1D24* lead to diseases with overlapping phenotypes, including seizures, ataxia and cerebellar atrophy, providing evidence for intersection in function between the two genes [320] [341] [105]. In addition, all TLDc proteins have been shown to bind to the V-ATPase complex, and are suggested to exert regulatory effects on activity of the enzyme [342] [343]. To investigate these possibilities, crosses were set up between each of the Tbc1d24 mutant mouse lines, *Tbc1d24*^{R360L} and *Tbc1d24*^{INS2}, and the neuronal Oxr1 overexpressor line, *Oxr1*$^{Prnp/+}$.

5.6.1 *Oxr1*^{Prnp} x *Tbc1d24*^{R360L} protein expression

To generate experimental progeny for the *Oxr1*^{Prnp} x *Tbc1d24*^{R360L} cross, mice heterozygous for the Oxr1 transgene and the *Tbc1d24*^{R360L} mutation (*Tbc1d24*$^{R360L/+}$*/Oxr1*$^{Prnp/+}$) were crossed with *Tbc1d24*$^{R360L/+}$ mice. This cross produced offspring with four genotypic combinations: *Tbc1d24*$^{+/+}$*Oxr1*$^{+/+}$; *Tbc1d24*$^{+/+}$*Oxr1*$^{Prnp/+}$; *Tbc1d24*$^{R360L/R360L}$*Oxr1*$^{Prnp/+}$; and *Tbc1d24*$^{R360L/R360L}$*Oxr1*$^{+/+}$. Western blotting from the four genotypic groups confirmed that Oxr1$^{Prnp/+}$ mice showed approximately threefold increase in expression of Oxr1 compared with Oxr1$^{+/+}$ mice, and Tbc1d24$^{R360L/R360L}$ mice showed reduced abundance of Tbc1d24 protein by approximately 80% (**Figure 5.15**). Due to proximity on the western blot, all Oxr1 isoform bands were quantified together to calculate protein levels of Oxr1. These data confirm that the progeny from the cross express the correct transgene and/or mutant protein at the predicted levels.

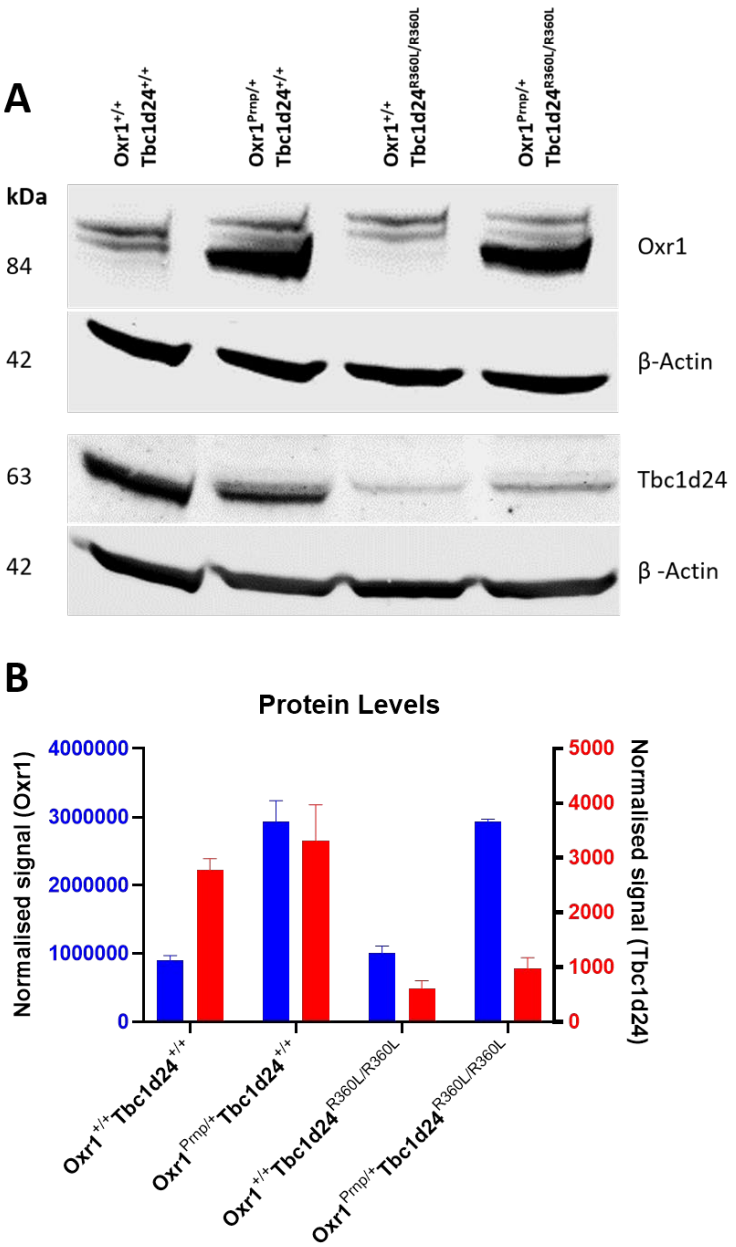


Figure 5.15 Progeny of the* Oxr1^{Prnp} *x* Tbc1d24^{R360L} *cross show expected protein levels. *Whole brains were taken for protein extraction and analysis by Western blotting.* ***A*** *– Representative western blots showing bands for Oxr1 isoforms around 84kDa and Tbc1d24 at 63kDa, which were each blotted separately using β-Actin at 42kDa to control for protein levels. All Oxr1 isoform bands were quantified. Bands show each of the four genotypes represented by progeny of the cross:* Tbc1d24$^{+/+}$Oxr1$^{+/+}$*;* Tbc1d24$^{+/+}$Oxr1$^{Prnp/+}$*;* Tbc1d24$^{R360L/R360L}$Oxr1$^{Prnp/+}$*; and* Tbc1d24$^{R360L/R360L}$Oxr1$^{+/+}$*.* ***B*** *- Graph of quantified protein signal for Tbc1d24 and Oxr1, normalised to β-Actin. Values show mean ± SEM. For each genotype, n=2.*

5.6.2 Preliminary video tracking analysis shows extended survival in *Oxr1^{Prnp}* x *Tbc1d24^{R360L}* compared with *Tbc1d24^{R360L}*

Home cage video tracking enables real time observation of mice in their habitual environment, with minimal disruption to conditions, and is therefore used to monitor a

variety of naturalistic behaviours [344]. Video tracking was therefore used to monitor litters from the *Oxr1*^{Prnp} x *Tbc1d24*^{R360L} cross, where minimal disruption to habitat was critical due to the young age of the mice, who were filmed between the ages of P15 and P25 in order to capture the short lifespan caused by the R360L mutation in Tbc1d24. Preliminary analysis of home cage video footage revealed that presence of the *Oxr1*$^{Prnp/+}$ transgene delayed onset of seizures and extended survival in *Tbc1d24*$^{R360L/R360L}$ mice. While *Tbc1d24*$^{R360L/R360L}$*Oxr1*$^{+/+}$ mice first display seizures between P14 and P16, which progress to fatal seizures at P16-P18, the earliest seizure recorded in *Tbc1d24*$^{R360L/R360L}$*Oxr1*$^{Prnp/+}$ mice was at P18, and survival was extended by up to a week in some mice, with the end-point as P25, an approximate 40% increase compared to the mean survival time in *Tbc1d24*$^{R360L/R360L}$ mice. However, some *Tbc1d24*$^{R360L/R360L}$ mice expressing the Oxr1 transgene experienced fatal seizures at P18, at the same time point as Tbc1d24$^{R360L/R360L}$ mice expressing wild type levels of Oxr1. Overall, the delayed onset of seizure phenotype, while short, is significant in that it suggests a potential compensatory mechanism for Oxr1 in the absence of normal levels of Tbc1d24, and provides further evidence for the role of Oxr1 in amelioration of neuronal disease.

Unfortunately, due to license restrictions and mouse breeding ratios, it was not possible to collect sufficient data to reliably report survival and seizure incidence from video tracked cages. With a larger sample size ($n \geq 5$ for each relevant genotype), a Kaplan-Meier estimation test could be performed in order to measure both survival in *Tbc1d24*$^{R360L/R360L}$ mice compared with wild type mice, and the effect of expression of the *Oxr1*^{Prnp} transgene on survival combined with the *Tbc1d24*^{R360L} mutation [345]. Kaplan-Meier estimation could also be applied to seizure incidence, plotting percentage of seizure-free mice over time [346]. In addition, recent advancements in video-tracking software – combining motion analysis with semi-automated seizure detection – would enable the automatic detection of seizure events, enabling more video footage to be scored, and likely more seizure events detected, than was feasible with manual seizure scoring as used in this experiment [347].

5.6.3 The gene c-Fos is influenced by neuronal overexpression of Oxr1

Overexpression of Oxr1 appears to extend survival in the *Tbc1d24*^{R360L} mutant, however, it was necessary to find other markers of disease progression in order to quantify potential rescue. While electroencephalography (EEG) is typically used in rodent models of epilepsy to characterize epileptiform events and seizure onset [348], this method was unavailable for mice of this size at MRC Harwell, therefore a molecular approach was required to understand how Oxr1 might affect neuronal activity. RNA-seq of the Tbc1d24^{R360L} frontal cortex showed upregulation of the immediate early gene (IEG) *c-fos* (**Figure 3.9**), which was also shown by be upregulated by over 10-fold in an adult inducible knockout model of Tbc1d24 (see Discussion, 6.2)(Oliver lab, unpublished). *C-fos* is a transcription factor understood to regulate neuronal excitability, and neuronal cell survival following excitotoxic insult [349], and is therefore used as a marker for neuronal activity, and a potential indicator of seizure-related excitability [350].

Due to the role of *c-fos* as an indicator of neuronal activation [351], it was predicted that any reduction in seizure activity due to Oxr1 overexpression might be shown by reduced expression of *c-fos*. RT-qPCR was performed on progeny of the *Oxr1*^{Prnp} x *Tbc1d24*^{R360L} cross, using mRNA extracted from whole brain. Contrary to predictions, there was no significant increase of *c-fos* expression in *Oxr1*$^{+/+}$*Tbc1d24*$^{R360L/R360L}$ compared with *Oxr1*$^{+/+}$*Tbc1d24*$^{+/+}$ (**Figure 5.16**). However, the presence of the *Oxr1*$^{Prnp/+}$ transgene was associated with reduced *c-fos* expression in both *Tbc1d24*$^{+/+}$ and *Tbc1d24*$^{R360L/R360L}$ progeny, although this difference was not statistically significant ($p = 0.199$ in *Oxr1*$^{Prnp/+}$*Tbc1d24*$^{+/+}$ cf. *Oxr1*$^{+/+}$*Tbc1d24*$^{+/+}$, and $p = 0.292$ in *Oxr1*$^{Prnp/+}$*Tbc1d24*$^{R360L/R360L}$ cf. *Oxr1*$^{+/+}$*Tbc1d24*$^{R360L/R360L}$). This suggests that the *Oxr1* transgene may alter *c-fos* expression in both *Tbc1d24*$^{+/+}$ and *Tbc1d24*$^{R360L/R360L}$, but as no significant increase in *c-fos* is observed in *Tbc1d24*$^{R360L/R360L}$ whole brain, it is not possible to comment on the effect of Oxr1 overexpression on seizure-related activity.

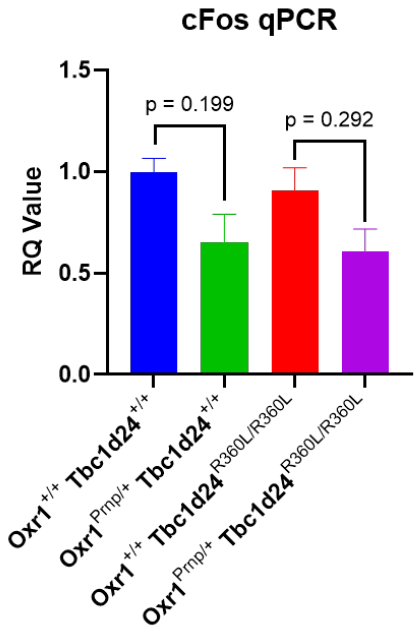


Figure 5.16 mRNA expression of c-fos in progeny of the* Oxr1^{Prnp} x Tbc1d24^{R360L} *cross. *RT-qPCR was performed using mRNA extracted from whole brain tissue. One way ANOVA using Tukey's multiple comparison's test performed using ΔCT values. Values are mean ± SEM, n = 4 for each genotype.*

5.7 Effect of Oxr1 overexpression on haematological disruption in loss-of-function Tbc1d24 mutants

As discussed in Chapter Four, the R360L and INS2 mutations in Tbc1d24 cause pronounced disruption to the haematological system, including disturbed haemoglobin synthesis and iron homeostasis. Markers associated with this disruption include Alas2, the rate-limiting enzyme for haemoglobin synthesis, and haemoglobin subunits Hbb and Hba. From previous transcriptomics experiments using microarrays in the *Tbc1d24*$^{R360L/R360L}$ mutant, expression changes have also been detected by in Contactin 3 (Cntn3), a cell adhesion molecule involved in development of the nervous system [352], while in the *Tbc1d24*$^{INS2/INS2}$ mutant, neuronal migration defects are observed in cortical layer 5. These four genes – *Alas2*, *Hbb-bt*, *Hba-a2* and *Cntn3* – appear therefore to be key markers for pathological alterations caused by disruption in Tbc1d24.

5.7.1 Rescue of Alas2 coincides with enhanced survival in *Oxr1*^{Prnp} x *Tbc1d24*^{R360L}

RT-qPCR was performed on progeny of the *Oxr1*^{Prnp} x *Tbc1d24*^{R360L} cross, to investigate levels of *Hba-a2*, *Hbb-bt*, *Alas2*, and *Cntn3*. As previously observed, the expression levels of *Hba-a2*, *Hbb-bt* and *Alas2* (**Figure 5.17**) were significantly higher in *Oxr1*$^{+/+}$*Tbc1d24*$^{R360L/R360L}$ compared with *Oxr1*$^{+/+}$*Tbc1d24*$^{+/+}$ mice (*Hba-a2*, p = 0.0001, *Hbb-bt*, p < 0.0001, *Alas2*, p < 0.0001); the expression of these genes was also higher in *Oxr1*$^{Prnp/+}$*Tbc1d24*$^{R360L/R360L}$ compared with *Oxr1*$^{+/+}$*Tbc1d24*$^{+/+}$ mice (*Hba-a2*, p = 0.0005, *Hbb-bt*, p < 0.0001, *Alas2*, p = 0.0001), indicating the magnitude of the effect of the R360L mutation on haematological gene expression. Interestingly, in *Oxr1*$^{Prnp/+}$*Tbc1d24*$^{+/+}$ mice, the presence of the *Oxr1* transgene caused a two-fold increase in expression of both *Hbb-bt* and *Alas2* compared with *Oxr1*$^{+/+}$*Tbc1d24*$^{+/+}$ (*Hbb-bt*, p = 0.0002, *Alas2*, p = 0.0017), suggesting possible downstream interaction with Oxr1. Most strikingly, the presence of the transgene caused a reduction in levels of *Alas2* in *Oxr1*$^{Prnp/+}$*Tbc1d24*$^{R360L/R360L}$ compared with *Oxr1*$^{+/+}$*Tbc1d24*$^{R360L/R360L}$ mice (p = 0.0233), with no significant difference in the levels of *Alas2* between *Oxr1*$^{Prnp/+}$*Tbc1d24*$^{+/+}$ and *Oxr1*$^{+/+}$*Tbc1d24*$^{R360L/R360L}$ mice, supporting a potential interaction of Oxr1 with the haematological system, which could affect the anaemic phenotype in the mutant. No effect was observed on levels of *Cntn3*, although there is a trend towards reduced *Cntn3* expression in *Tbc1d24*$^{R360L/R360L}$ mice with or without the *Oxr1* transgene. Oxr1 has been demonstrated to promote cell survival, but this has only been demonstrated *in vivo* through its protective effect on neurons. This data therefore suggests a new potential role for Oxr1 in ameliorating dysfunction in the haematological system.

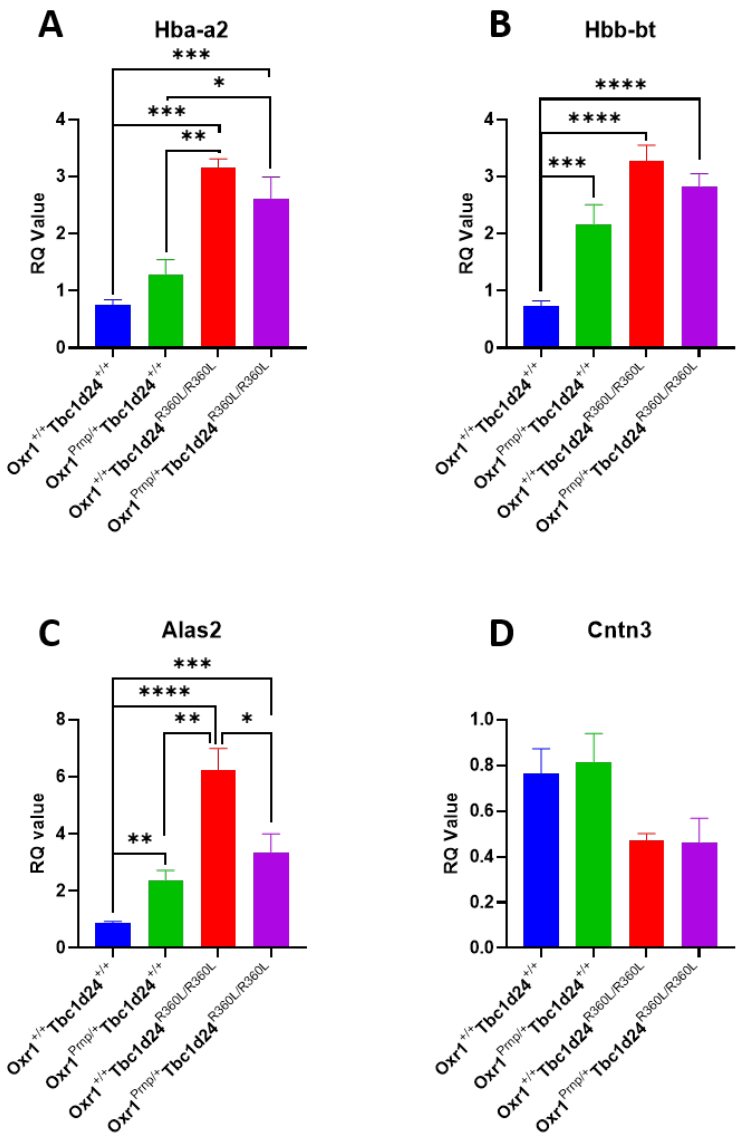


Figure 5.17 Overexpression of Oxr1 rescues pathological induction of Alas2 in Tbc1d24^{R360L}. *Expression of haematological and neurodevelopmental targets in progeny of the* Oxr1^{Prnp} x Tbc1d24^{R360L} *cross. RT-qPCR was performed using mRNA extracted from whole brain tissue to measure expression levels of* Hba-a2 *(A),* Hbb-bt *(B),* Alas2 *(C) and* Cntn3 *(D) mRNA. One way ANOVA with Tukey's multiple comparisons testing performed using ΔCT values. Both male and female mice were used. Values are mean ± SEM, n = 4 for each genotype.*

5.7.2 Haematological markers in *Oxr1^{Prnp}* x *Tbc1d24^{INS2}*

The *Prnp-Oxr1* transgene has been demonstrated to be strongly expressed from E13.5 [125], therefore it was postulated that its expression, and consequent overexpression of *Oxr1*, might modulate the embryonic lethal phenotype of the *Tbc1d24$^{INS2/INS2}$* mutant. Similarly to the cross with the *Tbc1d24^{R360L}* mutant line, experimental progeny were generated for a cross between *Oxr1^{Prnp}* x *Tbc1d24^{INS2}* to produce offspring with four

genotypic combinations: *Tbc1d24*$^{+/+}$*Oxr1*$^{+/+}$; *Tbc1d24*$^{+/+}$*Oxr1*$^{Prnp/+}$; *Tbc1d24*$^{INS2/INS2}$*Oxr1*$^{Prnp/+}$; and *Tbc1d24*$^{INS2/INS2}$*Oxr1*$^{+/+}$.

Due to the embryonic lethality of the *Tbc1d24*$^{INS2/INS2}$ mutant, the effect of the *Oxr1*$^{Prnp/+}$ transgene on neonatal survival (for example, from P0) could not be measured without suitable negative controls and was limited by animal licence stipulations. Instead, RT-qPCR was performed using mRNA extracted from whole brains of progeny, to determine levels of *Hba-a2*, *Hbb-bt*, *Alas2*, and *Cntn3*. RNAseq of the *Tbc1d24*^{INS2} line showed upregulation of the haematological genes *Hba-a2, Hbb-bt* and *Alas2*, consistent with the *Tbc1d24*^{R360L} line (**Chapter Four**), and the three genes were consequently chosen as markers for potential rescue of haematological dysfunction. Additionally, the *Tbc1d24*$^{INS2/INS2}$ mutant shows a defective cortical layering phenotype (**Chapter Three**), therefore the cell-adhesion gene *Cntn3* was again chosen as a marker for rescue, due to its role in neuronal migration and downregulation in the *Tbc1d24*$^{R360L/R360L}$ mutant, as shown by microarray transcriptomics (**Chapter Four**).

In this cross, the presence of the Oxr1 transgene did not appear to rescue levels of haematological markers, however, a trend towards decrease was observed in *Cntn3* in *Tbc1d24*$^{INS2/INS2}$*Oxr1*$^{Prnp/+}$ compared with *Tbc1d24*$^{INS2/INS2}$*Oxr1*$^{+/+}$, returning *Cntn3* expression closer to endogenous levels ($p = 0.0530$) (**Figure 5.18**). Predictably, based on observations of alterations in cortical layering in the *Tbc1d24*$^{INS2/INS2}$ mutant (Chapter Three), expression of *Cntn3* is significantly higher in *Oxr1*$^{+/+}$*Tbc1d24*$^{INS2/INS2}$ compared to both *Oxr1*$^{+/+}$*Tbc1d24*$^{+/+}$ ($p = 0.0029$) and *Oxr1*$^{Prnp/+}$*Tbc1d24*$^{+/+}$ ($p = 0.0084$). Changes in expression of haematological markers are less marked at earlier time points, as shown by RT-qPCR at P0 and P8 in *Tbc1d24*$^{R360L/R360L}$ (**Chapter Four**), which could explain the

apparent lack of effect of overexpression of *Oxr1*, whereas *Cntn3* plays an important role in early neuronal development [353].

5.7.3 Summary of the effects of overexpression of Oxr1 *in vivo*

In summary, the overexpression of Oxr1 *in vivo* by expression of the transgene

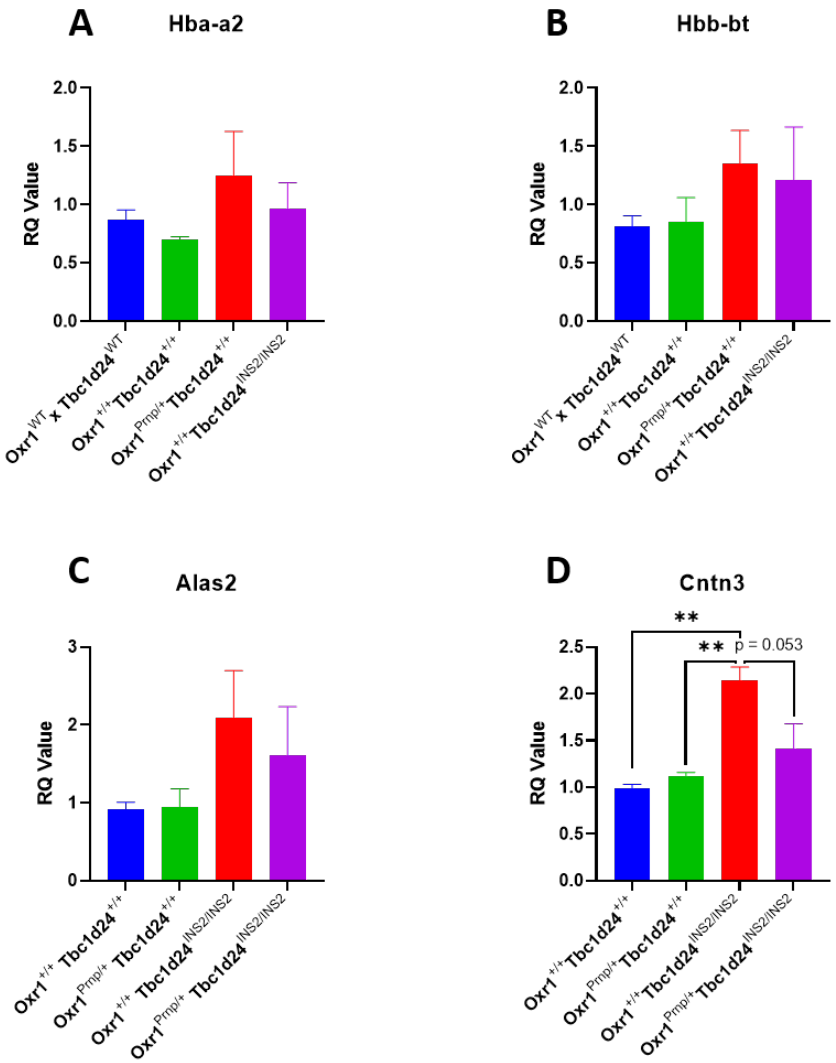


***Figure 5.18 Overexpression of Oxr1 may reduce marker of neurodevelopmental dysfunction in* Tbc1d24^{INS2}.** *Expression of haematological and neurodevelopmental targets in progeny of the* Oxr1^{Prnp} *x* Tbc1d24^{INS2} *cross. RT-qPCR was performed using mRNA extracted from whole brain tissue to measure expression levels of Hba-a2 (A), Hbb-bt (B), Alas2 (C) and Cntn3 (D) mRNA. One way ANOVA with Tukey's multiple comparisons test performed using ΔCT values. Both male and female mice were used. Values are mean ± SEM, n = 4 for each genotype.*

Tg(m*Prnp*-Oxr1) causes modulation of the seizure phenotype caused by the *Tbc1d24*^{R360L} mutation, with the earliest seizure in the *Oxr1*$^{Prnp/+}$*Tbc1d24*$^{R360L/R360L}$ line recorded at P18, compared with P14 in the *Tbc1d24*$^{R360L/R360L}$ line. Survival was also extended by up to a week, from P18 in *Tbc1d24*$^{R360L/R360L}$ to up to P25 in *Oxr1*$^{Prnp/+}$*Tbc1d24*$^{R360L/R360L}$.

Interestingly, expression of the haemoglobin synthesis enzyme *Alas2* was reduced in *Oxr1*$^{Prnp/+}$*Tbc1d24*$^{R360L/R360L}$ compared with in *Oxr1*$^{+/+}$*Tbc1d24*$^{R360L/R360L}$, suggesting potential rescue of the haematological disruption caused by the R360L mutation (described in Chapter Four) and indicating a novel protective role of Oxr1 outside of the nervous system. Finally, overexpression of Oxr1 in the *Tbc1d24*$^{INS2/INS2}$ mutant was investigated and a trend towards decreasing levels of *Cntn3* indicated that Oxr1 upregulation may prevent the increase of *Cntn3* expression due to defects in neuronal migration, which is disrupted in the Tbc1d24$^{INS2/INS2}$ mutant.

5.8 Discussion

5.8.1 Strategies for the transcriptional control of Oxr1 expression

The compound screen demonstrated that the dual luciferase reporter system is an effective tool for drug discovery, allowing interaction with a chosen promoter to be directly measured using robust readout of luciferase signals. The coincident reporter system is capable of recognising false positives, increasing the overall efficiency by removing additional validation stages. The stable cell lines generated expressing the luciferase reporters driven by the OXR1-C promoter are useful tools that could be used in larger-scale screens with additional compound libraries. Similar approaches have been successful; for example, a compound screen for upregulation of Frataxin (*FXN*), using the luciferase reporter line *FXN*-GAA-Luc, identified a group of histone methyltransferase inhibitors which increased readout of the luciferase assay. The screen determined that the SUV4-20 family of methyl transferases are involved in regulation of *FXN* expression, thus identifying a novel therapeutic target for Friedreich's ataxia [354]. In addition, a screen for novel therapeutic targets to treat Charcot-Marie-Tooth 1A, caused by the genetic duplication and resultant overexpression of Peripheral Myelin Protein 22 (*PMP22*), used a coincidence reporter assay to identify compounds able to downregulate *PMP22* expression, including protein kinase C (PKC) activators such as bryostatin, which had already reached clinical trials for use in Alzheimer's disease [355].

The Pharmakon 1600 compound library comprises a range of structurally diverse biologically active drugs, all with existing approval for use by the FDA and many of which are available on the market, thus enabling transition from *in vitro* screens for new biological activity to *in vivo* testing for clinical suitability. Of the 800 hits tested, approximately 50 were shown to activate both reporters in the 1 kb promoter line, which was narrowed-down to eight compounds which activated both reporters in the 400 bp promoter line, three of which were tested for transcriptional activation of *Oxr1-C* by RT-qPCR. While the positive hits identified in the screen were not taken forward for further testing, they demonstrated an ability to upregulate expression of mOXR1-C, at least in the cell line expressing the full length *Oxr1-C* promoter, which could be useful in murine *in vivo* research to increase *Oxr1* expression by drug administration.

Of the three compounds which reached testing for transcriptional activation – erythromycin estolate (A6), phenothrin (C9), and cyclamic acid (F5) (**Figure 5.10**) – all three had previously been tested in mice [356] [357] [358] and all except erythromycin estolate were capable of crossing the blood-brain-barrier to a measurable extent [359] [360], which is an important property for any potential therapeutic for neurological disorders. The compound library includes drugs with a range of active concentrations and routes of drug delivery, for example, some compounds can be given orally; cyclamic acid (F5) is a sweetener which is already used as a food additive. However, cyclamic acid has little known basis for direct transcriptional activation of Oxr1; in fact, the compound was shown to increase parameters of OS in the rat brain, and induce changes in haematological parameters indicative of microcytic anaemia [361]. The possible induction of OS by cyclamic acid suggests that it could indirectly lead to activation of Oxr1 expression, however this would not be a viable therapeutic strategy.

Compound ‘A6’, erythromycin estolate, is a macrolide antibiotic with known functions including inhibition of protein synthesis in bacteria, and destruction of viral lipid membranes to prevent infection with viruses such as the Zika Virus [356]. A study using

transcriptomics analysis of the livers from rats treated with erythromycin estolate identified expression changes in several of the target genes of Nrf2 [362], a nuclear transcription factor involved in the OS response through the Nrf2/ARE pathway [363]. Interestingly, a role for Oxr1 has been suggested in regulating the Nrf2-dependent OS response, due to the dependence of downstream effectors GPX2 and HMOX1 on levels of OXR1 [312], and the direct interaction between OXR1 and KEAP1, which regulates Nrf2 activity [364]. Compound 'C9' is Phenothrin, an insecticide which is used widely in agriculture due to its safe metabolism and low toxicity in mammals [357]. Phenothrin has been shown in rats to activate the nuclear receptor Peroxisome-Proliferator Activated Receptor α (PPARα) [365], which regulates genes involved in the uptake and oxidation of fatty acids, in addition to inflammation and vascular function [366]. Agonists of PPARα have been investigated as therapeutics for a wide range of disorders, including epilepsy [367], and the PPAR signalling pathway was found by transcriptomic analysis to be differentially regulated after hOXR1 depletion [308]. The possibility for either of these drugs to transcriptionally activate Oxr1 via known biological pathways makes both erythromycin estolate and phenothrin promising targets for further investigation, although this was not possible within the scope of this project given the time constraints, in addition to considerations of the weak effect of their administration on *Oxr1-C* expression in the cell line expressing the shorter *Oxr1-C* promoter, and the low ability of erythromycin estolate to cross the blood-brain-barrier [368].

Some hits, which did not reach expression analysis, may also have had strong molecular bases for effects on Oxr1 expression, such as 'H10' of plate MS20 - amlexanox, an anti-inflammatory, anti-histamine drug – which may be promising as a therapeutic due to the strong mechanistic links between neuroinflammation and oxidative stress, particularly in relation to epilepsy [318]. The compound 'G1' of plate MS09 is trazodone hydrochloride, a serotonin antagonist, which also shows promise due to the modulatory effects of serotonin on glutamate neurotransmission and excitotoxicity [369], and the potential role of Oxr1 in glutamate clearance (Oliver lab, unpublished findings – discussed below). Interestingly,

some compounds tested may have induced downregulation in Oxr1-C expression as measured by luciferase assay, for example, the compounds A5, Piroctone Olamine, which is an ethanolamine salt with fungicidal properties frequently used in anti-dandruff cosmetics [370], and E6, Benzalkonium Chloride, which is a cationic surfactanat and antimicrobial agent often used as a cosmetic preservative [371], from plate MS10 as shown in **Figure 5.8**. Some, including compound C2, the immunosuppressant drug Mitoxantrone hydrochloride [372], are dark in colour, and can therefore quench luminescence readings due to interference with the detection wavelength [373]. Although no further testing was performed on putative downregulators, these compounds may be useful for applications in which knock down of Oxr1 expression may be beneficial; low expression of h*OXR1* was identified by bioinformatics analysis as an adverse prognostic factor in patients with urothelial carcinoma [374], therefore application of a compound to downregulate *OXR1* could be used to elucidate the pathological effects of downregulation *in vitro*. This approach may be particularly advantageous if a compound is capable of selectively targeting one isoform for downregulation, in contrast with siRNA approaches which have been used to decrease expression of all hOXR1 isoforms [308].

Screening of the full PHARMAKON 1600 library was not possible due to time constraints, but in future investigation of the compound library, expression changes resulting from compound addition should be measured by RT-qPCR before moving to dose-response and cellular toxicity assays, to confirm that hits directly influence expression of Oxr1-C. Future use of the compounds would require initial testing of their effect on OS, to ensure that their upregulating effect on Oxr1 is not an indirect response to increased OS within the cell. Transcriptomics approaches should also be utilised to determine the specificity of effects of the compound, and investigate the pathways affected by its application. It is also important to note that the compounds, at the concentrations tested, increase Oxr1 expression to a lesser extent than has been shown to be protective *in vivo*; the Tg(mPrnp-Oxr1) produced a five-fold increase in expression of Oxr1-FL when crossed

with a mouse model of ALS [125], and three-fold in the cross described in this chapter between Oxr1$^{Prnp/+}$ and Tbc1d24^{R360L} mouse lines.

As an alternate method of genetic overexpression, CRISPRa represents a key strategy for targeted upregulation of endogenous genes, which shows great promise for therapeutic use. Indeed, the luciferase coincidence reporter system has recently been used as a method to validate the transcriptional activation by CRISPRa of the anti-aging and neuroprotective gene *Klotho*, through transfection of CRISPRa constructs including sgRNAs complementary to the *Klotho* promoter, into a cell line expressing the promoter ahead of NanoLuc and FireflyLuc [375]. Expression of the *Klotho* gene was shown by both RT-qPCR and luciferase assay to be upregulated by transfection with the CRISPRa constructs, suggesting the promise of this strategy for therapeutic use.

The CRISPRa system used here combines a nuclease-deficient dCas9 protein fused to a transcriptional activator of viral origin, VP64; the complex is guided by sgRNAs which are complementary to a specific gene promoter sequence [376]. The use of a single sgRNA, while capable of achieving transcriptional upregulation, has been demonstrated in many cases to produce a significantly lower magnitude of upregulation compared with the use of several sgRNAs targeting the same promoter at different sequences [377] [378]. This is concordant with the findings shown in **Figure 5.14**, that co-transfection with three CRISPRa constructs A, B and C, each with a different sgRNA sequence, produced robust upregulation of *Oxr1-C*, by 1.5 fold, while transfection with a single construct produced no significant difference in *Oxr1-C* expression. Importantly, the efficiency of transfection of the CRISPRa constructs, including co-transfection of all three, was low, ranging from 1.8% to 10.6% (**Figure 5.13**), and higher transfection efficiency could be expected to produce a higher magnitude of upregulation. For example, taking only the transfection efficiency into account, if a transfection efficiency of 5.0% produces a 1.5 fold increase for co-transfection with all three constructs, a transfection efficiency of 100% could produce up to a 30 fold increase in *Oxr1-C* expression. It is also very likely that single transfection of constructs A,

B, or C, with enhanced transfection efficiency, may produce significant upregulation of *Oxr1-C.* Despite this being an over-simplification, as *Oxr1-C* upregulation by CRISPRa may be limited by other factors including binding strength of the CRISPRa complex and chromatin packing [379], increasing the transfection efficiency would be desirable to produce high levels of *Oxr1-C* upregulation for use as a therapeutic strategy.

5.8.2 Overexpression of Oxr1 produces mild amelioration of pathology caused by loss-of-function mutations in Tbc1d24

There is a growing body of evidence for the protective role endogenously played by Oxr1 against OS-related cell death [304] and neuroinflammation [125], and for the potential remedial effect of upregulating Oxr1 to combat neurodegeneration [311]. Here, overexpression of Oxr1 in vivo through the presence of the $Oxr1^{Prnp/+}$ transgene demonstrated a potential ameliorative effect on the phenotypes caused by disruption of the related TLDc gene, Tbc1d24. Fatal seizure onset was delayed, suggesting a potential compensatory mechanism between the TLDc family members; however, upregulation of Oxr1 was not sufficient to prevent seizures altogether, Oxr1 has been shown to reduce OS, and is elevated at the site of oxidative injury (as seen in the $SOD1^{G93A}$ model of ALS), whereas a growing body of evidence supports a role for Tbc1d24 in the endolysosomal pathway, and there is little evidence of oxidative insult in the $Tbc1d24^{R360L}$ disease model from **Chapter Three**. Our findings suggest that neuronal expression of a full length Oxr1 isoform is not sufficient to functionally compensate for homozygous loss-of-function Tbc1d24 alleles. This points towards the functionally distinct roles of the TLDc family members, and supports a critical role for Tbc1d24 in mammalian survival. This is supported by findings in a recent cross between a knockout *Ncoa7* mouse model and an *Oxr1* loss-of-function model, in which no double-null mutants were obtained, including at early embryonic time-points, indicating that other TLDc family members were unable to functionally compensate for the loss of these two genes [380].

The rescue of key targets on the molecular level is an interesting indication of how these targets affect disease progression in models of Tbc1d24 dysfunction. A trend towards

the reduction of c-fos in mice expressing the *Oxr1*$^{Prnp/+}$ transgene accompanies a delay in onset of fatal seizures, as a possible indication of reduced neuronal excitability compared with Tbc1d24$^{R360L/R360L}$ counterparts with no expression of the Oxr1 transgene. Importantly, while RNA-seq analysis from the frontal cortex of Tbc1d24$^{R360L/R360L}$ mutants shows a significant upregulation of *c-Fos* (**Chapter Three**), RT-qPCR of mRNA extracted from whole brain does not show the same level of significance, suggesting that aberrant neuronal excitation and resultant seizure activity may be limited to the frontal cortex. In addition, it is likely that c-fos as a readout of excitability may depend on recent seizure activity [381].

It is important also to note that, although the *Prnp* promoter is commonly used in mouse models to alter neuronal gene expression, the gene has a leaky pattern of expression and is also expressed in the immune system, including in hematopoietic cells [382]. This suggests the possibility that overexpression of *Oxr1* in the mouse cross may extend to components of the blood, such as erythroid progenitors and platelets. Therefore, the observed reduction in *Alas2* expression in Tbc1d24$^{R360L/R360L}$ mutants expressing the *Oxr1*$^{Prnp/+}$ transgene may be due to increased expression of *Oxr1* in erythroid progenitors, which may reduce oxidative stress caused by hypoxia due to the R360L mutation, ultimately reducing the upregulation of *Alas2*. This hypothesis could be tested using ISH to visualise expression of *Oxr1* and *Prnp* in mouse hematopoietic cells of the bone marrow and liver.

Electrophysiological studies of the *Tbc1d24*^{R360L} mutant have shown that neurons of cortical layer 5 (L5) in these mutants display hyperexcitability, indicated by a lower excitation threshold, and random bursts of excitation consistent with epileptiform brain activity (Rial, D. – Oliver lab, unpublished). In addition, layer patterning defects are observed in cortical L5 (**Chapter Three**). Tbc1d24 has been identified as a binding partner of Ephrin-B2, the two proteins forming a complex mediated by Dishevelled during neural crest cell migration, and potentially playing a key role in formation of the CNS [383]. Additionally, Tbc1d24 has been shown to interact with ADP ribosylation factor 6 (ARF6) to regulate neuronal migration and cortical patterning [138]. Overexpression of the *Oxr1*$^{Prnp/+}$

transgene leads to a near-significant decrease in expression of Contactin 3 in the *Tbc1d24*^{INS2} mutant, suggesting that Oxr1 overexpression may reduce the upregulation of *Cntn3* linked with defects in neuronal migration caused by disruption in Tbc1d24. However, as Oxr1 isoforms are localized in the cytosol and mitochondria [323], it is unclear whether overexpression of Oxr1 protein could functionally compensate for interactions between Tbc1d24 and membrane bound proteins such as Ephrin-B2 and ARF6, and in fact, expression of *Cntn3* was not significantly different between *Tbc1d24*$^{INS2/INS2}$ mice with or without expression of the *Oxr1*$^{Prnp/+}$ transgene.

The brain is a highly vascularised organ, and increased OS is associated with a range of haematological disorders, including haemolytic anaemia [384] and iron-deficiency anaemia [385]. The haematological effects of Tbc1d24 disruption have been extensively described in Chapter Four, including the time-point dynamics of Alas2 expression, which becomes dramatically upregulated between P8 – P16, coinciding with an increase in disease severity. Alas2 catalyses the first step of heme biosynthesis, converting glycine and succinyl-CoA into 5-aminolevulinic acid (ALA) in the mitochondria [386]. Upregulation of Alas2 in the Tbc1d24$^{R360L/R360L}$ mutant is likely due to lack of functional haemoglobin caused by disrupted iron homeostasis. Interestingly, overexpression of Oxr1 via the Oxr1$^{Prnp/+}$ transgene was shown to prevent Alas2 upregulation in Tbc1d24$^{R360L/R360L}$ mutants, compared with Oxr1$^{Prnp/+}$Tbc1d24$^{WT/WT}$ mice. This suggests a link between Oxr1 and haemoglobin synthesis, despite its expression, in this case, being driven by a neuron-selective promoter. As shown in Chapter Four, saline-perfused brains of Tbc1d24$^{R360L/R360L}$ mutants show no significant increase in expression of Alas2, confirming that increased Alas2 expression originates in the blood. However, haemoglobin synthesis also takes place in neurons; interestingly, Alas2 has been shown to be neuronally upregulated in mouse models of Parkinson's disease [387] and social stress [388]. Increased ALAS2 expression has been identified as a survival-related marker in ALS, which has been attributed to the effect of Alas2 in indirectly reducing hypoxia, thereby preventing redox imbalance,

inflammation and metabolic dysfunction [389]. Knockdown of ALAS2 is associated with reduced erythroid differentiation, and downregulation of the mitophagy receptor BNIP3L [390]. The transgene Tg(mPrnp-Oxr1) expresses Oxr1-FL, which is endogenously localized in the cytosol, whereas Alas2 is functionally active in the mitochondria, therefore a direct interaction between the two proteins is unlikely. However, given the potential role of glutamate in causing seizures in the Tbc1d24 mutants, suggested in **Chapter Three**, overexpression of Oxr1 may increase glutamate uptake, either directly through functional compensation for Tbc1d24 or indirectly through enhanced protection against neuroinflammation and OS leading to increased survival. The enzyme glutamate dehydrogenase (GDH) converts glutamate into α-ketoglutarate, which directly enters the Krebs cycle, being converted into succinyl-CoA by the enzyme α-ketoglutarate dehydrogenase [391]. Increased glutamate availability may thus enhance mitochondrial metabolism, and, through increasing availability of the substrate of Alas2, may increase haemoglobin synthesis. Reduced serum glucose and increased lactic acid are observed in the *Tbc1d24*$^{R360L/R360L}$ mutant compared with wild type mice (**Chapter Four**), which indicates that aerobic metabolism is disrupted by the mutation. Overexpression of Oxr1, and increased uptake of glutamate, may enhance mitochondrial metabolism and therefore haemoglobin synthesis, which may help to prevent or delay anaemia caused by disruption in Tbc1d24.

5.8.3 Concluding Remarks

This chapter has investigated the potential for overexpression of Oxr1 as a neuroprotective strategy. The cell line stably expressing the dual luciferase coincidence reporter system is an effective tool for drug discovery, with high throughput potential, and has provided some early leads for compound-based upregulation of *Oxr1*. However, new genetic approaches such as CRISPRa show more promise in future therapeutics against neurodegeneration.

Breeding and characterization of a genetic cross between the epileptic mouse model *Tbc1d24*^{R360L} and the neuroprotective overexpressor line *Oxr1*$^{Prnp/+}$ has shed further light on the lack of functional redundancy of TLDc family members. Furthermore, a novel protective role for Oxr1 in the haematological system has been demonstrated.

Chapter 6: Discussion & Conclusion

6.1 General summary of data

This thesis has investigated the function and dysfunction of two key members of the TLDc gene family, *Tbc1d24* and *Oxr1*. In **Chapter Three**, human pathogenic mutations in *TBC1D24* were modelled in the mouse mutants *Tbc1d24*^{R360L} and *Tbc1d24*^{P135L}, with a further mouse mutant providing a complete null model, *Tbc1d24*^{INS2}. Both *Tbc1d24*^{R360L} and *Tbc1d24*^{P135L} showed recurrent seizures, providing valuable preclinical tools to model disease phenotypes observed in patients with TBC1D24 mutations. Surprisingly, it was demonstrated that the R360L (within the TLDc domain) and P135L (within the TBC domain) mutations led to decreases in Tbc1d24 protein expression of over 90%, while mRNA expression was unaltered; this not only suggests that they are acting as loss-of-function mutations, but also that the mutations are causing post-transcriptional destabilisation of the Tbc1d24 protein. This finding provides insight into the genotype-phenotype correlation of mutations within TBC1D24, consistent with the hypothesis that epilepsy-associated mutations cause destabilization of the tertiary structure leading to a reduction in protein expression, corroborated by decreased protein expression in TBC1D24 patient fibroblasts [172]. In the *Tbc1d24*^{INS2} mutant, very early postnatal lethality was observed, associated with total loss of Tbc1d24 protein and an approximate 50% decrease in *Tbc1d24* mRNA, supporting a crucial role for Tbc1d24 in development. In addition, some disruption of cortical layer patterning in the *Tbc1d24*^{INS2} mutant indicates that Tbc1d24 is required for normal neuronal development. This chapter also confirmed the protein-protein interaction between Tbc1d24 and the cytosolic V1 subunits of the vacuolar ATPase (V-ATPase). It is predicted that loss-of-function mutations in Tbc1d24 may influence function of the V-ATPase, supported by the overlapping clinical phenotypes of human TBC1D24 and V-ATPase pathological mutations [162] [132].

Chapter Four explored an unexpected consequence of disrupting Tbc1d24 expression, namely, haemolytic anaemia, as supported by blood smears of this mutant.

Transcriptomic analyses were performed using both *Tbc1d24*^{INS2} and *Tbc1d24*^{R360L} mutants, identifying a dramatic upregulation in key genes related to haemoglobin biosynthesis, suggesting that decreased expression of Tbc1d24 leads to the deregulation of haemoglobin synthesis pathways. Despite superficially normal blood smears in the *Tbc1d24*^{R360L} mutant, clinical chemistry showed increased numbers of erythrocytes but decreased erythrocytic volume, accompanying decreased haemoglobin concentration. Serum analysis in this mutant showed increased concentrations of iron and ferritin, suggesting disrupted iron homeostasis, and RT-qPCR confirmed alterations in iron homeostasis markers Transferrin receptor 1 (*Tfr1*) and Divalent metal transporter 1 (*Dmt1*). Increased iron staining in the *Tbc1d24*^{R360L} mutant spleen indicates iron loading anaemia. Furthermore, splenomegaly indicates stress erythropoiesis, confirmed by flow cytometry, which indicated erythropoietic drive in the spleen but not in the bone marrow of the *Tbc1d24*^{R360L} mice. The findings in this chapter demonstrate a novel role for Tbc1d24 in the haematological system, with a hypothesised mechanism of action involving the essential interaction with the V-ATPase promoting vesicle acidification and iron transport during haemoglobin synthesis.

In **Chapter Five**, a stable cell line expressing a dual luciferase coincidence reporter system was successfully developed and validated for use in compound screening. A screen of 800 compounds was performed to identify compounds able to upregulate expression of the short Oxr1 isoform (Oxr1-C) through interaction with a 400 bp promoter region conserved between humans and mice. While compounds were identified that were able to upregulate Oxr1-C expression, as confirmed by RT-qPCR, these compounds were deduced to act upstream of the conserved promoter region, and therefore would not necessarily be useful as therapeutics in humans. However, the cell line shows promise for future use in high-throughput compound screening. CRISPR activation (CRISPRa) was tested as an alternative method for the targeted upregulation of Oxr1-C, and was able to successfully upregulate Oxr1-C up to 1.5 fold, although it was clear that increased

transfection efficiency would be necessary for greater upregulation. CRISPRa therefore shows promise for use as a future therapeutic strategy. This chapter also investigated the effects of *in vivo* upregulation of Oxr1 on mouse models of Tbc1d24 dysfunction. A cross was performed between the *Tbc1d24*^{R360L} mutant and a mouse model expressing the transgene *Tg(mPrnp-Oxr1)*, which expresses full length Oxr1 driven by a prion promoter, leading to increased neuronal expression of Oxr1. Offspring from the cross showed survival extended by up to 40% compared with the *Tbc1d24*^{R360L} mutant, and deregulation of the haematology-related gene *Alas2* was shown to be less pronounced in presence of the Oxr1 transgene. This suggests a novel protective role for Oxr1 outside of the central nervous system (CNS).

6.2 Tbc1d24 protein stability and future treatment for TBC1D24-related pathology

Mouse models of epilepsy-related mutations in Tbc1d24, including the *Tbc1d24*^{R360L} and *Tbc1d24*^{P135L} lines described here, have demonstrated that neonatal seizures result from a significantly reduced abundance of Tbc1d24 protein expression [106]. Mice heterozygous for loss-of-function mutations in Tbc1d24 do not exhibit visible seizures, and survival is unaffected, suggesting that 50% expression of Tbc1d24 is sufficient for normal neurological function (see **Table 3.1**). Interestingly, all loss-of-function mutants of Tbc1d24 display seizures at a similar time point, between P15 – P16, which may indicate a specific neurodevelopmental role for Tbc1d24. Of note, increasing expression of *Tbc1d24* is observed in mouse hippocampal neurons extracted at E18.5 and cultured for 14 days *in vitro*, which correlates with terminal differentiation of neurons and further supports a role for Tbc1d24 in development [105]. To determine whether seizure activity in loss-of-function mutants is due only to developmental loss of Tbc1d24 expression, a new tamoxifen-inducible knockout mouse model of Tbc1d24 has been generated so that the effect of temporal Tbc1d24 knockdown in adulthood can be studied. Using CRISPR, the Oliver lab generated a new cre-lox mouse line containing two floxed exons within the TLDc domain of Tbc1d24, *Tbc1d24*$^{flox/flox}$. First, when this line was crossed with the non-inducible

ubiquitous cre-driver line, the offspring were shown to experience seizures from P16, confirming that the *Tbc1d24*$^{flox/flox}$ allele acts as a true null when recombined. The *Tbc1d24*$^{flox/flox}$ line was then crossed with tamoxifen-inducible ubiquitous cre line (Ubiq-cre), and adult (8 week) offspring from the cross were dosed with tamoxifen for 5 days. Strikingly, *Tbc1d24*$^{flox/flox}$/Ubiq-cre+ mice displayed fatal seizures approximately 40 days following tamoxifen dosing, at which point an 80% reduction in Tbc1d24 protein expression was observed in the cortex by Western blot. These data therefore suggest that the epileptic phenotype of Tbc1d24 loss-of-function is not only as a result of disrupted prenatal neuronal development, and support the importance of Tbc1d24 protein dosage (Oliver lab, unpublished). This is consistent with the finding in mature hippocampal cell culture that knockdown in expression of *Tbc1d24* caused a reduction in the number of excitatory synapses; Tbc1d24 is likely to play a role in the maintenance of mature synapses [137]. Tbc1d24 is known to play a role in axonal specification through enhancing membrane trafficking during neuronal development [135]. Although development plays a clear role in the pathogenesis of many epilepsies (for example, loss-of-function mutations in G protein-coupled receptor 56 (*GPR56*) result in abnormal cortical lamination which causes epilepsy [392]) epileptic syndromes can also be adult-onset [393], and some forms of epilepsy are associated with aging, such as in pre-symptomatic Alzheimer's disease, in which neurodegeneration can lead to epilepsy, preceding symptoms of dementia [394]. The inducible *Tbc1d24*$^{flox/flox}$ line may, therefore, be more useful for pharmacological screening of drugs to treat forms of epilepsy that are independent of disrupted development.

A significant clinical concern is that loss-of-function mutations, resulting in impaired function or expression of a protein, limit the possibility for the treatment of genetic diseases by application of a therapeutic compound [395]. Gain-of-function mutations can sometimes be targeted by drugs with inhibitory effects, for example, gain-of-function mutations in *SCN8A*, encoding the voltage gated sodium channel $Na_v1.6$, lead to epilepsy which can be treated using sodium channel blockers [396]. However, loss-of-function mutations require

the highly complex approach of rescuing protein function - such as allosteric activation of an enzyme – or via gene replacement [397]. Alternatively, drugs can also be used to target genes with potential compensatory mechanisms; the potential for this therapeutic strategy to treat loss-of-function in Tbc1d24 was investigated in Chapter Five, through the *in vivo* overexpression of Oxr1 in the *Tbc1d24*^{R360L} x *Oxr1*^{Prnp} cross. Overexpression of Oxr1 was found to extend survival by up to 40% compared with the *Tbc1d24*^{R360L} mouse model, suggesting that a compound able to upregulate Oxr1-C by targeting the conserved 400 bp promoter region could provide ameliorative effects to human patients with loss-of-function mutations in TBC1D24. However, more promising may be the potential to rescue of TBC1D24 expression itself.

Recent advances in gene therapy have given hope that rare genetic diseases which were previously considered intractable might be successfully treated by modification with exogenous genetic material [398]. Genome editing approaches, such as CRISPR, enable precise targeting of mutated genes, or, as demonstrated in Chapter Five, activation and upregulation of protective genes. The first *in vivo* CRISPR therapy trial is currently underway, which aims to treat LCA10, a genetic blindness syndrome caused by an autosomal recessive point mutation IVS26 in the gene centrosomal protein 290 (*CEP290*). The mutation introduces a splice donor side which produces a premature stop codon, resulting in the production of a truncated protein product which leads to degradation of photoreceptors in the retina [399]. The treatment approach utilises an adeno-associated virus (AAV) carrying the Cas9 protein, with guide RNAs (gRNAs) targeting and excising the mutation in *CEP290*. Promising results have been observed in patient fibroblasts *in vitro* and in a CRISPR-engineered mouse model of the disease [400]. If successful, approaches such as this could be used in the treatment of other diseases caused by loss-of-function point mutations, and could be used to treat diseases caused by mutation in *TBC1D24*.

CRISPRa has been used successfully to reduce chronic seizures in a kainate mouse model of acquired epilepsy, by transcriptionally activating expression of *Kcna1*,

which encodes the voltage gated potassium channel $K_v1.1$ [401]. Through increasing the endogenous expression of *Kcna1*, neuronal excitability is reduced, which is able to rescue seizures, and shows promise in future treatment of epilepsy. However, the mechanism for the loss of function of TBC1D24 is through reduction in abundance of TBC1D24 protein through post-transcriptional events, although further research is required to uncover the effect of loss-of-function mutations on protein stability. Upregulation of endogenous *TBC1D24* through transcriptional activation would therefore not be suitable for treating patients with loss-of-function mutations in TBC1D24. Rather, gene replacement of wild type *TBC1D24* would be required. Use of an adeno-associated virus (AAV) vector to deliver *TBC1D24* mRNA may be an effective therapeutic strategy, applicable to patients with a variety of loss-of-function mutations, enabling prolonged expression of functional TBC1D24 protein [402].

Thus, gene editing approaches show great promise for the treatment of loss-of-function mutations, for which treatment by pharmacological therapies is challenging.

6.3 Tbc1d24, the V-ATPase and the endolysosomal pathway

The interaction between Tbc1d24 and cytosolic V1 subunits of the V-ATPase was confirmed in **Chapter Three**. This finding builds upon recent evidence that suggests the interaction between other TLDc family proteins and the V-ATPase may be crucial, and disruption in these interactions are involved in disease. Proteomic analysis of mouse kidney lysates, published in 2015, identified Oxr1 and Ncoa7 as binding partners of the V-ATPase [403], where the complex plays an important role in urine acidification. Further proteomic analysis has since confirmed the interaction between the V-ATPase and the remainder of the TLDc family: Meak-7 (also known as Tldc1), Tldc2 (formerly known as C20Orf118) and Tbc1d24 [186]. Using site-specific mutagenesis, it was determined that the interaction depends on specific amino acid residues within the TLDc domain, in particular, those that are buried within the protein, as opposed to residues at the surface of the protein tertiary structure. These crucial residues were found by solubility assay to be essential for folding

of the TLDc domain [186]. It is thus likely that the TLDc family plays a regulatory role in V-ATPase function.

Significantly, cryo-EM has been applied very recently to shown in detail the interaction between the TLDc domain of Meak-7 and the V-ATPase, in which Meak-7 appears to form a crosslink between the cytosolic 'rotor' sub-complex of the enzyme, which rotates following hydrolysis of ATP, and the stationary, peripheral 'stator' portion of the V-ATPase, which stabilizes the enzyme complex. The crosslink interaction mediated by Meak-7 is predicted to inhibit rotation of the complex [404]. The TLDc domain of Meak-7 was shown to interact with the stator of the V-ATPase, while the C-terminal α helix of Meak-7 binds to the rotor of the V-ATPase. However, this labile interaction was shown to be easily displaced by ATP-induced rotation of the enzyme, indicating that Meak-7 neither enhances nor disrupts V-ATPase activity; rather, it was suggested Meak-7 may act as a sensor of V-ATPase activity [404]. In contrast to this, the interaction between Oxr1p, the yeast orthologue of Oxr1, and the yeast V1 complex of the v-ATPase, has also been detailed using cryo-EM, revealing that binding of Oxr1p puts strain on the complex, promoting disassembly and inhibiting v-ATPase function [405]. Taken together, these two cryo-EM studies support the role of the TLDc family as regulators of the v-ATPase, and highlight potential variability among the TLDc family in the effects they exert on the complex.

Importantly, however, the studies above lack cellular functional data to support the hypotheses. Related data regarding Ncoa7, not as yet studied by cryo-EM, and the V-ATPase supported a role for this TLDc protein in promoting V-ATPase assembly; primary cortical neurons of a mouse model lacking all *Ncoa7* isoforms showed an increase in lysosomal pH of up to 0.5 units, suggesting disrupted acidification [406]. A significant reduction in the number of lysosomes was detected in primary neurons of the *Ncoa7* knockout mouse, which could be rescued by overexpression of *Ncoa7*. Furthermore, lysosomal function was shown to be disrupted through the use of two lysosomal degradation assays, in which exogenous compounds are introduced to the lysosome;

neurons of the *Ncoa7* knockout mouse showed reduced processing of these compounds [406]. Transmission electron microscopy (TEM) was used to investigate the functional consequences of lysosomal dysfunction in the *Ncoa7* knockout neurons, revealing an increase in cytosolic granules in the neuronal soma, likely as a result of lysosomal failure to process material [406]. To investigate the interaction between Ncoa7 and the V-ATPase, subcellular fractionation was performed using protein extracted from primary cortical neurons of *Ncoa7* knockout mice. In the membrane fraction there was found to be a reduction in the levels of the V1 (cytosolic) subunits Atp6v1b2 and Atp6v1a1, compared with wild type, suggesting that loss of Ncoa7 results in destabilization of the V-ATPase complex at the membrane [406]. Membrane-associated phosphoinositides (PIPs) are known to interact with and stabilize the V-ATPase complex [407, 408], therefore a protein-lipid overlap assay was used to determine the interaction between Ncoa7 and PIPs, which revealed binding between recombinant Ncoa7 protein and a variety of PIPs, including those determined to be necessary for V-ATPase activity [406]. Together, these data suggest that Ncoa7 regulates V-ATPase function through tethering to the endolysosomal membrane to facilitate assembly of the complex, and thus regulate lysosomal function.

Knockout of *Ncoa7* was found to cause anxiety and social impairments in mice, while *NCOA7* mutations are associated with autism in human patients [406]. Importantly, studies in *Drosophila* revealed a PIP-binding pocket in the TBC domain of the Tbc1d24 orthologue, Sky, which may suggest a similar tethering function for Tbc1d24 between the V-ATPase and the membrane [409]. Given the severity of disease phenotypes associated with loss-of-function in TBC1D24, it could be predicted that Tbc1d24 is a more critical, or ubiquitous, regulator of V-ATPase function. In order to test this hypothesis, the effects of Tbc1d24 disruption on endolysosomal function should be investigated using similar experiments as for Ncoa7, such as measurements of lysosomal acidification, and degradation of ectopically-applied compounds. There is a growing body of evidence for the role of the TLDc domain as a critical regulator of the function of the V-ATPase, although the

potential for overlapping function between TLDc family members remains unclear. It is possible that structural differences between the family, such as the TBC domain of Tbc1d24, enable varying strengths of interaction between the V-ATPase and the membrane. Interestingly, the short isoform of Ncoa7, but none of the longer isoforms, shows interferon-inducible expression and displays cytoplasmic staining rather than co-localizing with endosomal markers. This isoform of Ncoa7 was found to inhibit viral entry through interaction with the V-ATPase, suggesting a specific role not observed in any other TLDc protein [410].

Mutations in the V-ATPase are associated with epilepsy, while rare heritable disorders such as DOORS syndrome support an obvious clinical link between the V-ATPase and the TLDc family [132] [163]. Missense mutations in *ATP6V1A* have been linked to a variety of clinical features, including epileptic encephalopathy, intellectual disability and neurodegeneration. Similarly to observations in *Ncoa7* knockout neurons, fibroblasts from patients with *ATP6V1A* mutations show altered lysosomal pH, although a significant increase in pH was associated with severe disease phenotypes, while significantly decreased pH was observed in patients with milder disease [411]. This supports the hypothesis that forms of epilepsy caused by mutations in the V-ATPase are lysosomal disorders, in which altered lysosomal homeostasis lead to neuronal dysfunction.

The V-ATPase complex is vital for a great many cellular processes, including neuronal synaptogenesis and the endolysosomal pathway. Regulators of the V-ATPase support these vital functions, including through stabilization of the complex and interaction with lysosomal membranes, as performed by members of the TLDc family. A growing body of evidence supports the role of endolysosomal dysfunction in neurological diseases, such as epilepsy [412], giving urgency to the need for further research into the interaction between the V-ATPase and the TLDc family.

6.4 The overlapping aetiologies of anaemia and epilepsy

This thesis has provided evidence for a novel role for Tbc1d24 in the haematological system, and described the haematological consequences of disruption in Tbc1d24 expression. The severe haemolytic phenotype of the *Tbc1d24*$^{INS2/INS2}$ mouse is likely to be incompatible with life, as the low proportion of viable RBCs visible on peripheral blood smears indicates low capacity for oxygen transport. As shown by transcriptomics of this mutant, upregulated genes indicate erythropoietic drive and a switch towards anaerobic methods of ATP generation, which occurs under hypoxic conditions. The *Nan* model of haemolytic anaemia is embryonic lethal in homozygous mice, with pallor and persistent haemolysis, indicating that severe haemolysis is incompatible with life [413]. Iron-loading anaemia indicated in the *Tbc1d24*$^{R360L/R360L}$ mutant may exacerbate neurological dysfunction; iron accumulation in the brain is also associated with neurological disorders, as observed in aceruloplasminemia, in which cellular iron retention leads to oxidative damage, causing neurodegeneration and anaemia [414].

Interestingly, haematological changes including anaemia and platelet defects have been reported in patients with mutations in TBC1D24, comorbid with epilepsy (personnel communication, Prof. S. Sisodiya, UCL Institute of Neurology). Furthermore, microcytic anaemia was reported in a patient with DOORS syndrome caused by mutation in *TBC1D24* [415]. However, RNA-Seq analysis of the inducible knockout mouse model of Tbc1d24 (see **6.2**, above) shows no immediate haematological changes, suggesting that the anaemia in the *Tbc1d24*$^{R360L/R360L}$ mutant does not cause the seizures observed. In a recent study, CRISPR-Cas9 genetic screening was used to identify pathways sensitive to lysosomal pH, revealing that alteration of pH causes disruption of cellular iron uptake and depletion of intracellular iron, preventing cell proliferation, although this can be rescued by supplementation with iron [416]. In addition, a cell line conditionally deficient for the V-ATPase subunit ATP6V0C was found to stop proliferating when ATP6V0C was lost, which

was again rescued by iron supplementation [416]. Lysosomal acidification, mediated by the V-ATPase, is therefore essential for normal iron homeostasis.

Therefore, it is likely that defective endolysosomal trafficking caused by mutations in Tbc1d24 results in both disrupted neuronal function and haemoglobin synthesis. The mechanism proposed above - that association between Tbc1d24 and the V-ATPase is required for vesicle acidification - also applies to erythroblasts, where the association is necessary for iron to be released from transferrin and to associate with heme to produce functional haemoglobin. In order to test this hypothesis, iron uptake could be measured using the radioactive isotope ^{59}Fe to label endosomes of *Tbc1d24*^{INS2} primary cultures, followed by measurements of ^{59}Fe-labelled heme, to determine incorporation of iron into heme in the presence or absence of Tbc1d24 [302].

Iron deficiency anaemia has been linked to seizures, with decreased haemoglobin levels measured in children who had experienced a first attack seizure compared to those who had not, suggesting that iron status can be a risk factor for seizures [417]. Abnormal iron metabolism is associated with epilepsy. Iron overload has been shown to cause epilepsy following haemorrhagic stroke, which can be modelled in rodents through injection with iron (III) chloride into the cerebral cortex, leading to recurrent seizures [418]. Epilepsy is also more than twice as common in patients with sickle cell anaemia, which may be related to disrupted blood supply to the brain [419]. Anaemia is a commonly reported side effect of anti-seizure medications (ASMs), which can be caused, for example, by toxicity of the ASM affecting bone marrow cells, and disrupting erythropoiesis, or by direct interaction between ASMs and erythrocyte membrane resulting in haemolysis [420]. Further research is needed to understand the overlap between epilepsy and haematological dysfunction, which is necessary to avoid anaemic side effects of ASMs and improve quality of life for patients with epilepsy.

6.5 Glutamate, epilepsy and the V-ATPase

On-going studies in the Oliver group suggest that the epileptic phenotype of the *Tbc1d24*$^{R360L/R360L}$ mutant is causally related to the functionality or synaptic availability of Glt-1, a glutamate transporter predominantly expressed in astrocytes, termed EAAT2 in humans [421]. As introduced in **Chapter Three**, electrophysiological data from both single-cell (**Figure 6.1A,** below) and local field potential (**Figure 6.1B**) recordings of L5 cortical neurons at P16 show early saturation of Glt-1 in *Tbc1d24*$^{R360L/R360L}$ animals compared with *Tbc1d24*$^{+/+}$ when the Glt-1 blocker DL-threo-beta-Benzyloxyaspartate (DL-TBOA) is applied (Rial, D. – Oliver lab, unpublished). These data may be indicative of reduced expression of Glt-1 in the mutant cortex, which was confirmed subsequently by Western blot (Soares, T. – Oliver lab, unpublished). Together, these data indicate that the epileptic phenotype of the *Tbc1d24*$^{R360L/R360L}$ mutant may in part originate from, or be exacerbated by, aberrant glutamate clearance, likely in astrocytes. To support this hypothesis, the conditional Tbc1d24 line has been crossed with a cre-driver line expressing specifically in calcium/calmodulin dependent protein kinase II α- (CamKIIα) Cre positive neurons in the forebrain [422]. The CamKIIα promoter is known to cause specific expression in glutamatergic, excitatory neurons, although recent studies have demonstrated expression of CamKIIα in GABAergic, inhibitory neurons [423] [424]. Interestingly, mice homozygous for the floxed allele show no visible seizure activity, *c-fos* induction by RT-qPCR or a reduction in lifespan (Oliver lab, unpublished). These data suggest that loss of Tbc1d24 functionality in non-neuronal cells is a key feature of seizures in the mouse. Tbc1d24 is expressed in both neurons and astrocytes, although neuronal expression of TBC1D24 is higher than that of astrocytes in both humans and mice, shown by search of the single-cell

RNASeq data base *Brain RNA-Seq* [425] [426]. Therefore Tbc1d24 may play important functional roles, as described, in both neurons and astrocytes.

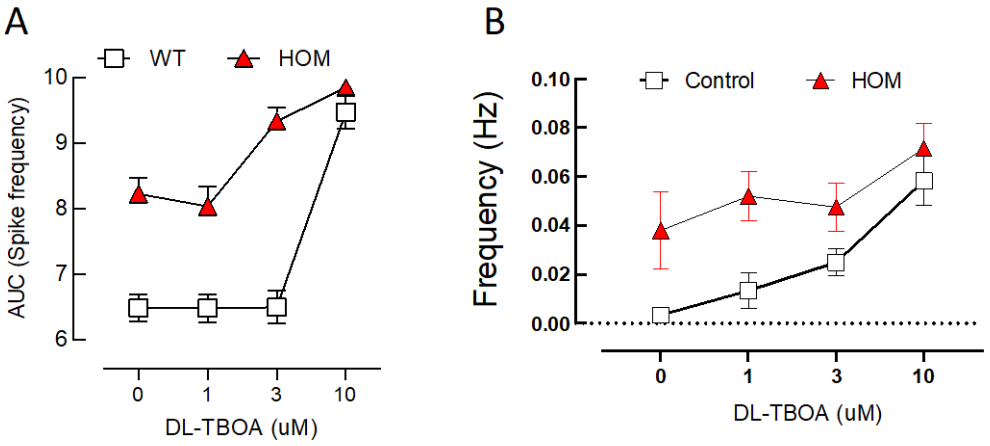


Figure 6.1 Electrophysiological recordings show hyperexcitability and increased saturation of Glt-1 in the* Tbc1d24$^{R360L/R360L}$ *mutant. *Single cell recordings (**A**) and local field potential recordings (**B**) of layer 5 cortical neurons show increased baseline spike frequency in* Tbc1d24$^{R360L/R360L}$ *(HOM) compared with* Tbc1d24$^{+/+}$ *(WT). Application of the Glt-1 blocker DL-threo-beta-Benzyloxyaspartate (DL-TBOA) showed supramaximal saturation in* Tbc1d24$^{R360L/R360L}$ *neurons at 3 μM, compared with 10 μM in* Tbc1d24$^{+/+}$ *neurons, indicating lower expression of Glt-1 in the* Tbc1d24$^{R360L/R360L}$ *mutant. (Data from Rial, D., Oliver lab, unpublished).*

Mice homozygous for the knockout of *Glt-1* exhibit spontaneous seizures and early death, similarly to mouse models of Tbc1d24 dysfunction [427]. However, conditional deletion of Glt-1 in either astrocytes or neurons produces very different phenotypes in mouse models; deletion of Glt-1 in astrocytes led to seizures, reduced body weight and early mortality in homozygous mice, whereas neuronal deletion of Glt-1 did not affect survival or weight, or produce seizures in the mice, but did produce a 40% reduction in glutamate uptake at the synapse [428]. Crucially, downregulation of synaptosomal Glt-1 has been observed during epileptogenesis, suggesting that insufficient glutamate clearance contributes to the pathology of epilepsy. In an induced epilepsy mouse, the intrahippocampal kainic acid (IHKA) model, significant downregulation of Glt-1 was measured 7 days post injection with kainic acid, corresponding with the onset of spontaneous seizures [429]. Furthermore, Glt-1 has been shown in astrocytes to co-compartmentalise with hexokinase-1 (the first enzyme in the glycolytic pathway), suggesting a spatial and mechanistic link between glutamate transport and glycolytic

metabolism [430]. As shown by transcriptomics in the *Tbc1d24*^{INS2} mutant and serum analysis in the *Tbc1d24*^{R360L} mutant, knockdown in Tbc1d24 expression is associated with a switch towards glycolysis.

Reduced synaptosomal Glt-1 expression in the *Tbc1d24*^{R360L} mutant may result in a seizure phenotype that originates from the astrocytes, although importantly, a mouse model of conditional astrocytic deletion of *Glt-1* led to a mortality rate of 50% by 23 weeks of age, while *Tbc1d24*$^{R360L/R360L}$ mice experienced fatal seizures from P18 (license restrictions prevented a longitudinal survival study). Endolysosomal defects due to pathogenic mutations in *Tbc1d24* may explain the phenotypic severity of neurological dysfunction observed in the *Tbc1d24*^{R360L} and *Tbc1d24*^{P135L} mouse models. The vesicular glutamate transporter, VGLUT, is responsible for refilling synaptic vesicles with glutamate, requiring an electrochemical gradient established by the V-ATPase to exchange glutamate for protons [431]. This process takes place both in neurons and in astrocytes; astrocytic recycling of glutamate from the synaptic cleft following uptake by Glt-1 is dependent on uptake into SVs by VGLUT [432]. Disruption of the electrochemical gradient required for VGLUT to function may result in an increase in intracellular glutamate within the astrocytes, which may also indirectly lead to downregulation of Glt-1 to prevent further glutamate uptake. However, a decrease in Glt-1 expression would likely result in the detrimental accumulation of glutamate in the synaptic cleft, and eventual excitotoxicity. The proposed mechanism for disrupted glutamate homeostasis caused by loss-of-function in TBC1D24 is depicted in **Figure 6.2**.

Interestingly, Glt-1 has been shown to be downregulated in a mouse model of Lafora disease, which is a fatal disorder characterized by epilepsy and neurodegeneration, with two known causative genes which encode laforin, a phosphatase, and malin, a ubiquitin ligase. Laforin and malin together form a laforin/malin complex. It was demonstrated that loss of expression of either gene results in decreased glutamate uptake in the astrocytes, while upregulation of laforin or malin expression was shown to prevent ubiquitination-

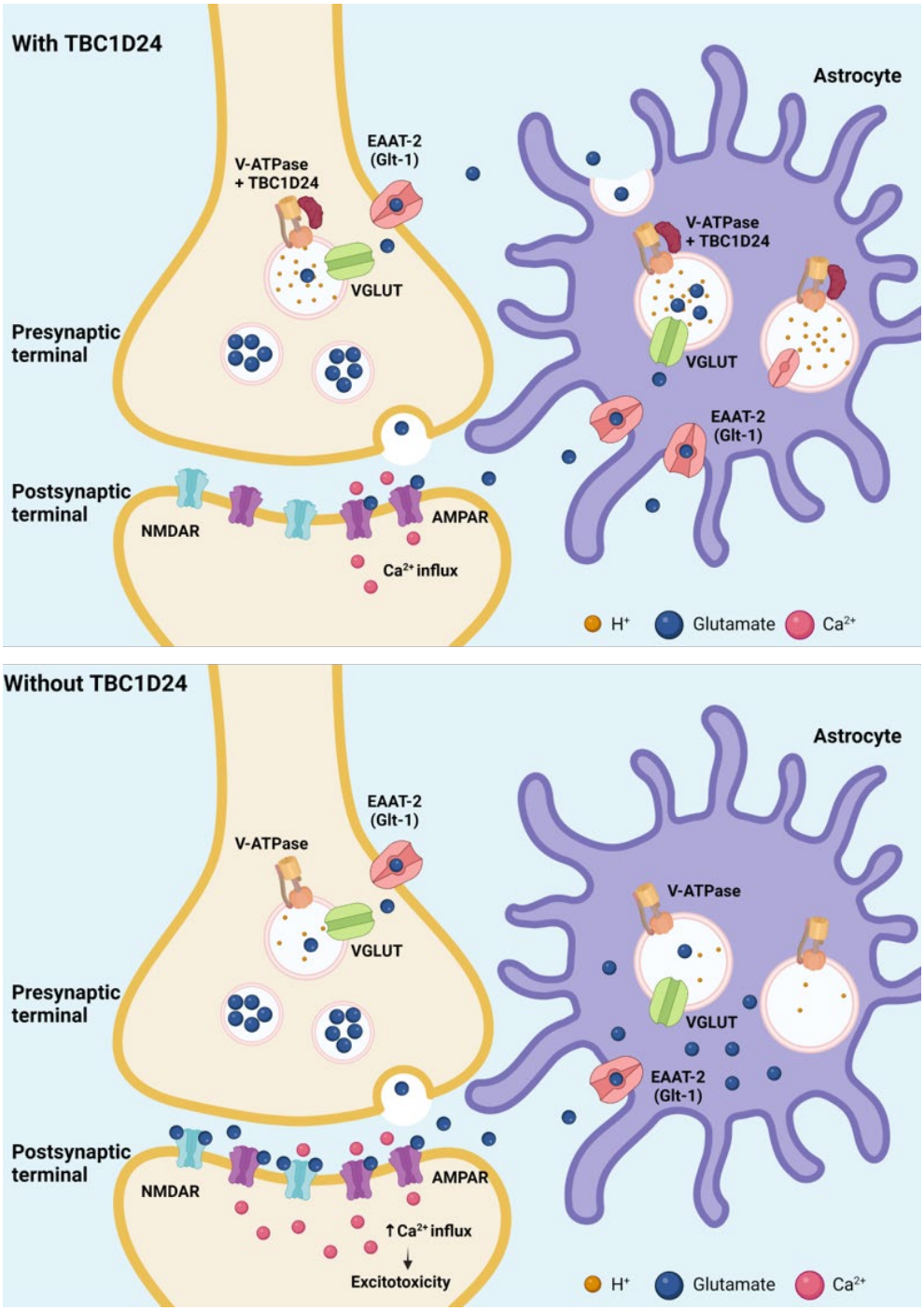


Figure 6.2 – The interaction between TBC1D24 and the V-ATPase is required for glutamate homeostasis between neurons and astrocytes. *Proposed mechanism for epilepsy observed as a result of loss-of-function mutations in TBC1D24 (for simplicity, the glutamate-glutamine cycle is not depicted). (**Top**) Glutamate is concentrated into synaptic vesicles by VGLUT, requiring an electrochemical gradient generated by the V-ATPase. TBC1D24 interacts with the V-ATPase to enhance acidification of vesicles. Glutamate is released from synaptic vesicles of excitatory neurons through calcium-mediated exocytosis. Glutamate crosses the synaptic cleft to bind to postsynaptic glutamate receptors such as AMPAR and NMDAR, inducing calcium influx and signal transduction in the postsynaptic neuron. Astrocytes are responsible for the bulk of glutamate clearance from the synaptic cleft through EAAT-2 (Glt-1 in mice). Glutamate is concentrated into vesicles for calcium-mediated exocytosis from astrocytes, to be released to neurons for recycling. EAAT-2 is delivered to the astrocytic membrane through the endosomal pathway, involving the V-ATPase. (**Bottom**) In the absence of TBC1D24, vesicle acidification is reduced. In astrocytes this prevents concentration of glutamate into vesicles, leading to build up of glutamate in astrocytes and downregulation of EAAT-2 expression, resulting in an excess of glutamate in the synaptic cleft, which leads to hyperexcitability of postsynaptic neurons, and eventual excitotoxicity. Created with Biorender.com.*

that the laforin/malin complex delays endocytosis of Glt-1 by mediating ubiquitination, and that disruption of laforin or malin expression caused deleterious alteration of Glt-1 homeostasis, leading to Lafora disease [434]. Therefore, endolysosomal dysfunction may similarly affect Glt-1 expression in loss-of-function mutations of Tbc1d24.

Increased survival observed in the offspring from the *Tbc1d24*$^{R360L/R360L}$ x *Oxr1*$^{Prnp/+}$ cross introduced in **Chapter Five** may be explained by increased neuronal glutamate uptake due to overexpression of Oxr1, either by functionally compensating for loss of Tbc1d24 or by generally increasing neuronal survival through resisting OS and neuroinflammation. This hypothesis could be tested using microdialysis to measure glutamate uptake in cortical sections of mice expressing the transgene Tg(m*Prnp*-Oxr1) compared with wild type mice [435]. Increased neuronal uptake of glutamate may reduce hyperexcitability and excitotoxicity [436]. However, as the majority of Glt-1 expression, and glutamate clearance, occurs in astrocytes, neuronal expression of Oxr1 does not prevent seizures or early mortality.

6.6 OXR1 as a future therapeutic target

Oxr1 has been shown both *in vitro* [310] and *in vivo* [125] to protect against oxidative stress and provide neuroprotection. In **Chapter Five**, the potential for the neuroprotective mechanisms of Oxr1 to be harnessed therapeutically was investigated in a small compound screen. Although the compounds which were identified to increase expression of Oxr1 were determined to be unsuitable for translational use, the stable cell line generated has high throughput potential, and testing of further libraries may yield more promising compounds. Screens for compounds which achieve upregulation of a target gene through interaction with an endogenous promoter have shown successes, such as screens for overexpression of the dystrophin paralogue utrophin for the treatment of Duchenne muscular dystrophy (DMD), which have identified several therapeutic candidates able to act on the utrophin promoter [437]. This particular approach relies of the availability of a suitable paralogue, as

overexpression of dystrophin itself has been shown to elicit a strong immune response, limiting its therapeutic potential [438].

However, a more reliable treatment option may be through gene therapy, as discussed above in the context of therapeutic options for loss-of-function mutations. CRISPR activation of *OXR1* in order to upregulate OXR1 may be a more promising therapeutic strategy. Furthermore, gene therapy can be applied to other members of the TLDc family for therapeutic purposes. *In vivo*, subretinal injection of AAV-packaged hOXR1 has been shown to be neuroprotective in a mouse model of retinopathy, improving photoreceptor function and delaying retinal degeneration [309]. *In vitro* expression of NCOA7 has been shown to inhibit viral entry, by preventing fusion of the viral membrane with the endosome, and enhancing vesicle acidification, through its interaction with the V-ATPase [410]. This mechanism could be harnessed therapeutically, to enhance immune regulation of the endolysosomal pathway in viral infection. Thus, TLDc proteins present a variety of useful mechanisms that may give promise for their application as therapeutics.

6.7 Conclusion

This thesis has investigated the TLDc family in the context of neurological and haematological dysfunction, and therapeutic strategies of neuroprotection. Key findings of this thesis are that loss-of-function mutations in Tbc1d24 result in severe neurological phenotypes including seizures, thus Tbc1d24 is necessary for normal neuronal function, and that loss of Tbc1d24 expression, unexpectedly, also leads to haematological dysfunction and disrupted iron homeostasis. Importantly, this is the first work to uncover a role for Tbc1d24 in the haematological system, and a link between mutations in Tbc1d24 and anaemia. Findings of this thesis support a key interaction between Tbc1d24 and the V-ATPase, suggesting disease mechanisms for both epilepsy and anaemia involving the disruption of this interaction. Finally, a therapeutic strategy involving the upregulation of Oxr1 has been examined, and a cell line suitable for future compound screening has been established. It is hoped that this thesis will contribute to a deeper understanding of the roles

of the TLDc family mediated through their varied interactions with the V-ATPase, which have been shown to play vital roles within many biological pathways. Furthermore, that the preclinical tools generated will help to define new therapeutic interventions to prevent severe neurological disease caused by TBC1D24 mutations.

Chapter 7: Appendices

Table 7.1 Genes identified as differentially expressed in the* Tbc1d24$^{INS2/INS2}$ *mutant cortex, determined by RNA-Seq. *Table shows all genes with false discovery rate adjusted P values (FDRs) < 0.01, to a total of 26 genes.*

Gene	Gene Name	logFC	FC	P Value	FDR
Tbc1d24	TBC1 Domain Family Member 24	-0.77483	0.584459	5.54E-88	6.70E-84
Alas2	δ-Aminolevulinate Synthase 2	1.560295	2.949142	7.98E-32	4.83E-28
Tent5c	Terminal Nucleotidyltransferase 5C	1.311316	2.481677	1.03E-17	3.22E-14
Slc16a3	Solute Carrier Family 16 Member 3 (aka Monocarboxylic Acid Transporter 4, MCT4)	1.097702	2.140136	1.07E-17	3.22E-14
Hbb-bt	Haemoglobin beta adult t chain	1.265436	2.403999	2.54E-14	6.15E-11
Hbb-bs	Haemoglobin beta adult s chain	0.961118	1.946819	2.17E-12	4.38E-09
Slc40a1	Ferroportin	0.663842	1.584296	5.17E-11	8.93E-08
Hmox1	Heme Oxgenase 1	1.238909	2.360201	8.93E-10	1.35E-06
Eno1	Enolase 1	0.237502	1.17895	4.65E-09	6.25E-06
Ldha	Lactate Dehydrogenase A	0.276954	1.211634	2.19E-08	2.65E-05
Pfkl	Phosphofructokinase, liver type	0.223179	1.167303	4.22E-08	4.50E-05
Gpi1	Glucose-6-Phosphate Isomerase	0.347329	1.272203	4.47E-08	4.50E-05
Gja4	Gap Junction Protein Alpha 4	0.505682	1.419794	1.60E-07	0.000148
Hba-a1	Haemoglobin alpha, adult chain 1	0.847253	1.799072	2.02E-07	0.000174
Bnip3	BCL2 Interacting Protein 3	0.317599	1.246255	2.44E-07	0.000196
Ube2l6	Ubiquitin Conjugating Enzyme E2 L6	0.550868	1.464966	2.61E-07	0.000198
Vegfa	Vascular Endothelial Growth Factor A	0.34648	1.271455	3.63E-07	0.000258
Hba-a2	Haemoglobin alpha, adult chain 2	0.802149	1.743697	1.23E-06	0.000829
Ecm1	Extracellular Matrix Protein 1	0.397456	1.317184	1.53E-06	0.000973
P4ha1	Prolyl 4-Hydroxylase Subunit Alpha 1	0.267398	1.203635	1.94E-06	0.00113

Gm42047	Predicted gene, 42047	0.608484	1.524656	1.96E-06	0.00113
Vwf	Von Willebrand Factor	0.314654	1.243713	3.09E-06	0.001696
Pdk1	Pyruvate Dehydrogenase Kinase 1	0.27363	1.208846	3.33E-06	0.001749
Slc17a7	Solute Carrier Family 17 Member 7 (aka Vesicular Glutamate Transporter 1, GLUT1)	-0.3178	0.802293	4.06E-06	0.002047
Tpi1	Triosephosphate Isomerase 1	0.22626	1.169798	7.39E-06	0.003573
Ucp2	Uncoupling Protein 2 (Mitochondrial, Proton Carrier)	0.303827	1.234415	1.63E-05	0.007558

Table 7.2 Genes identified as differentially expressed in the* Tbc1d24$^{R360L/R360L}$ *mutant cortex, determined by RNA-Seq. *Table shows all genes with false discovery rate adjusted P values (FDRs) < 0.01, to a total of 150 genes.*

Gene	Gene Name	logFC	FC	P Value	FDR
Tmem181b-ps	Transmembrane Protein 181B, Pseudogene	0.898061	1.863559	1.04E-27	1.23E-23
Hbb-bt	Haemoglobin beta adult t chain	1.747814	3.358494	1.59E-17	9.39E-14
Hba-a1	Haemoglobin alpha, adult chain 1	1.468531	2.767399	1.75E-16	6.86E-13
Hba-a2	Haemoglobin alpha, adult chain 2	1.529503	2.886864	2.78E-16	8.20E-13
Fkbp5	FK506 Binding Protein 5	-0.69692	0.616887	4.50E-16	1.06E-12
Hif3a	Hypoxia Inducible Factor 3, alpha subunit	-0.57438	0.671573	1.15E-15	2.27E-12
Arc	Activity Regulated Cytoskeletal-Associated Protein	2.122747	4.355224	1.38E-15	2.33E-12
Alas2	δ-Aminolevulinate Synthase 2	1.578446	2.98648	2.27E-13	3.35E-10
Zbtb16	Zinc Finger and BTB Domain Containing 16	-0.6347	0.644077	7.02E-13	9.20E-10
Klf10	Kruppel-like factor 10	0.831153	1.779107	1.25E-12	1.48E-09
Arl4d	ADP-ribosylation factor-like 4D	1.022322	2.031185	1.70E-12	1.82E-09
Ptgds	Prostaglandin D2 Synthase (brain)	-0.83897	0.559044	2.96E-11	2.91E-08
Tfrc	Transferrin Receptor	-0.43703	0.738656	7.73E-11	7.02E-08
Hbb-bs	Haemoglobin beta adult s chain	1.391524	2.623557	1.28E-10	1.08E-07
Stra6	Stimulated By Retinoic Acid Gene 6	-0.5797	0.669104	1.78E-10	1.40E-07

Kcnj2	Potassium Inwardly-Rectifying Channel, Subfamily J, Member 2	-0.71284	0.610116	2.38E-10	1.76E-07
Ier5l	Immediate Early Response 5-like	0.71186	1.637914	4.35E-10	3.02E-07
Junb	Jun B Proto-Oncogene	1.26917	2.410229	3.00E-09	1.96E-06
Slc13a4	Solute Carrier Family 13 (Sodium/Sulfate symporters), Member 4	-0.7148	0.609288	7.72E-09	4.79E-06
Nab2	Ngfi-A Binding Protein 2	0.554561	1.468721	1.53E-08	9.03E-06
Zfp143	Zinc Finger Protein 143	-0.39919	0.758285	2.64E-08	1.48E-05
Nrde2	Nrde-2 Necessary for RNA Interference, Domain Containing	-0.40948	0.752897	2.82E-08	1.51E-05
Pprc1	Peroxisome Proliferative Activated Receptor, Gamma, Coactivator-related 1	0.332572	1.259256	5.17E-08	2.65E-05
Clk1	CDC-like Kinase 1	0.479766	1.394518	6.56E-08	3.22E-05
Fos	FBJ Osteosarcoma Oncogene	1.489406	2.807734	7.38E-08	3.48E-05
Smim3	Small Integral Membrane Protein 3	-0.3899	0.763184	9.29E-08	4.22E-05
Ppp2r1b	Protein Phosphatase 2, Regulatory Subunit A, Beta	0.409672	1.328384	1.02E-07	4.45E-05
Tnfrsf19	Tumor Necrosis Factor Receptor Superfamily, Member 19	0.3069	1.237046	1.11E-07	4.53E-05
Islr	Immunoglobulin Superfamily Containing Leucine-Rich Repeat	-0.43951	0.737385	1.11E-07	4.53E-05
Dlc1	Deleted in Liver Cancer 1	0.286784	1.219918	1.29E-07	5.09E-05
Fmod	Fibromodulin	-0.65358	0.635701	1.49E-07	5.67E-05
Irf2bpl	Interferon Regulatory Factor 2 Binding Protein-like	0.282683	1.216455	1.62E-07	5.96E-05
Zfp867	Zinc Finger Protein 867	-0.4834	0.715291	1.72E-07	6.13E-05
Kdm6b	KDM1 Lysine (K)-Specific Demethylase 6B	0.392856	1.31299	1.80E-07	6.16E-05
Ier2	Immediate Early Response 2	1.118003	2.170463	1.87E-07	6.16E-05
Cep192	Centrosomal Protein 192	0.343681	1.26899	1.88E-07	6.16E-05
Nt5e	5' Nucleotidase, Ecto	-0.46733	0.723304	1.95E-07	6.23E-05
Frmpd1	FERM and PDZ Domain Containing 1	-0.34844	0.785434	2.02E-07	6.28E-05
Slc13a3	Solute Carrier Family 13 (Sodium-Dependent Dicarboxylate Transporter), Member 3	-0.40065	0.757515	2.25E-07	6.82E-05

Gm43843	Predicted Gene 43843	0.358496	1.282088	2.90E-07	8.56E-05
Ushbp1	USH1 Protein Network Component Harmonin Binding Protein 1	0.356283	1.280124	4.02E-07	0.000115
Rnf213	Ring Finger Protein 213	0.515815	1.429802	4.08E-07	0.000115
Mcl1	Myeloid Cell Leukemia Sequence 1	0.264149	1.200927	4.26E-07	0.000117
Cited4	Cbp/p300-Interacting Transactivator, with Glu/Asp-rich Carboxy-terminal Domain, 4	-0.39304	0.761524	4.40E-07	0.000118
Clk4	CDC Like Kinase 4	0.374892	1.296742	4.71E-07	0.000123
Dact1	Dishevelled-Binding Antagonist of Beta-Catenin 1	0.420702	1.338579	5.75E-07	0.000147
Sik1	Salt Inducible Kinase 1	1.114511	2.165217	9.32E-07	0.000234
Lyst	Lysosomal Trafficking Regulator	-0.24898	0.841489	9.84E-07	0.000242
Insig1	Insulin Induced Gene 1	0.229739	1.172623	1.14E-06	0.000274
Lrfn2	Leucine Rich Repeat and Fibronectin Type III Domain Containing 2	-0.32157	0.800199	1.26E-06	0.000296
Zfp658	Zinc Finger Protein 658	0.5079	1.421979	1.29E-06	0.000296
Igfbp3	Insulin-like Growth Factor Binding Protein 3	-0.44823	0.732942	1.31E-06	0.000296
Tnfrsf25	Tumor Necrosis Factor Receptor Superfamily, Member 25	0.95768	1.942184	1.35E-06	0.0003
Egr4	Early Growth Response 4	0.63949	1.557778	1.38E-06	0.000302
Lef1	Lymphoid Enhancer Binding Factor 1	0.458089	1.373721	1.50E-06	0.00032
Btg2	BTG Anti-Proliferation Factor 2	1.382051	2.606387	1.52E-06	0.00032
Arid3b	AT Rich Interactive Domain 3B (BRIGHT-like)	0.561458	1.47576	2.03E-06	0.000417
Fam43b	Family With Sequence Similarity 43, Member B	0.290369	1.222953	2.05E-06	0.000417
Egr2	Early Growth Response 2	1.673105	3.189002	2.20E-06	0.000439
Trib1	Tribbles Pseudokinase 1	0.740566	1.670831	2.28E-06	0.000445
Kdr	Kinase Insert Domain Protein Receptor	0.326421	1.253899	2.30E-06	0.000445
Bend5	BEN Domain Containing 5	-0.45595	0.729028	2.52E-06	0.00048
Fosb	FBJ Osteosarcoma Oncogene B	1.267241	2.407009	2.57E-06	0.000482

Csmd2	CUB and Sushi Multiple Domains 2	0.206249	1.153685	2.61E-06	0.000482
Nr4a1	Nuclear Receptor Subfamily 4, Group A, Member 1	1.066002	2.093624	2.88E-06	0.000523
Dusp1	Dual Specificity Phosphatase 1	1.127955	2.185487	4.00E-06	0.000715
Pnpla2	Patatin-like Phospholipase Domain Containing 2	-0.33662	0.791894	4.14E-06	0.00073
Rcor2	REST Corepressor 2	0.343113	1.268491	4.35E-06	0.000746
Slc7a5	Solute Carrier Family 7 (Cationic Amino Acid Transporter, y+ System), Member 5	-0.27067	0.828934	4.36E-06	0.000746
Prkd2	Protein Kinase D2	0.486165	1.400716	5.09E-06	0.000848
Cep250	Centrosomal Protein 250	0.233906	1.176014	5.10E-06	0.000848
Cttnbp2	Cortactin Binding Protein 2	0.185868	1.137501	5.38E-06	0.000882
Jun	Jun Proto-oncogene	0.360075	1.283493	5.54E-06	0.000895
Pik3r3	Phosphoinositide-3-kinase Regulatory Subunit 3	0.263627	1.200493	5.78E-06	0.000915
Ism1	Isthmin 1, Angiogenesis Inhibitor	-0.48444	0.714773	5.82E-06	0.000915
Ccnd2	Cyclin D2	0.213868	1.159794	5.90E-06	0.000916
Bcorl1	BCL6 Co-repressor-like 1	0.300196	1.231312	6.26E-06	0.000959
Apold1	Apolipoprotein L Domain Containing 1	1.007717	2.010727	7.48E-06	0.001129
Jdp2	Jun Dimerization Protein 2	-0.31719	0.802632	7.56E-06	0.001129
Megf6	Multiple EGF-Like-Domains 6	-0.35927	0.779556	8.06E-06	0.001175
Vegfa	Vascular Endothelial Growth Factor A	0.21432	1.160157	8.07E-06	0.001175
Stk40	Serine/Threonine Kinase 40	0.360383	1.283766	8.24E-06	0.001185
Cckbr	Cholecystokinin B Receptor	0.237827	1.179215	8.39E-06	0.001192
Plk3	Polo Like Kinase 3	0.343196	1.268564	8.75E-06	0.001222
Phf13	PHD Finger Protein 13	0.335958	1.262215	8.81E-06	0.001222
Adamts1	A Disintegrin-like and Metallopeptidase (Reprolysin Type) with Thrombospondin type 1 Motif, 1	0.885896	1.847912	9.07E-06	0.001232
1700016P03Rik	RIKEN cDNA 1700016P03 Gene	1.242018	2.365291	9.12E-06	0.001232

Per1	Period Circadian Clock 1	0.502167	1.41634	9.19E-06	0.001232
C730002L08Rik	RIKEN cDNA C730002L08 gene	-0.48324	0.715369	9.55E-06	0.001266
Tmem267	Transmembrane Protein 267	-0.58507	0.666615	1.07E-05	0.001404
Bhlhe40	Basic helix-loop-helix Family, Member E40	0.574617	1.489282	1.27E-05	0.001646
Nr2e1	Nuclear Receptor Subfamily 2, Group E, Member 1	0.337283	1.263375	1.32E-05	0.001692
Kdm2a	Lysine (K)-Specific Demethylase 2A	0.17597	1.129724	1.35E-05	0.001711
Egr1	Early Growth Response 1	0.611484	1.52783	1.38E-05	0.001722
Lmna	Lamin A	0.249598	1.188876	1.39E-05	0.001722
Dusp6	Dual Specificity Phosphatase 6	0.503357	1.417508	1.43E-05	0.001759
Rilpl2	Rab Interacting Lysosomal Protein-like 2	0.265472	1.202029	1.97E-05	0.002385
Zcchc2	Zinc Finger, CCHC Domain Containing 2	0.222259	1.166559	2.00E-05	0.002385
Zkscan3	Zinc Finger With KRAB and SCAN Domains 3	0.304705	1.235166	2.00E-05	0.002385
Id2	Inhibitor of DNA Binding 2	-0.21729	0.86018	2.12E-05	0.002482
Mecom	MDS1 and EVI1 complex locus	0.457998	1.373634	2.13E-05	0.002482
Cobll1	Cobl-like 1	0.368309	1.290839	2.23E-05	0.002575
Rexo1	REX1, RNA Exonuclease 1	-0.17335	0.886782	2.37E-05	0.002693
Tbc1d2	TBC1 Domain Family, Member 2	0.421753	1.339554	2.37E-05	0.002693
Fam13c	Family With Sequence Similarity 13, Member C	0.251924	1.190794	2.55E-05	0.002867
Dnajb5	DnaJ Heat Shock Protein Family (Hsp40) Member B5	0.316391	1.245212	2.58E-05	0.002872
Skp2	S-Phase Kinase-Associated Protein 2	0.332696	1.259365	2.99E-05	0.003295
Tshz2	Teashirt Zinc Finger Family Member 2	-0.52666	0.694162	3.06E-05	0.003339
Inpp5d	Inositol Polyphosphate-5-Phosphatase D	-0.21967	0.858763	3.40E-05	0.003679
Itpkc	Inositol 1,4,5-Trisphosphate 3-Kinase C	0.384988	1.305849	3.66E-05	0.003893
Dcn	Decorin	-0.44719	0.733471	3.66E-05	0.003893

Aebp1	AE Binding Protein 1	-0.58316	0.667498	4.04E-05	0.00426
Yeats2	YEATS Domain Containing 2	0.193854	1.143815	4.15E-05	0.00433
Ccn1	Cellular Communication Network Factor 1	2.18851	4.558346	4.47E-05	0.004569
Nr4a3	Nuclear Receptor Subfamily 4, Group A, Member 3	0.584327	1.499339	4.49E-05	0.004569
Il10ra	Interleukin 10 Receptor, Alpha	0.512137	1.426161	4.49E-05	0.004569
Traf5	TNF Receptor-Associated Factor 5	0.436124	1.352964	4.78E-05	0.004822
Sox2	SRY (sex determining region Y)-Box 2	0.230785	1.173473	5.02E-05	0.005019
Marchf11	Membrane Associated Ring-CH-type Finger 11	0.435991	1.35284	5.14E-05	0.005094
Ankrd34c	Ankyrin Repeat Domain 34C	-0.37657	0.770268	5.35E-05	0.005261
Ttr	Transthyretin	-1.88269	0.271178	5.62E-05	0.00548
Nes	Nestin	0.421046	1.338898	5.85E-05	0.005661
Stac3	SH3 and Cysteine Rich Domain 3	0.478331	1.393131	6.28E-05	0.006022
Slc22a6	Solute Carrier Family 22 (Organic Anion Transporter), Member 6	-0.4106	0.752313	6.53E-05	0.006213
Maml3	Mastermind Like Transcriptional Coactivator 3	-0.31715	0.802652	6.62E-05	0.006247
Sesn1	Sestrin 1	-0.19632	0.872775	6.87E-05	0.00643
Ier5	Immediate Early Response 5	0.40375	1.322942	7.05E-05	0.006545
Sp2	Sp2 Transcription Factor	-0.31272	0.805122	7.23E-05	0.006647
Zfp579	Zinc Finger Protein 579	0.267168	1.203443	7.27E-05	0.006647
Nrros	Negative Regulator of Reactive Oxygen Species	-0.34139	0.789279	7.40E-05	0.006711
Mbd4	Methyl-CpG Binding Domain Protein 4	0.281835	1.21574	7.54E-05	0.006793
Ace	Angiotensin I Converting Enzyme (Peptidyl-Dipeptidase A) 1	-0.38393	0.766349	7.68E-05	0.00686
Lfng	LFNG O-fucosylpeptide 3-beta-N-acetylglucosaminyltransferase	-0.23635	0.848892	7.89E-05	0.006995
Sema6d	Sema Domain, Transmembrane Domain (TM), and Cytoplasmic Domain, (Semaphorin) 6D	0.203531	1.151513	8.12E-05	0.007148
Smad7	SMAD Family Member 7	0.319506	1.247903	8.30E-05	0.007222

Mxd1	MAX Dimerization Protein 1	0.202215	1.150463	8.33E-05	0.007222
Csrnp1	Cysteine-Serine-Rich Nuclear Protein 1	0.683476	1.606004	8.75E-05	0.007536
Gramd2	GRAM Domain Containing 2	0.261287	1.198547	9.11E-05	0.007734
Erf	Ets2 Repressor Factor	0.205834	1.153353	9.11E-05	0.007734
Fgfr3	Fibroblast Growth Factor Receptor 3	-0.21975	0.858712	9.65E-05	0.008129
Nemp2	Nuclear Envelope Integral Membrane Protein 2	-0.31804	0.802161	0.000103	0.008641
Bmp2k	BMP2 Inducible Kinase	0.281723	1.215646	0.000105	0.008685
Obscn	Obscurin, Cytoskeletal Calmodulin and Titin-Interacting RhoGEF	0.358395	1.281999	0.000106	0.00877
Mir100hg	Mir100 Mirlet7a-2 Mir125b-1 Cluster Host Gene	0.270154	1.205937	0.000111	0.009118
Dusp5	Dual Specificity Phosphatase 5	0.60626	1.522308	0.000113	0.009174
Kcnd3	Potassium Voltage-Gated Channel, Shal-related family, Member 3	-0.19436	0.873963	0.000116	0.009394
Irf2bp2	Interferon Regulatory Factor 2 Binding Protein 2	0.370676	1.292958	0.00012	0.009604
Coq10b	Coenzyme Q10B	0.285458	1.218797	0.000122	0.009706
Btf3l4	Basic Transcription Factor 3-like 4	-0.28627	0.820022	0.000123	0.009706
Stx2	Syntaxin 2	0.193274	1.143356	0.000125	0.009862

Bibliography

[1] I. Scheffer, S. Berkovic, G. Capovilla, M. Connolly, J. French, L. Guilhoto, E. Hirsch, S. Jain, G. Mathern, S. Moshé and D. Nordli, "ILAE classification of the epilepsies: position paper of the ILAE Commission for Classification and Terminology," *Epilepsia,* vol. 58, no. 4, pp. 512-521, 2017.

[2] J. Bowman, F. Dudek and M. Spitz, "Epilepsy," *eLS,* 2001.

[3] S. Moshé, E. Perucca, P. Ryvlin and T. Tomson, "Epilepsy: new advances," *The Lancet,* vol. 385, no. 9971, pp. 884-898, 2015.

[4] C. Espinosa-Jovel, R. Toledano, Á. Aledo-Serrano, I. García-Morales and A. Gil-Nagel, "Epidemiological profile of epilepsy in low income populations," *Seizure,* vol. 56, pp. 67-72, 2018.

[5] R. Thijs, R. Surges, T. O'Brien and J. Sander, "Epilepsy in adults," *The Lancet,* vol. 393, no. 10172, pp. 689-701, 2019.

[6] P. Perucca, M. Bahlo and S. Berkovic, "The genetics of epilepsy," *Annual review of genomics and human genetics,* vol. 21, pp. 205-230, 2020.

[7] I. Helbig and C. Ellis, "Personalized medicine in genetic epilepsies–possibilities, challenges, and new frontiers.," *Neuropharmacology,* vol. 172, p. 107970, 2020.

[8] P. Ferguson, G. Smith, B. Wannamaker, D. Thurman, E. Pickelsimer and A. Selassie, "A population-based study of risk of epilepsy after hospitalization for traumatic brain injury," *Epilepsia,* vol. 51, no. 5, pp. 891-898, 2010.

[9] M. van Breemen, E. Wilms and C. Vecht, "Epilepsy in patients with brain tumours: epidemiology, mechanisms, and management.," *The Lancet Neurology,* vol. 6, no. 5, pp. 421-430, 2007.

[10] K. Howell, K. Katanyuwong, M. Mackay, C. Bailey, I. Scheffer, J. Freeman, S. Berkovic and A. Harvey, "Long-term follow-up of febrile infection–related epilepsy syndrome," *Epilepsia,* vol. 53, no. 1, pp. 101-110, 2012.

[11] R. Fisher, C. Acevedo, A. Arzimanoglou, A. Bogacz, J. Cross, C. Elger, J. Engel Jr, L. Forsgren, J. French, M. Glynn and D. Hesdorffer, " ILAE official report: a practical clinical definition of epilepsy," *Epilepsia,* vol. 55, no. 4, pp. 475-482, 2014.

[12] P. Gloor and R. Fariello, "Generalized epilepsy: some of its cellular mechanisms differ from those of focal epilepsy.," *Trends in neurosciences,* vol. 11, no. 2, pp. 63-68, 1988.

[13] R. Fisher, "The new classification of seizures by the International League Against Epilepsy," *Current neurology and neuroscience reports,* vol. 17, no. 6, pp. 1-6, 2017.

[14] K. Tufenkjian and H. Lüders, “Seizure semiology: its value and limitations in localizing the epileptogenic zone,” *Journal of Clinical Neurology,* vol. 8, no. 4, pp. 243-250, 2012.

[15] D. Englot, “A modern epilepsy surgery treatment algorithm: incorporating traditional and emerging technologies,” *Epilepsy & Behaviour,* vol. 80, pp. 68-74, 2018.

[16] J. Duncan, J. Sander, S. Sisodiya and M. Walker, “Adult epilepsy,” *The Lancet,* vol. 367, no. 9516, pp. 1087-1100, 2006.

[17] G. Sarlo and K. Holton, “Brain concentrations of glutamate and GABA in human epilepsy: A review,” *Seizure,* vol. 91, pp. 213-217, 2021.

[18] B. Meldrum, “Neurotransmission in epilepsy,” *Epilepsia,* vol. 36, pp. 30-35, 1995.

[19] D. Nuytten, J. Van Hees, A. Meulemans and H. Carton, “Magnesium deficiency as a cause of acute intractable seizures,” *Journal of neurology,* vol. 238, no. 5, pp. 262-264, 1991.

[20] P. Nwani, M. Nwosu and M. Nwosu, “Epidemiology of acute symptomatic seizures among adult medical admissions,” *Epilepsy Research and Treatment,* 2016.

[21] S. Hyman, “Neurotransmitters,” *Current biology,* vol. 15, no. 5, pp. R154-R158, 2005.

[22] Z. Farsi, R. Jahn and A. Woehler, “Proton electrochemical gradient: driving and regulating neurotransmitter uptake,” *Bioessays,* vol. 39, no. 5, p. 1600240, 2017.

[23] T. Südhof, “The synaptic vesicle cycle,” *Annual Review of Neuroscience,* vol. 27, pp. 509-547, 2004.

[24] I. Helbig, I. Scheffer, J. Mulley and S. Berkovic, “Navigating the channels and beyond: unravelling the genetics of the epilepsies,” *The Lancet Neurology,* vol. 7, no. 3, pp. 231-245, 2008.

[25] J. Symonds, S. Zuberi, K. Stewart, A. McLellan, M. O ‘Regan, S. MacLeod, A. Jollands, S. Joss, M. Kirkpatrick, A. Brunklaus and D. Pilz, “Incidence and phenotypes of childhood-onset genetic epilepsies: a prospective population-based national cohort,” *Brain,* vol. 142, no. 8, pp. 2303-2318, 2019.

[26] A. Escayg and A. Goldin, “Sodium channel SCN1A and epilepsy: mutations and mechanisms,” *Epilepsia,* vol. 51, no. 9, pp. 1650-1658, 2010.

[27] M. Li, S. Maljevic, A. Phillips, S. Petrovski, M. Hildebrand, R. Burgess, T. Mount, F. Zara, P. Striano, J. Schubert and H. Thiele, “Gain-of-function HCN2 variants in genetic epilepsy,” *Human mutation,* vol. 39, no. 2, pp. 202-209, 2018.

[28] T. Soykan, T. Maritzen and V. Haucke, “Modes and mechanisms of synaptic vesicle recycling,” *Current opinion in neurobiology,* vol. 39, pp. 17-23, 2016.

[29] R. Dhindsa, S. Bradrick, X. Yao, E. Heinzen, S. Petrovski, B. Krueger, M. Johnson, W. Frankel, S. Petrou, R. Boumil and D. Goldstein, “Epileptic encephalopathy-causing mutations in DNM1 impair synaptic vesicle endocytosis,” *Neurology Genetics,* vol. 1, no. 1, 2015.

[30] J. Gonçalves-Ribeiro, C. Pina, A. Sebastião and S. Vaz, “Glutamate Transporters in Hippocampal LTD/LTP: Not Just Prevention of Excitotoxicity,” *Frontiers in Cellular Neuroscience,* vol. 13, p. 357, 2019.

[31] J. Andersen, K. Markussen, E. Jakobsen, A. Schousboe, H. Waagepetersen, P. Rosenberg and B. Aldana, “Glutamate metabolism and recycling at the excitatory synapse in health and neurodegeneration,” *Glutamate metabolism and recycling at the excitatory synapse in health and neurodegeneration,* vol. 196, p. 108719, 2021.

[32] S. Holmseth, Y. Dehnes, Y. Huang, V. Follin-Arbelet, N. Grutle, M. Mylonakou, C. Plachez, Y. Zhou, D. Furness, D. Bergles and K. Lehre, “The density of EAAC1 (EAAT3) glutamate transporters expressed by neurons in the mammalian CNS,” *Journal of Neuroscience,* vol. 32, no. 17, pp. 6000-6013, 2012.

[33] J. Sepkuty, A. Cohen, C. Eccles, A. Rafiq, K. Behar, R. Ganel, D. Coulter and J. Rothstein, “A neuronal glutamate transporter contributes to neurotransmitter GABA synthesis and epilepsy,” *Journal of Neuroscience,* vol. 22, no. 15, pp. 6372-6379, 2002.

[34] C. Ong, E. Damisah, S. Gruenbaum, R. Dhaher, Y. Deng, M. Sandhu, H. Zaveri, D. Spencer and T. Eid, “ Increased branched-chain amino acids at baseline and hours before a spontaneous seizure in the human epileptic brain,” *Epilepsia,* vol. 62, no. 6, pp. e88-e97, 2021.

[35] M. During, “In vivo neurochemistry of the conscious human brain: intrahippocampal microdialysis in epilepsy,” *Techniques in the behavioral and neural sciences,* vol. 7, pp. 425-442, 1991.

[36] R. Guerriero, C. Giza and A. Rotenberg, “Glutamate and GABA imbalance following traumatic brain injury,” *Current neurology and neuroscience reports,* vol. 15, no. 5, pp. 1-11, 2015.

[37] S. Balestrini, A. Arzimanoglou, I. Blümcke, I. Scheffer, S. Wiebe, J. Zelano and M. Walker, “The aetiologies of epilepsy,” *Epileptic Disorders,* vol. 23, no. 1, pp. 1-16, 2021.

[38] A. Suls, S. Mullen, Y. Weber, K. Verhaert, B. Ceulemans, R. Guerrini, T. Wuttke, A. Salvo-Vargas, L. Deprez, L. Claes and A. Jordanova, “Early-onset absence epilepsy caused by mutations in the glucose transporter GLUT1,” *Annals of Neurology: Official Journal of the American Neurological Association and the Child Neurology Society,* vol. 66, no. 3, pp. 415-419, 2009.

[39] D. De Vivo, R. Trifiletti, R. Jacobson, G. Ronen, R. Behmand and S. Harik, “Defective glucose transport across the blood-brain barrier as a cause of persistent hypoglycorrhachia, seizures, and developmental delay,” *New England Journal of Medicine,* vol. 325, no. 10, pp. 703-709, 1991.

[40] M. Petit-Pedrol, T. Armangue, X. Peng, L. Bataller, T. Cellucci, R. Davis, L. McCracken, E. Martinez-Hernandez, W. Mason, M. Kruer and D. Ritacco, “Encephalitis with refractory seizures, status epilepticus, and antibodies to the GABAA receptor: a case series,

characterisation of the antigen, and analysis of the effects of antibodies," *The Lancet Neurology,* vol. 13, no. 3, pp. 276-286, 2014.

[41] W. Xue-Ping, W. Hai-Jiao, Z. Li-Na, D. Xu and L. Ling, "Risk factors for drug-resistant epilepsy: A systematic review and meta-analysis," *Medicine,* vol. 98, no. 30, 2019.

[42] J. Ochoa and W. Kilgo, "The Role of Benzodiazepines in the Treatment of Epilepsy," *Current treatment options in neurology,* vol. 18, no. 4, pp. 1-11, 2016.

[43] B. Miziak, A. Konarzewska, M. Ułamek-Kozioł, M. Dudra-Jastrzębska, R. Pluta and S. Czuczwar, "Anti-Epileptogenic Effects of Antiepileptic Drugs," *International Journal of Molecular Sciences,* vol. 21, no. 7, p. 2340, 2020.

[44] M. McLean and R. Macdonald, "Sodium valproate, but not ethosuximide, produces use- and voltage-dependent limitation of high frequency repetitive firing of action potentials of mouse central neurons in cell culture," *Journal of Pharmacology and Experimental therapeutics,* vol. 237, no. 3, pp. 1001-1011, 1986.

[45] W. Löscher, "Basic Pharmacology of Valproate," *CNS Drugs,* vol. 16, pp. 669-694, 2002.

[46] A. Kudin, G. Debska-Vielhaber, S. Vielhaber, C. Elger and W. Kunz, "The mechanism of neuroprotection by topiramate in an animal model of epilepsy," *Epilepsia,* vol. 45, no. 12, pp. 1478-1487, 2004.

[47] L. Kalilani, X. Sun, B. Pelgrims, M. Noack-Rink and V. Villanueva, "The epidemiology of drug-resistant epilepsy: a systematic review and meta-analysis," *Epilepsia,* vol. 59, no. 12, pp. 2179-2193, 2018.

[48] F. Tang, A. Hartz and B. Bauer, "Drug-Resistant Epilepsy: Multiple Hypotheses, Few Answers," *Frontiers in neurology,* vol. 8, p. 301, 2017.

[49] G. Marshall, A. Gonzalez-Sulser and C. Abbott, "Modelling epilepsy in the mouse: challenges and solutions," *Disease Models & Mechanisms,* vol. 14, no. 3, p. dmm047449, 2021.

[50] P. Willner, "The validity of animal models of depression," *Psychopharmacology,* vol. 83, no. 1, pp. 1-16, 1984.

[51] R. Racine, "Modification of seizure activity by electrical stimulation: II. Motor seizure," *Electroencephalography and clinical neurophysiology,* vol. 32, no. 3, pp. 281-294, 1972.

[52] K. Strohl, L. Gallaugher, A. Lynn, L. Friedman, A. Hill, J. Singer, E. Lander and J. Nadeau, "Sleep-related epilepsy in the A/J mouse," *Sleep,* vol. 30, no. 2, pp. 169-176, 2007.

[53] Q. Tieng, A. Anbazhagan, M. Chen and D. Reutens, "Mouse epileptic seizure detection with multiple EEG features and simple thresholding technique," *Journal of neural engineering,* vol. 14, no. 6, p. 066006, 2017.

[54] R. Bergstrom, J. Choi, A. Manduca, H. Shin, G. Worrell and C. Howe, “Automated identification of multiple seizure-related and interictal epileptiform event types in the EEG of mice.,” *Scientific reports,* vol. 3, no. 1, pp. 1-8, 2013.

[55] T. Singh, A. Mishra and R. Goel, “PTZ kindling model for epileptogenesis, refractory epilepsy, and associated comorbidities: relevance and reliability,” *Metabolic Brain Disease,* vol. 36, no. 7, pp. 1573-1590, 2021.

[56] V. Bouilleret, V. Ridoux, A. Depaulis, C. Marescaux, A. Nehlig and G. La Salle, “Recurrent seizures and hippocampal sclerosis following intrahippocampal kainate injection in adult mice: electroencephalography, histopathology and synaptic reorganization similar to mesial temporal lobe epilepsy,” *Neuroscience,* vol. 89, no. 3, pp. 717-729, 1999.

[57] W. Löscher, “Animal Models of Seizures and Epilepsy: Past, Present, and Future Role for the Discovery of Antiseizure Drugs,” *Neurochemical research,* vol. 42, no. 7, pp. 1873-1888, 2017.

[58] W. Löscher, “Critical review of current animal models of seizures and epilepsy used in the discovery and development of new antiepileptic drugs,” *Seizure,* vol. 20, no. 5, pp. 359-368, 2011.

[59] B. Grone and S. Baraban, “Animal models in epilepsy research: legacies and new directions,” *Nature neuroscience,* vol. 18, no. 3, pp. 339-343, 2015.

[60] R. Waterston and L. Pachter, “Inital sequencing and comparative analysis of the mouse genome,” *Nature,* vol. 420, no. 6915, pp. 520-562, 2002.

[61] A. Strand, A. Aragaki, Z. Baquet, A. Hodges, P. Cunningham, P. Holmans, K. Jones, L. Jones, C. Kooperberg and J. Olson, “Conservation of regional gene expression in mouse and human brain,” *PLoS genetics,* vol. 3, no. 4, p. e59, 2007.

[62] M. Meisler, “SCN8A encephalopathy: mechanisms and models,” *Epilepsia,* vol. 60, pp. S86-S91, 2019.

[63] R. Janz, Y. Goda, M. Geppert, M. Missler and T. Südhof, “SV2A and SV2B function as redundant Ca2+ regulators in neurotransmitter release,” *Neuron,* vol. 4, pp. 1003-1016, 1999.

[64] C. Harper, C. Small, E. Davenport, D. Low, K. Smillie, R. Martínez-Mármol, F. Meunier and M. Cousin, “An epilepsy-associated SV2A mutation disrupts synaptotagmin-1 expression and activity-dependent trafficking,” *Journal of Neuroscience,* vol. 40, no. 23, pp. 4586-4595, 2020.

[65] S. Ganesh, A. Delgado-Escueta, T. Sakamoto, M. Avila, J. Machado-Salas, Y. Hoshii, T. Akagi, H. Gomi, T. Suzuki, K. Amano and K. Agarwala, “Targeted disruption of the Epm2a gene causes formation of Lafora inclusion bodies, neurodegeneration, ataxia, myoclonus epilepsy and impaired behavioral response in mice,” *Human molecular genetics,* vol. 11, no. 11, pp. 1251-1262, 2002.

[66] Harris, J.J., Jolivet, R. & Attwell, D., “Synaptic Energy Use and Supply,” *Neuron,* vol. 75, no. 5, pp. 762-777, 2012.

[67] Mink, J.W., Blumenschine, R.J. & Adams, D.B., “Ratio of central nervous system to body metabolism in vertebrates: its constancy and functional basis,” *American Journal of Physiology-Regulatory, Integrative and Comparative Physiology,* vol. 241, no. 3, pp. 203-212, 1981.

[68] Cobley, J.N., Fiorello, M.L. & Bailey, D.M., “13 reasons why the brain is susceptible to oxidative stress,” *Redox Biology,* vol. 15, pp. 490-503, 2018.

[69] Valko, M., Leibfritz, D., Moncol, J., Cronin, M.T.D., Mazur, M. & Telser, J., “Free radicals and antioxidants in normal physiologcial functions and human disease,” *The International Journal of Biochemistry & Cell Biology,* vol. 39, no. 1, pp. 44-84, 2007.

[70] A. Sabogal-Guáqueta, F. Hobbie, A. Keerthi, A. Oun, A. Kortholt, E. Boddeke and A. Dolga, “Linalool attenuates oxidative stress and mitochondrial dysfunction mediated by glutamate and NMDA toxicity,” *Biomedicine & Pharmacotherapy,* vol. 118, p. 109295, 2019.

[71] M. Morimoto, S. Satomura, T. Hashimoto, E. Ito and S. Kyotani, “Oxidative stress measurement and prediction of epileptic seizure in children and adults with severe motor and intellectual disabilities,” *Journal of Clinical Medicine Research,* vol. 8, no. 6, p. 437, 2016.

[72] M. Gluck, E. Jayatilleke, S. Shaw, A. Rowan and V. Haroutunian, “CNS oxidative stress associated with the kainic acid rodent model of experimental epilepsy,” *CNS oxidative stress associated with the kainic acid rodent model of experimental epilepsy,* vol. 39, no. 1, pp. 63-71, 2000.

[73] M. Patel, B. Day, J. Crapo, I. Fridovich and J. McNamara, “Requirement for superoxide in excitotoxic cell death,” *Neuron,* vol. 16, no. 2, pp. 345-355, 1996.

[74] B. Menon, K. Ramalingam and R. Kumar, “Low plasma antioxidant status in patients with epilepsy and the role of antiepileptic drugs on oxidative stress,” *Annals of Indian Academy of Neurology,* vol. 17, no. 4, p. 398, 2014.

[75] A. Parsons, E. Bucknor, E. Castroflorio, T. Soares, P. Oliver and D. Rial, “The Interconnected Mechanisms of Oxidative Stress and Neuroinflammation in Epilepsy,” *Antioxidants,* vol. 11, no. 1, p. 157, 2022.

[76] S. Marklund, “Human copper-containing superoxide dismutase of high molecular weight,” *Proceedings of the National Academy of Sciences,* vol. 79, no. 24, pp. 7634-7638, 1982.

[77] E. Niki, N. Noguchi, H. Tsuchihashi and N. Gotoh, “Interaction among vitamin C, vitamin E, and beta-carotene,” *The American journal of clinical nutrition,* vol. 62, no. 6, pp. 1322S-1326S, 1995.

[78] J. Masuoka and P. Saltman, “Zinc (II) and copper (II) binding to serum albumin. A comparative study of dog, bovine, and human albumin,” *Journal of Biological Chemistry,* vol. 269, no. 41, pp. 25557-25561, 1994.

[79] R. Eisenstein and K. Blemings, “Iron regulatory proteins, iron responsive elements and iron homeostasis,” *The Journal of nutrition,* vol. 128, no. 12, pp. 2295-2298, 1998.

[80] L. Favreau and C. Pickett, “Transcriptional regulation of the rat NAD(P)H:quinone reductase gene: Identification of regulatory elements controlling basal level expression and inducible expression by planar aromatic compounds and phenolic antioxidants,” *Journal of Biological Chemistry,* vol. 266, no. 7, pp. 4556-4561, 1991.

[81] M. Kwong, Y. Wai Kan and J. Chan, “The CNC Basic Leucine Zipper Factor, Nrf1, Is Essential for Cell Survival in Response to Oxidative Stress-inducing Agents: ROLE FOR Nrf1 IN γ-gcs L AND gssEXPRESSION IN MOUSE FIBROBLASTS,” *Journal of Biological Chemistry,* vol. 274, no. 52, pp. 37491-37498, 1999.

[82] L. Leung, M. Kwong, S. Hou, C. Lee and J. Chan, “Deficiency of the Nrf1 and Nrf2 Transcription Factors Results in Early Embryonic Lethality and Severe Oxidative Stress,” *Journal of Biological Chemistry,* vol. 278, no. 48, pp. 48021-48029, 2003.

[83] J. Johnson, D. Johnson, A. Kraft, M. Calkins, R. Jakel, M. Vargas and P. Chen, “The Nrf2–ARE pathway: an indicator and modulator of oxidative stress in neurodegeneration,” *Annals of the new York Academy of Sciences,* vol. 1147, no. 1, pp. 61-69, 2008.

[84] T. Nguyen, P. Sherratt, P. Nioi, C. Yang and C. Pickett, “Nrf2 Controls Constitutive and Inducible Expression of ARE-driven Genes through a Dynamic Pathway Involving Nucleocytoplasmic Shuttling by Keap1,” *Journal of Biological Chemistry,* vol. 280, no. 37, pp. 32485-32492, 2005.

[85] J. Mehvari, F. Motlagh, M. Najafi, M. Ghazvini, A. Naeini and M. Zare, “Effects of vitamin E on seizure frequency, electroencephalogram findings, and oxidative stress status of refractory epileptic patients,” *Advanced biomedical research,* vol. 5, 2016.

[86] M. Volkert and D. Crowley, “Preventing Neurodegeneration by Controlling Oxidative Stress: The Role of OXR1,” *Frontiers in Neuroscience,* vol. 14, p. 611904, 2020.

[87] Volkert, M.R., Elliott, N.A. and Housman, D.E., “Functional genomics reveals a family of eukaryotic oxidation protection genes,” *PNAS,* vol. 97, no. 26, pp. 14530-14535, 2000.

[88] M. Finelli and P. Oliver, “TLDc proteins: new players in the oxidative stress response and neurological disease,” *Mammalian Genome,* vol. 28, pp. 395-406, 2017.

[89] M. Durand, A. Kolpak, T. Farrell, N. Elliott, W. Shao, M. Brown and M. Volkert, “The OXR domain defines a conserved family of eukaryotic oxidation resistance proteins,” *BMC cell biology,* vol. 8, no. 1, pp. 1-10, 2007.

[90] Doerks, T., Copley, R.R., Schultz, J., Ponting, C.P. and Bork, P., “Systematic Identification of Novel Protein Domain Families Associated with Nuclear Functions,” *Genome Research,* vol. 12, no. 1, pp. 47-56, 2002.

[91] Alsarraf, H.M., Laroche, F., Spaink, H., Thirup, S. and Blaise, M., "Purification, crystallization and preliminary crystallographic studies of the TLDc domain of oxidation resistance protein 2 from zebrafish," *Acta Crystallographica Section F: Structural Biology and Crystallization Communications,* vol. 67, no. 10, pp. 1253-1256, 2011.

[92] Finelli, M.J., Sanchez-Pulido, L., Liu, K.X., Davies, K.E. & Oliver, P.L., "The Evolutionarily Conserved Tre2/Bub2/Cdc16 (TBC), Lysin Motif (LysM), Domain Catalytic (TLDc) Domain Is Neuroprotective against Oxidative Stress," *The Journal of Biological Chemistry,* vol. 291, no. 6, pp. 2751-2765, 2016.

[93] Fukuda, M., "TBC proteins: GAPs for mammalian small GTPase Rab?," *Bioscience Reports,* vol. 31, no. 3, pp. 159-168, 2011.

[94] M. Corbett, M. Bahlo, L. Jolly, Z. Afawi, A. Gardner, K. Oliver, S. Tan, A. Coffey, J. Mulley, L. Dibbens and W. Simri, "A focal epilepsy and intellectual disability syndrome is due to a mutation in TBC1D24," *The American Journal of Human Genetics,* vol. 87, no. 3, pp. 371-375, 2010.

[95] A. Guven and A. Tolun, "TBC1D24 truncating mutation resulting in severe neurodegeneration," *Journal of medical genetics,* vol. 50, no. 3, pp. 199-202, 2013.

[96] M. Milh, A. Falace, N. Villeneuve, N. Vanni, P. Cacciagli, S. Assereto, R. Nabbout, F. Benfenati, F. Zara, B. Chabrol and L. Villard, "Novel compound heterozygous mutations in TBC 1 D 24 cause familial malignant migrating partial seizures of infancy," *Human mutation,* vol. 34, no. 6, pp. 869-872, 2013.

[97] T. Uzunhan and B. Uyanik, "Disrupted oxidative stress resistance: A homozygous mutation in the catalytic (TLDc) domain of TBC1D24 gene associated with epileptic encephalopathy," *Clinical Neurology and Neurosurgery,* vol. 196, p. 106080, 2020.

[98] B. Appavu, N. Guido-Estrada, K. Lindstrom, T. Grebe, J. Kerrigan and M. Troester, "Electroclinical phenotypes and outcomes in TBC1D24 -related epilepsy," *Epileptic Disorders,* vol. 18, no. 3, pp. 324-328, 2016.

[99] Falace, A., Filipello, F., La Padula, V., Vanni, N., Madia, F., Tonelli, D.D.P., de Falco, F.A., Striano, P., Bricarelli, F.D., Minetti, C. & Benfenati, F, "TBC1D24, an ARF6-interacting protein, is mutated in familial infantile myoclonic epilepsy," *The American Journal of Human Genetics,* vol. 87, no. 3, pp. 365-370, 2010.

[100] Mucha, B.E., Hennekam, R.C., Sisodiya, S. & Campeau, P.M., "TBC1D24-related disorders," GeneReviews, University of Washington, Seattle, 2017.

[101] P. Campeau, D. Kasperaviciute, J. Lu, L. Burrage, C. Kim, M. Hori, B. Powell, F. Stewart, T. Félix, J. van den Ende and M. Wisniewska, "The genetic basis of DOORS syndrome: an exome-sequencing study," *The Lancet Neurology,* vol. 13, no. 1, pp. 44-58, 2014.

[102] A. Rehman, R. Santos-Cortez, R. Morell, M. Drummond, T. Ito, K. Lee, A. Khan, M. Basra, N. Wasif, M. Ayub and R. Ali, "Mutations in TBC1D24, a gene associated with epilepsy, also cause nonsyndromic deafness DFNB86.," *The American Journal of Human Genetics,* vol. 94, no. 1, pp. 144-152, 2014.

[103] R. Tona, I. Lopez, C. Fenollar-Ferrer, R. Faridi, C. Anselmi, A. Khan, M. Shahzad, R. Morell, S. Gu, M. Hoa and L. Dong, "Mouse models of human pathogenic variants of TBC1D24 associated with non-syndromic deafness DFNB86 and DFNA65 and syndromes involving deafness," *Genes,* vol. 11, no. 10, p. 1122, 2020.

[104] N. Duru, S. Iseri, N. Selç and A. Tolun, "Early-onset progressive myoclonic epilepsy with dystonia mapping to 16pter-p13. 3," *Journal of neurogenetics,* vol. 24, no. 4, pp. 207-215, 2010.

[105] M. Corbett, M. Bahlo, L. Jolly, Z. Afawi, A. Gardner, K. Oliver, S. Tan, A. Coffey, J. Mulley, L. Dibbens and W. Simri, "A Focal Epilepsy and Intellectual Disability Syndrome Is Due to a Mutation in TBC1D24," *The American Journal of Human Genetics,* vol. 87, no. 3, pp. 371-375, 2010.

[106] Balestrini, S., Milh, M., Castiglioni, C., Lüthy, K., Finelli, M.J., Verstreken, P., Cardon, A., Stražišar, B.G., Holder, J.L., Lesca, G. & Mancardi, M.M., "TBC1D24 genotype-phenotype correlation: Epilepsies and other neurologic features," *Neurology,* vol. 87, no. 1, pp. 77-85, 2016.

[107] V. Uytterhoeven, S. Kuenen, J. Kasprowicz, K. Miskiewicz and P. Verstreken, " Loss of skywalker reveals synaptic endosomes as sorting stations for synaptic vesicle proteins.," *Cell,* vol. 145, no. 1, pp. 117-132, 2011.

[108] A. Fernandes, V. Uytterhoeven, S. Kuenen, Y. Wang, J. Slabbaert, J. Swerts, J. Kasprowicz, S. Aerts and P. Verstreken, "Reduced synaptic vesicle protein degradation at lysosomes curbs TBC1D24/sky-induced neurodegeneration," *Journal of Cell Biology,* vol. 207, no. 4, pp. 453-462, 2014.

[109] Fischer, B., Lüthy, K., Paesmans, J., De Koninck, C., Maes, I., Swerts, J., Kuenen, S., Uytterhoeven, V., Verstreken, P. & Versées, W., "Skywalker-TBC1D24 has a lipid-binding pocket mutated in epilepsy and required for synaptic function," *Nature Structural and Molecular Biology,* vol. 23, no. 11, pp. 965-973, 2016.

[110] Stowers, R.S., Russell, S. and Garza, D., "The 82F Late Puff Contains the L82 Gene, an Essential Member of a Novel Gene Family," *Developmental Biology,* vol. 213, pp. 116-130, 1999.

[111] H. Fischer, X. Zhang, K. O'Brien, P. Kylsten and E. Engvall, "C7, a novel nucleolar protein, is the mouse homologue of the Drosophila late puff product L82 and an isoform of human OXR1," *Biochemical and biophysical research communications,* vol. 281, no. 3, pp. 795-803, 2001.

[112] Elliott, N.A. and Volkert, M.R., "Stress Induction and Mitochondrial Localization of OXR1 Proteins in Yeast and Humans," *Molecular and Cellular Biology,* vol. 24, no. 8, pp. 3180-3187, 2004.

[113] P. Oliver, M. Finelli, B. Edwards, E. Bitoun, D. Butts, E. Becker, M. Cheeseman, B. Davies and K. Davies, "Oxr1 is essential for protecton against oxidative stress-induced neurodegeneration," *PLoS Genetics,* vol. 7, no. 10, p. e1002338, 2011.

[114] J. Wang, J. Rousseau, E. Kim, S. Ehresmann, Y. Cheng, L. Duraine, Z. Zuo, Y. Park, D. Li-Kroeger, W. Bi and L. Wong, " Loss of oxidation resistance 1, OXR1, is associated with an autosomal-recessive neurological disease with cerebellar atrophy and lysosomal dysfunction," *American Journal of Human Genetics,* vol. 105, no. 6, pp. 1237-1253, 2019.

[115] X. Lin, W. Wang, M. Yang, N. Damseh, M. de Sousa, F. Jacob, A. Lang, E. Kristiansen, M. Pannone, M. Kissova and R. Almaas, "Loss-of-function mutation in human Oxidation Resistance gene 1 disrupts the spatial-temporal regulation of histone arginine methylation in early brain development.," *bioRxiv,* 2022.

[116] Dickinson, M.E. et al., "High-throughput discovery of novel developmental phenotypes," *Nature,* vol. 537, no. 7621, pp. 508-514, 2016.

[117] X. Chen, R. Reader, A. Hoischen, J. Veltman, N. Simpson, C. Francks, D. Newbury and S. Fisher, "Next-generation DNA sequencing identifies novel gene variants and pathways involved in specific language impairment.," *Scientific reports,* vol. 7, no. 1, pp. 1-17, 2017.

[118] X. Wang, A. Zaidi, R. Pal, A. Garrett, R. Braceras, X. Chen, M. Michaelis and E. Michaelis, "Genomic and biochemical approaches in the discovery of mechanisms for selective neuronal vulnerability to oxidative stress," *BMC Neuroscience,* vol. 10, no. 1, pp. 1-20, 2009.

[119] N. Li, X. Pan, J. Zhang, A. Ma, S. Yang, J. Ma and A. Xie, "Plasma levels of miR-137 and miR-124 are associated with Parkinson's disease but not with Parkinson's disease with depression," *Neurological sciences,* vol. 38, no. 5, pp. 761-767, 2017.

[120] M. Yang, L. Luna, J. Sørbø, I. Alseth, R. Johansen, P. Backe, N. Danbolt, L. Eide and M. Bjørås, "Human OXR1 maintains mitochondrial DNA integrity and counteracts hydrogen peroxide-induced oxidative stress by regulating antioxidant pathways involving p21," *Free Radical Biology and Medicine,* vol. 77, pp. 41-48, 2014.

[121] Finelli, M.J., Liu, K.X., Wu, Y., Oliver, P.L. and Davies, K.E., "Oxr1 improves pathogenic cellular features of ALS-associated FUS and TDP-43 mutations," *Human Molecular Genetics,* vol. 24, no. 12, pp. 3529-3544, 2015.

[122] Liu, K.X., Edwards, B., Lee, S., Finelle, M.J., Davies, B., Davies, K.E. & Oliver, P.L., "Neuron-specific antioxidant OXR1 extends survival of a mouse model of amyotrophic lateral sclerosis," *Brain,* vol. 138, pp. 1167-1181, 2015.

[123] J. Mianné, G. Codner, A. Caulder, R. Fell, M. Hutchison, R. King, M. Stewart, S. Wells and L. Teboul, "Analysing the outcome of CRISPR-aided genome editing in embryos: Screening, genotyping and quality control," *Methods,* vol. 121, pp. 68-76, 2017.

[124] M. Haeussler, K. Schönig, H. Eckert, A. Eschstruth, J. Mianné, J. Renaud, S. Schneider-Maunoury, A. Shkumatava, L. Teboul, J. Kent and J. Joly, "Evaluation of off-target and on-target scoring algorithms and integration into the guide RNA selection tool CRISPOR," *Genome biology,* vol. 17, no. 1, pp. 1-12, 2016.

[125] K. Liu, B. Edwards, S. Lee, M. FinellI, B. Davies, K. Davies and P. Oliver, “Neuron-specific antioxidant OXR1 extends survival of a mouse model of amyotrophic lateral sclerosis,” *Brain,* vol. 138, pp. 1167-1181, 2015.

[126] L. Hobson, R. Bains, S. Greenaway, S. Wells and P. Nolan, “Phenotyping in Mice Using Continuous Home Cage Monitoring and Ultrasonic Vocalization Recordings,” *Current Protocols in Mouse Biology,* vol. 10, no. 3, p. e80, 2020.

[127] D. Barto, C. Bird, D. Hamilton and B. Fink, “The Simple Video Coder: A free tool for efficicently coding social video data,” *Behaviour Research Methods,* vol. 49, no. 4, pp. 1563-1568, 2017.

[128] R. Kurapati, C. McKenna, J. Lindqvist, D. Williams, M. Simon, E. LeProust, J. Baker, M. Cheeseman, N. Carroll, P. Denny and S. Laval, “Myofibrillar myopathy caused by a mutation in the motor domain of mouse MyHC IIb,” *Human molecular genetics,* vol. 21, no. 8, pp. 1706-1724, 2012.

[129] S. Amend, K. Valkenburg and K. Pienta, “Murine hind limb long bone dissection and bone marrow isolation.,” *Journal of Visualized Experiments,* vol. 110, p. e53936, 2016.

[130] B. Schuck, R. MacArthur and J. Inglese, “Quantitative High-Throughput Screening Using a Coincidence Reporter Biocircuit,” *Current Protocols in Neuroscience,* vol. 79, no. 1, pp. 5-32, 2017.

[131] A. Guven and A. Tolun, “TBC1D24 truncating mutation resulting in severe neurodegeneration,” *Phenotypes,* vol. 50, no. 3, pp. 199-202, 2013.

[132] B. Mucha, R. Hennekam, S. Sisodiya and P. Campeau, TBC1D24-related disorders, 2017.

[133] K. Lüthy, D. Mei, B. Fischer, M. De Fusco, J. Swerts, J. Paesmans, E. Parrini, N. Lubarr, I. Meijer, K. Mackenzie and W. Lee, “TBC1D24-TLDc-related epilepsy exercise-induced dystonia: rescue by antioxidants in a disease model,” *Brain,* vol. 142, no. 8, pp. 2319-2335, 2019.

[134] U. Pandey and C. Nichols, “Human disease models in Drosophila melanogaster and the role of the fly in therapeutic drug discovery,” *Pharmacological reviews,* vol. 63, no. 2, pp. 411-436, 2011.

[135] D. Aprile, F. Fruscione, S. Baldassari, M. Fadda, D. Ferrante, A. Falace, E. Buhler, J. Sartorelli, A. Represa, P. Baldelli and F. Benfenati, “TBC1D24 regulates axonal outgrowth and membrane trafficking at the growth cone in rodent and human neurons,” *Cell Death & Differentiation,* vol. 26, no. 11, pp. 2464-2478, 2019.

[136] Finelli, M.J., Aprile, D., Castroflorio, E., Jeans, A., Moschetta, M., Chessum, L., Degiacomi, M.T., Grasegger, J., Lupien-Meilleur, A., Bassett, A. & Rossignol, E., “ The epilepsy-associated protein TBC1D24 is required for normal development, survival and vesicle trafficking in mammalian neurons,” *Human molecular genetics,* 2018.

[137] L. Lin, Q. Lyu, P. Kwan, J. Zhao, R. Fan, A. Chai, C. Lai, Y. Chan, X. Shen and K. Lai, “The epilepsy and intellectual disability-associated protein TBC1D24 regulates the maintenance

of excitatory synapses and animal behaviors," *PLoS genetics,* vol. 16, no. 1, p. e1008587, 2020.

[138] A. Falace, E. Buhler, M. Fadda, F. Watrin, P. Lippiello, E. Pallesi-Pocachard, P. Baldelli, F. Benfenati, F. Zara, A. Represa and A. Fassio, "TBC1D24 regulates neuronal migration and maturation through modulation of the ARF6-dependent pathway," *PNAS,* vol. 111, no. 6, pp. 2337-2342, 2014.

[139] B. Brant, T. Stern, H. Shekhidem, L. Mizrahi, I. Rosh, Y. Stern, P. Ofer, A. Asleh, G. Umanah, R. Jada and N. Levy, "IQSEC2 mutation associated with epilepsy, intellectual disability, and autism results in hyperexcitability of patient-derived neurons and deficient synaptic transmission.," *Molecular psychiatry,* vol. 26, no. 12, pp. 7498-7508, 2021.

[140] M. Jackson, K. Loring, C. Homan, M. Thai, L. Määttänen, M. Arvio, I. Jarvela, M. Shaw, A. Gardner, J. Gecz and C. Shoubridge, "Heterozygous loss of function of IQSEC2/Iqsec2 leads to increased activated Arf6 and severe neurocognitive seizure phenotype in females," *Life science alliance,* vol. 2, no. 4, 2019.

[141] Nucleic Acids Research, "UniProt: the universal protein knowledgebase in 2021," *Nucleic acids research,* vol. 49, no. D1, pp. D480-D489, 2021.

[142] Muona, M., Berkovic, S.F., Dibbens, L.M., Oliver, K.L., Maljevic, S., Bayly, M.A., Joensuu, T., Canafoglia, L., Franceschetti, S., Michelucci, R. & Markkinen, S, "A recurrent de novo mutation in KCNC1 causes progressive myoclonus epilepsy," *Nature genetics,* vol. 47, no. 1, p. 39, 2015.

[143] P. Oliver, M. Finelli, B. Edwards, E. Bitoun, D. Butts, E. Becker, M. Cheeseman, B. Davies and K. Davies, "Oxr1 is essential for protection against oxidative stress-induced neurodegeneration," *PLoS genetics,* vol. 7, no. 10, p. e1002338, 2011.

[144] E. Banuelos, K. Ramsey, N. Belnap, M. Krishnan, C. Balak, S. Szelinger, A. Siniard, M. Russell, R. Richholt, M. De Both and I. Piras, "Case Report: Novel mutations in TBC1D24 are associated with autosomal dominant tonic-clonic and myoclonic epilepsy and recessive Parkinsonism, psychosis, and intellectual disability," *F1000Research,* vol. 6, 2017.

[145] T. O'Leary, H. Mantolino, K. Stover and R. Brown, "Age-related deterioration of motor function in male and female 5xFAD mice from 3 to 16 months of age," *Genes, Brain and Behavior,* vol. 19, no. 3, p. e12538, 2020.

[146] D. Avgustinovich, T. Lipina, N. Bondar, O. Alekseyenko and N. Kudryavtseva, "Features of the genetically defined anxiety in mice," *Behavior Genetics,* vol. 30, no. 2, pp. 101-109, 2000.

[147] M. Finelli, L. Sanchez-Pulido, K. Liu, K. Davies and P. Oliver, "The evolutionarily conserved Tre2/Bub2/Cdc16 (TBC), lysin motif (LysM), domain catalytic (TLDc) domain is neuroprotective against oxidative stress," *Journal of Biological Chemistry,* vol. 291, no. 6, pp. 2751-2763, 2016.

[148] D. Wu, F. Chang, D. Peng, S. Xie, X. Li and W. Zheng, “The morphological characteristics of hippocampus and thalamus in mesial temporal lobe epilepsy.,” *BMC Neurology,* vol. 20, no. 1, pp. 1-9, 2020.

[149] K. Powell, H. Tang, C. Ng, I. Guillemain, G. Dieuset, G. Dezsi, N. Çarçak, F. Onat, B. Martin, T. O'Brien and A. Depaulis, “Seizure expression, behavior, and brain morphology differences in colonies of Genetic Absence Epilepsy Rats from Strasbourg,” *Epilepsia,* vol. 55, no. 12, pp. 1959-1968, 2014.

[150] J. Wang, J. Rousseau, E. Kim, S. Ehresmann, Y. Cheng, L. Duraine, Z. Zuo, Y. Park, D. Li-Kroeger, W. Bi and L. Wong, “Loss of oxidation resistance 1, OXR1, is associated with an autosomal-recessive neurological disease with cerebellar atrophy and lysosomal dysfunction,” *The American Journal of Human Genetics,* vol. 105, no. 6, pp. 1237-1253, 2019.

[151] J. Marques-Carneiro, A. Nehlig, J. Cassel, E. Castro-Neto, J. Litzahn, A. Pereira de Vasconcelos, M. Naffah-Mazacoratti and M. Fernandes, “Neurochemical Changes and c-Fos Mapping in the Brain after Carisbamate Treatment of Rats Subjected to Lithium–Pilocarpine-Induced Status Epilepticus,” *Pharmaceuticals,* vol. 10, no. 4, p. 85, 2017.

[152] H. Yang, W. Shan, F. Zhu, T. Yu, J. Fan, A. Guo, F. Li, X. Yang and Q. Wang, “C-Fos mapping and EEG characteristics of multiple mice brain regions in pentylenetetrazol-induced seizure mice model,” *Neurological Research,* vol. 41, no. 8, pp. 749-761, 2019.

[153] S. Piredda and K. Gale, “A crucial epileptogenic site in the deep prepiriform cortex,” *Nature,* vol. 317, no. 6038, pp. 623-625, 1985.

[154] M. Galovic, I. Baudracco, E. Wright-Goff, G. Pillajo, P. Nachev, B. Wandschneider, F. Woermann, P. Thompson, S. Baxendale, A. McEvoy and M. Nowell, “Association of Piriform Cortex Resection With Surgical Outcomes in Patients With Temporal Lobe Epilepsy,” *JAMA Neurology,* vol. 76, no. 6, pp. 690-700, 2019.

[155] D. N. Vaughan and G. D. Jackson, “The piriform cortex and human focal epilepsy,” *Frontiers in neurology,* vol. 5, p. 259, 2014.

[156] A. Eaton, M. Merkulova and D. Brown, “The H+-ATPase (V-ATPase): from proton pump to signaling complex in health and disease,” *American Journal of Physiology-Cell Physiology,* vol. 320, no. 3, pp. C392-C414, 2021.

[157] A. Fassio, A. Esposito, M. Kato, H. Saitsu, D. Mei, C. Marini, V. Conti, M. Nakashima, N. Okamoto, A. Olmez Turker and B. Albuz, “De novo mutations of the ATP6V1A gene cause developmental encephalopathy with epilepsy,” *Brain,* vol. 141, no. 6, pp. 1703-1718, 2018.

[158] R. Guerrini, D. Mei, K. Kerti-Szigeti, S. Pepe, M. Koenig, G. Von Allmen, M. Cho, K. McDonald, J. Baker, V. Bhambhani and Z. Powis, “Phenotypic and genetic spectrum of ATP6V1A encephalopathy: a disorder of lysosomal homeostasis,” *Brain,* 2022.

[159] L. Bott, M. Forouhan, M. Lieto, A. Sala, R. Ellerington, J. Johnson, A. Speciale, C. Criscuolo, A. Filla, D. Chitayat and E. Alkhunaizi, “Variants in ATP6V0A1 cause progressive myoclonus

epilepsy and developmental and epileptic encephalopathy," *Brain Communications,* vol. 3, no. 4, p. fcab245, 2021.

[160] K. Aoto, M. Kato, T. Akita, M. Nakashima, H. Mutoh, N. Akasaka, J. Tohyama, Y. Nomura, K. Hoshino, Y. Ago and R. Tanaka, "ATP6V0A1 encoding the a1-subunit of the V0 domain of vacuolar H+-ATPases is essential for brain development in humans and mice," *Nature communications,* vol. 12, no. 1, pp. 1-17, 2021.

[161] Y. Tian, Q. Zhai, X. Li, Z. Shi, C. Cheng, C. Fan, B. Tang, Y. Zhang, Y. He, W. Li and S. Luo, "ATP6V0C Is Associated With Febrile Seizures and Epilepsy With Febrile Seizures Plus," *Frontiers in Molecular Neuroscience,* p. 206, 2022.

[162] I. Menendez, C. Carranza, M. Herrera, N. Marroquin, I. Joseph Foster, F. Cengiz, G. Bademci and M. Tekin, "Dominant deafness–onychodystrophy syndrome caused by an ATP6V1B2 mutation," *Clinical case reports,* vol. 5, no. 4, p. 376, 2017.

[163] E. Beauregard-Lacroix, G. Pacheco-Cuellar, N. Ajeawung, J. Tardif, K. Dieterich, T. Dabir, D. Vind-Kezunovic, S. White, D. Zadori, C. Castiglioni and L. Tranebjærg, "DOORS syndrome and a recurrent truncating ATP6V1B2 variant," *Genetics in medicine,* vol. 23, no. 1, pp. 149-154, 2021.

[164] B. Mucha, S. Banka, N. Ajeawung, S. Molidperee, G. Chen, M. Koenig, R. Adejumo, M. Till, M. Harbord, R. Perrier and E. Lemyre, "A new microdeletion syndrome involving TBC1D24, ATP6V0C, and PDPK1 causes epilepsy, microcephaly, and developmental delay.," *Genetics in Medicine,* vol. 21, no. 5, pp. 1058-1064, 2019.

[165] Y. Kuroda, Y. U. T. Kimura, K. Kosaki and K. Kurosawa, "Refinement of 16p13. 3 microdeletion syndrome from a case presentation of a girl with epilepsy and intellectual disability," *Congenital Abnormalities,* vol. 60, no. 2, pp. 75-77, 2020.

[166] Y. Shi, P. Kirwan, J. Smith, H. Robinson and F. Livesey, "Human cerebral cortex development from pluripotent stem cells to functional excitatory synapses," *Nature neuroscience,* vol. 15, no. 3, pp. 477-486, 2012.

[167] J. Yoon, Y. L. M. Hwang, J. Sun, H. Cho, L. Knaik and I. Daar, "TBC1d24-ephrinB2 interaction regulates contact inhibition of locomotion in neural crest cell migration," *Nature communications,* vol. 9, no. 1, pp. 1-14, 2018.

[168] J. Calhoun, N. Hawkins, N. Zachwieja and J. Kearney, "Cacna1g is a genetic modifier of epilepsy caused by mutation of voltage-gated sodium channel Scn2a," *Epilepsia,* vol. 57, no. 6, pp. e103-e107, 2016.

[169] R. Tona, W. Chen, Y. Nakano, L. Reyes, R. Petralia, Y. Wang, M. Starost, T. Wafa, R. Morell, K. Cravedi, J. du Hoffmann, T. Miyoshi, J. Munasinghe, T. Fitzgerald, Y. Chudasama, K. Omori, et al and T. Friedman, "The phenotypic landscape of a Tbc1d24 mutant mouse includes convulsive seizures resembling human early infantile epileptic encephalopathy.," *Human molecular genetics,* vol. 28, no. 9, pp. 1530-1547, 2019.

[170] R. Tona, I. Lopez, C. Fenollar-Ferrer, R. Faridi, C. Anselmi, A. Khan, M. Shahzad, R. Morell, S. Gu, M. Hoa and L. Dong, "Mouse models of human pathogenic variants of TBC1D24

associated with non-syndromic deafness DFNB86 and DFNA65 and syndromes involving deafness," *Genes,* vol. 11, no. 10, p. 1122, 2020.

[171] B. Semple, K. Blomgren, K. Gimlin, D. Ferriero and L. Noble-Haeusslein, "Brain development in rodents and humans: Identifying benchmarks of maturation and vulnerability to injury across species," *Progress in neurobiology,* vol. 106, pp. 1-16, 2013.

[172] R. Lozano, K. Herman, M. Rothfuss, H. Rieger, P. Bayrak-Toydemir, D. Aprile, F. Fruscione, F. Zara and A. Fassio, "Clinical intrafamilial variability in lethal familial neonatal seizure disorder caused by TBC1D24 mutations," *American Journal of Medical Genetics Part A,* vol. 170, no. 12, pp. 3207-3214, 2016.

[173] M. Arnaud-Arnould, M. Tauziet, O. Moncorgé, C. Goujon and M. Blaise, "Crystal structure of the TLDc domain of human NCOA7-AS," *Acta Crystallographica Section F: Structural Biology Communications,* vol. 77, no. 8, 2021.

[174] A. &. K. Y. Ciechanover, "Degradation of misfolded proteins in neurodegenerative diseases: therapeutic targets and strategies," *Experimental & Molecular Medicine,* vol. 47, p. e147, 2015.

[175] G. Kleiger and T. Mayor, "Perilous journey: a tour of the ubiquitin–proteasome system," *Trends in Cell Biology,* vol. 24, no. 6, pp. 352-359, 2014.

[176] T. &. K. D. Yorimutsu, "Autophagy: molecular machinery for self-eating," *Cell Death & Differentiation,* vol. 12, pp. 1542-1552, 2005.

[177] M. Lee, J. Lee and D. Rubinsztein, "Tau degradation: The ubiquitin–proteasome system versus the autophagy-lysosome system," *Progress in Neurobiology,* vol. 105, pp. 49-59, 2013.

[178] X. Lin, W. Wang, M. Yang, N. Damseh, M. de Sousa, F. Jacob, A. Lang, E. Kristiansen, M. Pannone, M. Kissova and R. Almaas, "Loss-of-function mutation in human Oxidation Resistance gene 1 disrupts the spatial-temporal regulation of histone arginine methylation in early brain development," *bioRxiv,* 2022.

[179] M. McMackin, C. Henderson and G. Cortopassi, "Neurobehavioral deficits in the KIKO mouse model of Friedreich's ataxia.," *Behavioural brain research,* vol. 316, pp. 183-188, 2017.

[180] Z. Afawi, S. Mandelstam, A. Korczyn, S. Kivity, S. Walid, A. Shalata, K. Oliver, M. Corbett, J. Gecz, S. Berkovic and G. Jackson, "TBC1D24 mutation associated with focal epilepsy, cognitive impairment and a distinctive cerebro-cerebellar malformation," *Epilepsy research,* vol. 105, no. 1-2, pp. 240-244, 2013.

[181] T. Chae, Y. Kwon, R. Bronson, P. Dikkes, E. Li and L. Tsai, "Mice Lacking p35, a Neuronal Specific Activator of Cdk5, Display Cortical Lamination Defects, Seizures, and Adult Lethality," *Neuron,* vol. 18, no. 1, pp. 29-42, 1997.

[182] R. Li, C. Hu, L. Wang, D. Liu, D. Liu, W. Liao, B. Xiao, H. Chen and L. Feng, "Disruption of functional connectivity among subcortical arousal system and cortical networks in temporal lobe epilepsy," *Brain Imaging and Behaviour,* vol. 14, no. 3, pp. 762-771, 2020.

[183] N. Zhang, M. Hou, S. Ma, Y. Liu, W. Wei and Z. Chen, "Novel variants in TBC1D24 associated with epilepsy and deafness: Report of two cases," *International Journal of Developmental Neuroscience,* vol. 81, no. 1, pp. 98-105, 2021.

[184] S. Vavassori and A. Mayer, "A new life for an old pump: V-ATPase and neurotransmitter release," *Journal of Cell Biology,* vol. 205, no. 1, pp. 7-9, 2014.

[185] Q. Song, B. Meng, H. Xu and Z. Mao, "The emerging roles of vacuolar-type ATPase-dependent Lysosomal acidification in neurodegenerative diseases.," *Tranlsational Neurodegeneration,* vol. 9, no. 1, pp. 1-14, 2020.

[186] A. Eaton, D. Brown and M. Merkulova, "The evolutionary conserved TLDc domain defines a new class of (H+) V-ATPase interacting proteins," *Scientific reports,* vol. 11, no. 1, pp. 1-15, 2021.

[187] E. Castroflorio, J. Den Hoed, D. Svistunova, M. Finelli, A. Cebrian-Serrano, S. Corrochano, A. Bassett, B. Davies and P. Oliver, "The Ncoa7 locus regulates V-ATPase formation and function, neurodevelopment and behaviour.," *Cellular and molecular life sciences,* vol. 78, no. 7, pp. 3503-3524, 2021.

[188] S. Banerjee, K. Clapp, M. Tarsio and P. Kane, "Interaction of the late endo-lysosomal lipid PI(3,5)P2 with the Vph1 isoform of yeast V-ATPase increases its activity and cellular stress tolerance," *Journal of Biological Chemistry,* vol. 294, no. 23, pp. 9161-9171, 2019.

[189] S. Li, T. Diakov, T. Xu, M. Tarsio, W. Zhu, S. Couoh-Cardel, L. Weisman and P. Kane, "The signaling lipid PI(3,5)P2 stabilizes V1–Vo sector interactions and activates the V-ATPase," *Molecular biology of the cell,* vol. 25, no. 8, pp. 1251-1262, 2014.

[190] D. Coulter and T. Eid, "Astrocytic regulation of glutamate homeostasis in epilepsy," *Glia,* vol. 60, no. 8, pp. 1215-1226, 2012.

[191] E. Benarroch, "Glutamate transporters: diversity, function, and involvement in neurologic disease," *Neurology,* vol. 74, no. 3, pp. 259-264, 2010.

[192] Y. Wang and E. Floor, "Hydrogen peroxide inhibits the vacuolar H+-ATPase in brain synaptic vesicles at micromolar concentrations," *Journal of neurochemistry,* vol. 70, no. 2, pp. 646-652, 1998.

[193] T. Vos, C. Allen, M. Arora, R. Barber, Z. Bhutta, A. Brown, A. Carter, D. Casey, F. Charlson, A. Chen and M. Coggeshall, "Global, regional, and national incidence, prevalence, and years lived with disability for 310 diseases and injuries, 1990–2015: a systematic analysis for the Global Burden of Disease Study 2015," *The Lancet,* vol. 388, no. 10053, pp. 1545-1602, 2015.

[194] A. Lopez, P. Cacoub, I. Macdougall and L. Peyrin-Biroulet, "Iron deficiency anaemia," *The Lancet,* vol. 387, no. 110021, pp. 907-916, 2016.

[195] C. Camaschella, “Iron-Deficiency Anemia,” *New England journal of medicine,* vol. 372, no. 19, pp. 1832-1843, 2015.

[196] R. Brodsky and R. Jones, “Aplastic Anaemia,” *The Lancet,* vol. 365, no. 9471, pp. 1647-1656, 2005.

[197] M. D. Cappellini and G. Fiorelli, “Glucose-6-phosphate dehydrogenase deficiency,” *The Lancet,* vol. 371, no. 9606, pp. 64-74, 2008.

[198] Q. Hill, R. Stamps, E. Massey, J. Grainger, D. Provan and A. Hill, “The diagnosis and management of primary autoimmune haemolytic anaemia,” *British journal of haematology,* vol. 176, no. 3, pp. 395-411, 2017.

[199] A. Piccin, C. Murphy, E. Eakins, M. Rondinelli, M. Daves, C. Vecchiato, D. Wolf, C. Mc Mahon and O. Smith, “Insight into the complex pathophysiology of sickle cell anaemia and possible treatment,” *European journal of haematology,* vol. 102, no. 4, pp. 319-330, 2019.

[200] S. Pasricha, K. Colman, E. Centeno-Tablante, M. Garcia-Casal and J. Peña-Rosas, “Revisiting WHO haemoglobin thresholds to define anaemia in clinical medicine and public health.,” *The Lancet Haematology,* vol. 5, no. 2, pp. e60-e62, 2018.

[201] V. Sankaran, J. Xu and S. Orkin, “Advances in the understanding of haemoglobin switching,” *British journal of haematology,* vol. 149, no. 2, pp. 181-194, 2010.

[202] J. Chung, C. Chen and B. Paw, “Heme metabolism and erythropoiesis,” *Current opinion in hematology,* vol. 19, no. 3, p. 156, 2012.

[203] X. Yin and H. Dailey, “Erythroid 5-aminolevulinate synthase is required for erythroid differentiation in mouse embryonic stem cells,” *Blood Cells, Molecules, and Diseases,* vol. 24, no. 1, pp. 41-53, 1998.

[204] R. Doty, S. Phelps, C. Shadle, M. Sanchez-Bonilla, S. Keel and J. Abkowitz, “Coordinate expression of heme and globin is essential for effective erythropoiesis,” *The Journal of clinical investigation,* vol. 125, no. 12, pp. 4681-4691, 2015.

[205] Z. Yang, S. Keel, A. Shimamura, L. Liu, A. Gerds, H. Li, B. Wood, B. Scott and J. Abkowitz, “Delayed globin synthesis leads to excess heme and the macrocytic anemia of Diamond Blackfan anemia and del (5q) myelodysplastic syndrome,” *Science translational medicine,* vol. 8, no. 338, pp. 338ra67-338ra67, 2016.

[206] A. Bank, “Understanding globin regulation in β-thalassemia: it’s as simple as α, β, γ, δ,” *The Journal of Clinical Investigation,* vol. 115, no. 6, pp. 1470-1473, 2005.

[207] E. Nagababu, S. Gulyani, C. Earley, R. Cutler, M. Mattson and J. Rifkind, “Iron-deficiency anaemia enhances red blood cell oxidative stress,” *Free radical research,* vol. 42, no. 9, pp. 824-829, 2008.

[208] R. Cellerino, G. Guidi and G. Perona, “Plasma iron and erythrocytic glutathione peroxidase activity: a possible mechanism for oxidative haemolysis in iron deficiency anaemia.,” *Scandinavian Journal of Haematology,* vol. 17, no. 2, pp. 111-116, 1976.

[209] G. Bagby, “Recent advances in understanding hematopoiesis in Fanconi Anemia,” *F1000 Research,* vol. 7, no. 105, 2018.

[210] S. Chen, Y. Su and J. Wang, “ROS-mediated platelet generation: a microenvironment-dependent manner for megakaryocyte proliferation, differentiation, and maturation,” *Cell death & disease,* vol. 4, no. 7, p. e722, 2013.

[211] A. Cozzi, B. Corsi, S. Levi, P. Santambrogio, G. Biasiotto and P. Arosio, “Analysis of the biologic functions of H-and L-ferritins in HeLa cells by transfection with siRNAs and cDNAs: evidence for a proliferative role of L-ferritin,” *Blood,* vol. 103, no. 6, pp. 2377-2383, 2004.

[212] P. L. S. Arosio, “Cytosolic and mitochondrial ferritins in the regulation of cellular iron homeostasis and oxidative damage,” *Biochimica et Biophysica Acta (BBA),* vol. 1800, no. 8, pp. 783-792, 2010.

[213] C. Wang and J. Babitt, “Liver iron sensing and body iron homeostasis,” *Blood, The Journal of the American Society of Hematology,* vol. 133, no. 1, pp. 18-29, 2019.

[214] M. Muckenthaler, S. Rivella, M. Hentze and B. Galy, “ A red carpet for iron metabolism,” *Cell,* vol. 168, no. 3, pp. 344-361, 2017.

[215] H. Gunshin, B. Mackenzie, U. Berger, Y. Gunshin, M. Romero, W. Boron, S. Nussberger, J. Gollan and M. Hediger, “Cloning and characterization of a mammalian proton-coupled metal-ion transporter,” *Nature,* vol. 388, no. 6641, pp. 482-488, 1997.

[216] H. Drakesmith, E. Nemeth and T. Ganz, “Ironing out ferroportin,” *Cell metabolism,* vol. 22, no. 5, pp. 777-787, 2015.

[217] B. Mackenzie, M. Ujwal, M. Chang, M. Romero and M. Hediger, “Divalent metal-ion transporter DMT1 mediates both H+-coupled Fe2+ transport and uncoupled fluxes.,” *Pflügers Archiv,* vol. 451, no. 4, pp. 544-558, 2006.

[218] A. Hamdi, T. Roshan, T. Kahawita, A. Mason, A. Sheftel and P. Ponka, “Erythroid cell mitochondria receive endosomal iron by a “kiss-and-run” mechanism,” *Biochimica Et Biophysica Acta (BBA)-Molecular Cell Research,* vol. 1863, no. 12, pp. 2859-2867, 2016.

[219] B. Mackenzie and M. Hediger, “SLC11 family of H+-coupled metal-ion transporters NRAMP1 and DMT1,” *Pflügers Archiv,* vol. 447, no. 5, pp. 571-579, 2004.

[220] K. Yambire, C. Rostosky, T. Watanabe, D. Pacheu-Grau, S. Torres-Odio, A. Sanchez-Guerrero, O. Senderovich, E. Meyron-Holtz, I. Milosevic, J. Frahm and A. West, “Impaired lysosomal acidification triggers iron deficiency and inflammation in vivo,” *Elife,* vol. 8, p. e51031, 2019.

[221] A. Eaton, D. Brown and M. Merkulova, “The evolutionary conserved TLDc domain defines a new class of (H+) V-ATPase interacting proteins,” *Scientific Reports ,* vol. 11, no. 1, pp. 1-15, 2021.

[222] E. Beauregard-Lacroix, G. Pacheco-Cuellar, N. Ajeawung, J. Tardif, K. Dieterich, T. Dabir, D. Vind-Kezunovic, S. White, D. Zadori, C. Castiglioni and L. Tranebjærg, “DOORS syndrome

and a recurrent truncating ATP6V1B2 variant," *Genetics in Medicine,* vol. 23, no. 1, pp. 149-154, 2021.

[223] B. Mucha, S. Banka, N. Ajeawung, S. Molidperee, G. Chen, M. Koenig, R. Adejumo, M. Till, M. Harbord, R. Perrier and E. Lemyre, "A new microdeletion syndrome involving TBC1D24, ATP6V0C, and PDPK1 causes epilepsy, microcephaly, and developmental delay," *Genetics in Medicine,* vol. 21, no. 5, pp. 1058-1064, 2019.

[224] A. Fassio, A. Esposito, M. Kato, H. Saitsu, D. Mei, C. Marini, V. Conti, M. Nakashima, N. Okamoto, A. Olmez Turker and B. Albuz, "De novo mutations of the ATP6V1A gene cause developmental encephalopathy with epilepsy," *Brain,* vol. 141, no. 6, pp. 1703-1718, 2018.

[225] M. Baron, A. Vacaru and J. Nieves, "Erythroid development in the mammalian embryo," *Blood Cells, Molecules, and Diseases,* vol. 51, no. 4, pp. 213-219, 2013.

[226] A. S. Adewoyin, "Peripheral blood film - a review," *Annals of Ibadan postgraduate medicine,* vol. 12, pp. 71-79, 2014.

[227] J. Petithory, F. Ardoin and L. Ash, "Rapid and inexpensive method of diluting Giemsa stain for diagnosis of malaria and other infestations by blood parasites.," *Journal of clinical microbiology,* vol. 43, no. 1, p. 528, 2005.

[228] A. Bunyaratvej, P. Butthep, S. Fucharoen and D. Saw, "Erythrocyte volume and haemoglobin concentration in haemoglobin H disease: discrimination between the two genotypes," *Acta haematologica,* vol. 87, no. 1-2, pp. 1-5, 1992.

[229] L. Chen, J. Wang, J. Liu, H. Wang, C. Hillyer, L. Blanc, X. An and N. Mohandas, "Dynamic changes in murine erythropoiesis from birth to adulthood: implications for the study of murine models of anemia," *Blood advances,* vol. 5, no. 1, pp. 16-25, 2021.

[230] J. Philips, "Heme biosynthesis and the porphyrins," *Molecular Genetics and Metabolism,* vol. 128, no. 3, pp. 164-177, 2019.

[231] E. Eden, R. Navon, I. Steinfeld, D. Lipson and Z. Yakhini, "GOrilla: a tool for discovery and visualization of enriched GO terms in ranked gene lists," *BMC Bioinformatics,* vol. 10, no. 1, pp. 1-7, 2009.

[232] E. Eden, D. Lipson, S. Yogev and Z. Yakhini, "Discovering Motifs in Ranked Lists of DNA sequences," *PLoS Computational Biology,* vol. 3, no. 3, p. e39, 2007.

[233] L. Kolberg, U. Raudvere, I. Kuzmin, J. Vilo and H. Peterson, "gprofiler2– an R package for gene list functional enrichment analysis and namespace conversion toolset g:Profiler," *F1000Research,* vol. 9 (ELIXIR), no. 709, 2020.

[234] Y. Chao, Z. Zhong, W. Sheng-Peng, V. Chi-Teng, Y. Bin and W. Yi-Tao, " HIF-1: structure, biology and natural modulators," *Chinese Journal of Natural Medicines,* vol. 19, no. 7, pp. 521-527, 2021.

[235] H. Auer, D. Newsom and K. Kornacker, "Expression profiling using Affymetrix GeneChip microarrays," *Microchip Methods in Diagnostics,* pp. 35-46, 2009.

[236] N. Wu, X. Nguyen, L. Wang, R. Appourchaux, C. Zhang, B. Panthu, H. Gruffat, C. Journo, S. Alais, J. Qin and N. Zhang, "The interferon stimulated gene 20 protein (ISG20) is an innate defense antiviral factor that discriminates self versus non-self translation," *PLoS pathogens,* vol. 15, no. 10, p. e1008093, 2019.

[237] M. Dalva, A. McClelland and M. Kayser, "Cell adhesion molecules: signalling functions at the synapse," *Nature Reviews Neuroscience,* vol. 8, no. 3, pp. 206-220, 2007.

[238] M. Cao, Z. Huang, H. Zhou, J. Lin and D. Zhang, "Clinical and molecular genetic analysis of a Chinese family with hereditary elliptocytosis caused by a novel mutation in the EPB41 gene," *Journal of Clinical Laboratory Analysis,* vol. 35, no. 6, p. e23781, 2021.

[239] P. Dörmer, E. Spitzer and W. Möller, "EDR is a stress-related survival factor from stroma and other tissues acting on early haematopoietic progenitors," *Cytokine,* vol. 27, no. 2-3, pp. 47-57, 2004.

[240] M. Shin, T. Beane, A. Quillien, I. Male, L. Zhu and N. Lawson, "Vegfa signals through ERK to promote angiogenesis, but not artery differentiation," *Development,* vol. 143, no. 20, pp. 3796-3805, 2016.

[241] J. Chappell, J. Cluceru, J. Nesmith, K. Mouillesseaux, V. Bradley, C. Hartland, Y. Hashambhoy-Ramsay, J. Walpole, S. Peirce, F. Mac Gabhann and V. Bautch, "Flt-1 (VEGFR-1) coordinates discrete stages of blood vessel formation," *Cardiovascular research,* vol. 111, no. 1, pp. 84-93, 2016.

[242] Z. Zhang, P. Dawson, M. Piper and D. Simmons, "Postnatal N-acetylcysteine administration rescues impaired social behaviors and neurogenesis in Slc13a4 haploinsufficient mice," *EBioMedicine,* vol. 43, pp. 435-446, 2019.

[243] X. Gu, G. Wan, Y. Yang, Y. Liu, X. Yang, Y. Zheng, L. Jiang, P. Zhang, D. Liu, W. Zhao and G. Huang, "SLFN5 influences proliferation and apoptosis by upregulating PTEN transcription via ZEB1 and inhibits the purine metabolic pathway in breast cancer," *American journal of cancer research,* vol. 10, no. 9, p. 2832, 2020.

[244] M. Codrich, M. Bertuzzi, R. Russo, M. Francescatto, S. Espinoza, L. Zentilin, M. Giacca, D. Cesselli, A. Beltrami, P. Ascenzi and S. Zucchelli, "Neuronal hemoglobin affects dopaminergic cells' response to stress," *Cell death & disease,* vol. 8, no. 1, p. e2538, 2018.

[245] A. Khan, Y. Wang, Y. Sun, X. Mao, L. Xie, E. Miles, J. Graboski, S. Chen, L. Ellerby, K. Jin and D. Grennberg, "Neuroglobin-overexpressing transgenic mice are resistant to cerebral and myocardial ischaemia," *Proceedings of the National Academy of Sciences,* vol. 103, no. 47, pp. 17944-17948, 2006.

[246] N. Harris, J. Kunicka and A. Kratz, "The ADVIA 2120 hematology system: flow cytometry-based analysis of blood and body fluids in the routine hematology laboratory," *Laboratory Hematology,* vol. 11, no. 1, pp. 47-61, 2005.

[247] K. Fixter, D. Rabbolini, B. Valecha, M. Morel-Kopp, S. Gabrielli, Q. Chen, W. Stevenson and C. Ward, "Mean platelet diameter measurements to classify inherited

thrombocytopenias," *International Journal of Laboratory Hematology,* vol. 40, no. 2, pp. 187-195, 2018.

[248] S. Salignac, V. Latger-Cannard, N. Schlegel and T. Lecompte, "Platelet counting," in *Haemostasis*, Totowa, NJ, Humana Press, 2013, pp. 193-205.

[249] C. University, "eClinpath.com," [Online]. Available: https://eclinpath.com/hematology/tests/wbc-count/. [Accessed 2 May 2022].

[250] A. Nienhuis and D. Nathan, "Pathophysiology and clinical manifestations of the β-thalassemias," *Cold Spring Harbor perspectives in medicine,* vol. 2, no. 12, p. a011726, 2012.

[251] R. Nilsson, I. Schultz, E. Pierce, K. Soltis, A. Naranuntarat, D. Ward, J. Baughman, P. Paradkar, P. Kingsley, V. Culotta and J. Kaplan, "Discovery of genes essential for heme biosynthesis through large-scale gene expression analysis," *Cell metabolism,* vol. 10, no. 2, pp. 119-130, 2009.

[252] C. Smith, T. Hayamizu, J. Finger, S. Bello, I. McCright, J. Xu, R. Baldarelli, J. Beal, J. Campbell, L. Corbani and P. Frost, "The mouse Gene Expression Database (GXD): 2019 update," Nucleic Acids Res., Maine, 2019.

[253] W. Wang, M. Knovich, L. Coffman, F. Torti and S. Torti, "Serum ferritin: past, present and future.," *Biochimica et Biophysica Acta ,* vol. 1800, no. 8, pp. 760-769, 2010.

[254] H. Kawabata, "Transferrin and transferrin receptors update," *Free Radical Biology and Medicine,* vol. 133, pp. 46-54, 2019.

[255] A. Pietrangelo, "Iron and the liver," *Liver international,* vol. 36, pp. 116-123, 2016.

[256] A. Pietrangelo, "Ferroportin disease: pathogenesis, diagnosis and treatment," *Haematologica,* vol. 102, no. 12, p. 1972, 2017.

[257] M. Rogatzki, B. Ferguson, M. Goodwin and L. Gladden, "Lactate is always the end product of glycolysis.," *Frontiers in neuroscience,* vol. 9, p. 22, 2015.

[258] J. Gutteridge and A. Smith, "Antioxidant protection by haemopexin of haem-stimulated lipid peroxidation," *Biochemical journal,* vol. 253, no. 3, pp. 861-865, 1988.

[259] J. Bourne, M. Colicchia, Y. Di, E. Martin, A. Slater, L. Roumenina, J. Dimitrov, S. Watson and J. Rayes, "Heme induces human and mouse platelet activation through C-type-lectin-like receptor-2," *Haematologica,* vol. 106, no. 2, p. 626, 2021.

[260] R. Moreau, D. Tshikudi Malu, M. Dumais, E. Dalko, V. Gaudreault, H. Romero, C. Martineau, O. Kevorkova, J. Dardon, E. Dodd and D. Bohle, "Alterations in bone and erythropoiesis in hemolytic anemia: comparative study in bled, phenylhydrazine-treated and Plasmodium-infected mice.," *PLoS One,* p. e46101, 2012.

[261] E. Turer, W. McAlpine, K. Wang, T. Lu, X. Li, M. Tang, X. Zhan, T. Wang, X. Zhan, C. Bu and A. Murray, “Creatine maintains intestinal homeostasis and protects against colitis,” *Proceedings of the National Academy of Sciences,* vol. 114, no. 7, pp. E1273-E1281, 2017.

[262] P. Zhao, H. Qian and Y. Xia, “GABA and glycine are protective to mature but toxic to immature rat cortical neurons under hypoxia,” *European Journal of Neuroscience,* vol. 22, no. 2, pp. 289-300, 2005.

[263] M. McCarty, J. O'Keefe and J. DiNicolantonio, “Dietary glycine is rate-limiting for glutathione synthesis and may have broad potential for health protection,” *Ochsner Journal,* vol. 18, no. 1, pp. 81-87, 2018.

[264] C. Camaschella and A. Nai, “Ineffective erythropoiesis and regulation of iron status in iron loading anaemias,” *British journal of haematology,* vol. 172, no. 4, pp. 512-523, 2016.

[265] R. Meguro, Y. Asano, S. Odagiri, C. Li, H. Iwatsuki and K. Shoumura, “The presence of ferric and ferrous iron in the nonheme iron store of resident macrophages in different tissues and organs: histochemical demonstrations by the perfusion-Perls and-Turnbull methods in the rat.,” *Archives of histology and cytology,* vol. 68, no. 3, pp. 171-183, 2005.

[266] H. Wang, D. Liu, P. Song, F. Jiang, X. Chi and T. Zhang, “Exposure to hypoxia causes stress erythropoiesis and downregulates immune response genes in spleen of mice.,” *BMC Genomics,* vol. 22, no. 1, pp. 1-14, 2021.

[267] J. Zhang, Y. Liu, X. Han, Y. Mei, J. Yang, Z. Zhang, X. Lu and P. Ji, “Rats provide a superior model of human stress erythropoiesis,” *Experimental hematology,* vol. 78, pp. 21-34, 2019.

[268] K. Chen, J. Liu, S. Heck, J. Chasis, X. An and N. Mohandas, “ Resolving the distinct stages in erythroid differentiation based on dynamic changes in membrane protein expression during erythropoiesis,” *Proceedings of the National Academy of Sciences,* vol. 106, no. 41, pp. 17413-17418, 2009.

[269] L. Pang, M. Weiss and M. Poncz, “Megakaryocyte biology and related disorders,” *The Journal of clinical investigation,* vol. 115, no. 12, pp. 3332-3338, 2005.

[270] E. Gautier, S. Ducamp, M. Leduc, V. Salnot, F. Guillonneau, M. Dussiot, J. Hale, M. Giarratana, A. Raimbault, L. Douay and C. Lacombe, “Comprehensive Proteomic Analysis of Human Erythropoiesis,” *Cell reports,* vol. 16, no. 5, pp. 1470-1484, 2016.

[271] Z. Warkocki, V. Liudkovska, O. Gewartowska, S. Mroczek and A. Dziembowski, “Terminal nucleotidyl transferases (TENTs) in mammalian RNA metabolism,” *Philosophical Transactions of the Royal Society B: Biological Sciences,* vol. 373, no. 1762, p. 20180162, 2018.

[272] S. Mroczek, J. Chlebowska, T. Kuliński, O. Gewartowska, J. Gruchota, D. Cysewski, V. Liudkovska, E. Borsuk, D. Nowis and A. Dziembowski, “The non-canonical poly (A) polymerase FAM46C acts as an onco-suppressor in multiple myeloma,” *Nature communications,* vol. 8, no. 1, pp. 1-17, 2017.

[273] A. Donovan, C. Lima, J. Pinkus, G. Pinkus, L. Zon, S. Robine and N. Andrews, “The iron exporter ferroportin/Slc40a1 is essential for iron homeostasis,” *Cell metabolism,* vol. 1, no. 3, pp. 191-200, 2005.

[274] L. Cheng, H. Yu, N. Yan, K. Lai and M. Xiang, “Hypoxia-inducible factor-1α target genes contribute to retinal neuroprotection,” *Frontiers in Cellular Neuroscience,* vol. 11, p. 20, 2017.

[275] L. Dunn, R. Midwinter, J. Ni, H. Hamid, C. Parish and R. Stocker, “ New insights into intracellular locations and functions of heme oxygenase-1,” *Antioxidants & redox signaling,* vol. 20, no. 11, pp. 1723-1742, 2014.

[276] P. Fisel, S. Kruck, S. Winter, J. Bedke, J. Hennenlotter, A. Nies, M. Scharpf, F. Fend, A. Stenzl, M. Schwab and E. Schaeffeler, “DNA methylation of the SLC16A3 promoter regulates expression of the human lactate transporter MCT4 in renal cancer with consequences for clinical outcome,” *Clinical Cancer Research,* vol. 19, no. 18, pp. 5170-5181, 2013.

[277] M. Ullah, A. Davies and A. Halestrap, “The plasma membrane lactate transporter MCT4, but not MCT1, is up-regulated by hypoxia through a HIF-1α-dependent mechanism.,” *Journal of Biological Chemistry,* vol. 281, no. 14, pp. 9030-9037, 2006.

[278] G. Semenza, “Hypoxia-inducible factor 1: oxygen homeostasis and disease pathophysiology,” *Trends in molecular medicine,* vol. 7, no. 8, pp. 345-350, 2001.

[279] N. Iyer, L. Kotch, F. Agani, S. Leung, E. Laughner, R. Wenger, M. Gassmann, J. Gearhart, A. Lawler, Y. Aimee and G. Semenza, “Cellular and developmental control of O2 homeostasis by hypoxia-inducible factor 1α,” *Genes & development,* vol. 12, no. 2, pp. 149-162, 1998.

[280] H. Hou, D. Li, Y. Yao, J. Lu, Y. Sun, Y. Hu, S. Wu, X. Chu, P. Xiao, G. Xu and S. Hu, “Proteomic analysis for identifying the differences in molecular profiling between fanconi anaemia and aplastic anaemia.,” *American Journal of Translational Research,* vol. 11, no. 10, p. 6522, 2019.

[281] Y. Chung, P. Swietach, M. Curtis, V. Ball, P. Robbins and S. Lakhal-Littleton, “ Iron-Deficiency Anemia Results in Transcriptional and Metabolic Remodeling in the Heart Toward a Glycolytic Phenotype,” *Frontiers in cardiovascular medicine,* p. 361, 2021.

[282] T. McDonald, M. Puchowicz and K. Borges, “Impairments in oxidative glucose metabolism in epilepsy and metabolic treatments thereof,” *Frontiers in Cellular Neuroscience,* vol. 12, p. 274, 2018.

[283] D. Hodge, E. Coghill, J. Keys, T. Maguire, B. Hartmann, A. McDowall, M. Weiss, S. Grimmond and A. Perkins, “A global role for EKLF in definitive and primitive erythropoiesis,” *Blood,* vol. 107, no. 8, pp. 3359-3370, 2006.

[284] X. Peng, J. Williams, P. Smallwood and J. Nathans, “Defining the binding interface of Amyloid Precursor Protein (APP) and Contactin3 (CNTN3) by site-directed mutagenesis.,” *Plos one,* vol. 14, no. 7, p. e0219384, 2019.

[285] A. Korotkov, M. Luinenburg, A. Romagnolo, T. Zimmer, J. van Scheppingen, A. Bongaarts, D. Broekaart, J. Anink, C. Mijnsbergen, F. Jansen and W. Van Hecke, "Down-regulation of the brain-specific cell-adhesion molecule contactin-3 in tuberous sclerosis complex during the early postnatal period," *Journal of neurodevelopmental disorders,* vol. 14, no. 1, pp. 1-16, 2022.

[286] M. Parra, P. Gascard, L. Walensky, S. Snyder, N. Mohandas and J. Conboy, "Cloning and characterization of 4.1 G (EPB41L2), a new member of the skeletal protein 4.1 (EPB41) gene family.," *Genomics,* vol. 49, no. 2, pp. 298-306, 1998.

[287] V. Revin, I. Grunyushkin, N. Gromova, E. Revina, A. Abdulvwahid, I. Solomadin, A. Tychkov and A. Kukina, "Effect of hypoxia on the composition and state of lipids and oxygen-transport properties of erythrocyte haemoglobin," *Biotechnology & Biotechnological Equipment,* vol. 31, no. 1, pp. 128-137, 2017.

[288] L. Bury, A. Malara, S. Momi, E. Petito, A. Balduini and P. Gresele, "Mechanisms of thrombocytopenia in platelet-type von Willebrand disease," *Haematologica,* vol. 104, no. 7, p. 1473, 2019.

[289] T. Nilsson, K. Sondell, B. Norberg and O. Bäck, "Plasma levels of endothelial-derived haemostatic factors in autoimmune thrombocytopenia and haemolytic anaemia.," *Journal of internal medicine,* vol. 228, no. 3, pp. 249-252, 1990.

[290] T. Bastian, S. Santarriaga, T. Nguyen, J. Prohaska, M. Georgieff and G. Anderson, "Fetal and neonatal iron deficiency but not copper deficiency increases vascular complexity in the developing rat brain.," *Nutritional neuroscience,* vol. 18, no. 8, pp. 365-375, 2015.

[291] N. Ferrara, "Role of vascular endothelial growth factor in physiologic and pathologic angiogenesis: therapeutic implications," *Seminars in oncology,* vol. 29, no. 6, pp. 10-14, 2002.

[292] H. Marti and W. Risau, "Systemic hypoxia changes the organ-specific distribution of vascular endothelial growth factor and its receptors.," *Proceedings of the National Academy of Sciences,* vol. 95, no. 26, pp. 15809-15814, 1998.

[293] P. Pichiule and J. LaManna, "Angiopoietin-2 and rat brain capillary remodeling during adaptation and deadaptation to prolonged mild hypoxia," *Journal of applied physiology,* vol. 93, no. 3, pp. 1131-1139, 2002.

[294] D. Simmons, J. Rakoczy, J. Jefferis, R. Lourie, H. McIntyre and P. Dawson, "Human placental sulfate transporter mRNA profiling from term pregnancies identifies abundant SLC13A4 in syncytiotrophoblasts and SLC26A2 in cytotrophoblasts.," *Placenta,* vol. 34, no. 4, pp. 381-384, 2013.

[295] N. Farsijani, Q. Liu, H. Kobayashi, O. Davidoff, F. Sha, J. Fandrey, T. Ikizler, P. O'Connor and V. Haase, "Renal epithelium regulates erythropoiesis via HIF-dependent suppression of erythropoietin," *The Journal of Clinical Investigation,* vol. 126, no. 4, pp. 1425-1437, 2016.

[296] F. Metzner, E. Huber, K. Hopfner and K. Lammens, “Structural and biochemical characterization of human Schlafen 5,” *Nucleic Acids Research,* vol. 50, no. 2, pp. 1147-1161, 2022.

[297] S. Cooperman, E. Meyron-Holtz, H. Olivierre-Wilson, M. Ghosh, J. McConnell and T. Rouault, “Microcytic anemia, erythropoietic protoporphyria, and neurodegeneration in mice with targeted deletion of iron-regulatory protein 2,” *Blood,* vol. 106, no. 3, pp. 1084-1091, 2005.

[298] E. Urrechaga, L. Borque and J. Escanero, “Erythrocyte and reticulocyte indices in the assessment of erythropoiesis activity and iron availability,” *Journal of Laboratory Hematology,* vol. 35, no. 2, pp. 144-149, 2013.

[299] I. Alamo, K. Kannan, M. Smith, P. Efron and A. Mohr, “ Characterization of erythropoietin and hepcidin in the regulation of persistent injury-associated anemia,” *The journal of trauma and acute care surgery,* vol. 81, no. 4, p. 705, 2016.

[300] Y. Abbas, D. Wu, S. Bueler, C. Robinson and J. Rubinstein, “Structure of V-ATPase from the mammalian brain,” *Science,* vol. 367, no. 6483, pp. 1240-1246, 2020.

[301] K. Kaneko, K. Ohba, T. Hirose, K. Totsune, K. Furuyama and K. Takahashi, “Expression of (pro) renin receptor during rapamycin-induced erythropoiesis in K562 erythroleukemia cells and its possible dual actions on erythropoiesis,” *The Tohoku Journal of Experimental Medicine,* vol. 241, no. 1, pp. 35-43, 2017.

[302] A. Zhang, A. Sheftel and P. Ponka, “Intracellular kinetics of iron in reticulocytes: evidence for endosome involvement in iron targeting to mitochondria,” *Blood,* vol. 105, no. 1, pp. 368-375, 2005.

[303] A. Sobh, A. Loguinov, J. Zhou, S. Jenkitkasemwong, R. Zeidan, N. El Ahmadie, A. Tagmount, M. Knutson, P. Fraenkel and C. Vulpe, “Genetic screens reveal CCDC115 as a modulator of erythroid iron and heme trafficking,” *American Journal of Hematology,* vol. 95, no. 9, pp. 1085-1098, 2020.

[304] P. L. Oliver, M. J. Finelli, B. Edwards, E. Bitoun, D. L. Butts, E. B. C. M. Becker, B. Davies and K. E. Davies, “Oxr1 is essential for protection against oxidative stress-induced neurodegeneration,” *PLoS Genetics,* vol. 7, no. 10, 2011.

[305] M. Yang, L. Luna, J. Sørbø, I. Alseth, R. Johansen, P. Backe, N. Danbolt, L. Eide and M. Bjørås, “Human OXR1 maintains mitochondrial DNA integrity and counteracts hydrogen peroxide-induced oxidative stress by regulating antioxidant pathways involving p21,” *Free Radical Biology and Medicine,* vol. 77, pp. 41-48, 2014.

[306] J. Mo, P. Z. X. Chen, Y. Lei, L. Lv, C. Qian and F. Sun, “MicroRNA-365 knockdown prevents ischemic neuronal injury by activating oxidation resistance 1-mediated antioxidant signals,” *Neuroscience bulletin,* vol. 35, no. 5, pp. 815-825, 2019.

[307] D. Svistunova, J. Simon, E. Rembeza, M. Crabtree, W. Yue, P. Oliver and M. Finelli, “Oxidation resistance 1 regulates post-translational modifications of peroxiredoxin 2 in the cerebellum,” *Free Radical Biology and Medicine,* vol. 130, pp. 151-162, 2019.

[308] M. Yang, X. Lin, A. Rowe, Rognes, E. L. T. and M. Bjørås, “Transcriptome analysis of human OXR1 depleted cells reveals its role in regulating the p53 signaling pathway,” *Scientific Reports,* vol. 5, no. 1, pp. 1-12, 2015.

[309] B. Sahu, L. Leon, W. Zhang, N. Puranik, R. Periasamy, H. Khanna and M. Volkert, “Oxidative Stress Resistance 1 Gene Therapy Retards Neurodegeneration in the rd1 Mutant Mouse Model of Retinopathy,” *Investigative ophthalmology & visual science,* vol. 62, no. 12, p. 8, 2021.

[310] M. Finelli, K. Liu, Y. Wu, P. Oliver and K. Davies, “Oxr1 improves pathogenic cellular features of ALS-associated FUS and TDP-43 mutations,” *Human Molecular Genetics,* vol. 24, no. 12, pp. 3529-3544, 2015.

[311] M. Williamson, M. Finelli, J. Sleigh, A. Reddington, D. Gordon, K. Talbot, K. Davies and P. Oliver, “Neuronal over-expression of Oxr1 is protective against ALS-associated mutant TDP-43 mislocalisation in motor neurons and neuromuscular defects in vivo,” *Human molecular genetics,* vol. 28, no. 21, pp. 3584-3599, 2019.

[312] M. Volkert and D. Crowley, “Preventing Neurodegeneration by Controlling Oxidative Stress: The Role of OXR1,” *Frontiers in Neuroscience,* vol. 14, p. 1318, 2020.

[313] M. Tawfik, “Coenzyme Q10 enhances the anticonvulsant effect of phenytoin in pilocarpine-induced seizures in rats and ameliorates phenytoin-induced cognitive impairment and oxidative stress,” *Epilepsy & Behaviour,* vol. 22, no. 4, pp. 671-677, 2011.

[314] W. Wang, Y. Wu, G. Zhang, H. Fang, H. Wang, H. Zang, T. Xie and W. Wang, “ctivation of Nrf2-ARE signal pathway protects the brain from damage induced by epileptic seizure,” *Brain research,* vol. 1544, pp. 54-61, 2014.

[315] S. Shakeel, M. Rehman, N. Tabassum and U. Amin, “Effect of naringenin (a naturally occurring flavanone) against pilocarpine-induced status epilepticus and oxidative stress in mice,” *Pharmacognosy Magazine,* vol. 13, p. 154, 2017.

[316] M. Murphy, “Antioxidants as therapies: can we improve on nature?,” *Free Radical Biology an,* vol. 66, pp. 20-23, 2014.

[317] G. Kim, J. Kim, S. Rhie and S. Yoon, “The Role of Oxidative Stress in Neurodegenerative Diseases,” *Experimental Neurobiology,* vol. 24, no. 4, pp. 325-340, 2015.

[318] A. Parsons, E. Bucknor, E. Castroflorio, T. Soares, P. Oliver and D. Rial, “The Interconnected Mechanisms of Oxidative Stress and Neuroinflammation in Epilepsy,” *Antioxidants,* vol. 11, no. 1, p. 157, 2022.

[319] M. Finelli, L. Sanchez-Pulido, K. Liu, K. Davies and P. Oliver, “The Evolutionarily Conserved Tre2/Bub2/Cdc16 (TBC), Lysin Motif (LysM), Domain Catalytic (TLDc) Domain Is Neuroprotective against Oxidative Stress,” *The Journal of Biological Chemistry,* vol. 291, no. 6, pp. 2751-2765, 2016.

[320] J. Wang, J. Rousseau, E. Kim, S. Ehresmann, Y. Cheng, L. Duraine, Z. Zuo, Y. Park, D. Li-Kroeger, W. Bi and L. Wong, “Loss of oxidation resistance 1, OXR1, is associated with an

autosomal-recessive neurological disease with cerebellar atrophy and lysosomal dysfunction," *The American Journal of Human Genetics,* vol. 105, no. 6, pp. 1237-1253, 2019.

[321] M. Durand, A. Kolpak, T. Farrell, N. Elliott, W. Shao, M. Brown and M. Volkert, "The OXR domain defines a conserved family of eukaryotic oxidation resistance proteins," *BMC Cell Biology,* vol. 8, no. 1, pp. 1-10, 2007.

[322] X. Chen, R. Reader, A. Hoischen, J. Veltman, N. Simpson, C. Francks, D. Newbury and S. Fisher, "Next-generation DNA sequencing identifies novel gene variants and pathways involved in specific language impairment," *Scientific Reports,* vol. 7, no. 1, pp. 1-17, 2017.

[323] Y. Wu, K. Davies and P. Oliver, "The antioxidant protein Oxr1 influences aspects of mitochondrial morphology.," *Free Radical Biology and Medicine,* vol. 95, pp. 255-267, 2016.

[324] B. Schuck, R. MacArthur and J. Inglese, "Quantitative High-Throughput Screening Using a Coincidence Reporter Biocircuit," *Current Protocols in Neuroscience,* vol. 79, no. 1, pp. 5-32, 2017.

[325] E. Conti, N. Franks and P. Brick, "Crystal structure of firefly luciferase throws light on a superfamily of adenylate-forming enzymes," *Structure,* vol. 4, no. 3, pp. 287-298, 1996.

[326] M. Hall, J. Unch, B. Binkowski, M. Valley, B. Butler, M. Wood, P. Otto, K. Zimmerman, G. Vidugiris, T. Machleidt and M. Robers, "Engineered luciferase reporter from a deep sea shrimp utilizing a novel imidazopyrazinone substrate," *ACS Chemical Biology,* vol. 7, no. 11, pp. 1848-1857, 2012.

[327] S. Hasson, A. Fogel, C. Wang, R. MacArthur, R. Guha, S. Heman-Ackah, S. Martin, R. Youle and J. Inglese, "Chemogenomic profiling of endogenous PARK2 expression using a genomeedited coincidence reporter," *ACS Chemical Biology,* vol. 10, no. 5, pp. 1188-1197, 2015.

[328] Z. Zhang, N. Guan, T. Li, D. Mais and M. Wang, "Quality control of cell-based high-throughput drug screening," *Acta Pharmaceutica Sinica B,* vol. 2, no. 5, pp. 429-438, 2012.

[329] B. Krampe and M. Al-Rubeai, "Cell death in mammalian cell culture: molecular mechanisms and cell line engineering strategies," *Cytotechnology,* vol. 62, no. 3, pp. 175-188, 2010.

[330] N. Choulis, "Miscellaneous drugs, materials, medical devices, and techniques,," *Side Effects of Drugs Annual,* vol. 34, pp. 785-800, 2012.

[331] K.-C. Cheng and J. Inglese, "A coincidence reporter-gene system for high-throughput screening," *Nature methods,* vol. 9, no. 10, p. 937, 2012.

[332] M. Maeder, S. Linder, V. Cascio, Y. Fu, Q. Ho and J. Joung, "CRISPR RNA–guided activation of endogenous human genes," *Nature methods,* vol. 10, no. 10, pp. 977-979, 2013.

[333] E. Becirovic, "Maybe you can turn me on: CRISPRa-based strategies for therapeutic applications," *Cellular and molecular life sciences,* vol. 79, no. 2, pp. 1-9, 2022.

[334] A. Cheng, H. Wang, H. Yang, L. Shi, Y. Katz, T. Theunissen, R. Sudharshan, C. Shivalila, D. Dadon and R. Jaenisch, "Multiplexed activation of endogenous genes by CRISPR-on, an RNA-guided transcriptional activator system," *Cell Research,* vol. 23, pp. 1163-1171, 2013.

[335] T. Jensen, N. Mikkelsen, Z. Gao, J. Foßelteder, G. Pabst, E. Axelgaard, A. Laustsen, S. König, A. Reinisch and R. Bak, "Targeted regulation of transcription in primary cells using CRISPRa and CRISPRi," *Genome research,* vol. 31, no. 11, pp. 2120-2130, 2021.

[336] K. Lüthy, D. Mei, B. Fischer, M. De Fusco, J. Swerts, J. Paesmans, E. Parrini, N. Lubarr, I. Meijer, K. Mackenzie and W. Lee, "TBC1D24-TLDc-related epilepsy exercise-induced dystonia: rescue by antioxidants in a disease model," *Brain,* vol. 142, no. 8, pp. 2319-2335, 2019.

[337] L. Liang, S. Waldbaum, S. Rowley, T. Huang, B. Day and M. Patel, "Mitochondrial oxidative stress and epilepsy in SOD2 deficient mice: Attenuation by a lipophilic metalloporphyrin," *Neurobiology of disease,* vol. 3, pp. 1068-1076, 2012.

[338] S. Keskin Guler, B. Aytac, Z. Durak, B. Gokce Cokal, N. Gunes, I. Durak and T. Yoldas, "Antioxidative-oxidative balance in epilepsy patients on antiepileptic therapy: A prospective case-control study," *Neurological Sciences,* vol. 5, pp. 763-767, 2016.

[339] M. Gluck, E. Jayatilleke, S. Shaw, A. Rowan and V. Haroutunian, "CNS oxidative stress associated with the kainic acid rodent model of experimental epilepsy," *Epilepsy Research,* vol. 39, pp. 63-71, 2000.

[340] N. Pandya, F. Koopmans, J. Slotman, I. Paliukhovich, A. Houtsmuller, A. Smit and K. Li, "Correlation profiling of brain sub-cellular proteomes reveals co-assembly of synaptic proteins and subcellular distribution," *Scientific Report,* vol. 7, no. 1, p. 12107, 2017.

[341] D. Doummar, C. Mignot, E. Apartis, L. Villard, D. Rodriguez, S. Chantot-Bastauraud and L. Burglen, "A novel homozygous TBC1D24 mutation causing multifocal myoclonus with cerebellar involvement," *Movement disorders: official journal of the Movement Disorder Society,* vol. 30, no. 10, pp. 1431-1432, 2015.

[342] A. Eaton, D. Brown and M. Merkulova, "The evolutionary conserved TLDc domain defines a new class of (H+) V-ATPase interacting proteins," *Scientific reports,* vol. 11, pp. 1-15, 2021.

[343] Y. Tan, Y. Abbas, J. Wu, D. Wu, G. Hesketh, S. Bueler, A. Gingras, C. Robinson, S. Grinstein and J. Rubinstein, "Structure of mammalian V-ATPase with the TLDc domain protein mEAK7 bound," *bioRxiv,* 2021.

[344] F. Grieco, B. Bernstein, B. Biemans, L. Bikovski, C. Burnett, J. Cushman, E. Van Dam, S. Fry, B. Richmond-Hacham, J. Homberg and M. Kas, "Measuring behavior in the home cage: Study design, applications, challenges, and perspectives," *Frontiers in behavioral neuroscience,* vol. 15, 2021.

[345] M. Goel, P. Khanna and J. Kishore, "Understanding survival analysis: Kaplan-Meier estimate," *International journal of Ayurveda research,* vol. 1, no. 4, p. 274, 2010.

[346] J. Burneo, V. Villanueva, R. Knowlton, R. Faught and R. Kuzniecky, “Kaplan–Meier analysis on seizure outcome after epilepsy surgery: Do gender and race influence it?,” *Seizure,* vol. 17, no. 4, pp. 314-319, 2008.

[347] D. Diaz-Arce, A. Ghouma, P. Scalmani, M. Mantegazza and F. Duprat, “A python-based package for long-lasting video acquisition,” *bioRxiv,* 2022.

[348] R. Bergstrom, J. Choi, A. Manduca, H. Shin, G. Worrell and C. Howe, “ Automated identification of multiple seizure-related and interictal epileptiform event types in the EEG of mice,” *Scientific reports,* vol. 3, no. 1, pp. 1-8, 2013.

[349] Z. Zhang, D. Zhang, J. Slane McQuade, M. Behbehani, J. Tsien and M. Xu, “c-fos regulates neuronal excitability and survival,” *Nature Genetics,* vol. 30, pp. 416-420, 2002.

[350] H. Yang, W. Shan, F. Zhu, T. Yu, J. Fan, A. Guo, F. Li, X. Yang and Q. Wang, “C-Fos mapping and EEG characteristics of multiple mice brain regions in pentylenetetrazol-induced seizure mice model,” *Neurological Research,* vol. 41, no. 8, pp. 749-761, 2019.

[351] J. Marques-Carneiro, A. Nehlig, J. Cassel, E. Castro-Neto, J. Litzahn, A. Pereira de Vasconcelos, M. Naffah-Mazacoratti and M. Fernandes, “Neurochemical Changes and c-Fos Mapping in the Brain after Carisbamate Treatment of Rats Subjected to Lithium–Pilocarpine-Induced Status Epilepticus,” *Pharmaceuticals,* vol. 10, no. 4, p. 85, 2017.

[352] A. Korotkov, M. Luinenburg, A. Romagnolo, T. Zimmer, J. van Scheppingen, A. Bongaarts, D. Broekaart, J. Anink, C. Mijnsbergen, F. Jansen and W. Van Hecke, “Down-regulation of the brain-specific cell-adhesion molecule contactin-3 in tuberous sclerosis complex during the early postnatal period,” *Journal of neurodevelopmental disorders,* vol. 14, no. 1, pp. 1-16, 2022.

[353] Y. Yoshihara, M. Kawasaki, A. Tani, A. Tamada, S. Nagata and H. &. M. K. Kagamiyama, “BIG-1: a new TAG-1/F3-related member of the immunoglobulin superfamily with neurite outgrowth-promoting activity,” *Neuron,* vol. 13, no. 2, pp. 415-426, 1994.

[354] G. Vilema-Enríquez, R. Quinlan, P. Kilfeather, R. Mazzone, S. Saqlain, I. Del Barrio, A. Donato, G. Corda, F. Li, M. Vedadi and A. Németh, “ Inhibition of the SUV4-20 H1 histone methyltransferase increases frataxin expression in Friedreich's ataxia patient cells,” *Journal of Biological Chemistry,* vol. 295, no. 52, pp. 17973-17985, 2020.

[355] N. Martinez, J. Braisted, P. Dranchak, J. Moran, H. Larson, B. Queme, E. Pak, A. Dutra, G. Rai, K. Cheng and J. Svaren, “Genome-Edited Coincidence and PMP22-HiBiT Fusion Reporter Cell Lines Enable an Artifact-Suppressive Quantitative High-Throughput Screening Strategy for PMP22 Gene-Dosage Disorder Drug Discovery,” *ACS Pharmacology & Translational Science,* vol. 4, no. 4, pp. 1422-1436, 2021.

[356] X. Wang, S. Xia, P. Zou and L. Lu, “Erythromycin estolate inhibits zika virus infection by blocking viral entry as a viral inactivator,” *Viruses,* vol. 11, no. 11, p. 1064, 2019.

[357] H. Kaneko, “Chapter 76 - Pyrethroid Chemistry and Metabolism,” *Hayes' Handbook of Pesticide Toxicology,* pp. 1635-1663, 2010.

[358] A. Bachmanov, M. Tordoff and G. Beauchamp, “Sweetener preference of C57BL/6ByJ and 129P3/J mice,” *Chemical senses,* vol. 26, no. 7, pp. 905-913, 2001.

[359] J. Miyamoto, T. Suzuki and C. Nakae, “Metabolism of phenothrin or 3-phenoxybenzyl d-trans-chrysanthemumate in mammals,” *Pesticide Biochemistry and Physiology,* vol. 4, no. 4, pp. 438-450, 1974.

[360] D. Voiculescu, V. Ostafe and A. Isvoran, “COMPUTATIONAL ASSESSMENT OF THE PHARMACOKINETICS AND TOXICITY OF THE INTENSIVE SWEETENERS,” *Farmacia,* vol. 69, no. 6, pp. 1032-1041, 2021.

[361] S. Ibragić, E. Fehratović, D. Suljević and M. Mitrašinović-Brulić, “Artificial sweeteners elicit oxidative stress in rat brain and development of microcytic anemia: Promising protective effects of vitamin C,” *Journal of Research in Pharmacy,* vol. 25, pp. 117-123, 2021.

[362] X. Lu, Y. Tian, X. Lian, Y. Jin, T. Jin, Q. Zhao, B. Hu, X. Shen and X. Fan, “Integrated systems toxicology approaches identified the possible involvement of ABC transporters pathway in erythromycin estolate-induced liver injury in rat,” *Food and chemical toxicology,* vol. 65, pp. 343-355, 2014.

[363] H. Bryan, A. Olayanju, C. Goldring and B. Park, “The Nrf2 cell defence pathway: Keap1-dependent and -independent mechanisms of regulation,” *Biochemical pharmacology,* vol. 85, no. 6, pp. 705-717, 2013.

[364] M. Yang, X. Lin, F. Segers, R. Suganthan, G. Hildrestrand, J. Rinholm, P. Aas, M. Sousa, S. Holm, N. Bolstad and D. Warren, “OXR1A, a coactivator of PRMT5 regulating histone arginine methylation,” *Cell reports,* vol. 30, no. 12, pp. 4165-4178, 2020.

[365] C. Fujino, Y. Watanabe, S. Sanoh, H. Nakajima, N. Uramaru, H. Kojima, K. Yoshinari, S. Ohta and S. Kitamura, “Activation of PXR, CAR and PPARα by pyrethroid pesticides and the effect of metabolism by rat liver microsomes,” *Heliyon,* vol. 5, no. 9, 2019.

[366] B. Staels and J. Fruchart, “Therapeutic roles of peroxisome proliferator–activated receptor agonists,” *Diabetes,* vol. 54, no. 8, pp. 2460-2470, 2005.

[367] M. Puligheddu, G. Pillolla, M. Melis, S. Lecca, F. Marrosu, M. De Montis, S. Scheggi, G. Carta, E. Murru, S. Aroni and A. Muntoni, “PPAR-alpha agonists as novel antiepileptic drugs: preclinical findings,” *PLoS One,* vol. 8, no. 5, 2013.

[368] G. Dette, “Serum and tissue concentrations of erythromycin: a review,” *Current Medical Research and Opinion,* vol. 6, no. 8, pp. 23-28, 1980.

[369] J. Kamei, H. Igarashi and Y. Kasuya, “Modulation by serotonin of glutamate-induced lethality in mice,” *Research Communications in Chemical Pathology and Pharmacology,* vol. 74, no. 2, pp. 167-184, 1991.

[370] Y. Kim, P. Alpmann, S. Blaum-Feder, S. Kraemer, T. Endo, D. Lu, D. Carson and I. Schmidt-Wolf, “Increased in vivo efficacy of lenalidomide by addition of piroctone olamine,” *In vivo,* vol. 25, no. 1, pp. 99-103, 2011.

[371] A. Houari and P. Di Martino, “Effect of chlorhexidine and benzalkonium chloride on bacterial biofilm formation,” *Letters in applied microbiology,* vol. 45, no. 6, pp. 652-656, 2007.

[372] J. Beijnen, A. Bult and W. Underberg, “Mitoxantrone hydrochloride,” *Analytical profiles of drug substances,* vol. 17, pp. 221-258, 1988.

[373] D. Auld and J. Inglese, “Interferences with Luciferase Reporter Enzymes,” 2018.

[374] C. Lai, T. Chen, T. Chan, W. Li and H. He, “Prognostic significance of OXR1 in urothelial carcinoma: low OXR1 expression is associated with worse survival,” *Future Oncology,* vol. 17, no. 31, pp. 4145-4156, 2021.

[375] C. Chen, E. Zeldich, Y. Li, A. Yuste and C. Abraham, “Activation of the Anti-Aging and Cognition-Enhancing Gene Klotho by CRISPR-dCas9 Transcriptional Effector Complex,” *Journal of Molecular Neuroscience,* vol. 64, no. 2, pp. 175-184, 2018.

[376] S. Konermann, M. Brigham, A. Trevino, J. Joung, O. Abudayyeh, C. Barcena, P. Hsu, N. Habib, J. Gootenberg, H. Nishimasu and O. Nureki, “Genome-scale transcriptional activation by an engineered CRISPR-Cas9 complex,” *Nature,* vol. 517, no. 7536, pp. 583-588, 2015.

[377] P. Perez-Pinera, D. Kocak, C. Vockley, A. Adler, A. Kabadi, L. Polstein, P. Thakore, K. Glass, D. Ousterout, K. Leong and F. Guilak, “RNA-guided gene activation by CRISPR-Cas9–based transcription factors,” *Nature methods,* vol. 10, no. 10, pp. 973-976, 2013.

[378] P. Mali, J. Aach, P. Stranges, K. Esvelt, M. Moosburner, S. Kosuri, L. Yang and G. Church, “CAS9 transcriptional activators for target specificity screening and paired nickases for cooperative genome engineering,” *Nature biotechnology,* vol. 31, no. 9, pp. 833-838, 2013.

[379] S. Vora, M. Tuttle, J. Cheng and G. Church, “Next stop for the CRISPR revolution: RNA-guided epigenetic regulators,” *The FEBS Journal,* vol. 283, no. 17, pp. 3181-3193, 2016.

[380] E. Castroflorio, J. Den Hoed, D. Svistunova, M. Finelli, A. Cebrian-Serrano, S. Corrochano, A. Bassett, B. Davies and P. Oliver, “The Ncoa7 locus regulates V-ATPase formation and function, neurodevelopment and behaviour,” *Cellular and Molecular Life Sciences,* vol. 78, no. 7, pp. 3503-3524, 2021.

[381] J. Morgan, D. Cohen, J. Hempstead and T. Curran, “Mapping patterns of c-fos expression in the central nervous system after seizure,” *Science,* vol. 237, no. 4811, pp. 192-197, 1987.

[382] J. Isaacs, G. Jackson and D. Altmann, “The role of cellular prion protein in the immune system,” *Clinical and experimental immunology,* vol. 146, no. 1, pp. 1-8, 2006.

[383] J. Yoon, Y. Hwang, M. Lee, J. Sun, H. Cho, L. Knapik and I. Daar, “TBC1d24-ephrinB2 interaction regulates contact inhibition of locomotion in neural crest cell migration,” *Nature communications,* vol. 9, no. 1, pp. 1-14, 2018.

[384] E. Fibach and E. Rachmilewitz, “The role of oxidative stress in hemolytic anaemia,” *Current molecular medicine,* vol. 8, no. 7, pp. 609-619, 2008.

[385] E. Nagababu, S. Gulyani, C. J. Earley, R. G. Cutler, M. P. Mattson and J. M. Rifkind, “Iron-deficiency anaemia enhances red blood cell oxidative stress,” *Free radical research,* vol. 42, no. 9, pp. 824-829, 2008.

[386] B. May, S. Dogra, T. Sadlon, C. Bhasker, T. Cox and S. Bottomley, “Molecular regulation of heme biosynthesis in higher vertebrates,” *Progress in nucleic acid research and molecular biology,* vol. 51, pp. 1-51, 1995.

[387] Y. Choi, S. Yeo, Y. Hong, S. Kim and S. Lim, “Changes of gene expression profiles in the cervical spinal cord by acupuncture in an MPTP-intoxicated mouse model: microarray analysis,” *Gene,* vol. 481, no. 1, pp. 7-16, 2011.

[388] A. Stankiewicz, J. Goscik, A. Swiergiel, A. Majewska, M. Wieczorek, G. Juszczak and P. Lisowski, “Social stress increases expression of hemoglobin genes in mouse prefrontal cortex,” *BMC neuroscience,* vol. 15, no. 1, pp. 1-16, 2014.

[389] H. Sun, M. Li, Y. Ji, J. Zhu, Z. Chen, L. Zhang, C. Deng, Q. Cheng, W. Wang, Y. Shen and D. Shen, “Identification of Regulatory Factors and Prognostic Markers in Amyotrophic Lateral Sclerosis,” *Antioxidants,* vol. 11, no. 2, p. 303, 2022.

[390] S. Hu, X. Li, H. Chen, L. Xu and J. Fang, “Knockdown of ALAS2 affects erythroid differentiation by down-regulating mitophagy receptor BNIP3L,” *Zhongguo shi yan xue ye xue za zhi,* vol. 28, no. 5, pp. 1710-1717, 2020.

[391] J. Van Hove, M. Saenz, J. Thomas, R. Gallagher, M. Lovell, L. Fenton, S. Shanske, S. Myers, R. Wanders, J. Ruiter and M. Turkenburg, “Succinyl-CoA ligase deficiency: a mitochondrial hepatoencephalomyopathy.,” *Pediatric Research,* vol. 68, no. 2, pp. 159-164, 2010.

[392] R. Santos-Silva, A. Passas, C. Rocha, R. Figueiredo, J. Mendes-Ribeiro, S. Fernandes, S. Biskup and M. Leão, “Bilateral frontoparietal polymicrogyria: a novel GPR56 mutation and an unusual phenotype.,” *Neuropediatrics,* vol. 46, no. 2, pp. 134-138, 2015.

[393] C. Marini, M. King, J. Archer, M. Newton and S. Berkovic, “Idiopathic generalised epilepsy of adult onset: clinical syndromes and genetics,” *Journal of Neurology, Neurosurgery & Psychiatry,* vol. 74, no. 2, pp. 192-196, 2003.

[394] J. DiFrancesco, L. Tremolizzo, V. Polonia, G. Giussani, E. Bianchi, C. Franchi, A. Nobili, I. Appollonio, E. Beghi and C. Ferrarese, “Adult-Onset Epilepsy in Presymptomatic Alzheimer’s Disease: A Retrospective Study,” *Journal of Alzheimer's Disease,* vol. 60, no. 4, pp. 1267-1274, 2017.

[395] L. Ségalat, “Loss-of-function genetic diseases and the concept of pharmaceutical targets,” *Orphanet journal of rare diseases,* vol. 2, no. 1, pp. 1-6, 2007.

[396] P. Perucca and E. Perucca, “Identifying mutations in epilepsy genes: impact on treatment selection,” *Epilepsy research,* vol. 152, pp. 18-30, 2019.

[397] B. Chen and R. Altman, “Opportunities for developing therapies for rare genetic diseases: focus on gain-of-function and allostery,” *Orphanet journal of rare diseases,* vol. 12, no. 1, pp. 1-7, 2017.

[398] C. Dunbar, K. High, J. Joung, D. Kohn, K. Ozawa and M. Sadelain, “Gene therapy comes of age,” *Science,* vol. 359, no. 6372, p. eaan4672, 2018.

[399] B. Leroy, D. Birch, J. Duncan, B. Lam, R. Koenekoop, F. Porto, S. Russell and A. Girach, “Leber congenital amaurosis due to cep290 mutations—Severe vision impairment with a high unmet medical need: A Review,” *Retina,* vol. 41, no. 5, p. 898, 2021.

[400] M. Maeder, M. Stefanidakis, C. Wilson, R. Baral, L. Barrera, G. Bounoutas, D. Bumcrot, H. Chao, D. Ciulla, J. DaSilva and A. Dass, “Development of a gene-editing approach to restore vision loss in Leber congenital amaurosis type 10,” *Nature medicine,* vol. 25, no. 2, pp. 229-233, 2019.

[401] G. Colasante, Y. Qiu, L. Massimino, C. Di Berardino, J. Cornford, A. Snowball, M. Weston, S. Jones, S. Giannelli, A. Lieb and S. Schorge, “In vivo CRISPRa decreases seizures and rescues cognitive deficits in a rodent model of epilepsy.,” *Brain,* vol. 143, no. 3, pp. 891-905, 2020.

[402] C. Falcicchia, M. Simonato and G. Verlengia, “New Tools for Epilepsy Therapy,” *Frontiers in cellular neuroscience,* vol. 12, p. 147, 2018.

[403] M. Merkulova, T. Păunescu, A. Azroyan, V. Marshansky, S. Breton and D. Brown, “Mapping the H+ (V)-ATPase interactome: identification of proteins involved in trafficking, folding, assembly and phosphorylation,” *Scientific reports,* vol. 5, no. 1, pp. 1-15, 2015.

[404] Y. Tan, Y. Abbas, J. Wu, D. Wu, K. Keon, G. Hesketh, S. Bueler, A. Gingras, C. Robinson, S. Grinstein and J. Rubinstein, “CryoEM of endogenous mammalian V-ATPase interacting with the TLDc protein mEAK-7,” *Life Science Alliance,* vol. 5, no. 11, 2022.

[405] M. Khan, S. Lee, S. Couoh-Cardel, R. Oot, H. Kim, S. Wilkens and S. Roh, “Oxidative stress protein Oxr1 promotes V-ATPase holoenzyme disassembly in catalytic activity-independent manner,” *The EMBO journal,* vol. 41, no. 3, p. e109360, 2022.

[406] E. Castroflorio, J. den Hoed, D. Svistunova, M. Finelli, A. Cebrian-Serrano, S. Corrochano, A. Bassett, B. Davies and P. Oliver, “The Ncoa7 locus regulates V-ATPase formation and function, neurodevelopment and behaviour,” *Cellular and Molecular Life Sciences,* vol. 78, pp. 3503-3524, 2020.

[407] S. Banerjee, K. Clapp, M. Tarsio and K. P.M., “Interaction of the late endo-lysosomal lipid PI(3,5)P2 with the Vph1 isoform of yeast V-ATPase increases its activity and cellular stress tolerance,” *Journal of Biological Chemistry,* vol. 294, pp. 9161-9171, 2019.

[408] S. Li, T. Diakov, T. Xu, M. Tarsio, W. Zhu, S. Couoh-Cardel, L. Weisman and P. Kane, “The signaling lipid PI(3,5)P2 stabilizes V1–Vo sector interactions and activates the V-ATPase,” *Molecular biology of the cell,* vol. 25, no. 8, pp. 1251-1262, 2014.

[409] B. Fischer, K. Lüthy, J. Paesmans, C. De Koninck, I. Maes, J. Swerts, S. Kuenen, V. Uytterhoeven, P. Verstreken and W. Versées, “Skywalker-TBC1D24 has a lipid-binding pocket mutated in epilepsy and required for synaptic function,” *Nature structural & molecular biology,* vol. 23, no. 11, pp. 965-973, 2016.

[410] T. Doyle, O. Moncorgé, B. Bonaventure, D. Pollpeter, M. Lussignol, M. Tauziet, L. Apolonia, M. Catanese, C. Goujon and M. Malim, "The interferon-inducible isoform of NCOA7 inhibits endosome-mediated viral entry.," *Nature microbiology,* vol. 3, no. 12, pp. 1369-1376, 2018.

[411] R. Guerrini, D. Mei, K. Kerti-Szigeti, S. Pepe, M. Koenig, G. Von Allmen, M. Cho, K. McDonald, J. Baker, V. Bhambhani and Z. Powis, "Phenotypic and genetic spectrum of ATP6V1A encephalopathy: a disorder of lysosomal homeostasis," *Brain,* 2022.

[412] A. Fassio, A. Falace, A. Esposito, D. Aprile, R. Guerrini and F. Benfenati, "Emerging Role of the Autophagy/Lysosomal Degradative Pathway in Neurodevelopmental Disorders With Epilepsy," *Frontiers in Cellular Neuroscience,* vol. 14, p. 39, 2020.

[413] R. White, I. Sokolovsky, M. Britt, N. Nsumu, D. Logsdon, S. McNulty, L. Wilmes, B. Brewer, E. Wirtz, H. Joyce and B. Fegley, "Hematologic characterization and chromosomal localization of the novel dominantly inherited mouse hemolytic anemia, neonatal anemia (Nan)," *Blood Cells, Molecules, and Diseases,* vol. 43, no. 2, pp. 141-148, 2009.

[414] G. Marchi, F. Busti, A. Lira Zidanes, A. Castagna and D. Girelli, "Aceruloplasminemia: a severe neurodegenerative disorder deserving an early diagnosis," *Frontiers in neuroscience,* vol. 13, p. 325, 2019.

[415] E. Atli, H. Gurkan, S. Ulusal, Y. Karal, E. Atli and H. Tozkir, "Identification of a novel homozygous TBC1D24 mutation in a Turkish family with DOORS syndrome," *Clinical Dysmorphology,* vol. 27, no. 1, pp. 1-3, 2018.

[416] R. Weber, F. Yen, S. Nicholson, H. Alwaseem, E. Bayraktar, M. Alam, R. Timson, K. La, M. Abu-Remaileh, H. Molina and K. Birsoy, "Maintaining Iron Homeostasis Is the Key Role of Lysosomal Acidity for Cell Proliferation," *Molecular Cell,* vol. 77, no. 3, pp. 645-655, 2020.

[417] R. Fallah, B. Tirandazi, F. Ferdosian and N. Fadavi, "Iron Deficiency and Iron Deficiency Anemia in Children With First Attack of Seizure and on Healthy Control Group: A Comparative Study," *Iranian journal of child neurology,* vol. 8, no. 3, p. 18, 2014.

[418] S. Chen, Y. Chen, Y. Zhang, X. Kuang, Y. Liu, M. Guo, L. Ma, D. Zhang and Q. Li, "Iron Metabolism and Ferroptosis in Epilepsy," *Frontiers in Neuroscience,* vol. 14, p. 601193, 2020.

[419] A. Galadanci, M. DeBaun and N. Galadanci, "Neurologic complications in children under five years with sickle cell disease," *Neuroscience letters,* vol. 706, pp. 201-206, 2019.

[420] P. Jaskamal, K. Khizer, S. Mohammad, K. Varsha, K. Gauvain, D. Richa, P. Sandeep, A. Cooper and J. Gutteridge, "Association of Anemia With Epilepsy and Antiepileptic Drugs," *Cureus,* vol. 13, no. 11, 2021.

[421] D. Furness, Y. Dehnes, A. Akhtar, D. Rossi, M. Hamann, N. Grutle, V. Gundersen, S. Holmseth, K. Lehre, K. Ullensvang and M. Wojewodzic, "A quantitative assessment of glutamate uptake into hippocampal synaptic terminals and astrocytes: new insights into a neuronal role for excitatory amino acid transporter 2 (EAAT2)," *Neuroscience,* vol. 157, no. 1, pp. 80-94, 2008.

[422] P. Nilsson, K. Loganathan, M. Sekiguchi, Y. Matsuba, K. Hui, S. Tsubuki, M. Tanaka, N. Iwata, T. Saito and T. Saido, “Aβ secretion and plaque formation depend on autophagy,” *Cell reports,* vol. 5, no. 1, pp. 61-69, 2013.

[423] P. Radhiyanti, A. Konno, Y. Matsuzaki and H. Hirai, “Comparative study of neuron-specific promoters in mouse brain transduced by intravenously administered AAV-PHP. eB,” *Neuroscience Letters,* vol. 756, p. 135956, 2021.

[424] Y. Egashira, Y. Mori, Y. Yanagawa and S. Takamori, “Development of lentiviral vectors for efficient glutamatergic-selective gene expression in cultured hippocampal neurons.,” *Scientific reports,* vol. 8, no. 1, pp. 1-13, 2018.

[425] Y. Zhang, K. Chen, S. Sloan, M. Bennett, A. Scholze, S. O'Keeffe, H. Phatnani, P. Guarnieri, C. Caneda, N. Ruderisch and S. Deng, “An RNA-sequencing transcriptome and splicing database of glia, neurons, and vascular cells of the cerebral cortex,” *Journal of Neuroscience,* vol. 34, no. 36, pp. 11929-11947, 2014.

[426] Y. Zhang, S. Sloan, L. Clarke, C. Caneda, C. Plaza, P. Blumenthal, H. Vogel, G. Steinberg, M. Edwards, G. Li and J. Duncan III, “Purification and Characterization of Progenitor and Mature Human Astrocytes Reveals Transcriptional and Functional Differences with Mouse,” *Neuron,* vol. 89, no. 1, pp. 37-53, 2016.

[427] K. Tanaka, K. Watase, T. Manabe, K. Yamada, M. Watanabe, K. Takahashi, H. Iwama, T. Nishikawa, N. Ichihara, T. Kikuchi and S. Okuyama, “Epilepsy and exacerbation of brain injury in mice lacking the glutamate transporter GLT-1,” *Science,* vol. 276, no. 5319, pp. 1699-1702, 1997.

[428] G. Petr, Y. Sun, N. Frederick, Y. Zhou, S. Dhamne, M. Hameed, C. Miranda, E. Bedoya, K. Fischer, W. Armsen and J. Wang, “Conditional deletion of the glutamate transporter GLT-1 reveals that astrocytic GLT-1 protects against fatal epilepsy while neuronal GLT-1 contributes significantly to glutamate uptake into synaptosomes,” *Journal of Neuroscience,* vol. 35, no. 13, pp. 5187-5201, 2015.

[429] A. Peterson and D. Binder, “Regulation of synaptosomal GLT-1 and GLAST during epileptogenesis.,” *Neuroscience,* vol. 411, pp. 185-201, 2019.

[430] E. Genda, J. Jackson, A. Sheldon, S. Locke, T. Greco, J. O'Donnell, L. Spruce, R. Xiao, W. Guo, M. Putt and S. Seeholzer, “Co-compartmentalization of the Astroglial Glutamate Transporter, GLT-1, with Glycolytic Enzymes and Mitochondria,” *Journal of Neuroscience,* vol. 31, no. 50, pp. 18275-18288, 2011.

[431] M. Martineau, R. Guzman, C. Fahlke and J. Klingauf, “VGLUT1 functions as a glutamate/proton exchanger with chloride channel activity in hippocampal glutamatergic synapses.,” *Nature communications,* vol. 8, no. 1, pp. 1-13, 2017.

[432] V. Montana, Y. Ni, X. Hua and V. Parpura, “ Vesicular glutamate transporter-dependent glutamate release from astrocytes.,” *Journal of Neuroscience,* vol. 24, no. 11, pp. 2633-2642, 2004.

[433] C. Muñoz-Ballester, A. Berthier, R. Viana and P. Sanz, “Homeostasis of the astrocytic glutamate transporter GLT-1 is altered in mouse models of Lafora disease,” *Biochimica Et Biophysica Acta (BBA)-Molecular Basis of Disease,* vol. 1862, no. 6, pp. 1074-1083, 2016.

[434] E. Perez-Jimenez, R. Viana, C. Muñoz-Ballester, C. Vendrell-Tornero, R. Moll-Diaz, M. Garcia-Gimeno and P. Sanz, “Endocytosis of the glutamate transporter 1 is regulated by laforin and malin: Implications in Lafora disease,” *Glia,* vol. 69, no. 5, pp. 1170-1183, 2021.

[435] S. Parrot, A. Corscadden, L. Lallemant, H. Benyamine, J. Comte, A. Huguet-Lachon, G. Gourdon and M. Gomes-Pereira, “Defects in Mouse Cortical Glutamate Uptake Can Be Unveiled In Vivo by a Two-in-One Quantitative Microdialysis,” *ACS Chemical Neuroscience,* vol. 13, no. 1, pp. 134-142, 2021.

[436] D. Patel, B. Tewari, L. Chaunsali and H. Sontheimer, “Neuron–glia interactions in the pathophysiology of epilepsy.,” *Nature Reviews Neuroscience,* vol. 20, no. 5, pp. 282-297, 2019.

[437] P. Soblechero-Martín, A. López-Martínez, L. de la Puente-Ovejero, A. Vallejo-Illarramendi and V. Arechavala-Gomeza, “Utrophin modulator drugs as potential therapies for Duchenne and Becker muscular dystrophies,” *Neuropathology and Applied Neurobiology,* vol. 47, no. 6, pp. 711-723, 2021.

[438] Y. Song, L. Morales, A. Malik, A. Mead, C. Greer, M. Mitchell, M. Petrov, L. Su, M. Choi, S. Rosenblum and X. Lu, “Non-immunogenic utrophin gene therapy for the treatment of muscular dystrophy animal models.,” *Nature medicine,* vol. 25, no. 10, pp. 1505-1511, 2019.

[439] B. Martin, G. Dieuset, J. Pawluski, N. Costet and A. Biraben, “Audiogenic seizure as a model of sudden death in epilepsy: A comparative study between four inbred mouse strains from early life to adulthood.,” *Epilepsia,* vol. 61, no. 2, pp. 342-349, 2020.

[440] V. Carola, F. D'Olimpio, E. Brunamonti, F. Mangia and P. Renzi, “Evaluation of the elevated plus-maze and open-field tests for the assessment of anxiety-related behaviour in inbred mice,” *Behavioural brain research,* vol. 134, no. 1-2, pp. 49-57, 2002.

[441] A. Falace, E. Buhler, M. Fadda, F. Watrin, P. Lippiello, E. Pallesi-Pocachard, P. Baldelli, F. Benfenati, F. Zara, A. Represa and A. Fassio, “TBC1D24 regulates neuronal migration and maturation through modulation of the ARF6-dependent pathway,” *Proceedings of the National Acadmeny of Sciences,* vol. 111, no. 6, pp. 2337-2342, 2014.

[442] D. Alapati, W. Zacharias, H. Hartman, A. Rossidis, J. Stratigis, N. Ahn, B. Coons, S. Zhou, H. Li, K. Singh and J. Katzen, “In utero gene editing for monogenic lung disease,” *Science translational medicine,* vol. 11, no. 488, p. eaav8375, 2019.

[443] M. Finelli, D. Aprile, E. Castroflorio, A. Jeans, M. Moschetta, L. Chessum, M. Degiacomi, J. Grasegger, A. Lupien-Meilleur, A. Bassett and E. Rossignol, “The epilepsy-associated protein TBC1D24 is required for normal development, survival and vesicle trafficking in mammalian neurons,” *Human molecular genetics,* vol. 28, no. 4, pp. 584-597, 2019.

[444] A. Bodzęta, M. Kahms and J. Klingauf, “The presynaptic v-ATPase reversibly disassembles and thereby modulates exocytosis but is not part of the fusion machinery,” *Cell reports,* vol. 20, no. 6, pp. 1348-1359, 2017.

[445] M. Corbett, M. Bahlo, L. Jolly, Z. Afawi, A. Gardner, K. Oliver, S. Tan, A. Coffey, J. Mulley, L. Dibbens and W. Simri, “A focal epilepsy and intellectual disability syndrome is due to a mutation in TBC1D24,” *The American Journal of Human Genetics,* vol. 87, no. 3, pp. 371-375, 2010.